NASA TECHNICAL MEMORANDUM

NASA TM X-3398

NASA TM X-3398

EFFECT OF DROOPED-NOSE FLAPS ON THE EXPERIMENTAL FORCE AND MOMENT CHARACTERISTICS OF AN OBLIQUE WING

Edward J. Hopkins and George H. Lovette

Ames Research Center
Moffett Field, Calif. 94035

NATIONAL AERONAUTICS AND SPACE ADMINISTRATION • WASHINGTON, D. C. • NOVEMBER 1976

1. Report No. NASA TM X - 3398	2. Government Accession No.	3. Recipient's Catalog No.
4. Title and Subtitle EFFECT OF DROOPED-NOSE FLAPS ON THE EXPERIMENTAL FORCE AND MOMENT CHARACTERISTICS OF AN OBLIQUE WING		5. Report Date November 1976 6. Performing Organization Code
7. Author(s) Edward J. Hopkins and George H. Lovette*		8. Performing Organization Report No. A-6461
9. Performing Organization Name and Address Ames Research Center Moffett Field, California 94035		10. Work Unit No. 505-11-12 11. Contract or Grant No.
12. Sponsoring Agency Name and Address National Aeronautics and Space Administration Washington, D. C. 20546		13. Type of Report and Period Covered Technical Memorandum 14. Sponsoring Agency Code
15. Supplementary Notes *Project Engineer, ARO, Inc., Moffett Field, Calif. 94035		

16. Abstract

Six-component experimental force and moment data are presented for a low aspect-ratio, oblique wing equipped with drooped-nose flaps and mounted on top of a body of revolution. These flaps were investigated on the downstream wing panel with the nose drooped 5°, 10°, 20°, and 30°, and on both wing panels with the nose drooped 30°. The purpose of the study was to determine if such flaps would make the moment curves more linear by controlling the flow separation on the downstream wing panel at high lift coefficients. The wing was elliptical in planform and had an aspect ratio of 6.0 (based on the unswept wing span). The wing was tested at sweep angles of 45° and 50° throughout the Mach number range from 0.25 to 0.95. The drooped-nose flaps alone were not effective in making the moment curves more linear; however, a previous study showed that Krüger nose flaps improved the linearity of the moment curves when the Krüger flaps were used on only the downstream wing panel equipped with drooped-nose flaps deflected 5°.

17. Key Words (Suggested by Author(s))		18. Distribution Statement
Leading-edge flaps Wing flaps Wing nose flaps Stability & control	Oblique wings Swept wings	Unlimited STAR Category – 08

19. Security Classif. (of this report)	20. Security Classif. (of this page)	21. No. of Pages	22. Price*
Unclassified	Unclassified	142	$5.75

*For sale by the National Technical Information Service, Springfield, Virginia 22161

NOMENCLATURE

The axes systems and sign conventions are presented in figure 1. Lift and drag are presented about the wind axes; side force, pitching moments, rolling moments and yawing moments are presented about the body axes.

b	wing span
C_D	drag coefficient, $\frac{\text{drag}}{qS}$
C_l	rolling-moment coefficient about the body axes, $\frac{\text{rolling moment}}{qSb}$
C_L	lift coefficient, $\frac{\text{lift}}{qS}$
C_m	pitching-moment coefficient (see fig. 2(a) for moment-center location), $\frac{\text{pitching moment}}{qS\bar{c}}$
C_n	yawing-moment coefficient about the body axes, $\frac{\text{yawing moment}}{qSb}$
C_Y	side-force coefficient about the body axes, $\frac{\text{side force}}{qS}$
c	wing chord
c_{aft}	portion of wing chord aft of the 0.25c line
c_{fwd}	portion of wing chord forward of the 0.25c line
c_{root}	wing root chord
$\bar{c}$	wing mean aerodynamic chord
H	vertical distance from wing reference plane to base line (see fig. (2b))
M	Mach number
q	free-stream dynamic pressure
RN/L	unit Reynolds number per meter times 10^{-6}
r	body radius
S	wing area
$(t/c)_{max}$	maximum thickness-to-chord ratio
V	free-stream velocity
x	chordwise distance along airfoil

x_1	axial distance along body from the 57.45 cm longitudinal station
Y	distance along wing span (see fig. 2(b))
z	vertical distance above the wing-chord plane
α	angle of attack, deg
δ_n	nose flap deflection (positive with nose down), deg
Λ	sweep angle measured between a perpendicular to the body axis and the 0.25c line of the wing in a horizontal plane (the right wing tip is forward for positive Λ's), deg

EFFECT OF DROOPED-NOSE FLAPS ON THE EXPERIMENTAL FORCE AND MOMENT CHARACTERISTICS OF AN OBLIQUE WING

Edward J. Hopkins and George H. Lovette*

Ames Research Center

SUMMARY

Six-component experimental force and moment data are presented for a low aspect-ratio, oblique wing equipped with drooped-nose flaps and mounted on top of a body of revolution. These flaps were investigated on the downstream wing panel with the nose drooped 5°, 10°, 20°, and 30°, and on both wing panels with the nose drooped 30°. The purpose of the study was to determine if such flaps would make the moment curves more linear by controlling the flow separation on the downstream wing panel at high lift coefficients. The wing was elliptical in planform and had an aspect ratio of 6.0 (based on the unswept wing span). The wing was tested at sweep angles of 45° and 50° throughout the Mach number range from 0.25 to 0.95. The drooped-nose flaps alone were not effective in making the moment curves more linear; however, a previous study showed that Krüger nose flaps improved the linearity of the moment curves when the Krüger flaps were used on only the downstream wing panel equipped with drooped-nose flaps deflected 5°.

INTRODUCTION

It was shown experimentally in references 1 and 2 that the low aspect-ratio, oblique wing (suitable for a highly maneuverable vehicle) is more efficient and has considerably higher maximum lift-to-drag ratios at transonic Mach numbers than a conventional swept wing of the same aspect ratio. At high lift coefficients, however, there is flow separation on the downstream wing panel of oblique wings; this separation results in very nonlinear pitching-, rolling-, and yawing-moment curves. In references 1 and 2, an attempt was made to alleviate the asymmetrical spanwise wing stall associated with oblique wings by bending the wing panels upward to produce washout on the downstream wing panel and washin on the upstream wing panel. It was found that although wing bending might produce more linear moment curves, an impractical wing pivot location would be required to eliminate the rolling moments at low lift coefficients. For this reason, two types of nose flaps (Krüger and drooped-nose flaps) were investigated as a possible means of delaying the flow separation on the trailing wing panel of oblique wings at high lift coefficients. In the previous investigation (ref. 3), it was found that Krüger nose flaps mounted only on the downstream wing panel with a nose flap deflected 5° was the most effective arrangement for delaying the flow separation and making the moment curves more linear.

The present investigation was undertaken to study the effectiveness of drooped-nose flaps alone, mounted on the same low aspect-ratio oblique wing of reference 3, for controlling the flow

*Project Engineer, ARO, Inc., Moffett Field, Calif. 94035

separation on the downstream wing panel and making the moment curves more linear at high lift coefficients. The effects of the drooped-nose flaps were studied with the flaps (1) mounted on the downstream panel only (nose drooped successively from 5° to 30°) and (2) with the flaps mounted on both panels (nose drooped 30° only). The wing was investigated at sweep angles of 45° and 50°. The use of nose flaps on both wing panels might eliminate the rolling and yawing moments at low lift without loss in effectiveness of the nose flaps at high lift. A limited comparison between the effectiveness of the Krüger flaps (investigated in ref. 3) and the drooped-nose flaps of the present investigation in making the moment curves more linear is also presented.

CONFIGURATION CODE

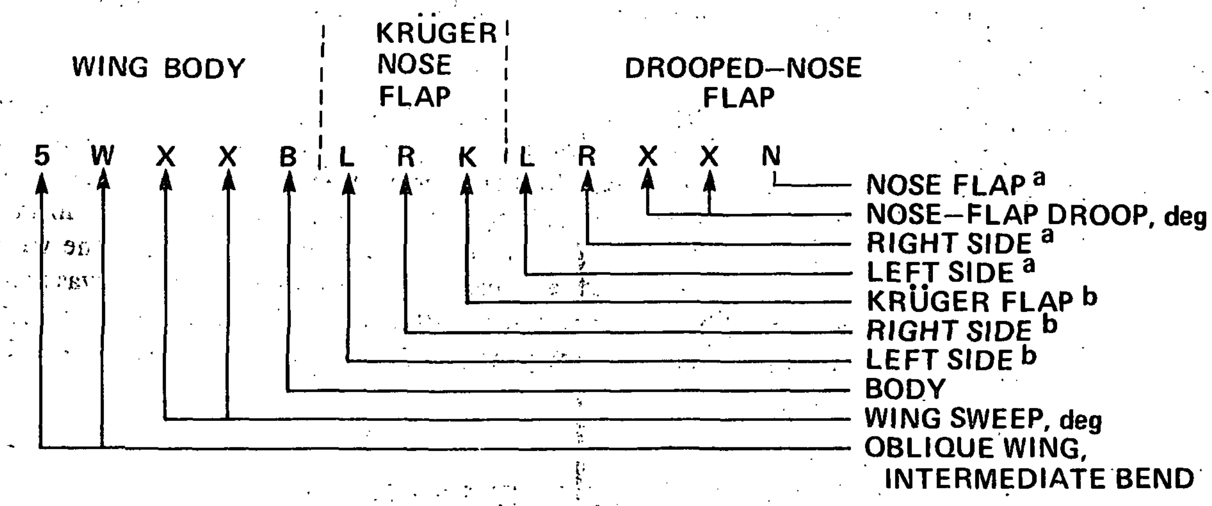

[a]WHEN SYMBOL IS DELETED, DROOPED-NOSE FLAP IS UNDEFLECTED

[b]WHEN SYMBOL IS DELETED, KRÜGER NOSE FLAP IS REMOVED

TEST FACILITY

The Ames 6- by 6-Foot Wind Tunnel is a variable pressure, continuous flow, closed return-type facility. The nozzle ahead of the test section consists of an asymmetric sliding block which permits a continuous variation of Mach number from 0.25 to 2.3. The test section has a perforated floor and ceiling for boundary-layer removal to permit transonic testing.

MODEL DESCRIPTION

The model consisted of an oblique wing mounted on top of a Sears-Haack body of revolution designed to have minimum wave drag for a given length and volume. By installing different fairing blocks under the wing, as shown in figure 2(a), the wing could be swept 45° and 50°. Details of the body and of the fairing blocks are given in table 3 of reference 4. Also, note in figure 2(a) that the wing pivot point and the moment center are located at 0.40 c_{root} ($\Lambda = 0$). The wing planform consisted of two semiellipses having the same major axis but different minor axes in the ratio of 3:1

so that the major axis is the quarter chord line. Effective geometric twist was accomplished by bending the wing panels upward so that the chord lines perpendicular to the quarter chord line remained in horizontal planes. This type of bending results in wing twist when the oblique wing is swept; that is, washout on the downstream panel and washin on the upstream panel. Equations for the bend lines of the wing with the intermediate bend of the present investigation, and the wing planform are shown in figure 2(b). Additional geometric details of the wing and body are presented in table 1.

A subcritical Garabedian profile with a design lift coefficient of 1.3 at $M = 0.6$, $(t/c)_{max} = 0.1016$, was used perpendicular to the quarter chord line. This profile, shown in figure 2(c), varied in maximum thickness from $0.11c$ at the wing root to $0.06c$ at the wing tip according to the elliptical equation given in figure 2(b). Coordinates for the Garabedian profile are given in table 2.

The drooped-nose flaps with which the model was equipped had a span that was 67 percent that of the wing and were segmented as shown in figure 2(d). The drooped-nose flaps were tested when mounted on both wing panels and deflected 30°, and when mounted on the downstream panel only and deflected 5°, 10°, 20°, and 30°. The drooped-nose flaps were pivoted about an axis located on the lower surface of the wing at about 15 percent of the wing chord behind the wing leading edge. All gaps between the nose segments were sealed and a radius fairing of wax was used on the upper wing surface between the main wing and the nose flap when the flap was deflected. A sketch of the Krüger nose flaps mounted on the nose flaps with a deflection of 5°, as investigated in reference 3, is also shown in figure 2(d).

DATA REDUCTION AND TEST PROCEDURE

The model was sting-supported through the base of the model on a six-component electrical strain-gage balance as shown in figure 3. Measured drag forces were corrected to a condition corresponding to that of having the free-stream static pressure on the base of the fuselage. Moment data are presented about a moment center located on the body axis at $0.4c_{root}$ of the unswept oblique wing (see fig. 2(a)). Reference lengths and the wing area used in the reduction of the data are given in table 1.

Boundary-layer transition strips (0.1905 cm wide) consisting of a random distribution of glass spheres (0.01905 cm diameter) were placed 0.762 cm downstream of the wing leading edge on both the upper and lower surfaces of the wing, and 2.54 cm downstream of the body tip. Sublimation studies made on the plain wing (with no leading-edge flaps) at wing sweep angles of 0 and 45° indicate that the boundary layer was tripped by the 0.01905 cm diameter spheres near the roughness strips at $\alpha = 0$ and 10° at Mach numbers of 0.6 and 0.9.

The unit Reynolds number was held constant at 8.2×10^6/m throughout the test except at the Mach number of 0.25; for $M = 0.25$, the unit Reynolds number was reduced to 5.7×10^6/m, because of the dynamic overload restrictions of the balance. The model was mounted on a sting that was bent 10° to increase the maximum angle of attack; the resulting angle-of-attack range was from -1° to 31°. Data were obtained at Mach numbers of 0.25, 0.4, 0.6, 0.8, 0.9, 0.95. Angle of attack was indicated by an electrical dangleometer mounted in the model support located downstream of the sting. Corrections were applied to the indicated angle of attack for balance and sting deflections.

RESULTS AND DISCUSSION

Experimental results for the oblique wing equipped with drooped-nose flaps on only the downstream wing panel are shown in figures 4-9 for a sweep angle of 45°, and in figures 10-15 for a sweep angle of 50°. Results for the case when the drooped-nose flaps were used on both wing panels are shown in figures 16-21 for a wing sweep angle of 45°, and in figures 22-27 for a sweep angle of 50°. A limited comparison of the drooped-nose flap results and the Krüger nose flap results of reference 3 is presented in figure 28.

Drooped-Nose Flaps on the Downstream Wing Panel

With the oblique wing swept either 45° or 50°, drooping the nose flap on the downstream wing panel successively from 5° to 30° had little effect on controlling the flow separation on the downstream panel. This result is shown by the highly nonlinear pitching-, rolling-, or yawing-moment curves in figures 9(b), 9(e), 15(b), and 15(e). It can also be observed that deflecting the nose flaps had a progressively detrimental effect on the lift/drag ratio as the deflection angle was increased (see figs. 9(d) and 15(d)).

Drooped-Nose Flaps on Both Wing Panels

With the oblique wing swept either 45° or 50°, deflecting the nose flap 30° on both wing panels did not improve the linearity of the moment curves at either high or low lift coefficients (see figs. 21(b), 21(e), 27(b) and 27(e)). Again, the lift/drag ratios for the oblique wing with drooped-nose flaps were generally lower than for the plain wing (see figs. 21(d) and 27(d)).

A Comparison of the Drooped-Nose Flap Results and Previous Krüger Nose Flap Results

The effects of mounting Krüger nose flaps on the drooped-nose flaps, which were deflected 5° and mounted on the downstream wing panel only, are shown in figures 28(b) and 28(e) for a Mach number of 0.95 and a sweep angle of 45°. Results for the Krüger nose flaps at other Mach numbers and sweep angles are presented in reference 3. At low lift coefficients, the Krüger nose flaps produced increments of yawing moment (fig. 28(e)) and lower lift/drag ratios (fig. 28(d)).

As pointed out in reference 3, with no upward bending of the wing panels the rolling moment coefficients of −0.01 to −0.02 could be eliminated at low lift coefficients. Bending the wing panels upward to the so-called intermediate bend did not improve the linearity of the moment curves.

CONCLUDING REMARKS

It was shown that drooped-nose flaps alone on a low-aspect ratio, oblique wing were not effective in making the pitching-, rolling-, and yawing-moment curves more linear at high lift coefficients. As previously reported, however, Krüger flaps were effective in producing more linear moment curves for the oblique wing when they were mounted on to downstream wing panel with the nose flap deflected 5°.

Ames Research Center
National Aeronautics and Space Administration
Moffett Field, California 94035, March 15, 1976

REFERENCES

1. Hopkins, Edward J.; and Levin, Alan D.: An Experimental and Theoretical Study of Low-Aspect Ratio Swept and Oblique Wings at Mach Numbers Between 0.6 and 1.4. AIAA Preprint 74-771, AIAA Mechanics and Control of Flight Conference, Anaheim, Calif. August 5–9, 1974.

2. Hopkins, Edward J.: Effects of Wing Bend on the Aerodynamic Characteristics of a Low Aspect Ratio Oblique Wing. AIAA Preprint 75-995, AIAA Aircraft Systems and Technology Meeting, Los Angeles, Calif. August 4-7, 1975.

3. Hopkins, Edward J.; and Lovette, George H.: Effect of Krüger Nose Flaps on the Experimental Force and Moment Characteristics of an Oblique Wing. NASA TM X-3372, 1976.

4. Hopkins, Edward J.; Meriwether, Frank D.; and Pena, Douglas F.: Experimental Aerodynamic Characteristics of Low Aspect-Ratio Swept and Oblique Wings at Mach Numbers Between 0.6 and 1.4. NASA TM X-62,317, 1973.

TABLE 1.– MODEL GEOMETRY

Body	
Radius	$r = 3.856[1 - (1 - 2x_1/114.91)^2]^{3/4}$ cm
Length	
Closed	114.91 cm
Cutoff	91.44 cm
Maximum diameter	7.71 cm
Wing	
Planform ellipticity about 0.25 *c* line	4.7:1
Span	90.51 cm
Span (reference)	71.12 cm
Area (reference)	1365.09 cm^2
Mean aerodynamic chord (reference), $\bar{c}$	20.88 cm
Root chord	19.20 cm
Aspect ratio ($\Lambda = 0$)	6.0
Aspect ratio ($\Lambda = 45°$)	3.2
Incidence relative to body centerline	0
Profile perpendicular to 0.25 *c* line	Garabedian, subcritical (see table 2)

TABLE 2.– COORDINATES FOR GARABEDIAN PROFILE
[$(t/c)_{max}$ = 0.1016, design lift coefficient = 1.3 at M = 0.6]

x/c	z/c	x/c	z/c
0	0	0	0
−.00045	.00079	.00048	−.00058
−.00073	.00146	.00104	−.00120
−.00086	.00191	.00165	−.00176
−.00097	.00244	.00257	−.00249
−.00103	.00290	.00343	−.00308
−.00106	.00345	.00467	−.00382
−.00104	.00403	.00592	−.00445
−.00098	.00463	.00674	−.00481
−.00077	.00572	.00774	−.00519
−.00052	.00653	.00943	−.00570
−.00021	.00732	.01149	−.00620
.00026	.00830	.01539	−.00694
.00073	.00909	.02583	−.00837
.00163	.01033	.03967	−.00970
.00276	.01161	.06022	−.01116
.00464	.01340	.09339	−.01288
.00709	.01538	.13965	−.01462
.01197	.01878	.19880	−.01601
.02179	.02443	.25034	−.01684
.03187	.02928	.31761	−.01738
.04250	.03373	.38597	−.01735
.06373	.04113	.45495	−.01657
.09353	.04969	.50010	−.01568
.13389	.05882	.54359	−.01456
.17545	.06597	.57465	−.01363
.22415	.07249	.61351	−.01232
.28227	.07822	.65330	−.01090
.34741	.08236	.68122	−.00988
.41444	.08434	.71655	−.00865
.48168	.08406	.74682	−.00771
.55738	.08094	.77611	−.00702
.62052	.07591	.82243	−.00642
.68276	.06852	.87054	−.00698
.72012	.06288	.89717	−.00810
.75413	.05684	.91595	−.00941
.82318	.04227	.94348	−.01235
.85663	.03370	.96854	−.01674
.89115	.02388	.98615	−.02126
.92448	.01327	.99596	−.02434
.95410	.00145	1.00000	−.02600
.97175	−.00538		
.99163	−.01450		
1.00000	−.01900		

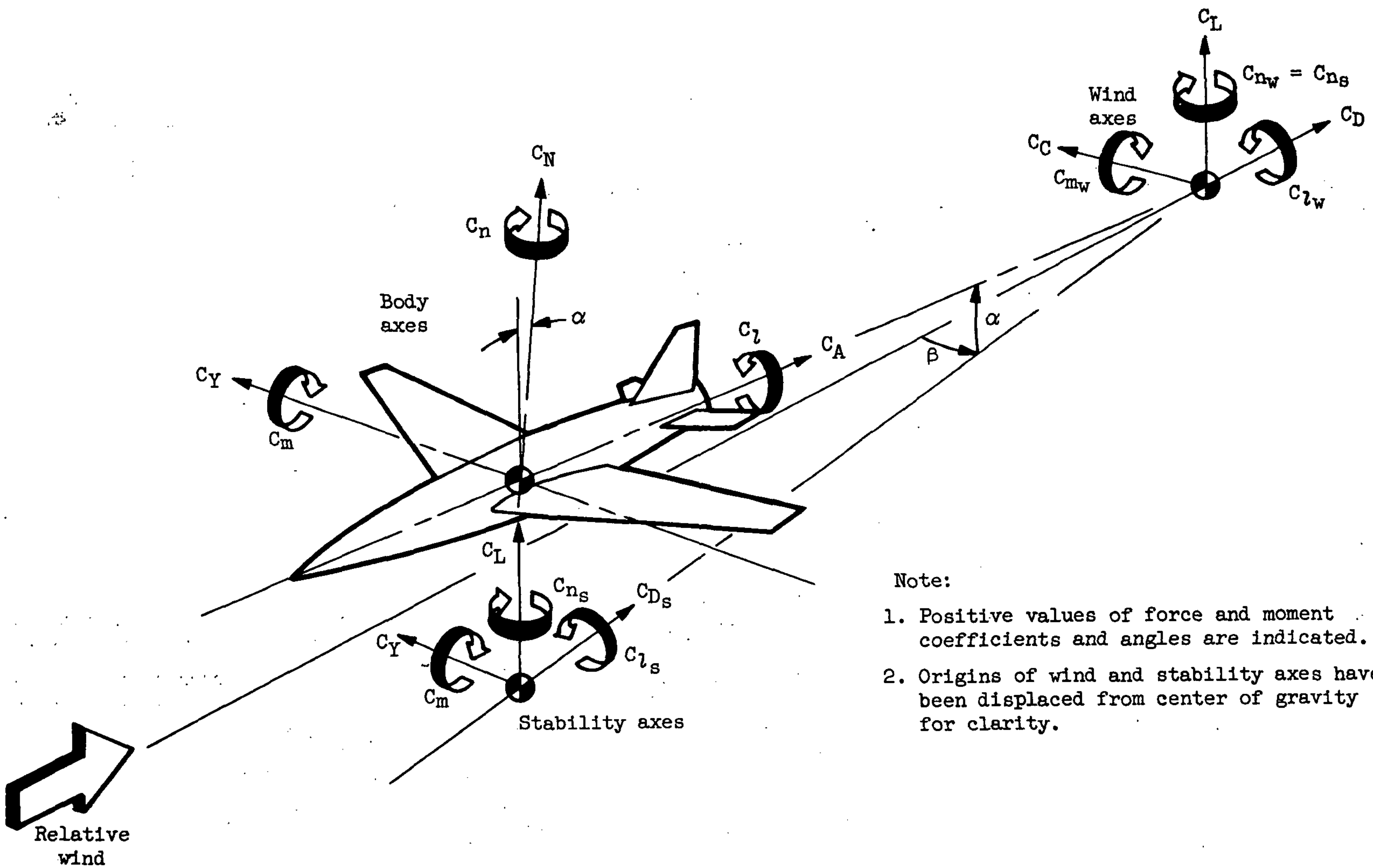

Figure 1.– Axes systems and sign conventions.

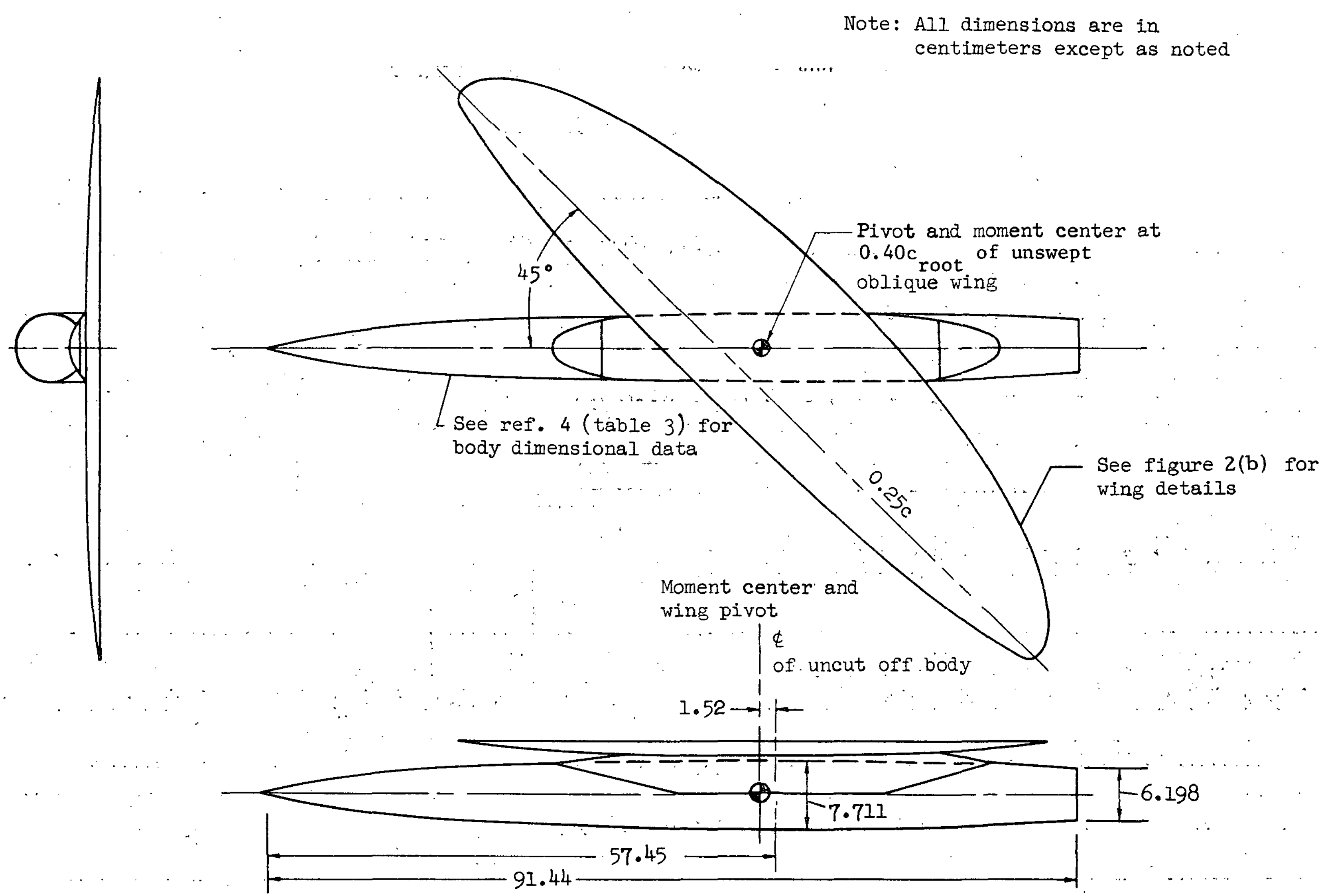

(a) Wing pivot and moment center.

Figure 2.– Geometric details for the oblique wing-body combination and the flaps.

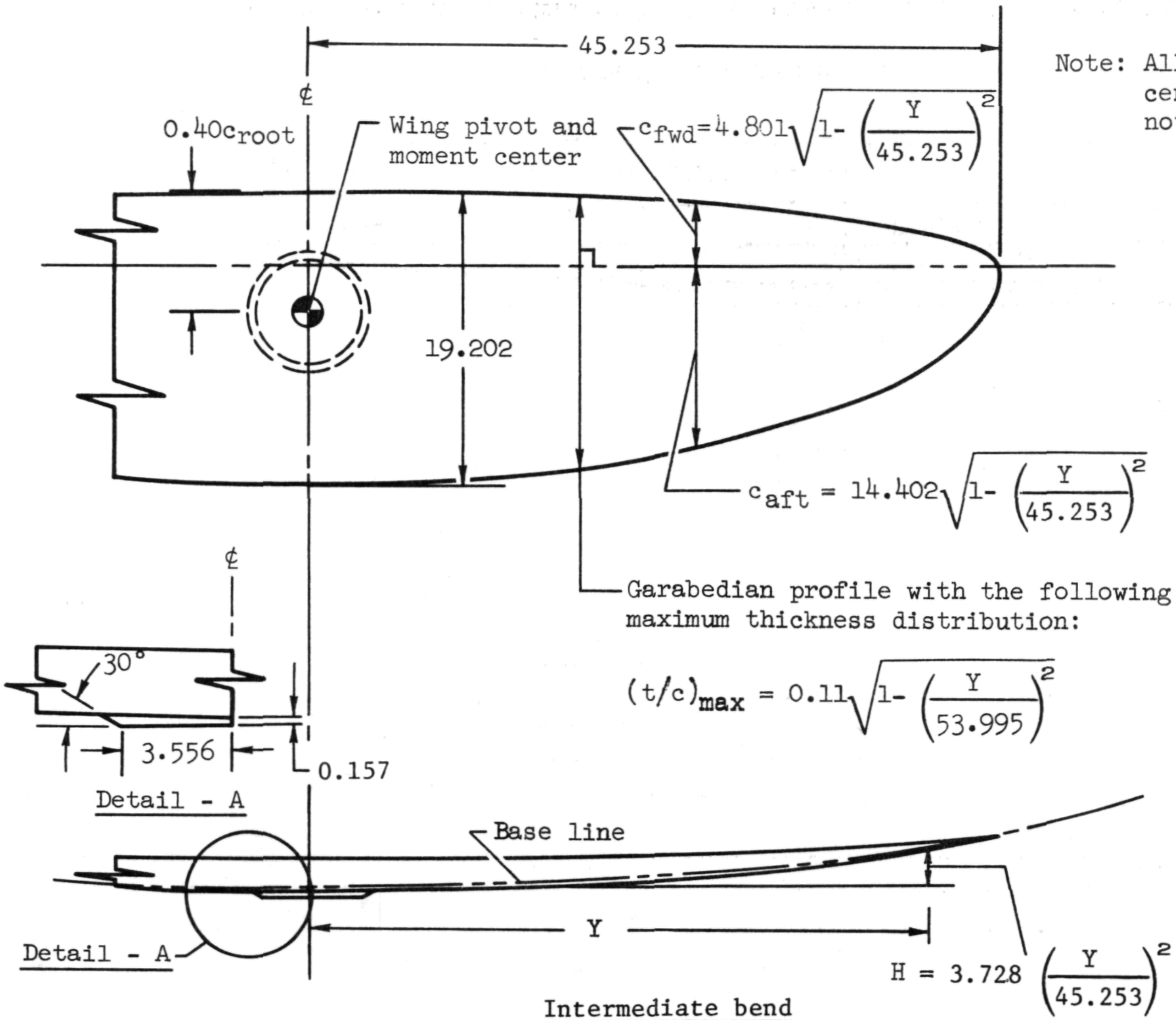

(b) Wing planform, thickness distribution and bend line.

Figure 2.– Continued.

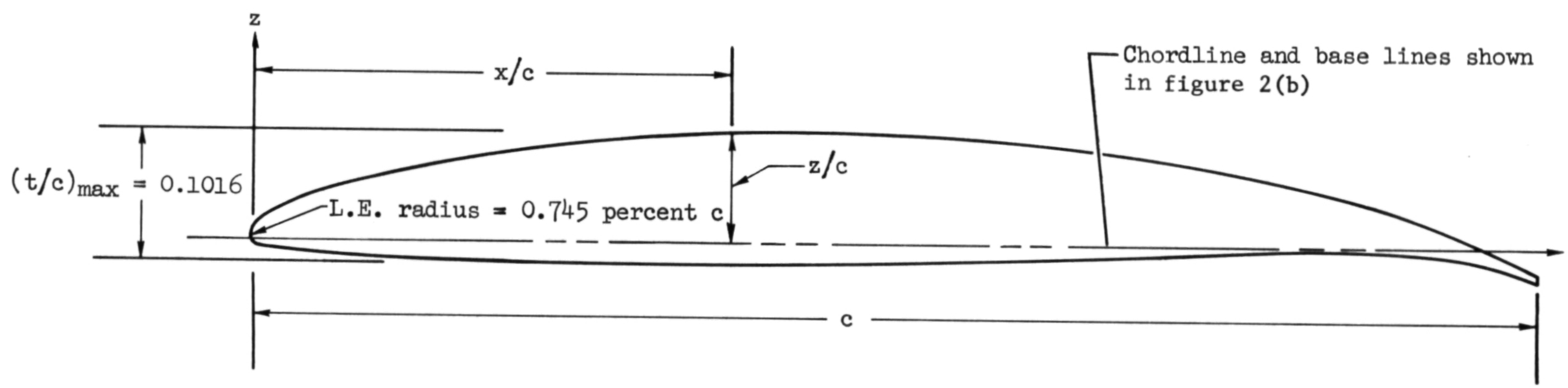

(c) Garabedian airfoil (designed for a section lift coefficient of 1.3 at $M = 0.6$, $(t/c)_{max} = 0.1016$).

Figure 2.– Continued.

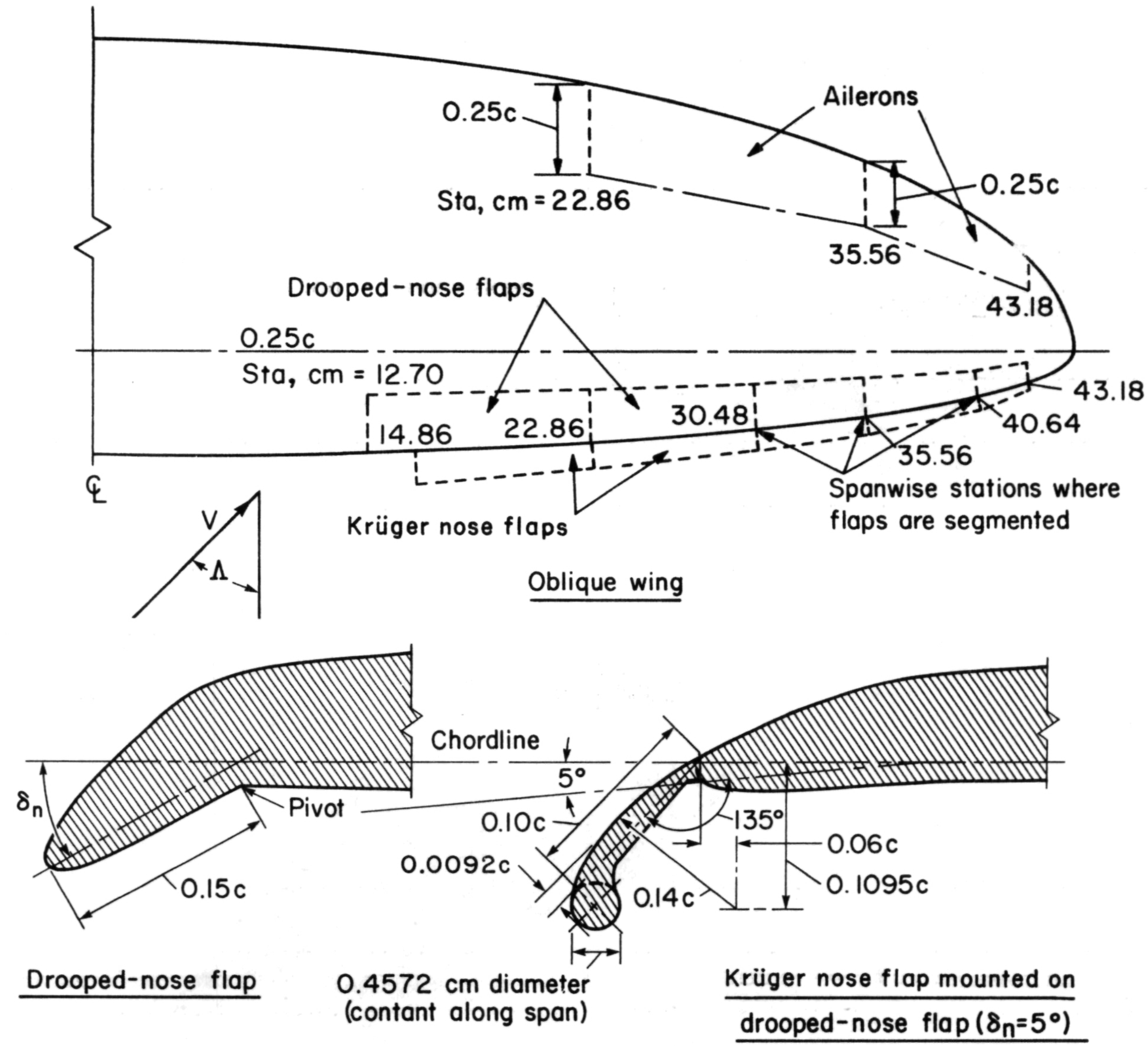

(d) Drooped-nose and Krüger nose flaps.

Figure 2.– Concluded.

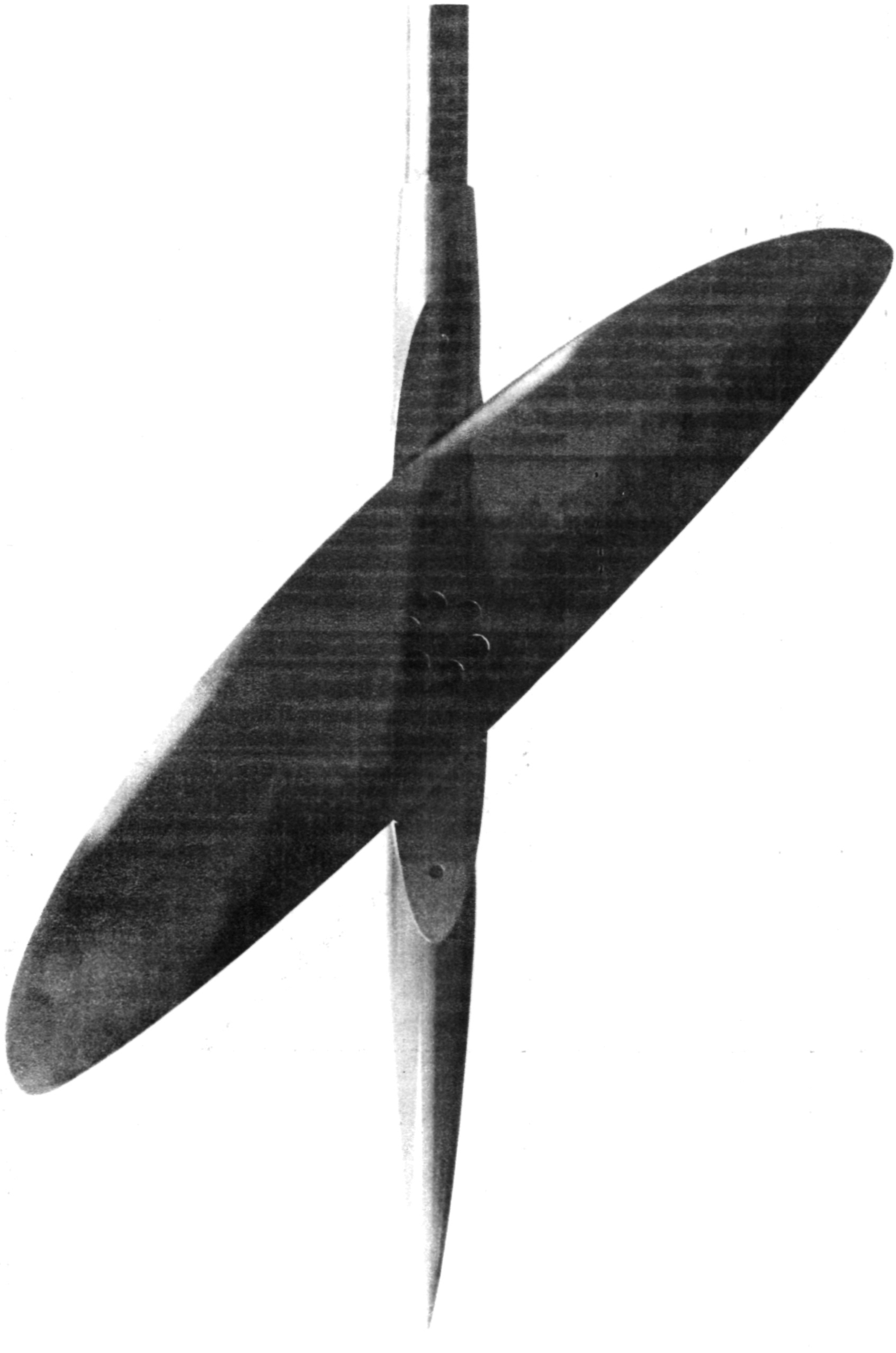

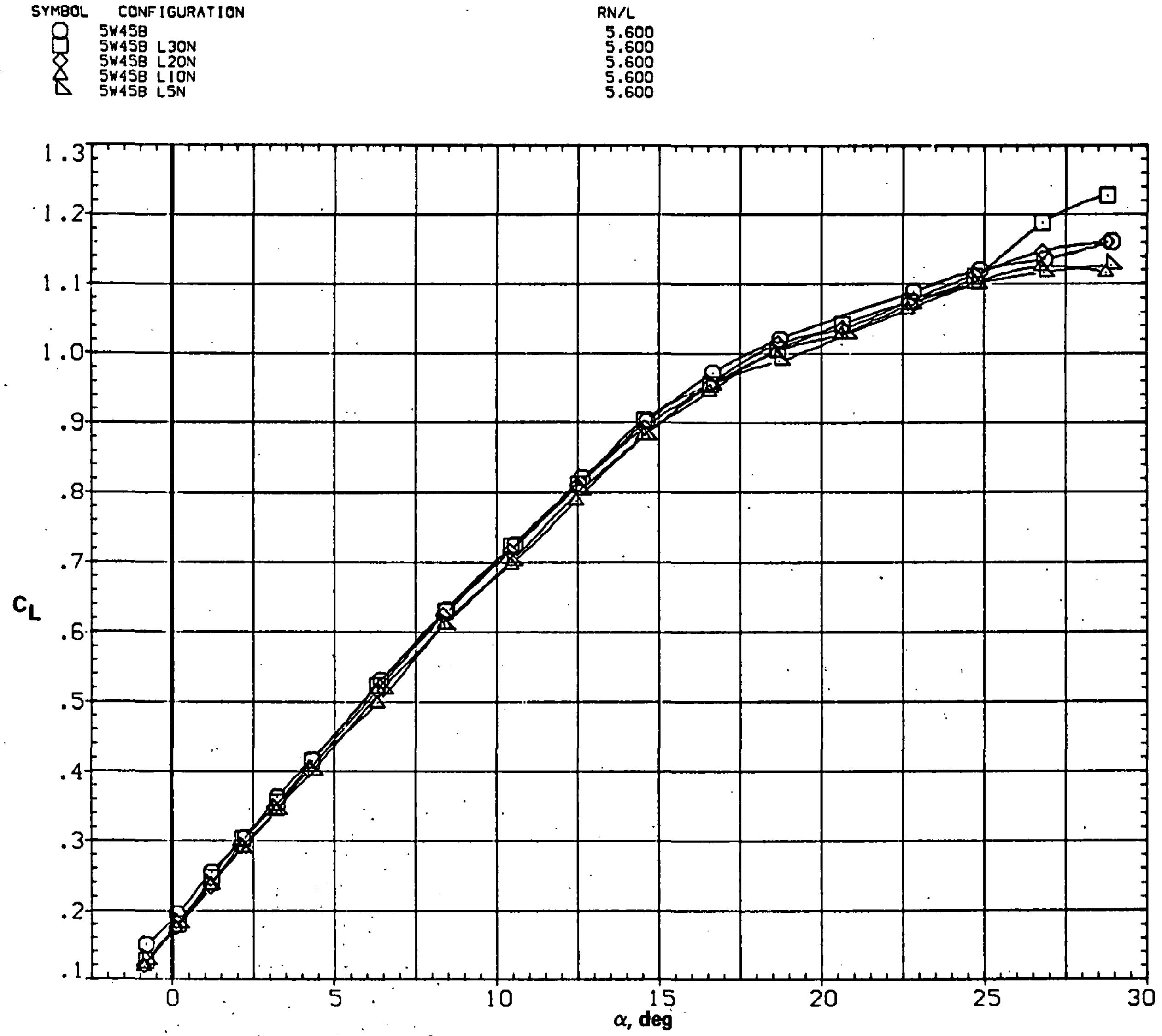

(a) C_L vs α

Figure 4.– Effect of drooped-nose flaps on the static longitudinal characteristics of the oblique wing: flaps on downstream wing panel only, $\Lambda = 45°$, $M = 0.25$.

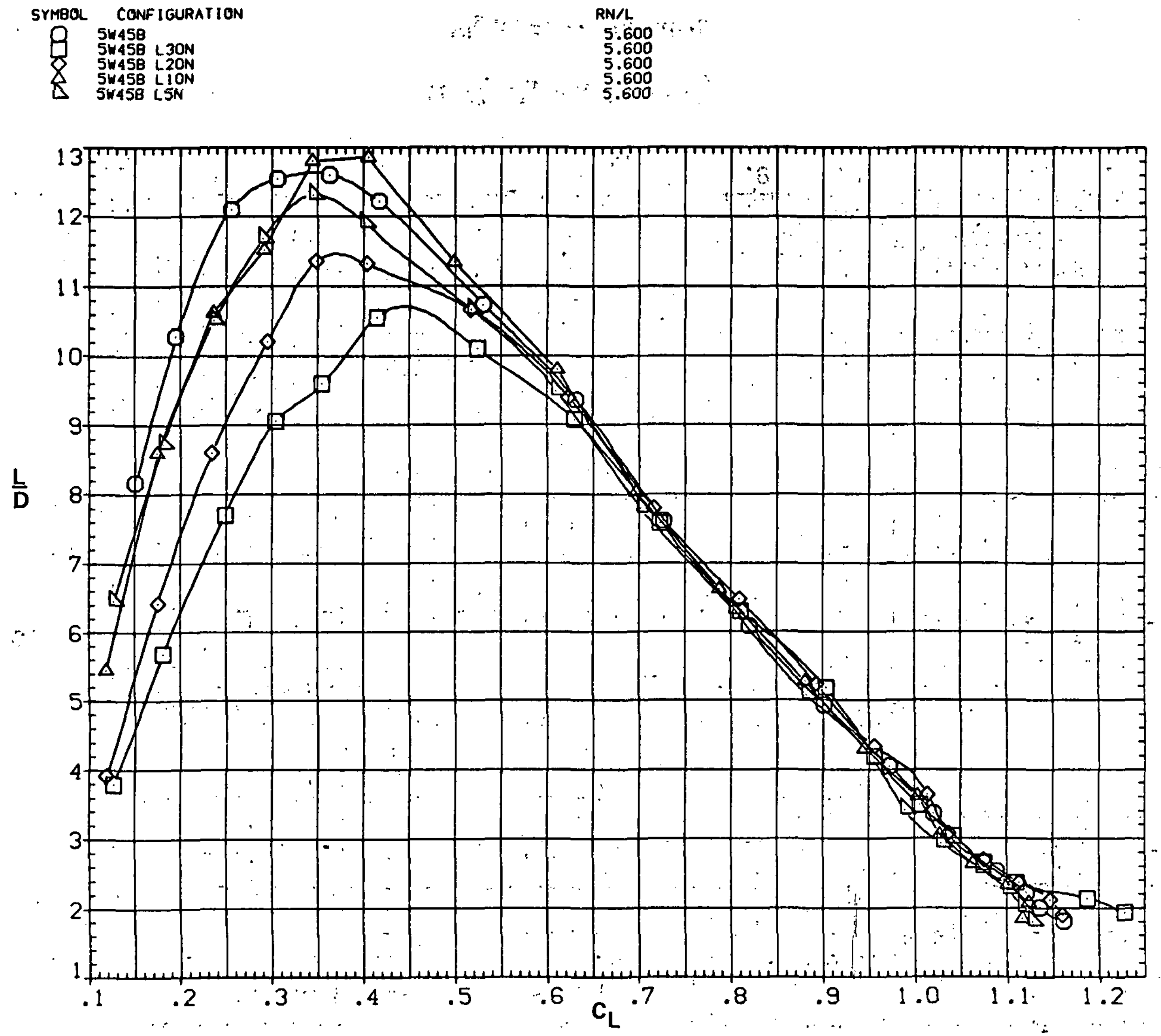

(d) L/D vs C_L

Figure 4.– Continued.

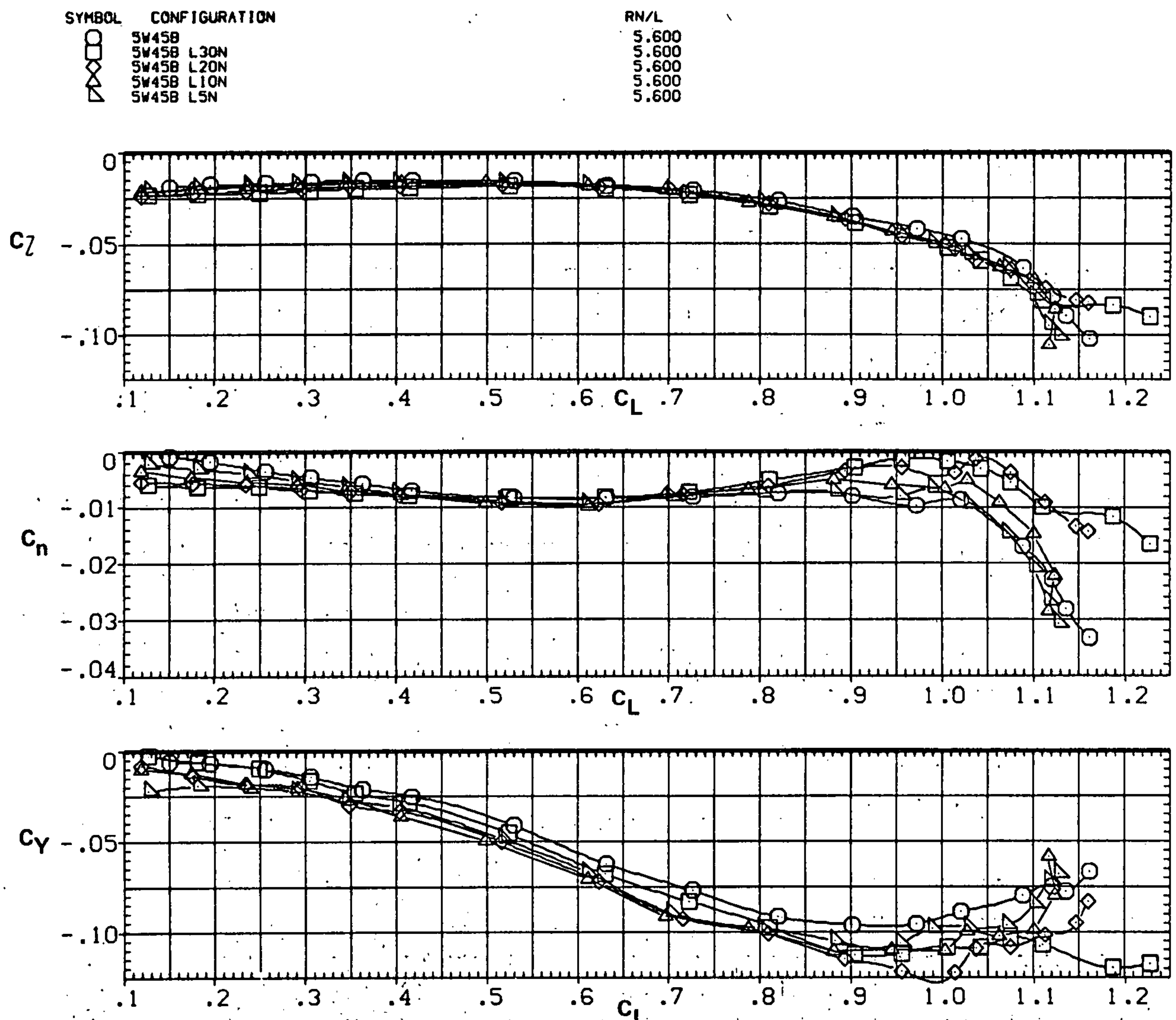

(e) C_l, C_n, and C_Y vs C_L

Figure 4.– Concluded.

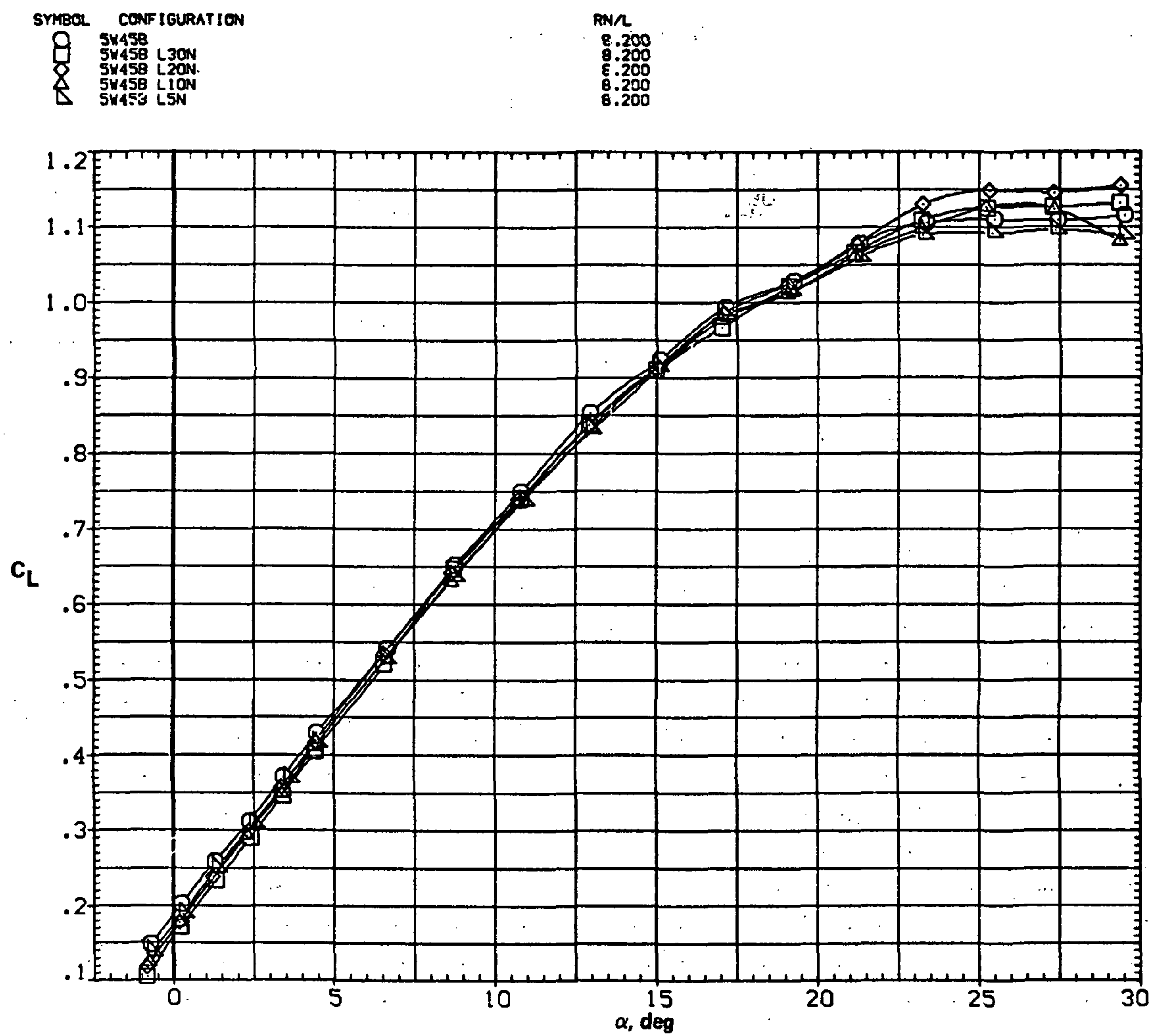

(a) C_L vs α

Figure 5.– Effect of drooped-nose flaps on the static longitudinal characteristics of the oblique wing: flaps on downstream wing panel only, $\Lambda = 45°$, $M = 0.4$.

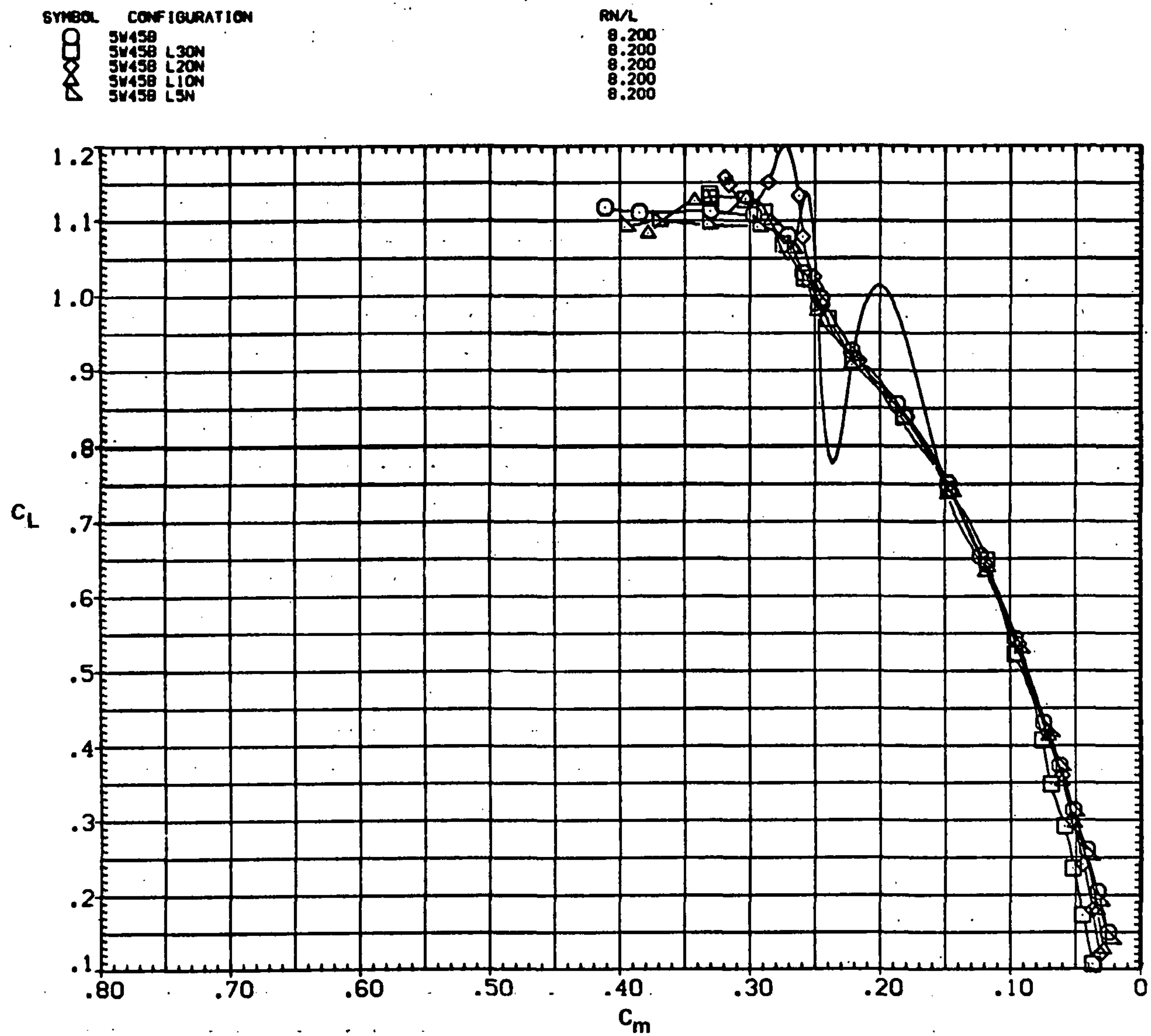

(b) C_L vs C_m

Figure 5.– Continued.

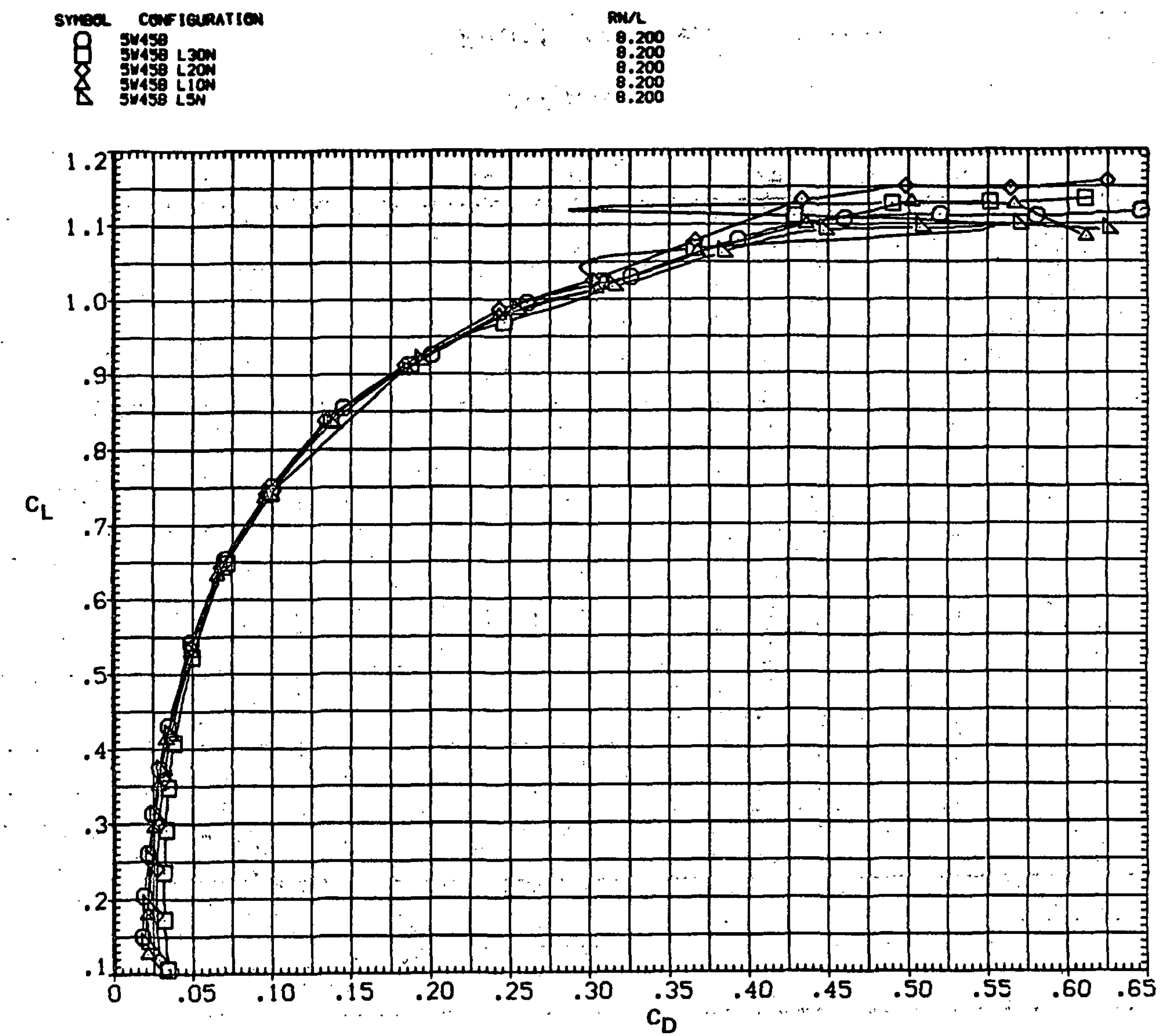

(c) C_L vs C_D

Figure 5.– Continued.

(d) L/D vs C_L

Figure 5.– Continued.

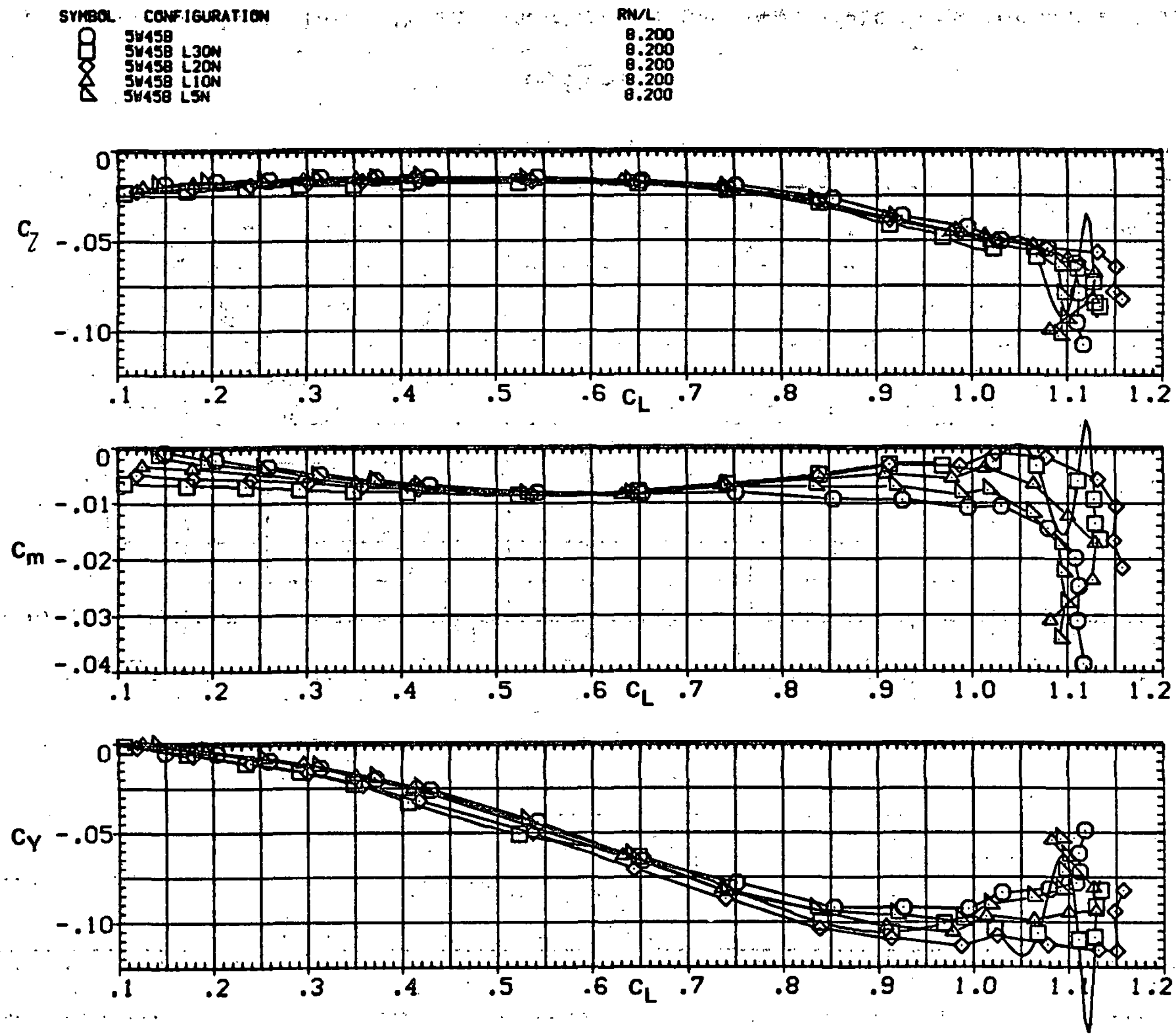

(e) C_l, C_n and C_Y vs. C_L

Figure 5.– Concluded.

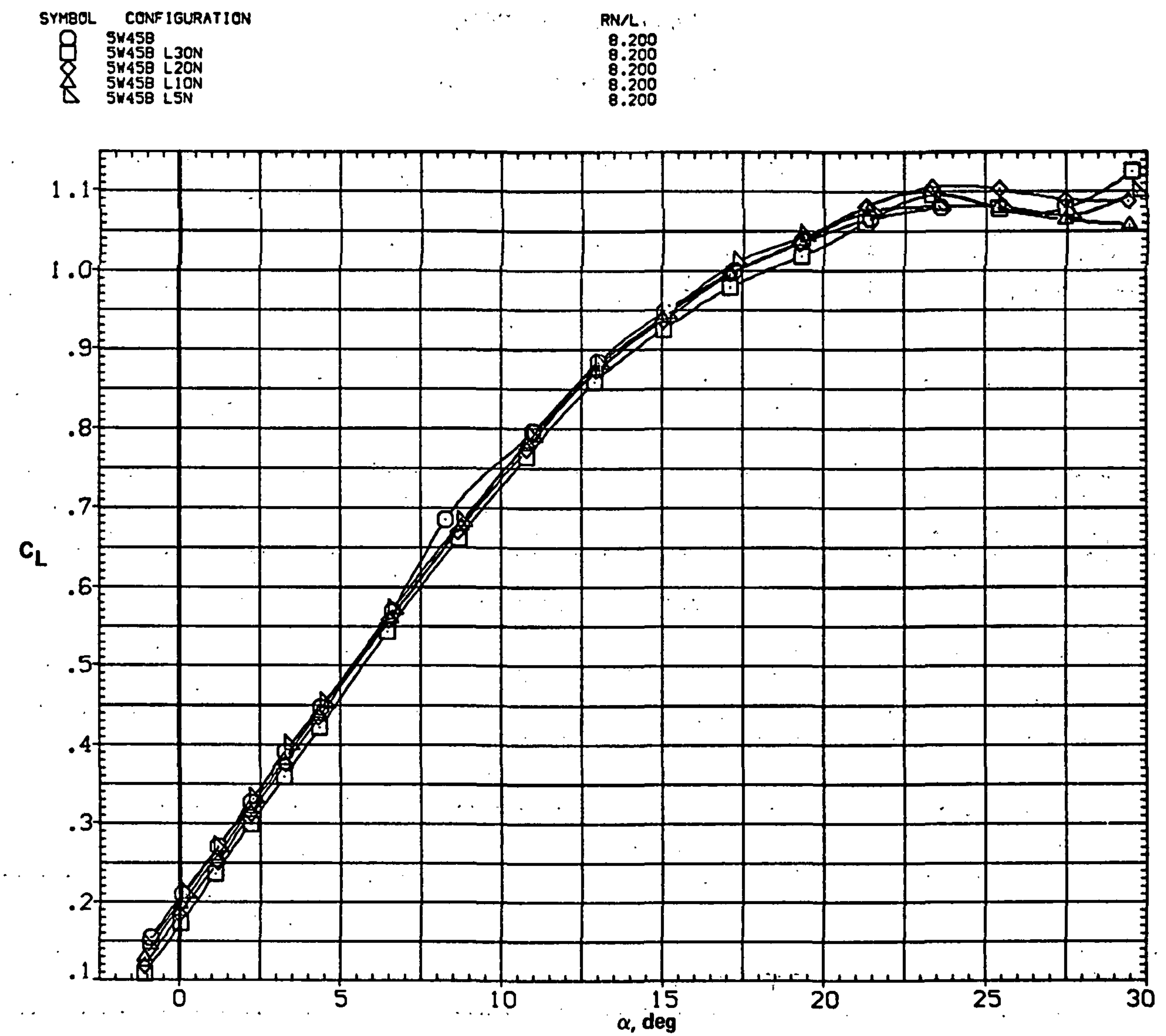

(a) C_L vs α

Figure 6.— Effect of drooped-nose flaps on the static longitudinal characteristics of the oblique wing: flaps on downstream wing panel only, $\Lambda = 45°$, $M = 0.6$.

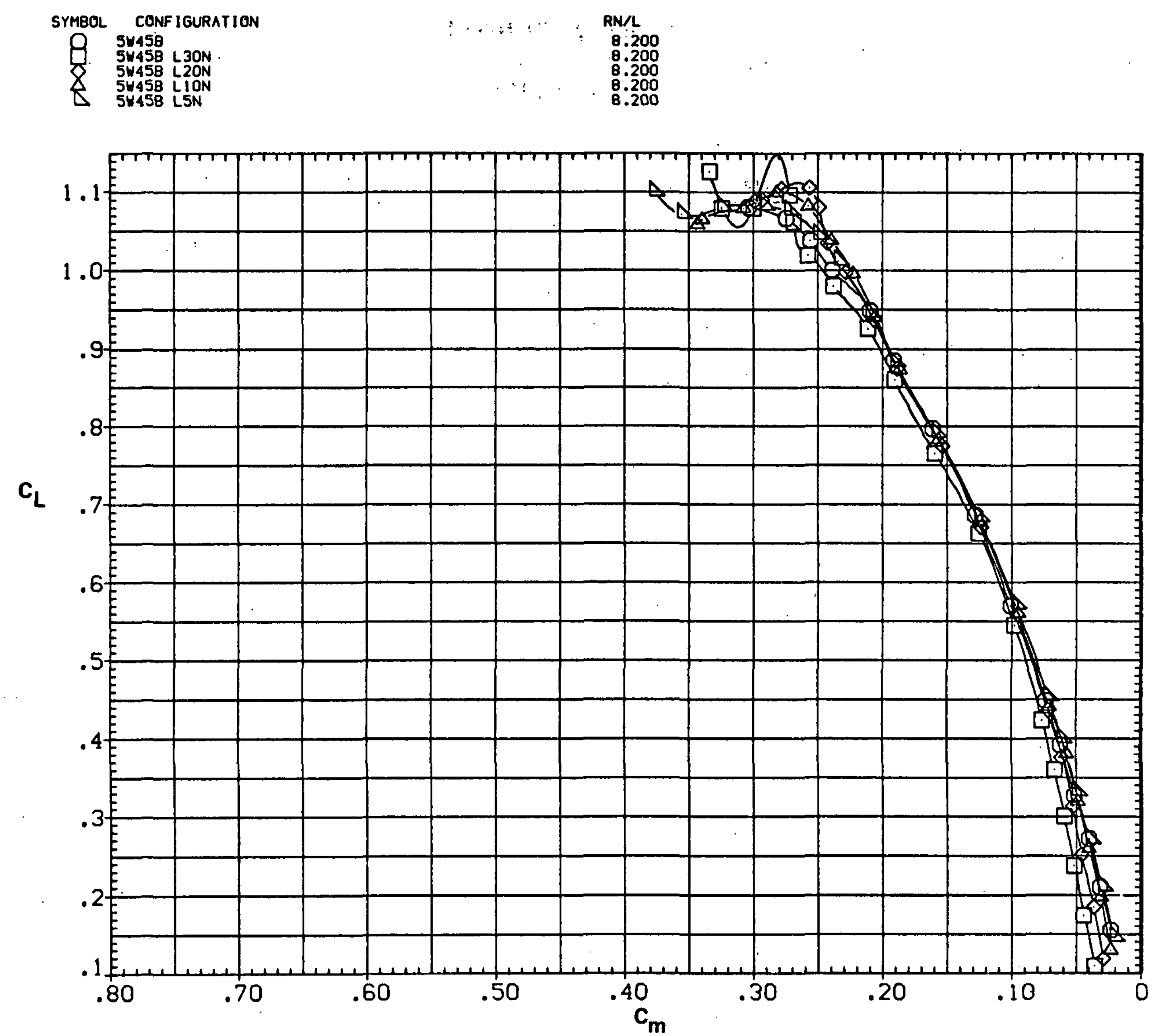

(b) C_L vs C_m

Figure 6.– Continued.

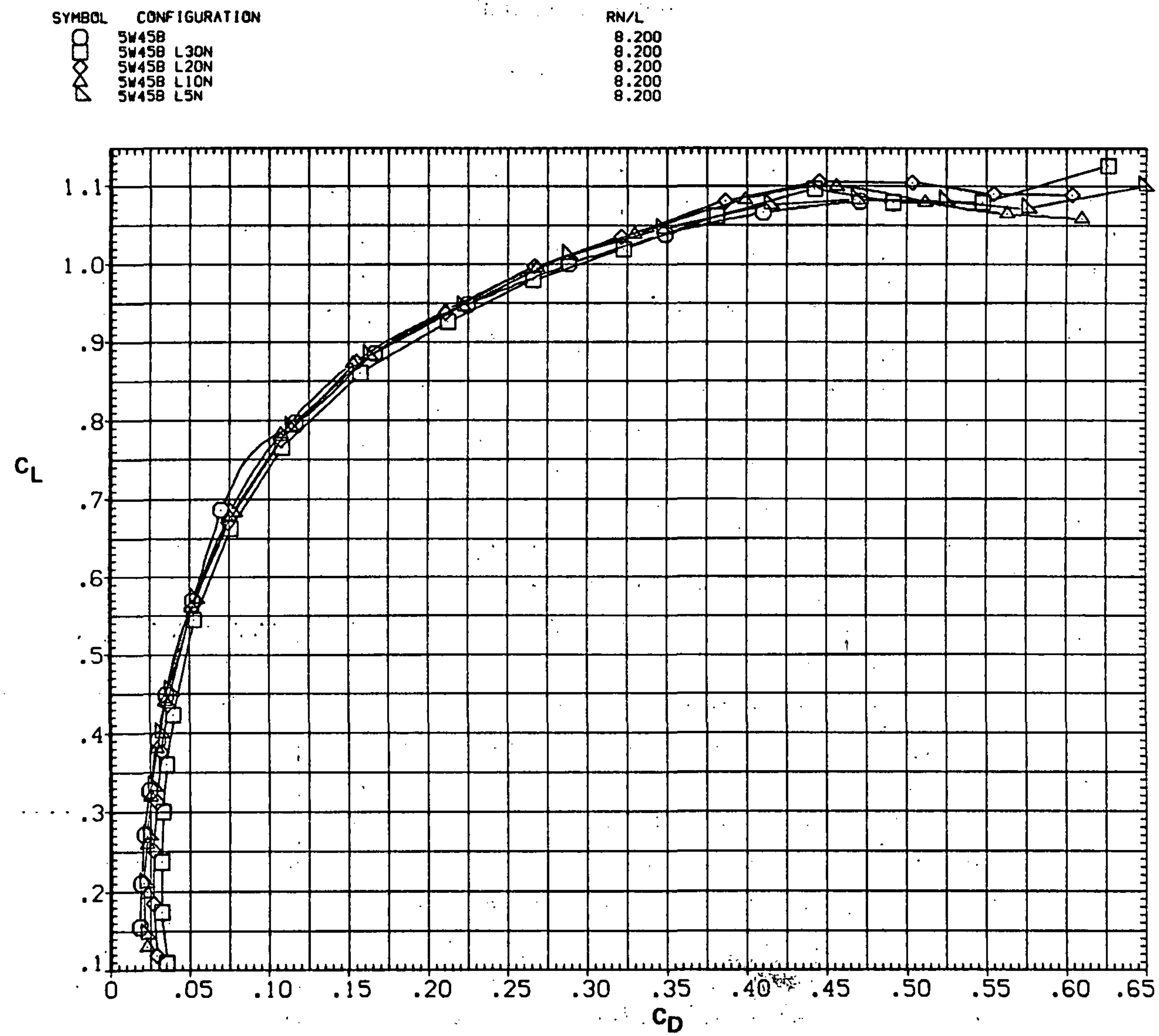

(c) C_L vs C_D

Figure 6.– Continued.

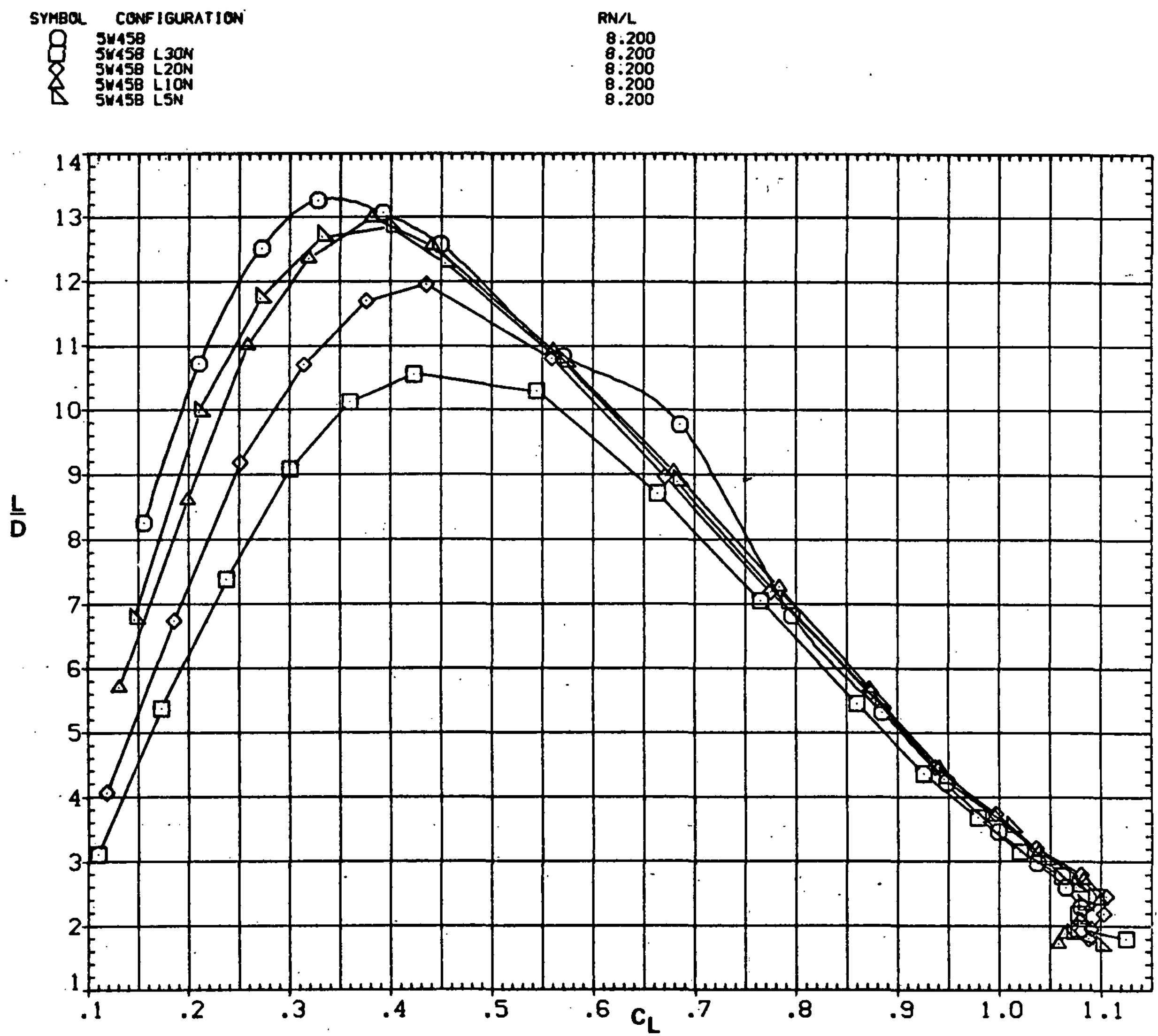

(d) L/D vs C_L

Figure 6.– Continued.

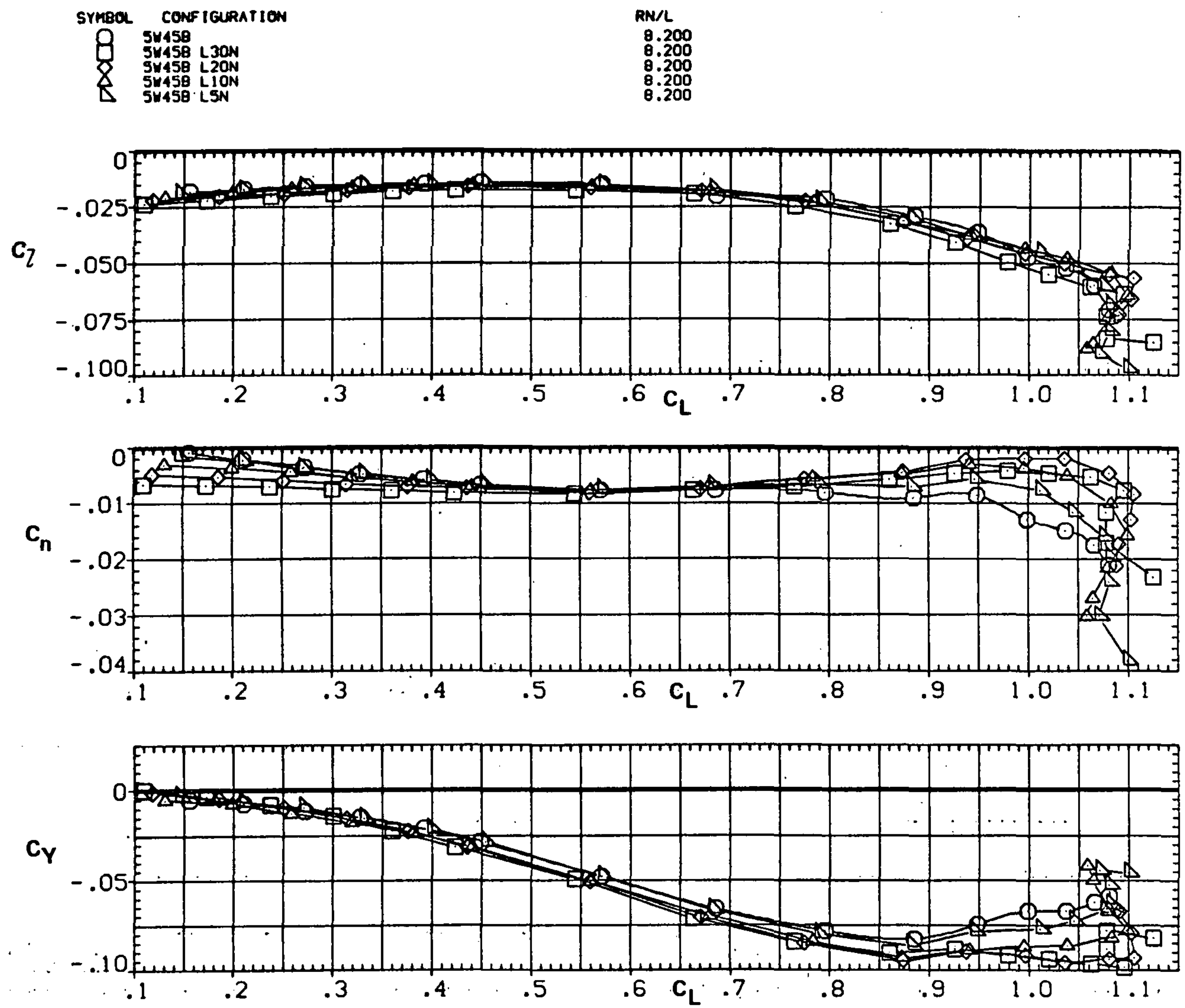

(e) C_l, C_n, and C_Y vs C_L

Figure 6.– Concluded.

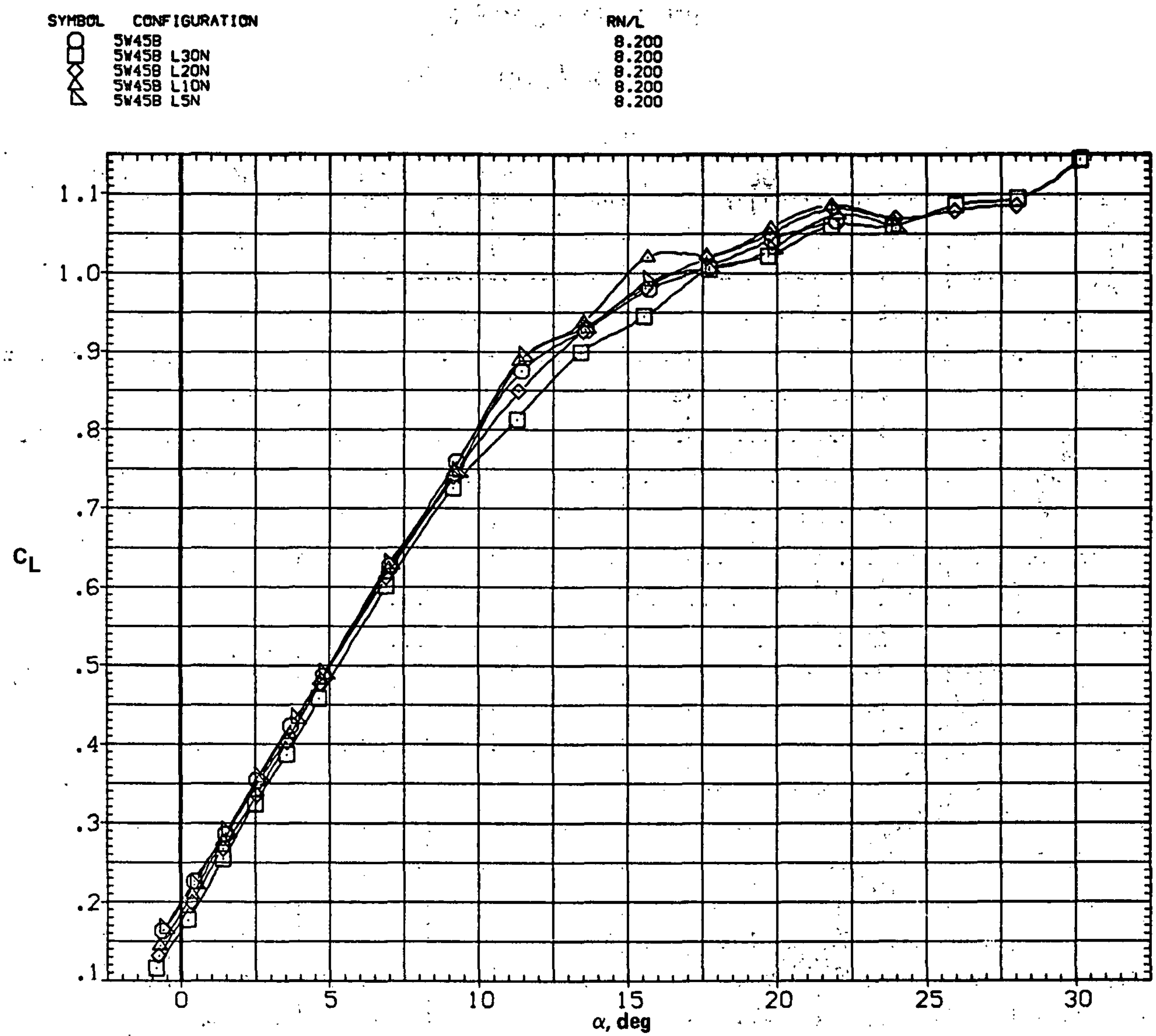

(a) C_L vs α

Figure 7.– Effect of drooped-nose flaps on the static longitudinal characteristics of the oblique wing: flaps on downstream wing panel only, $\Lambda = 45°$, $M = 0.8$.

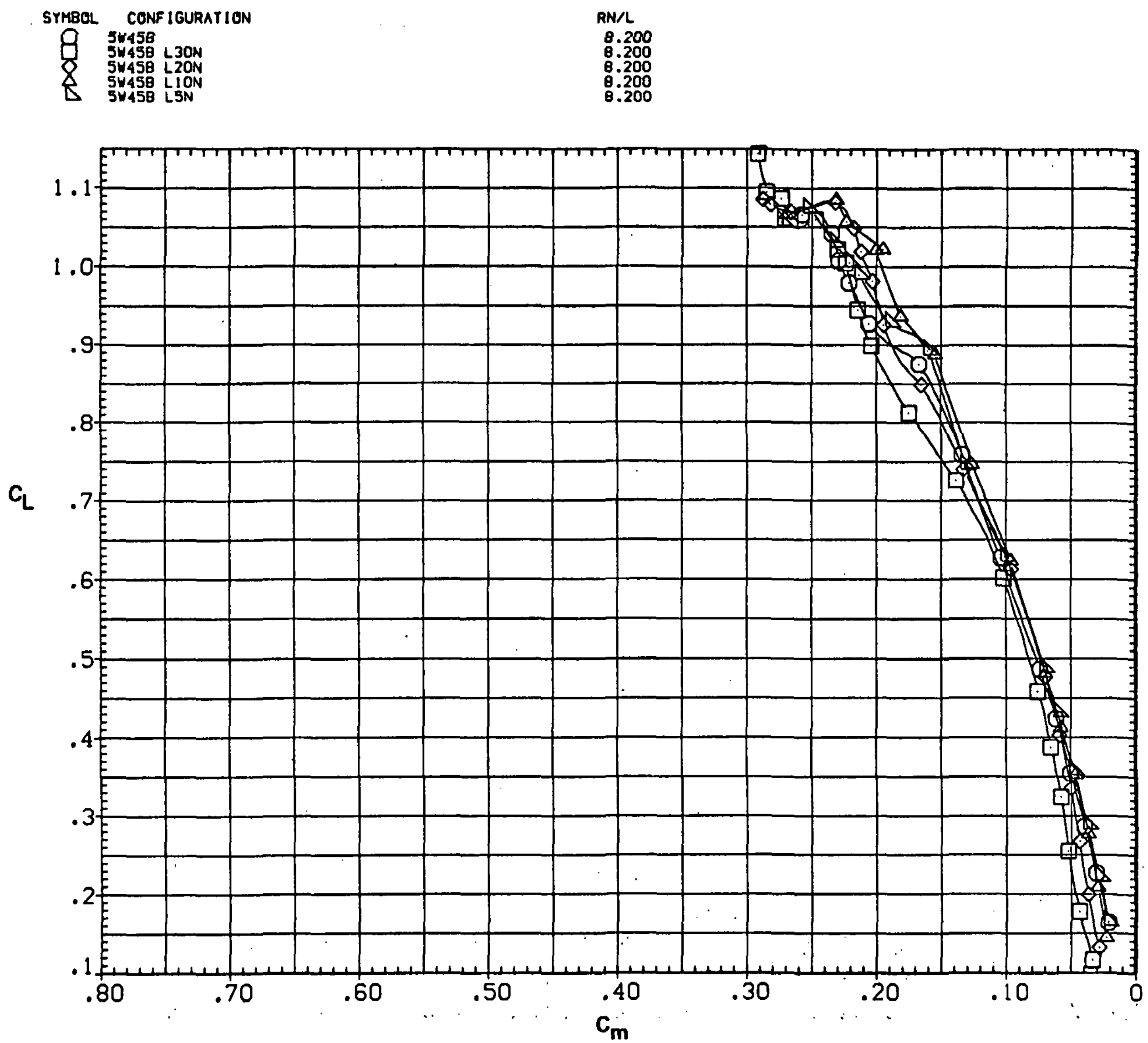

(b) C_L vs C_m

Figure 7.– Continued.

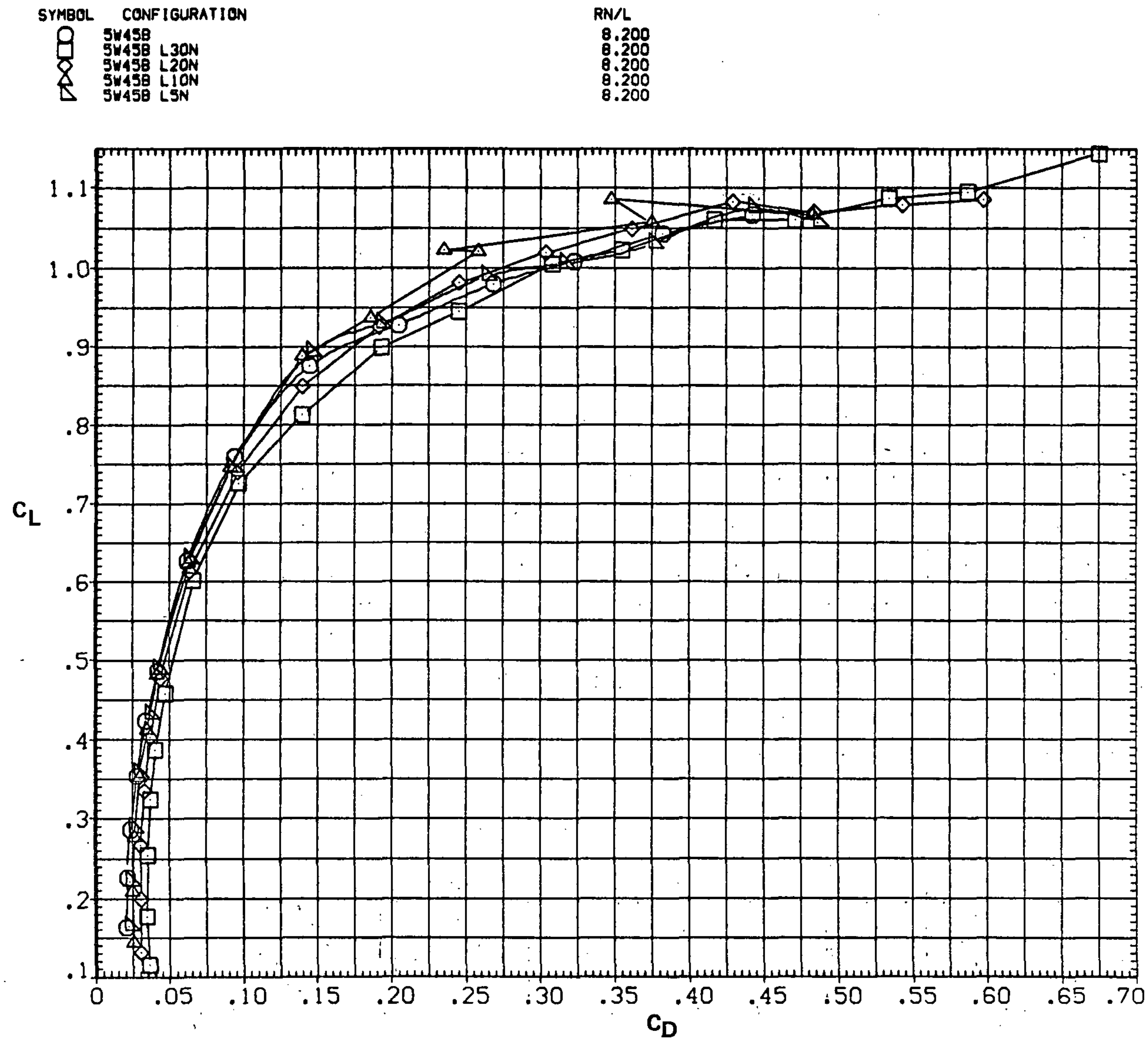

(c) C_L vs C_D

Figure 7.– Continued.

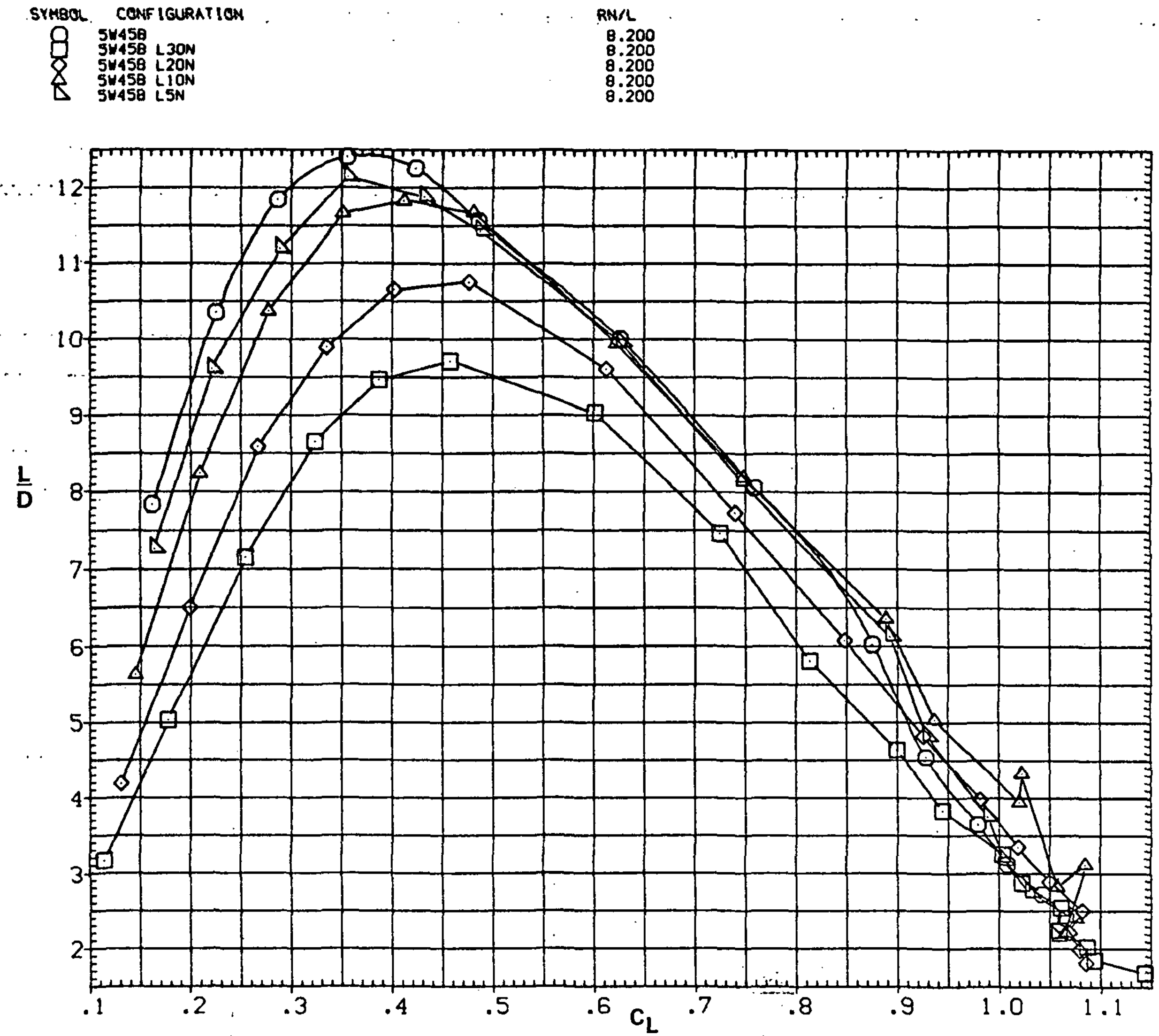

(d) L/D vs C_L

Figure 7.– Continued.

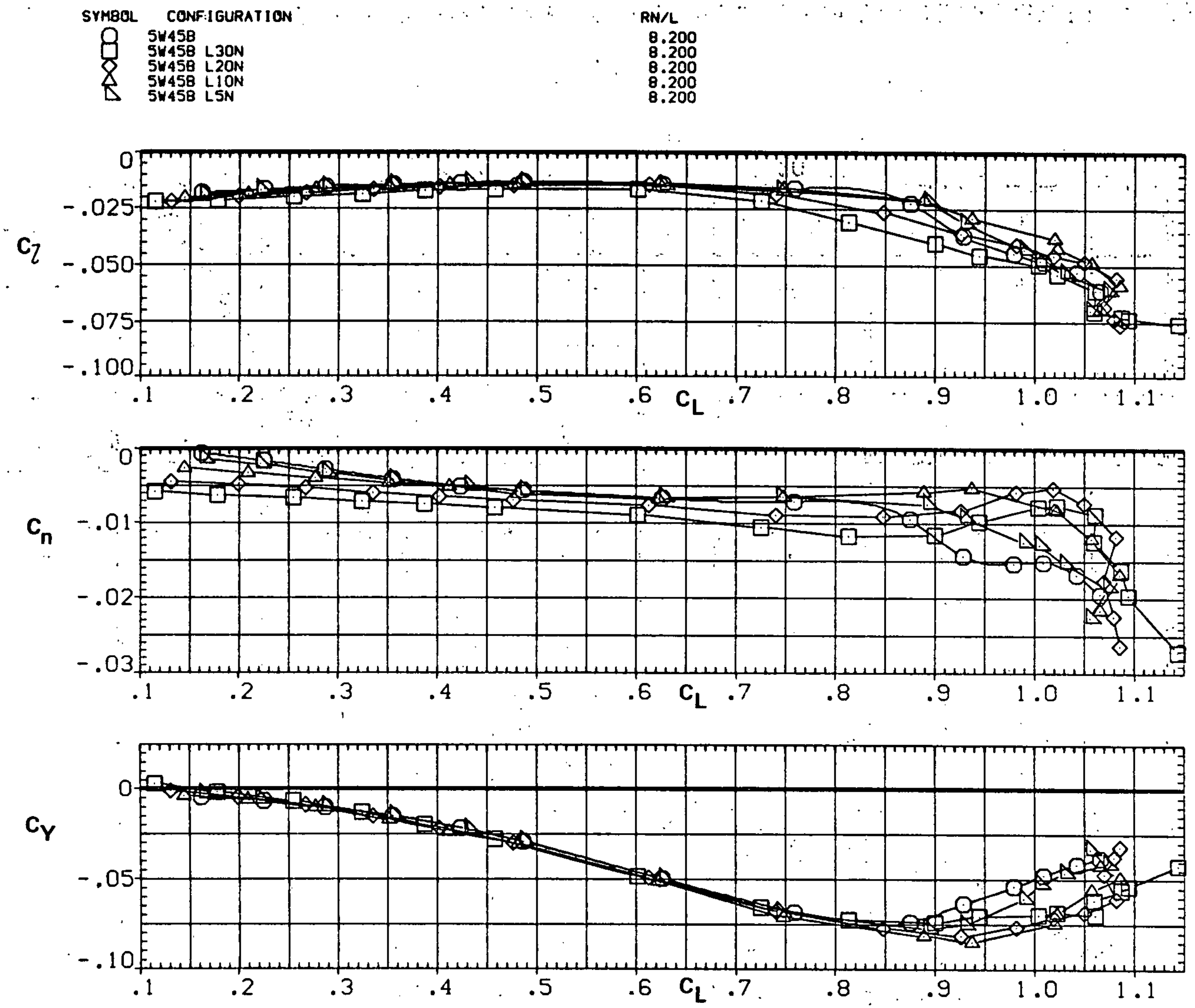

(e) C_l, C_n, and C_Y vs C_L

Figure 7.– Concluded.

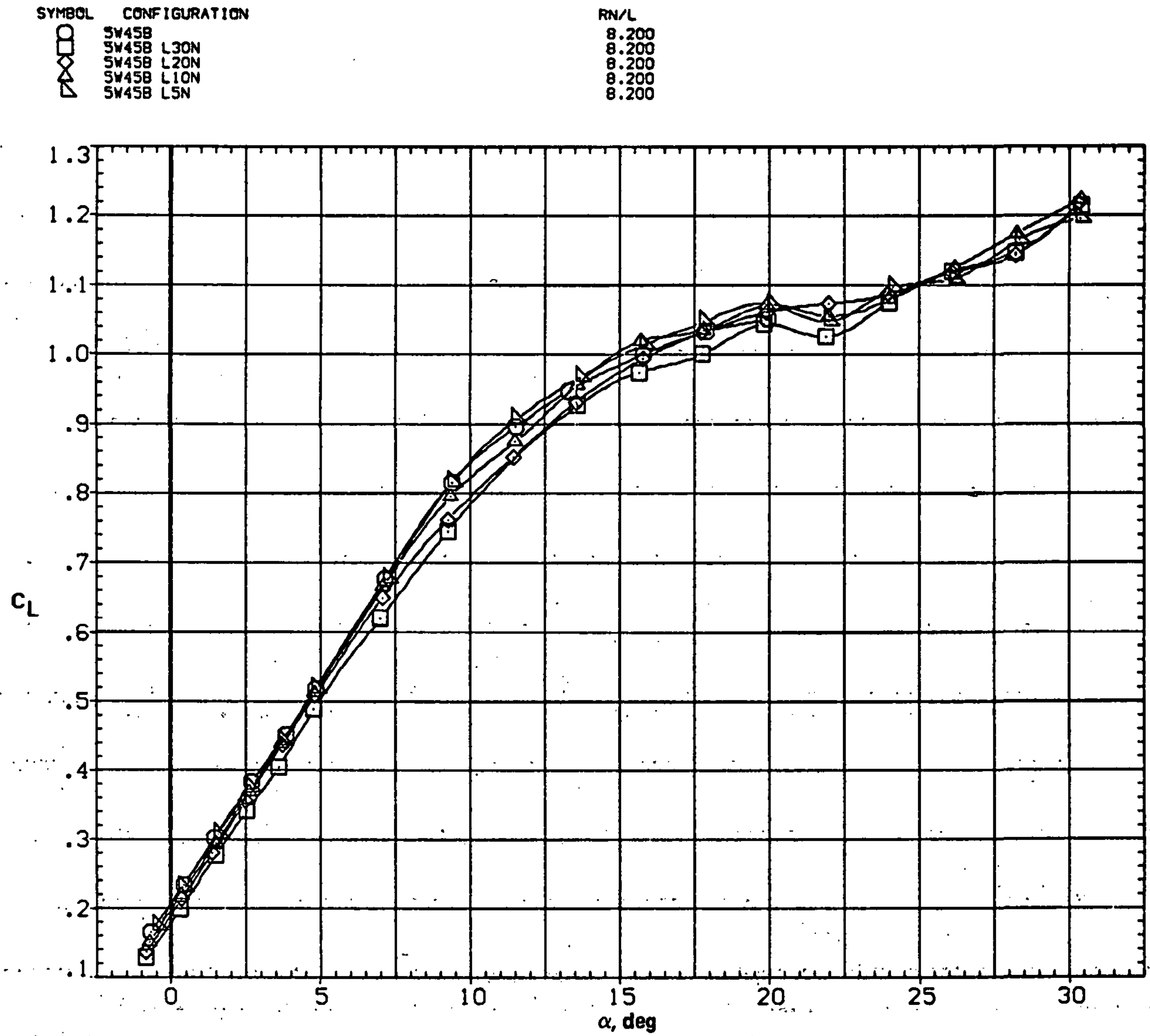

(a) C_L vs α

Figure 8.– Effect of drooped-nose flaps on the static longitudinal characteristics of the oblique wing: flaps on downstream wing panel only, $\Lambda = 45°$, $M = 0.9$.

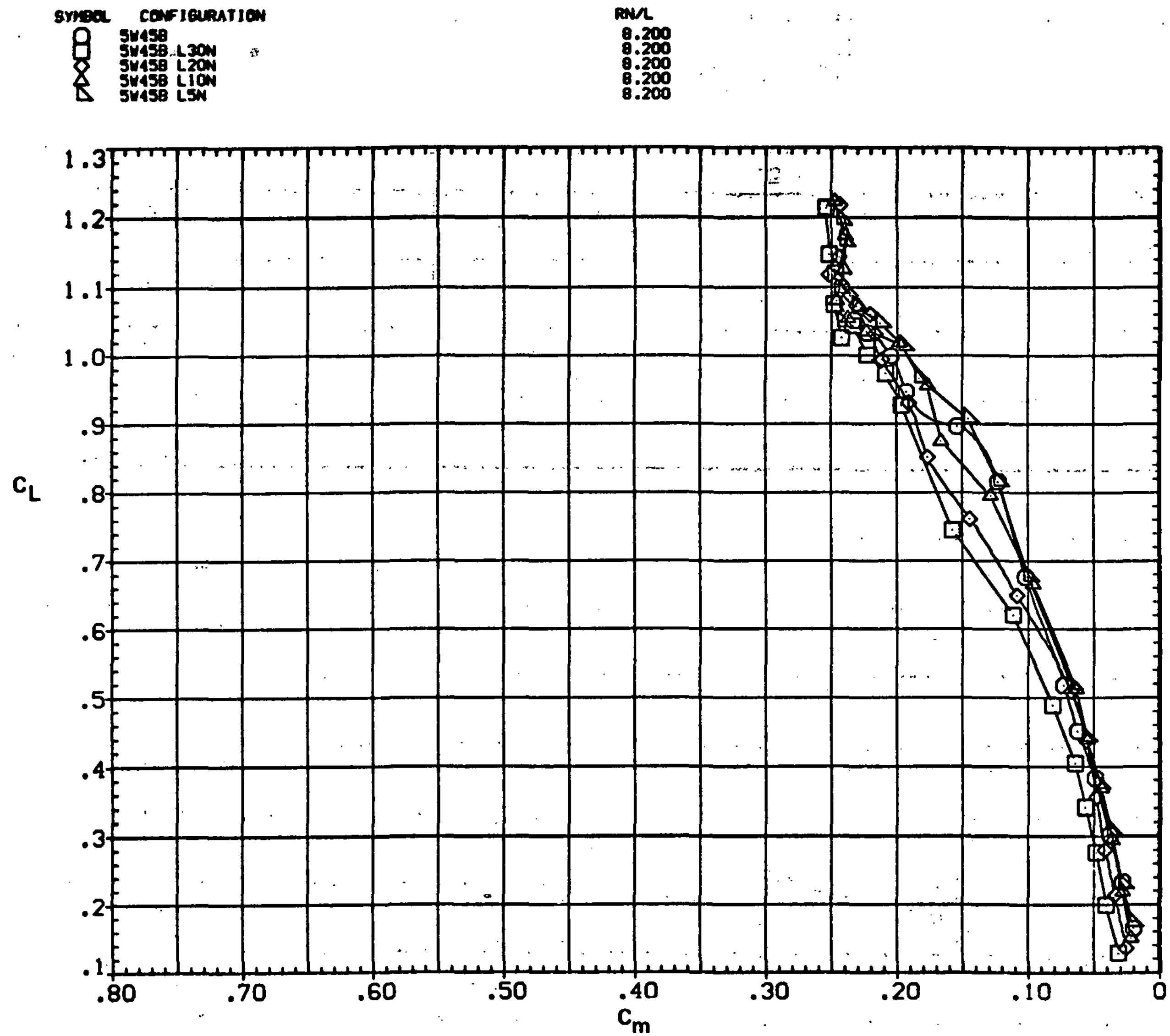

(b) C_L vs C_m

Figure 8.– Continued.

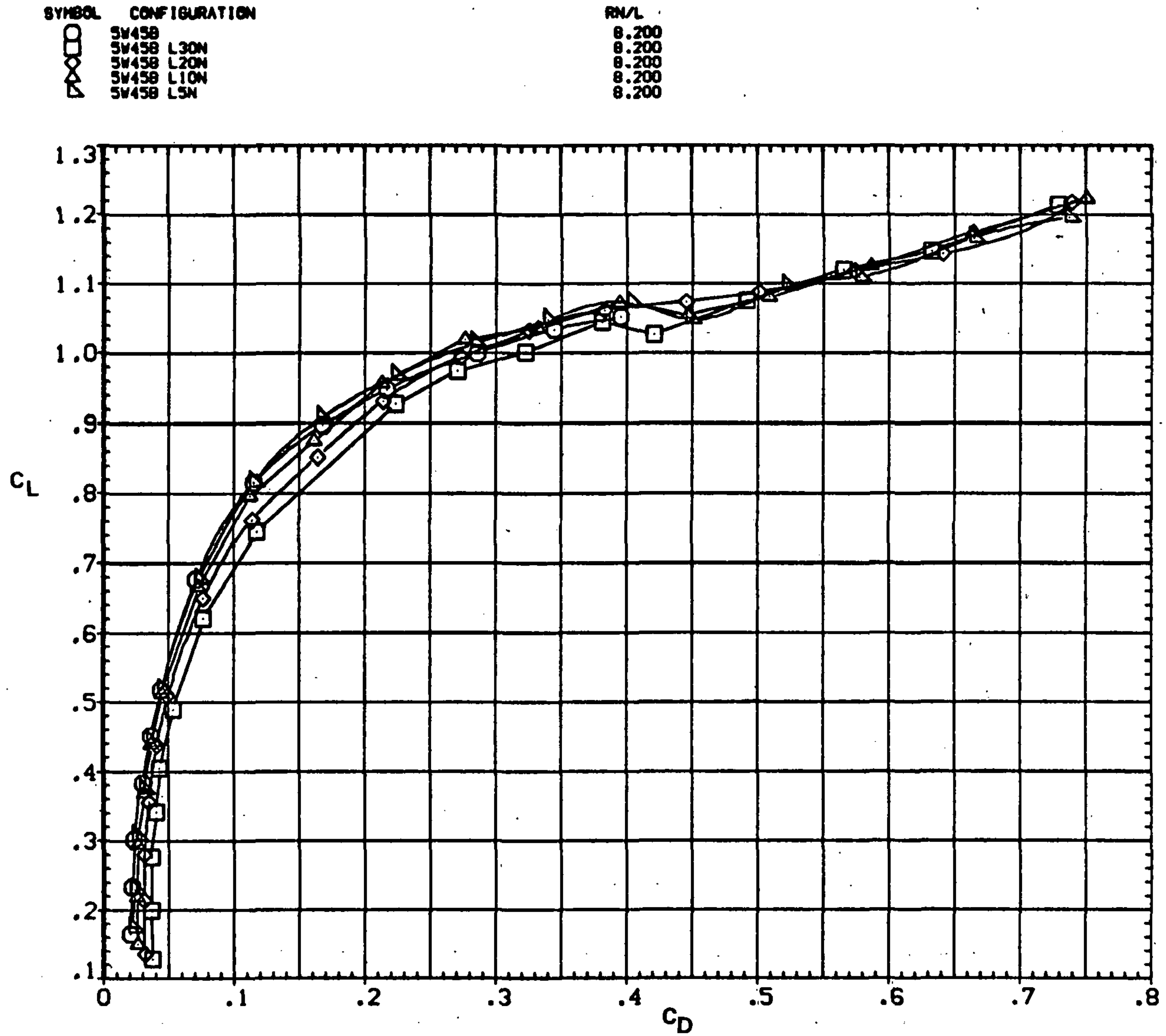

(c) C_L vs C_D

Figure 8.– Continued.

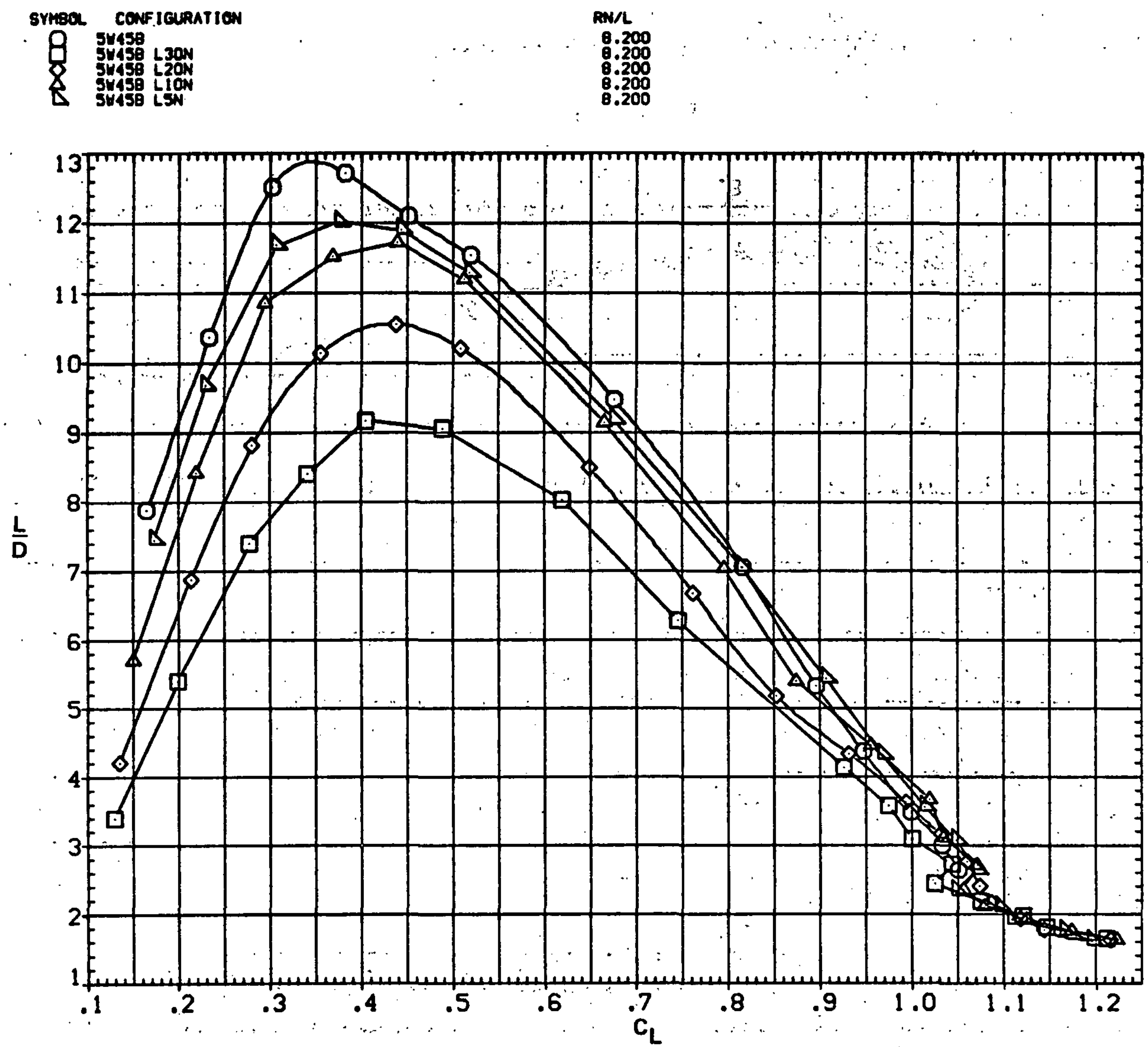

(d) L/D vs C_L

Figure 8.– Continued.

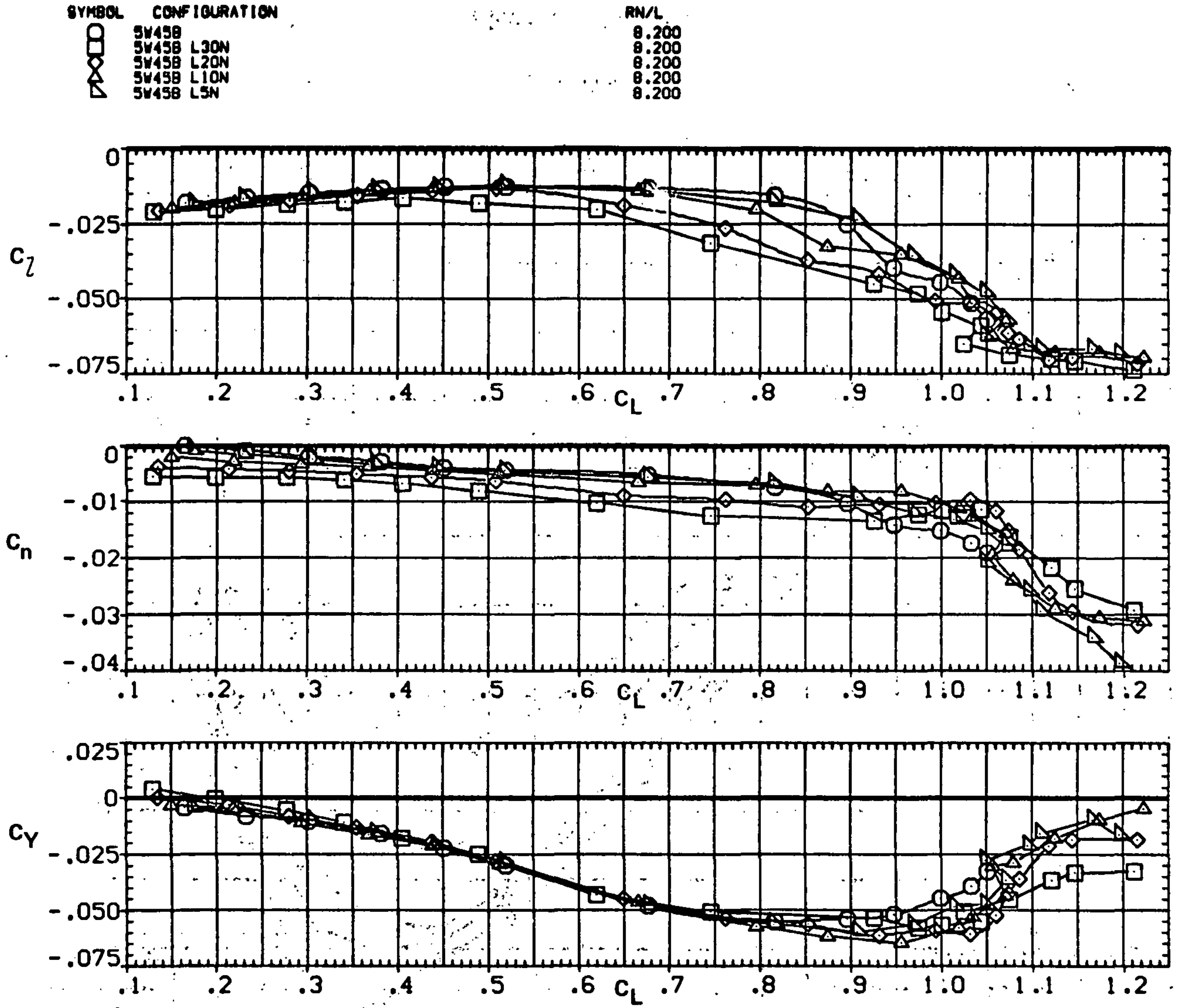

(e) C_l, C_n, and C_Y vs C_L

Figure 8.– Concluded.

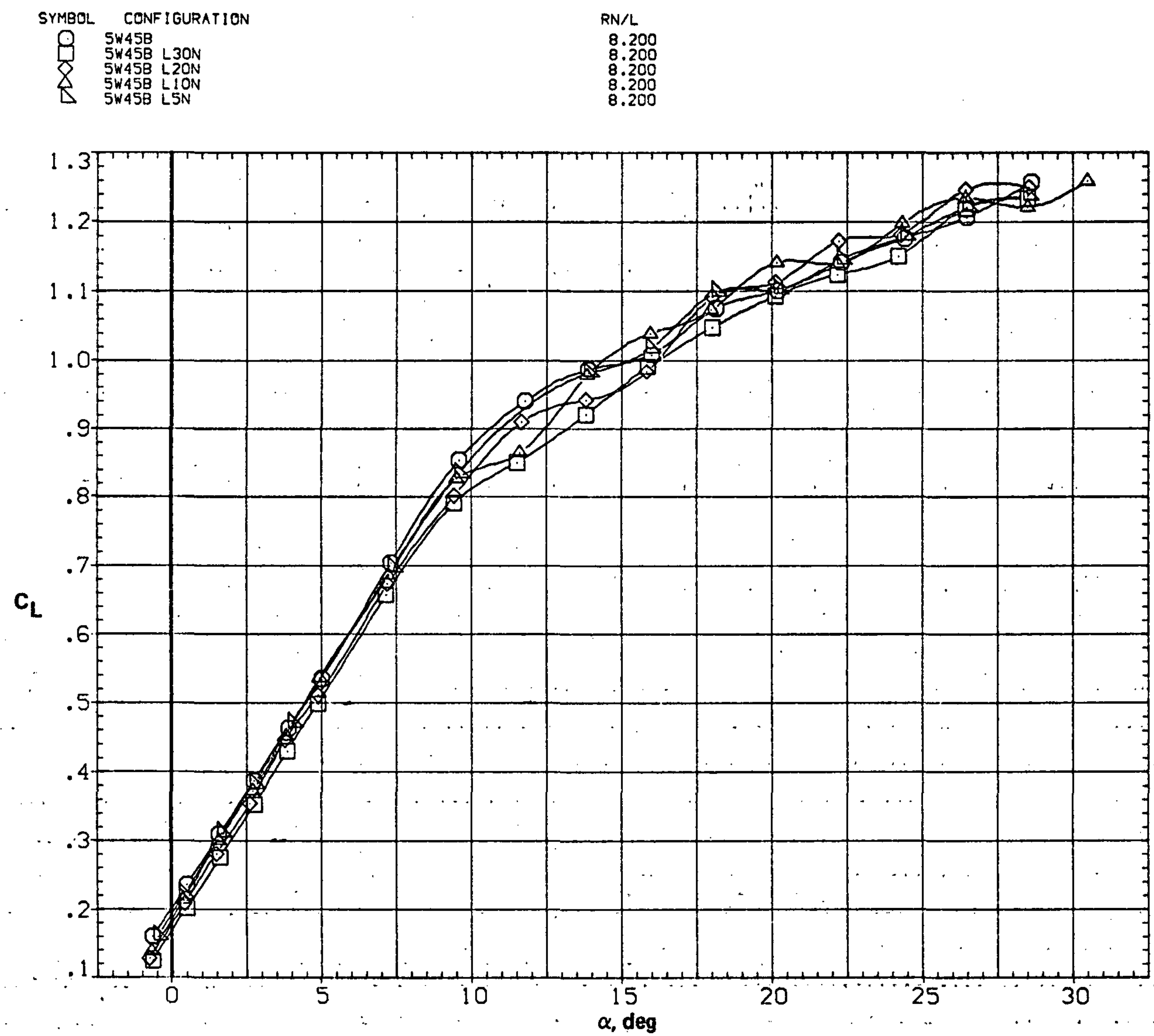

(a) C_L vs. α

Figure 9.– Effect of drooped-nose flaps on the static longitudinal characteristics of the oblique wing: flaps on downstream wing panel only, $\Lambda = 45°$, $M = 0.95$.

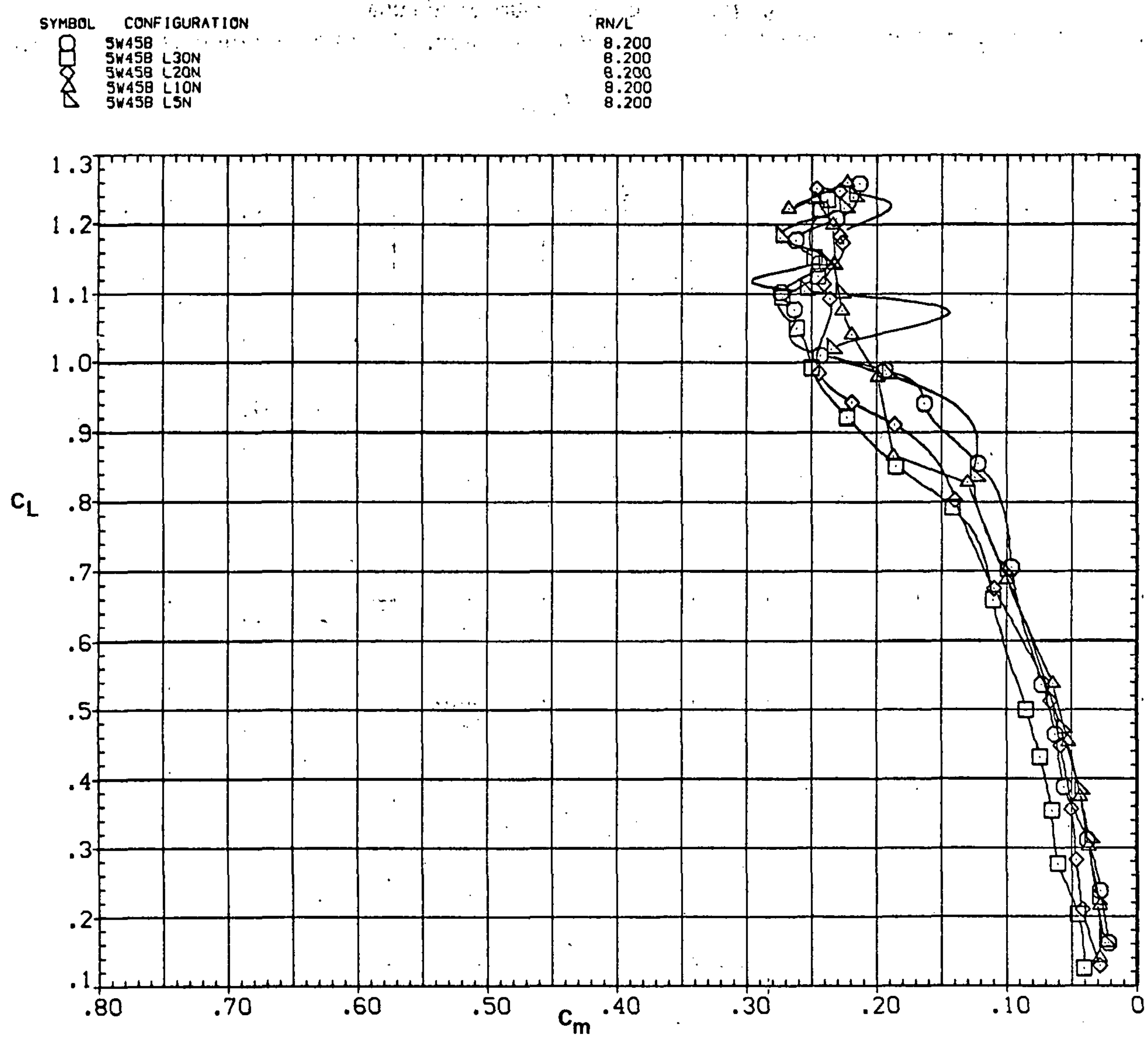

(b) C_L vs C_m

Figure 9.— Continued.

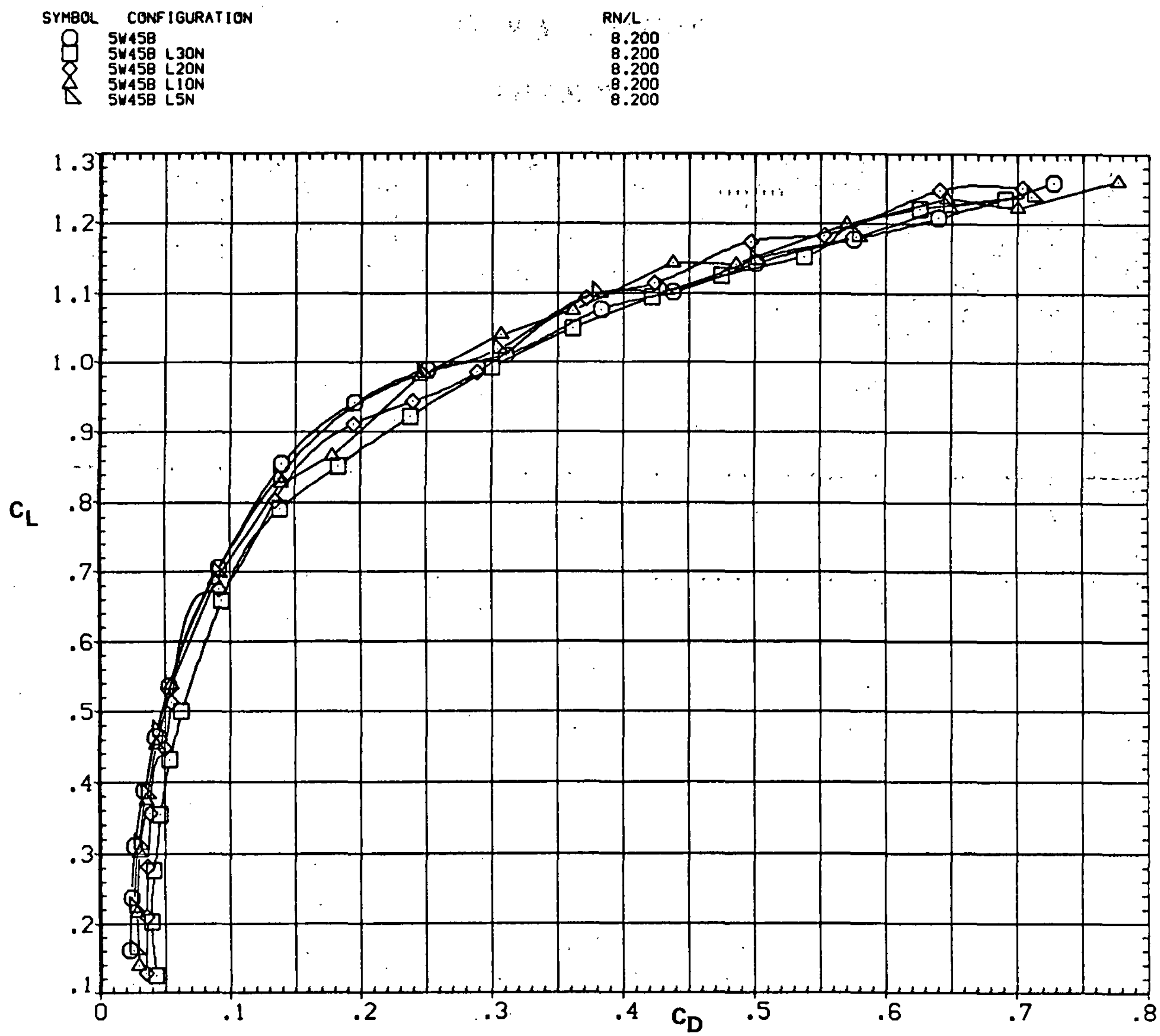

(c) C_L vs C_D

Figure 9.– Continued.

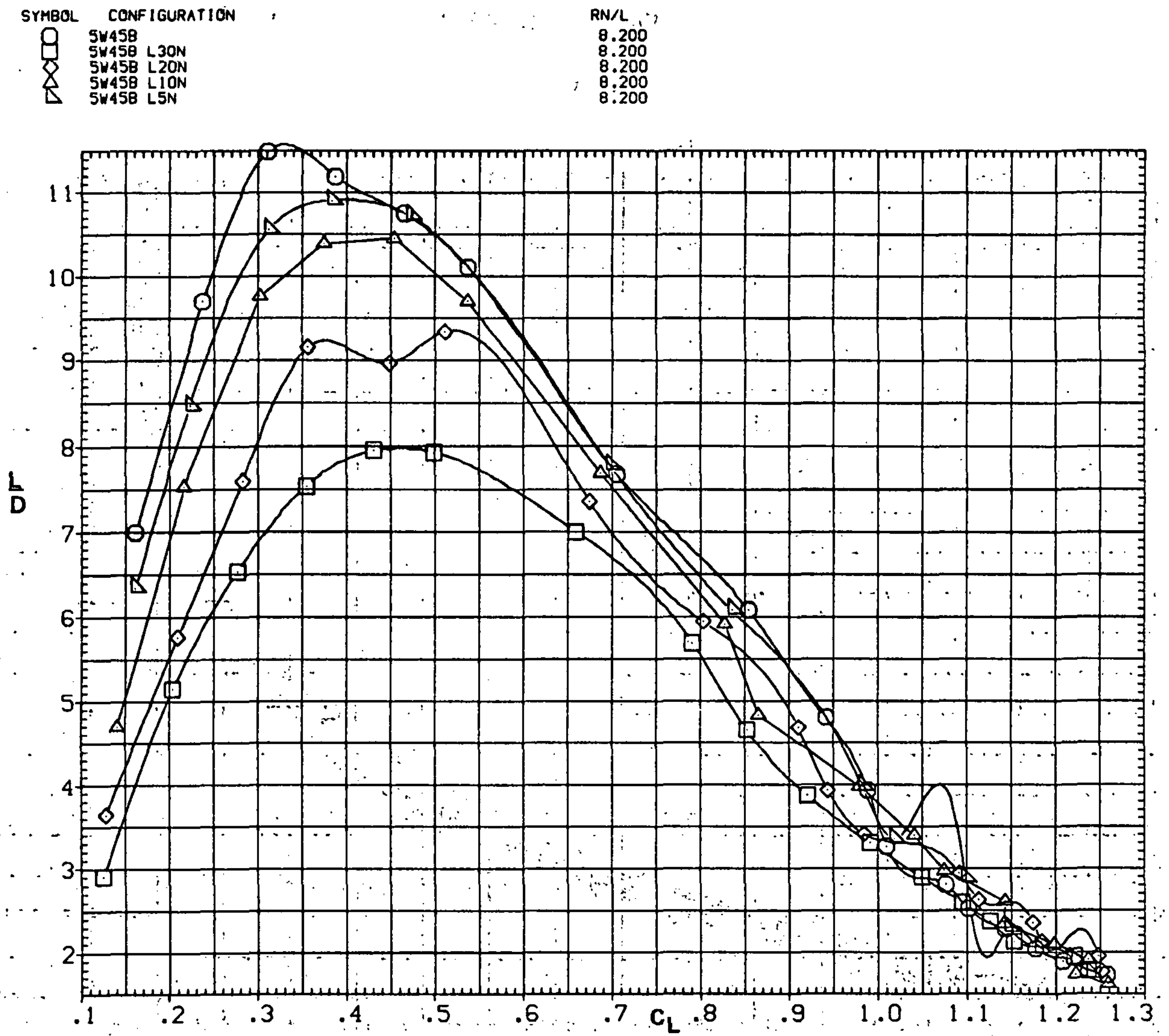

(d) L/D vs C_L

Figure 9.– Continued.

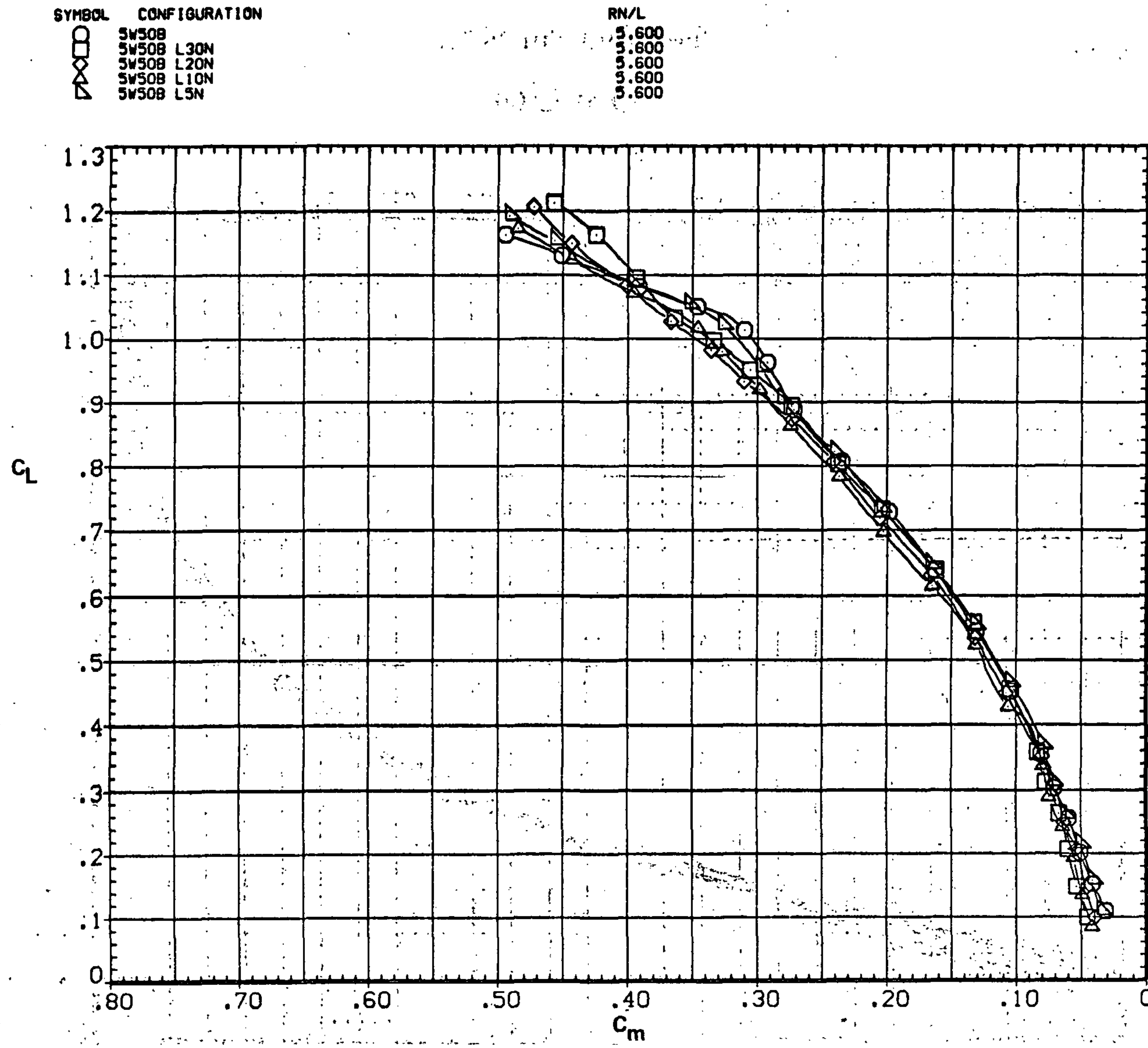

(b) C_L vs C_m

Figure 10.– Continued.

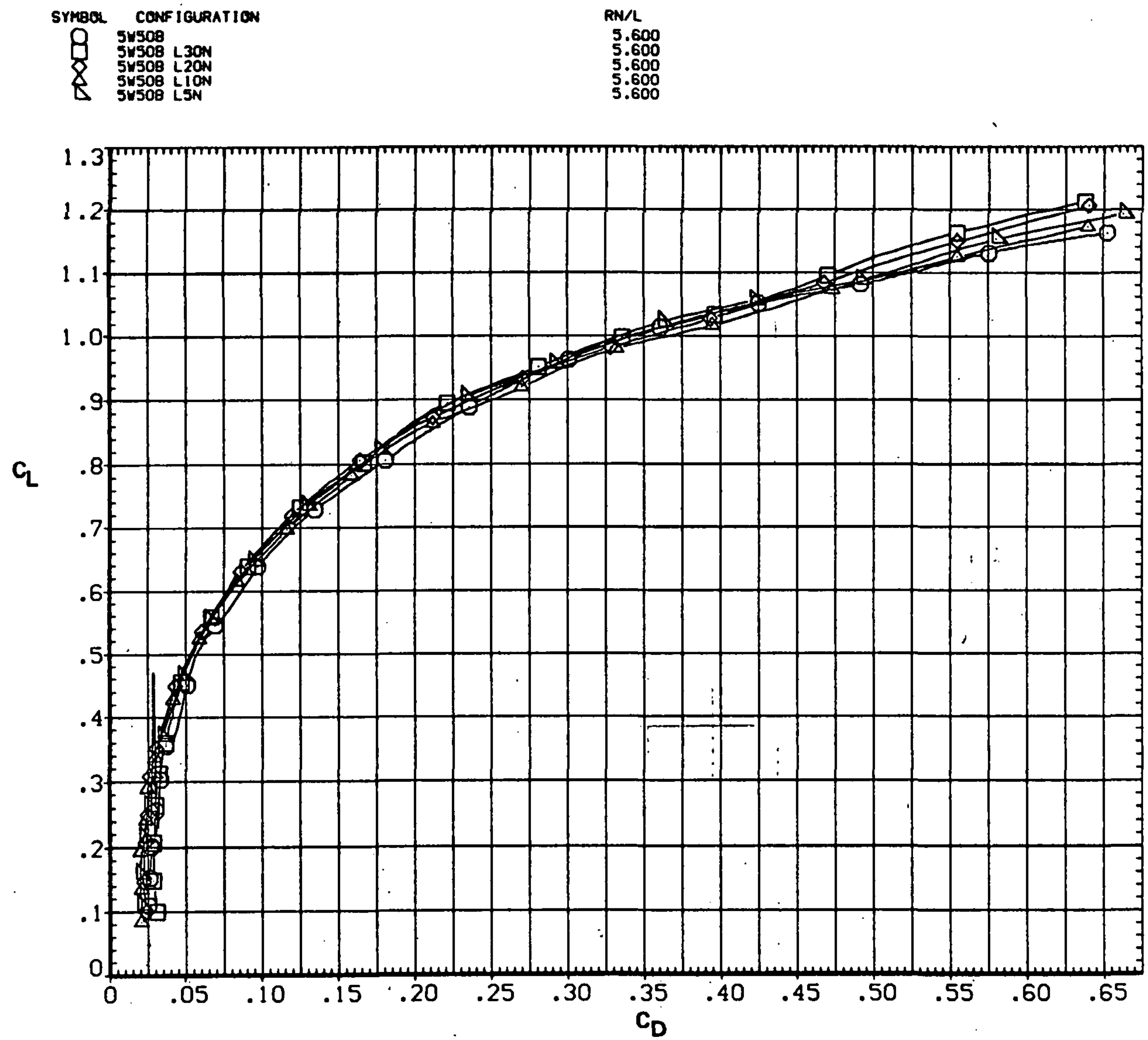

(c) C_L vs C_D

Figure 10.– Continued.

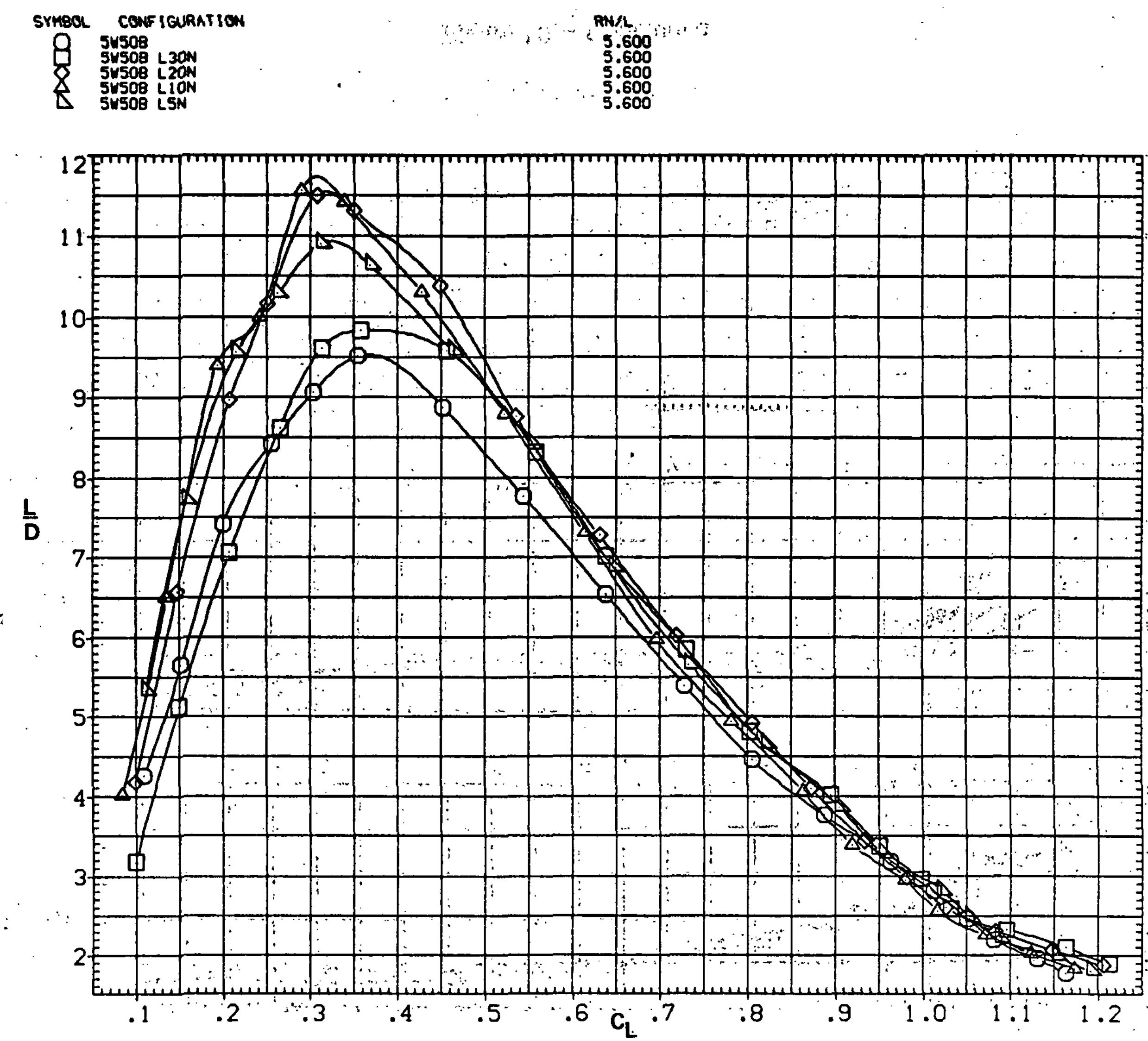

(d) L/D vs C_L

Figure 10.– Continued.

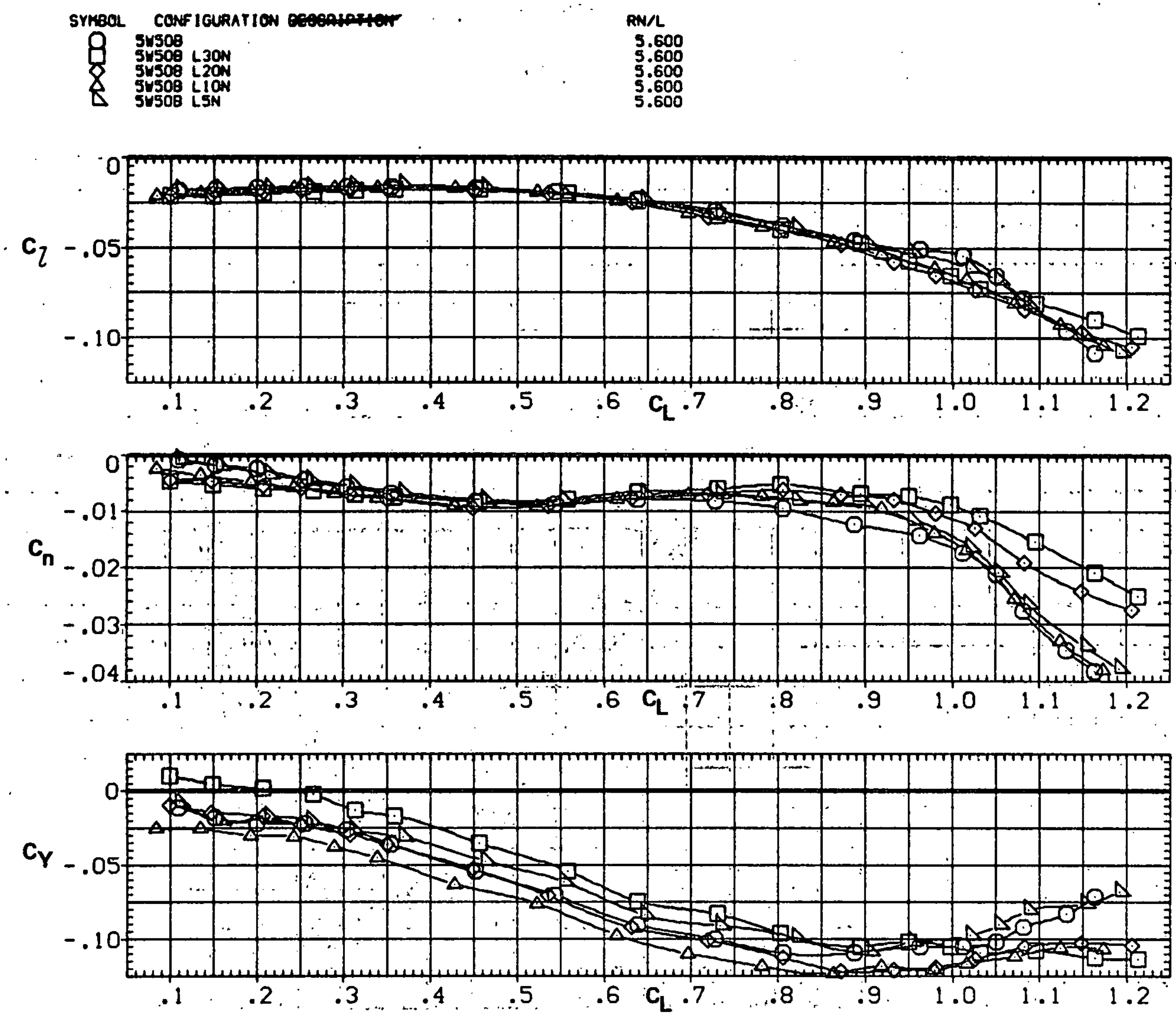

(e) C_l, C_n, and C_Y vs. C_L

Figure 10.– Concluded.

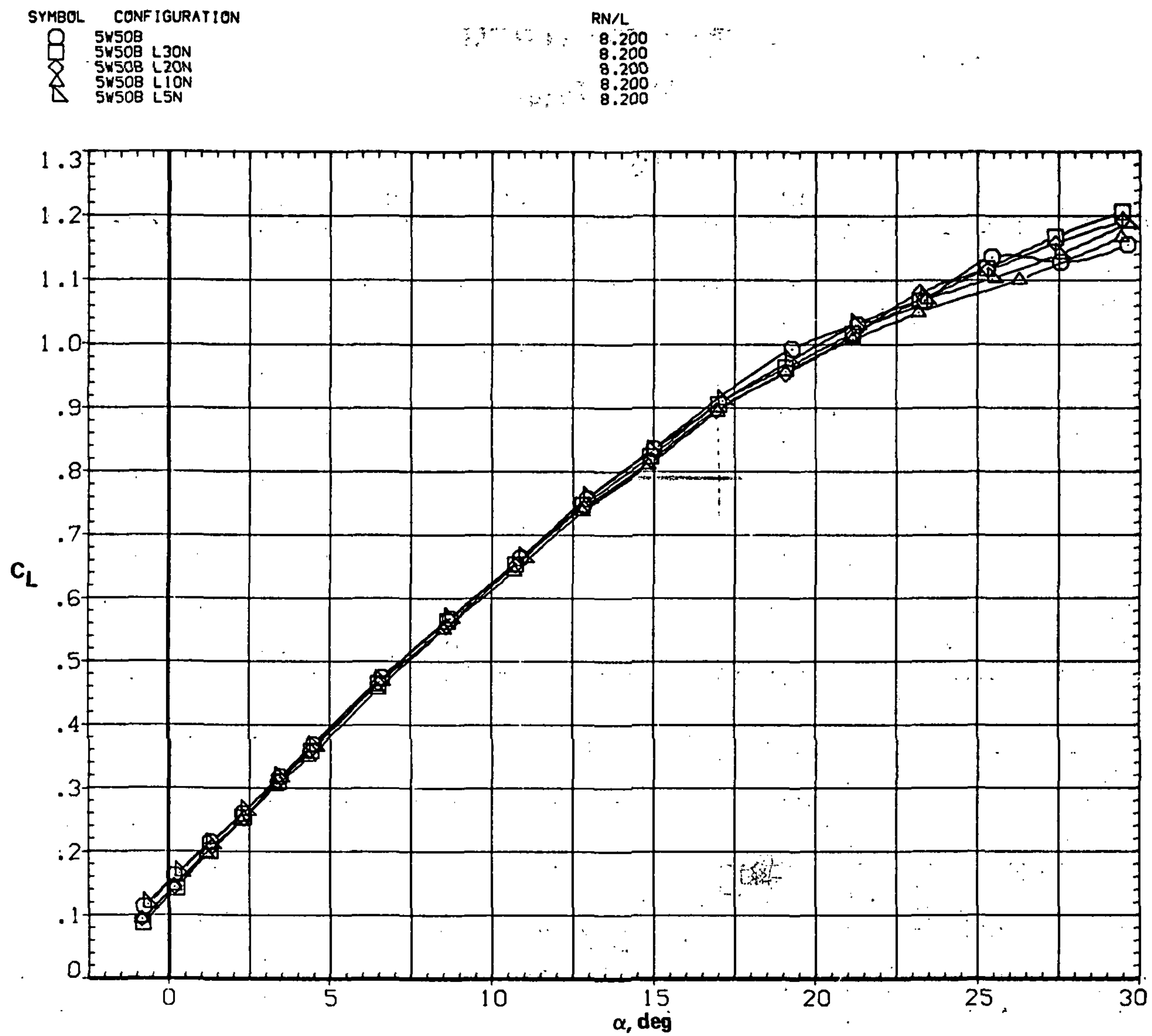

(a) C_L vs α

Figure 11.– Effect of drooped-nose flaps on the static longitudinal characteristics of the oblique wing: flaps on downstream wing panel only, $\Lambda = 50°$, $M = 0.4$.

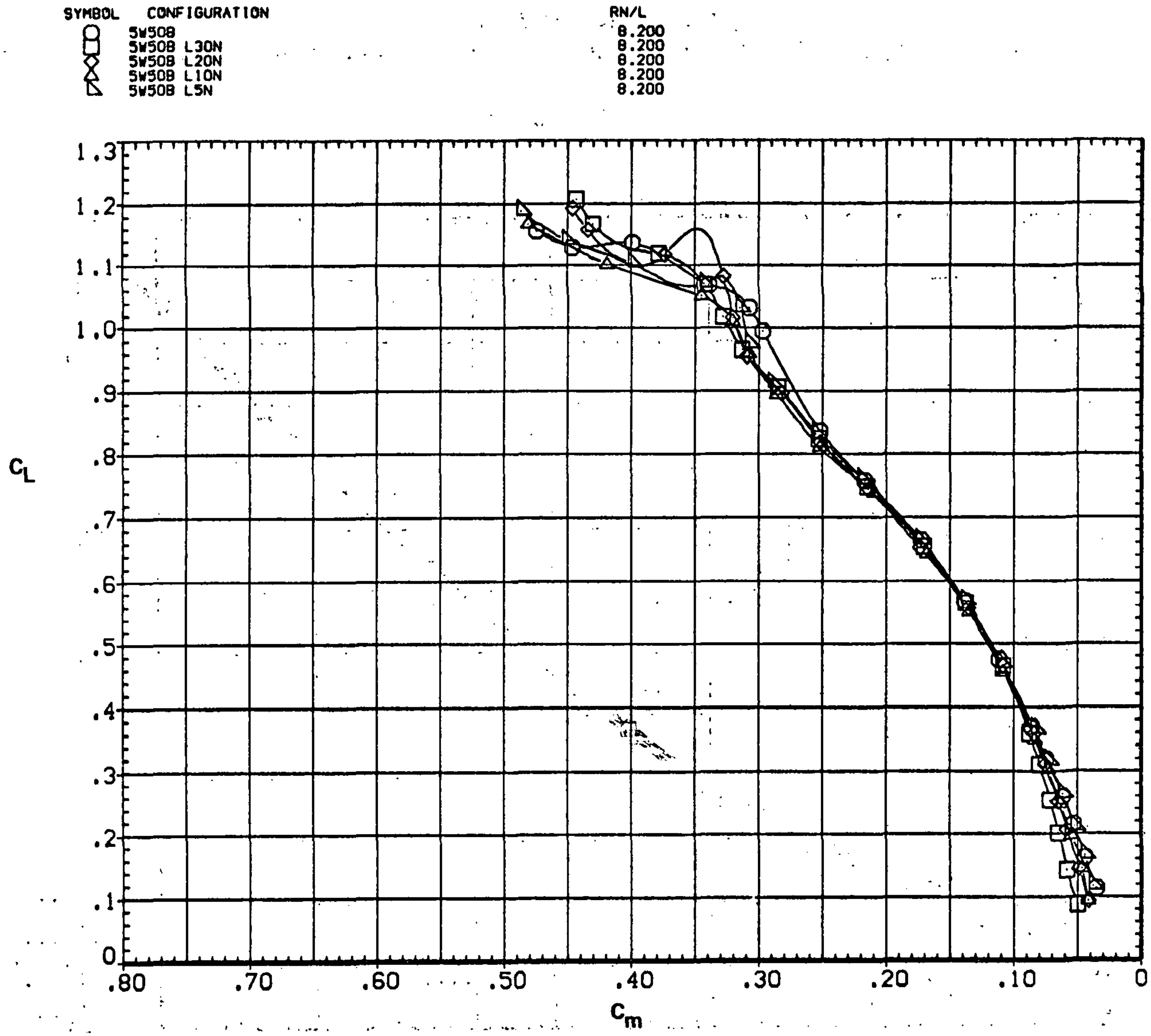

(b) C_L vs C_m

Figure 11.—Continued.

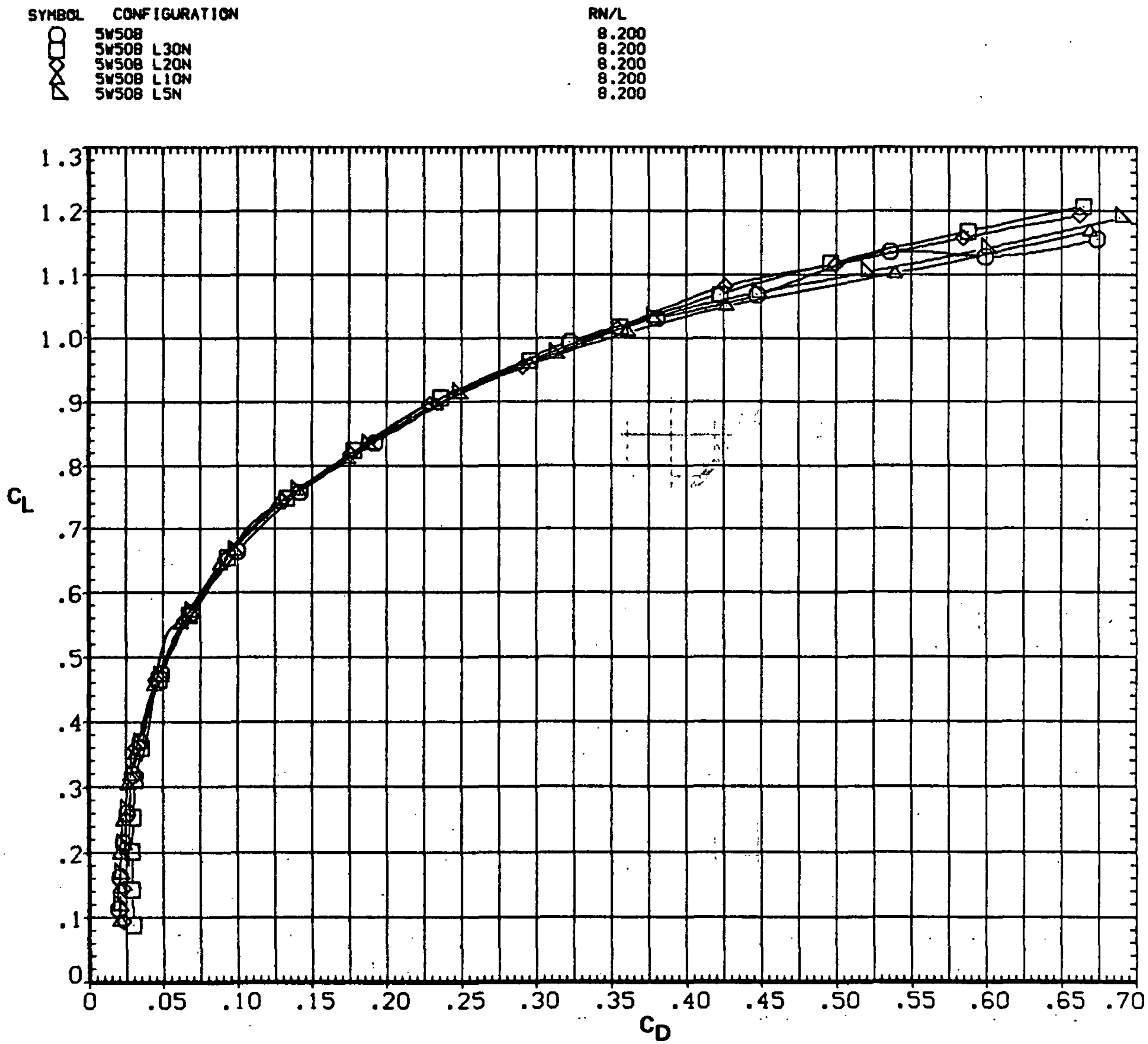

(c) C_L vs C_D

Figure 11.– Continued.

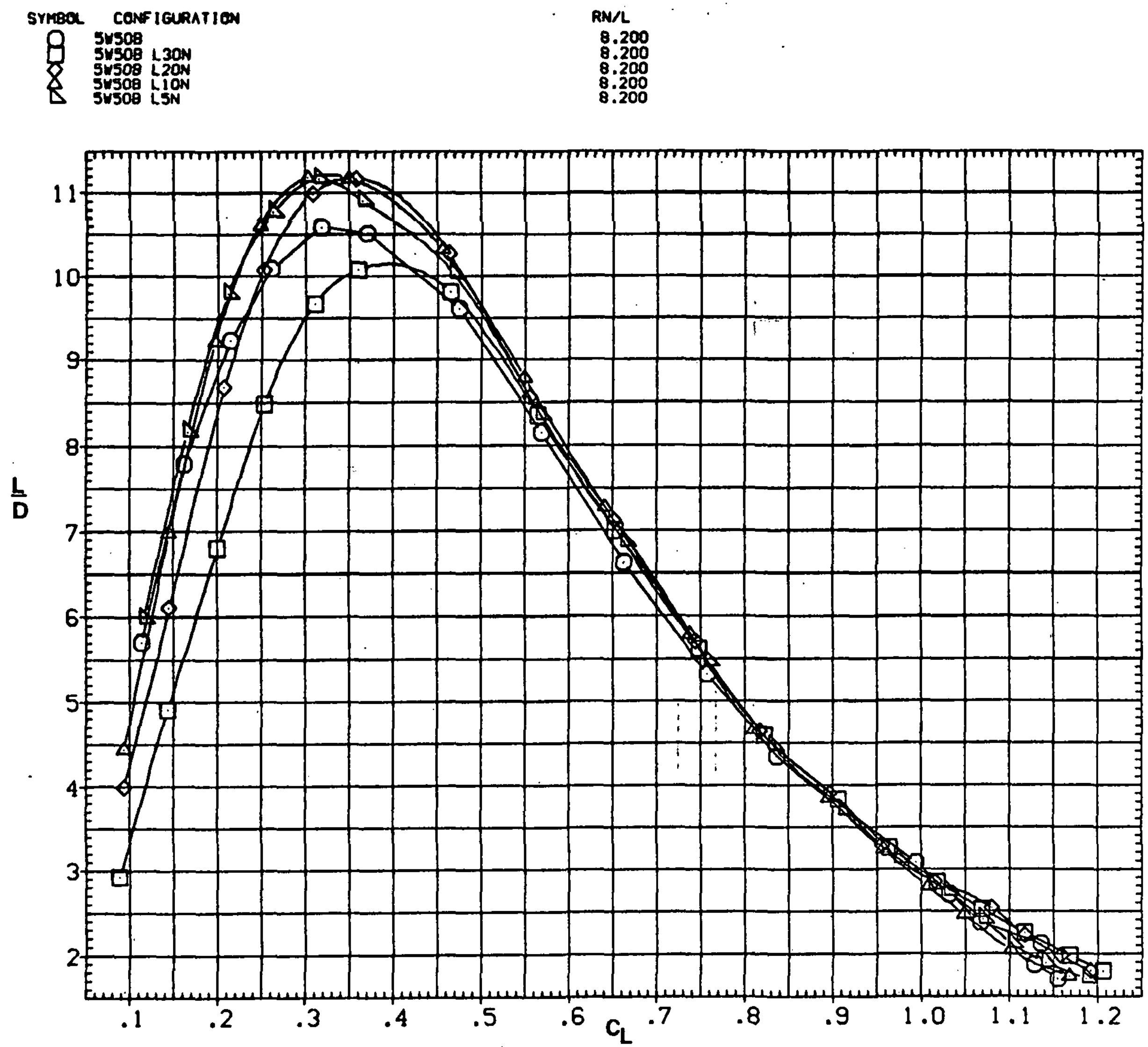

(d) L/D vs C_L

Figure 11.– Continued.

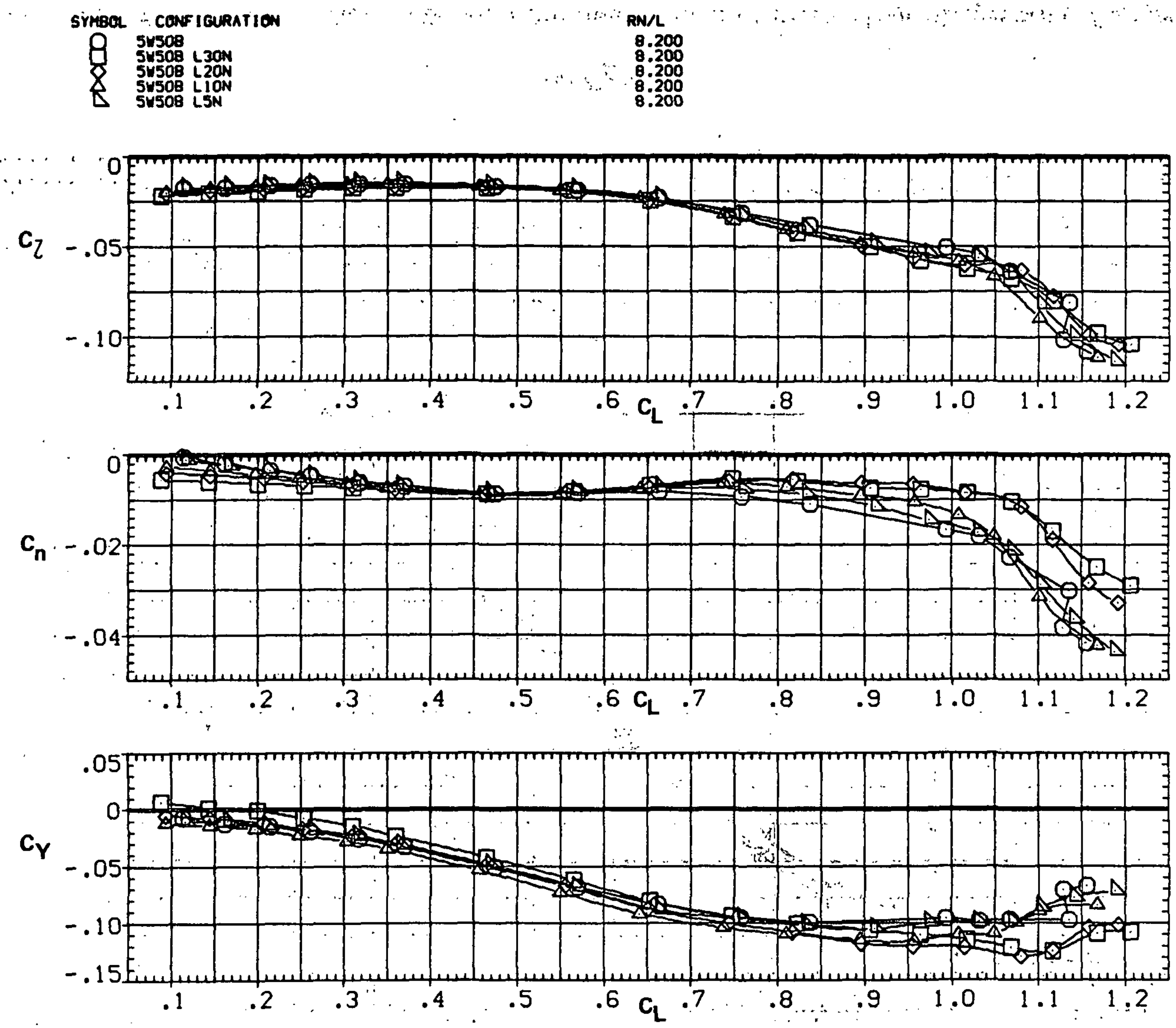

(e) C_l, C_n, and C_Y vs C_L

Figure 11.– Concluded.

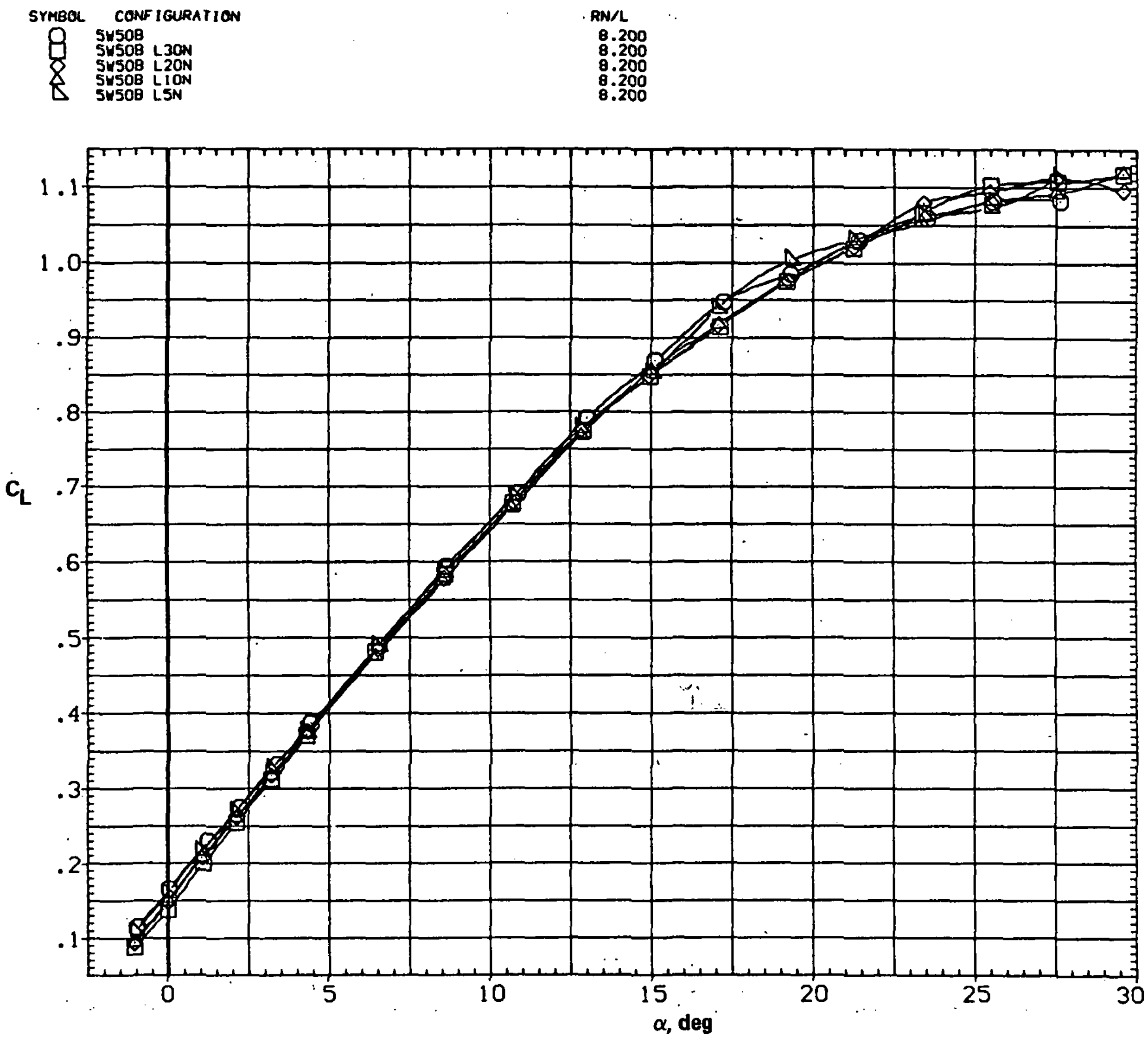

(a) C_L vs. α

Figure 12.– Effect of drooped-nose flaps on the static longitudinal characteristics of the oblique wing: flaps on downstream wing panel only, $\Lambda = 50°$, $M = 0.6$.

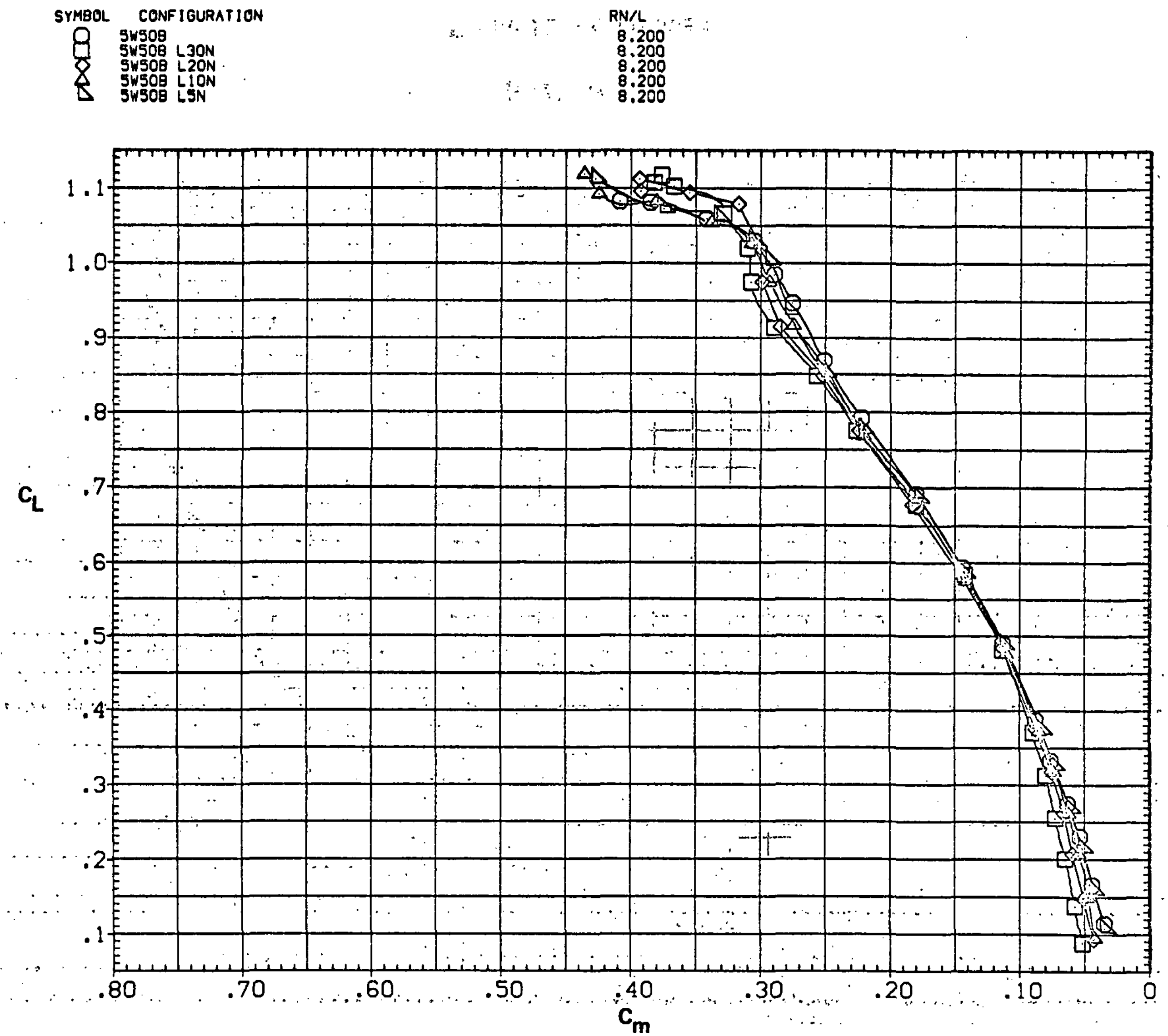

(b) C_L vs C_m

Figure 12.– Continued.

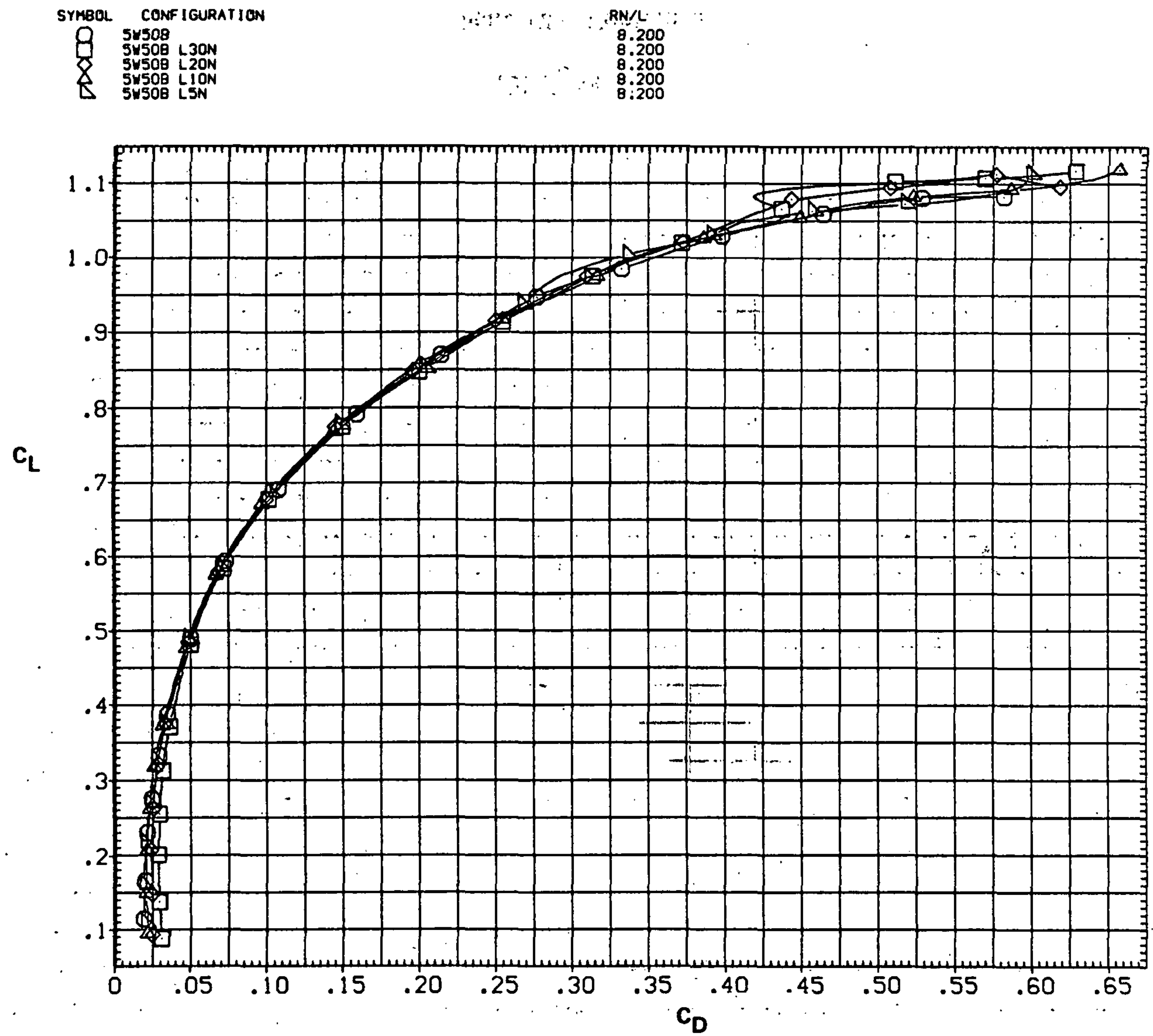

(c) C_L vs C_D

Figure 12.– Continued.

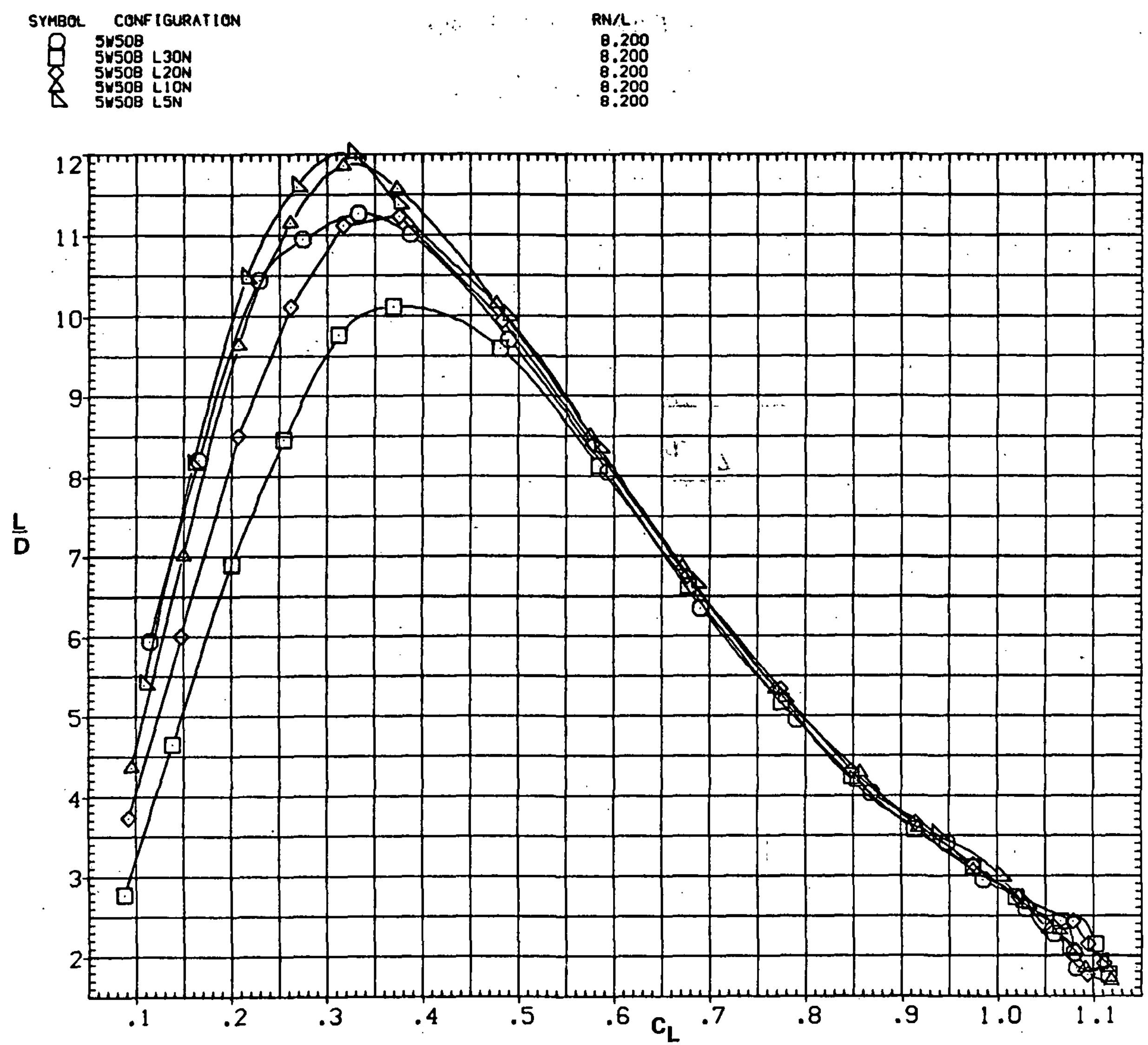

(d) L/D vs C_L

Figure 12.– Continued.

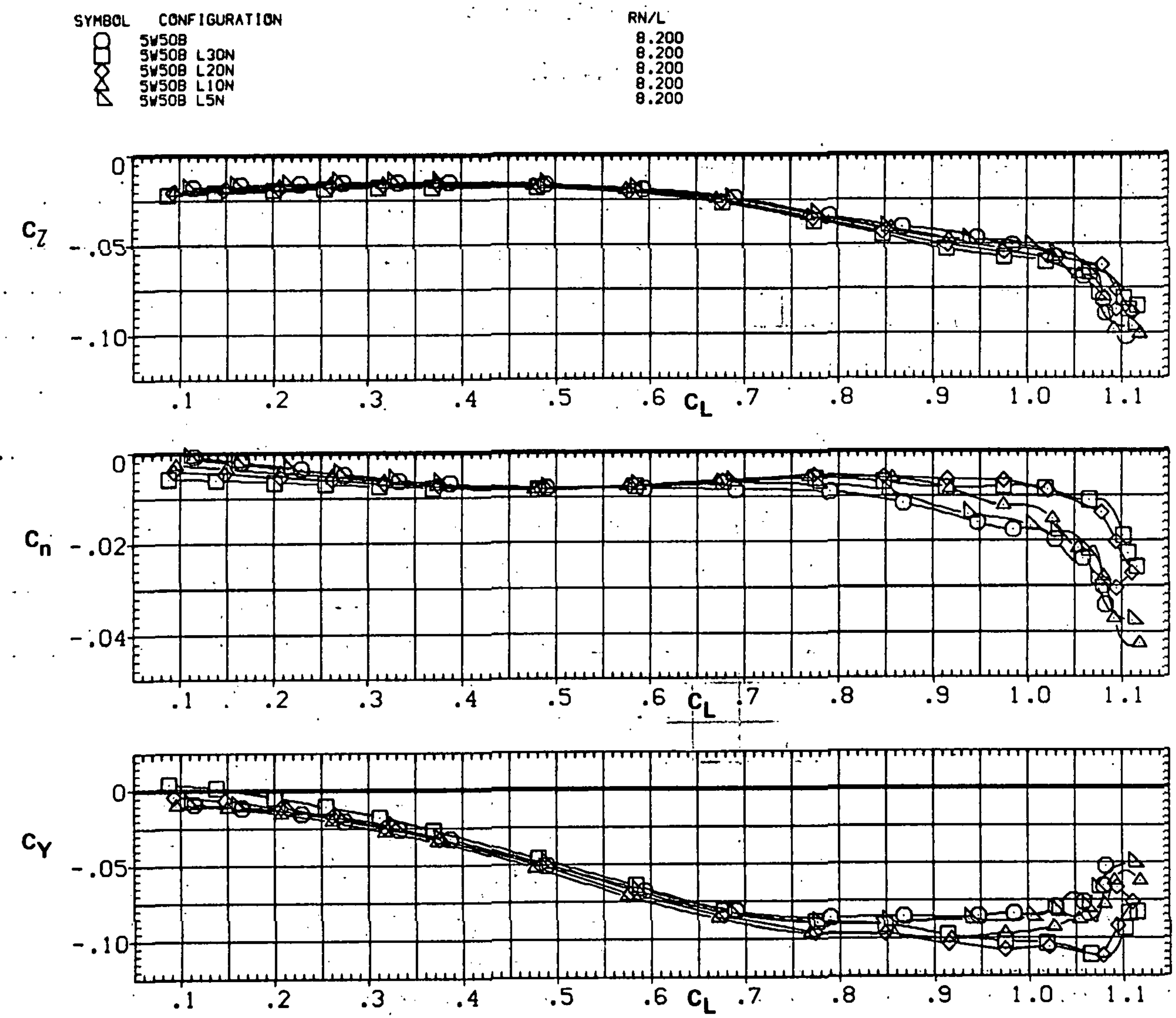

(e) C_l, C_n, and C_Y vs C_L

Figure 12.– Concluded.

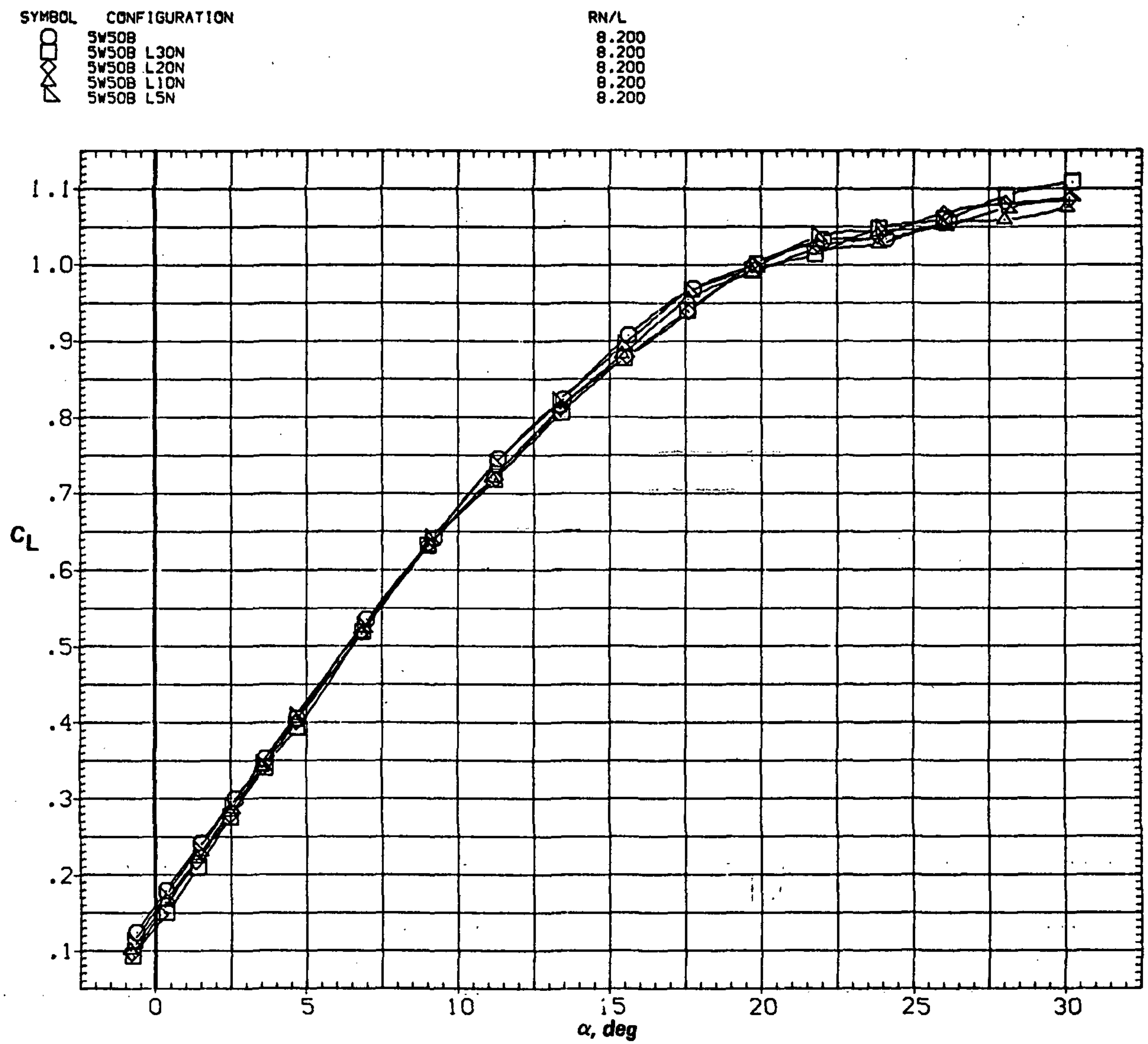

(a) C_L vs α

Figure 13.– Effect of drooped-nose flaps on the static longitudinal characteristics of the oblique wing: flaps on downstream wing panel only, $\Lambda = 50°$, $M = 0.8$.

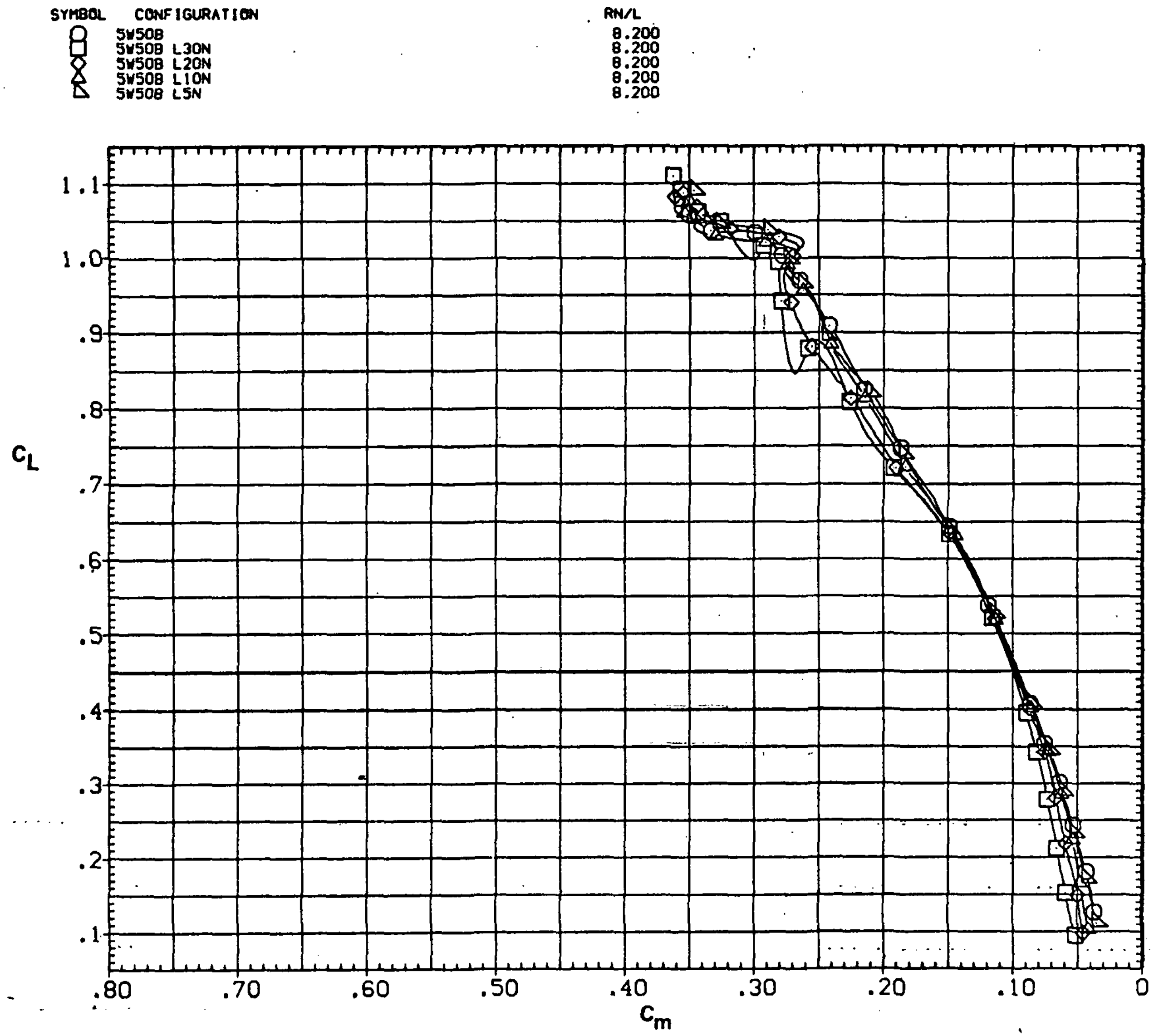

(b) C_L vs C_m

Figure 13.– Continued.

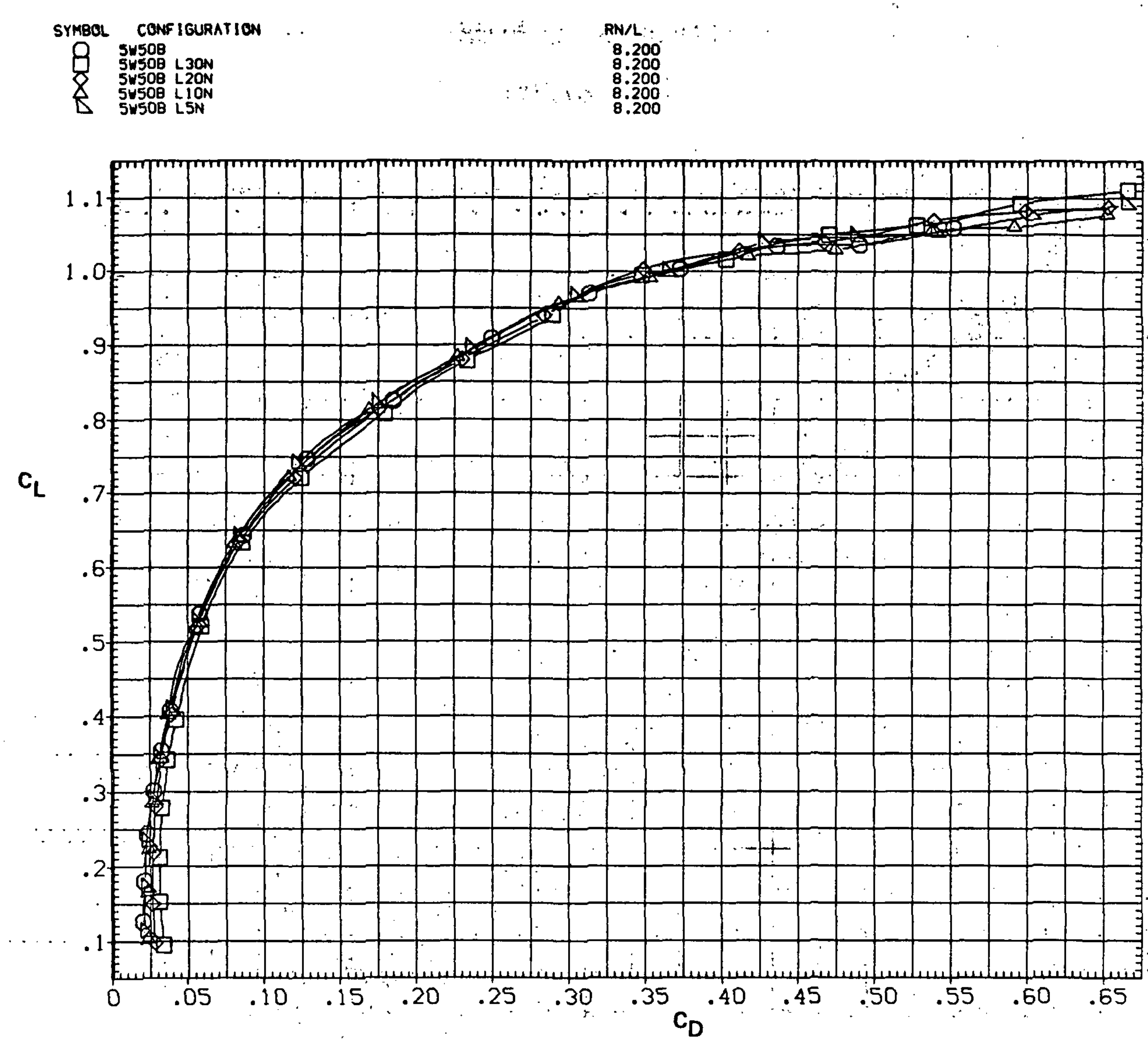

(c) C_L vs C_D

Figure 13.– Continued.

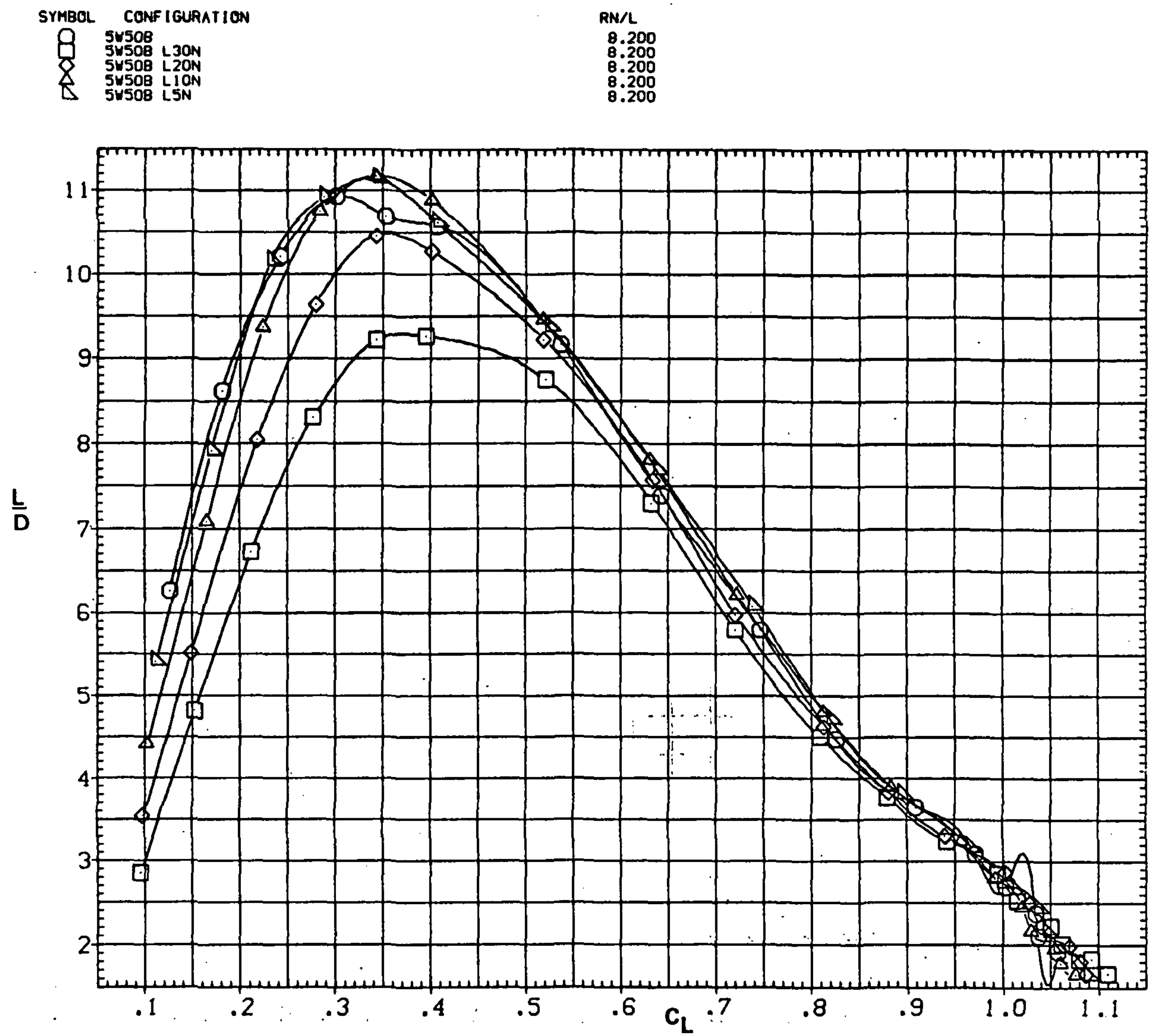

(d) L/D vs C_L

Figure 13.– Continued.

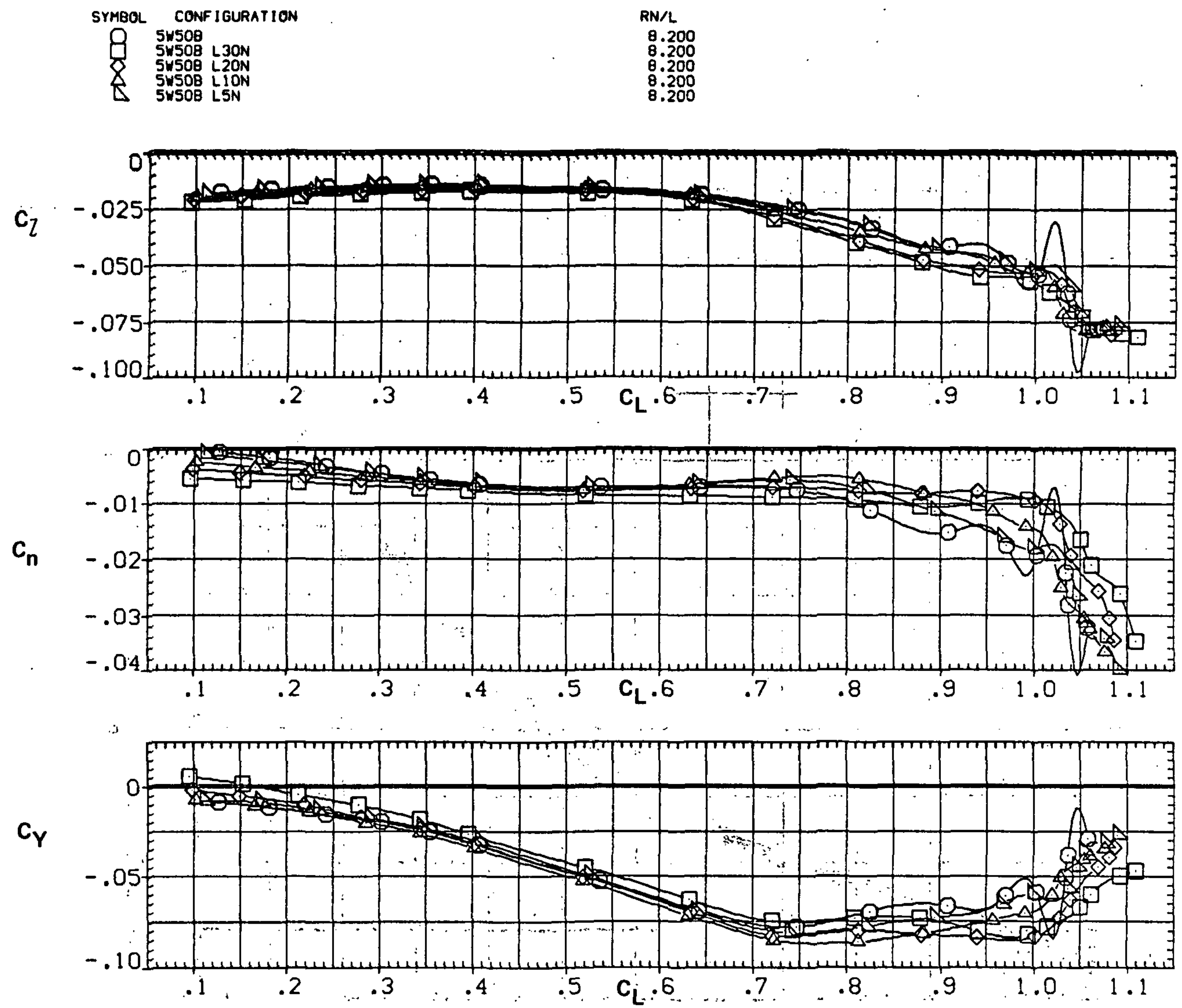

(e) C_l, C_n, and C_Y vs C_L

Figure 13.– Concluded.

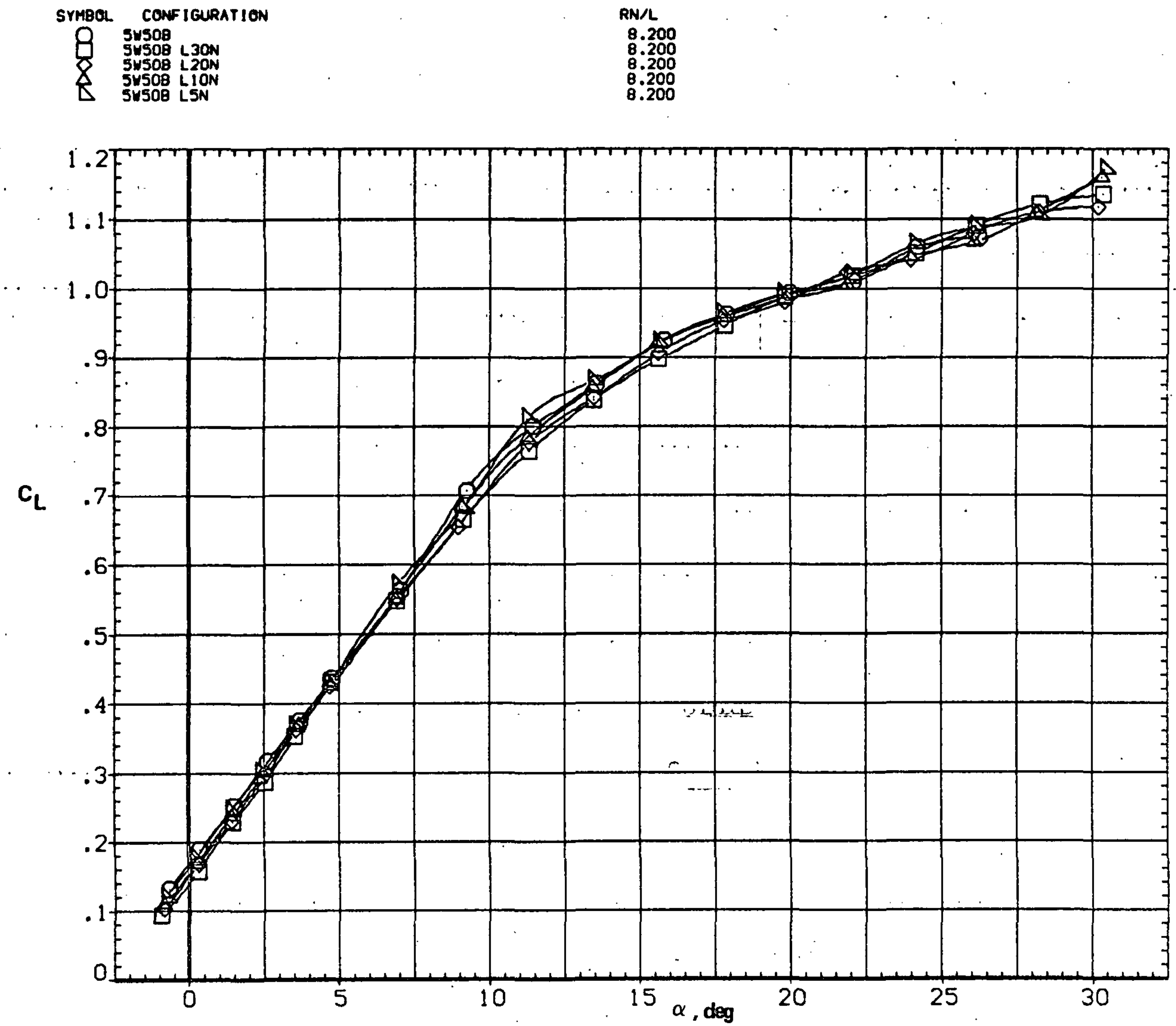

(a) C_L vs α

Figure 14.— Effect of drooped-nose flaps on the static longitudinal characteristics of the oblique wing: flaps on downstream wing panel only, $\Lambda = 50°$, $M = 0.9$.

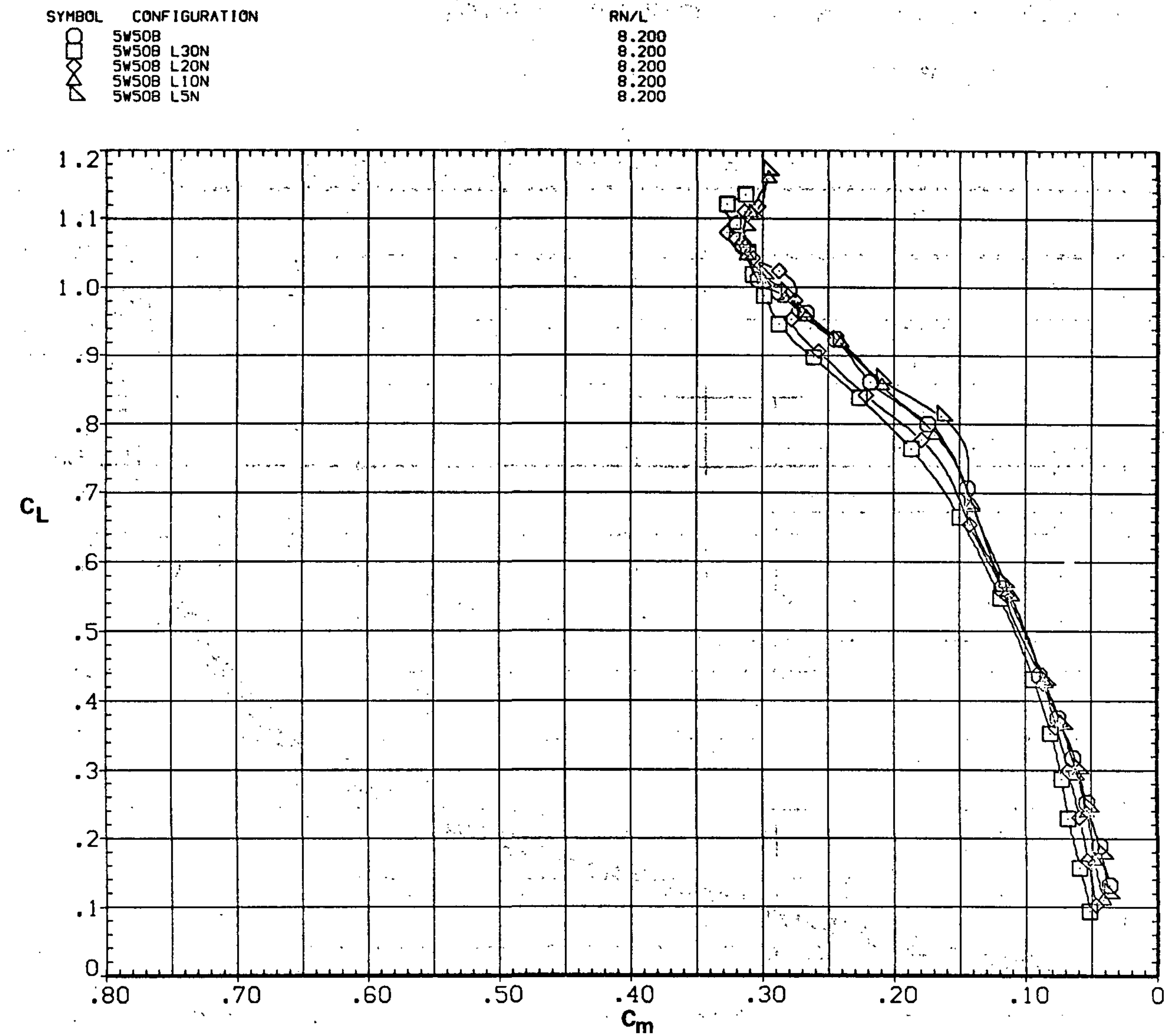

(b) C_L vs C_m

Figure 14.– Continued.

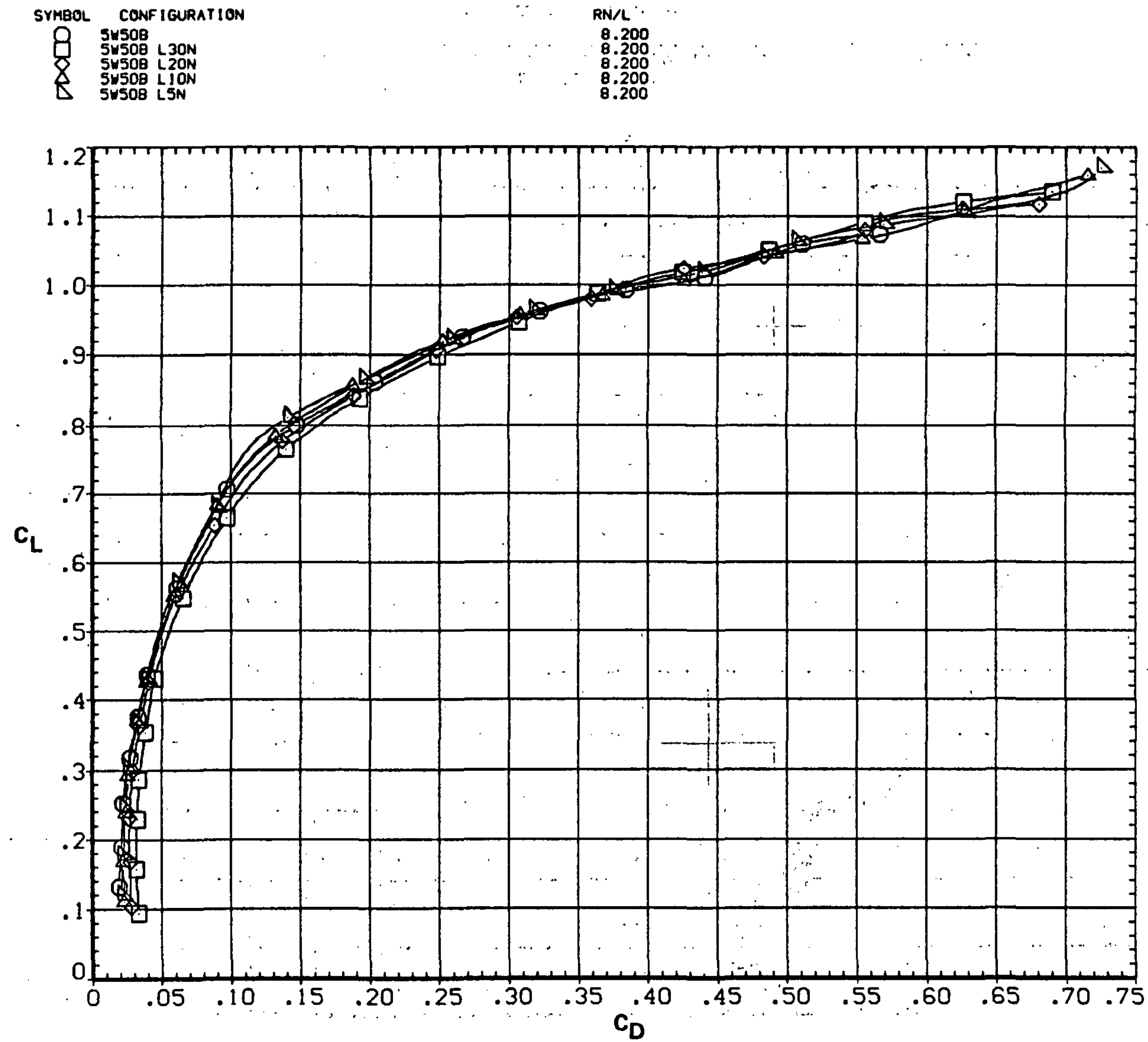

(c) C_L vs C_D

Figure 14.– Continued.

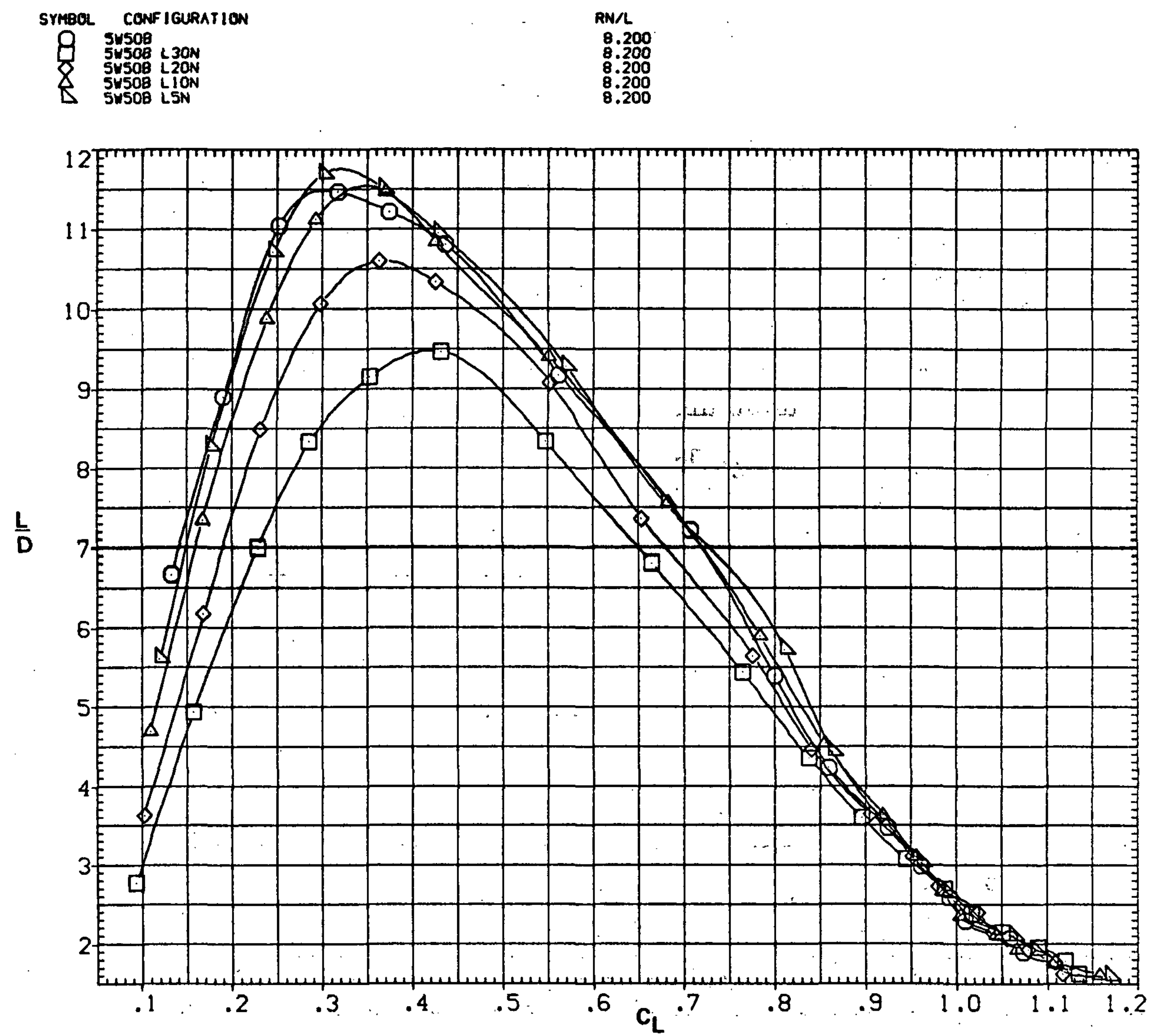

(d) L/D vs C_L

Figure 14.– Continued.

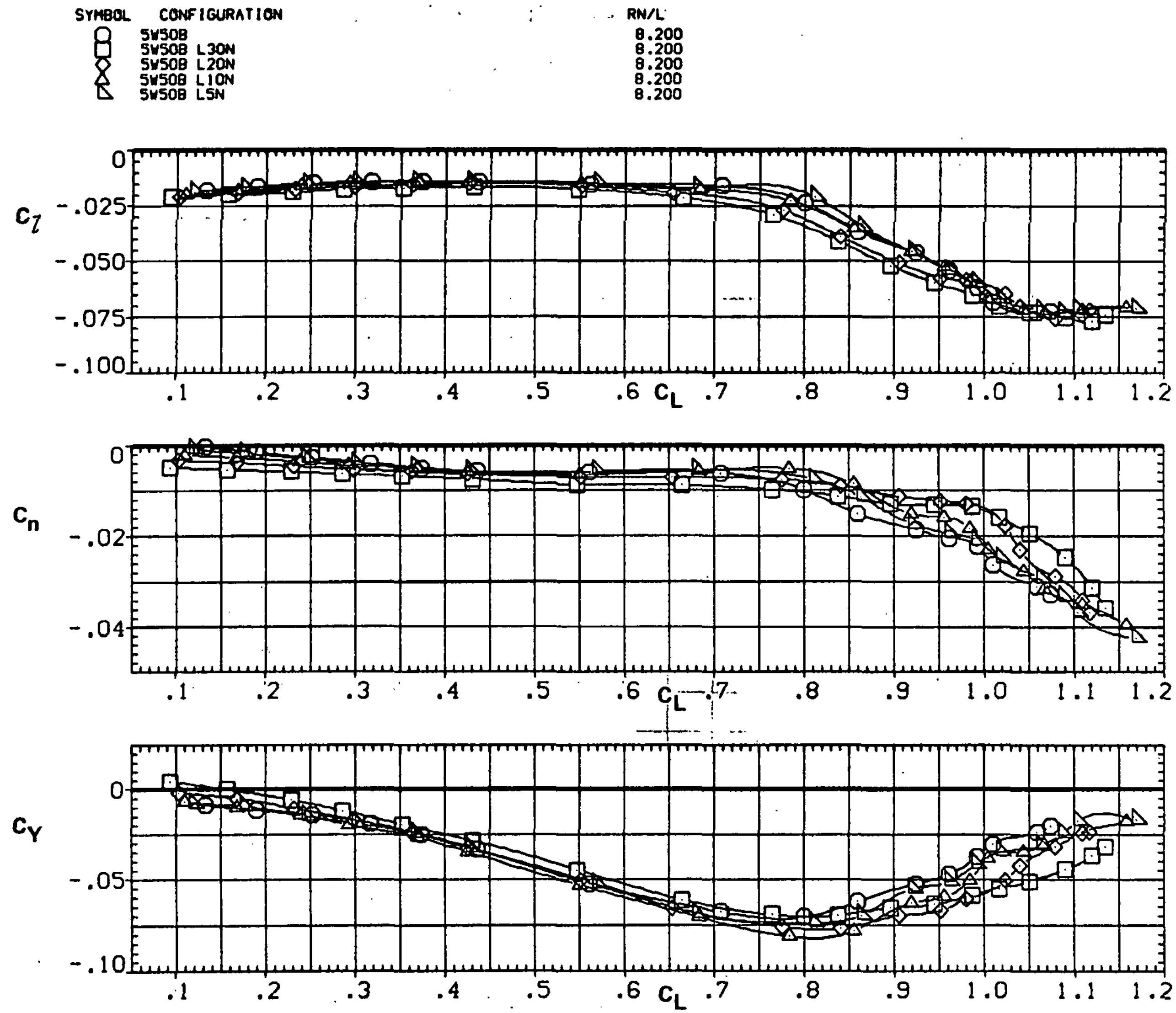

(e) C_l, C_n, and C_Y vs C_L

Figure 14.– Concluded.

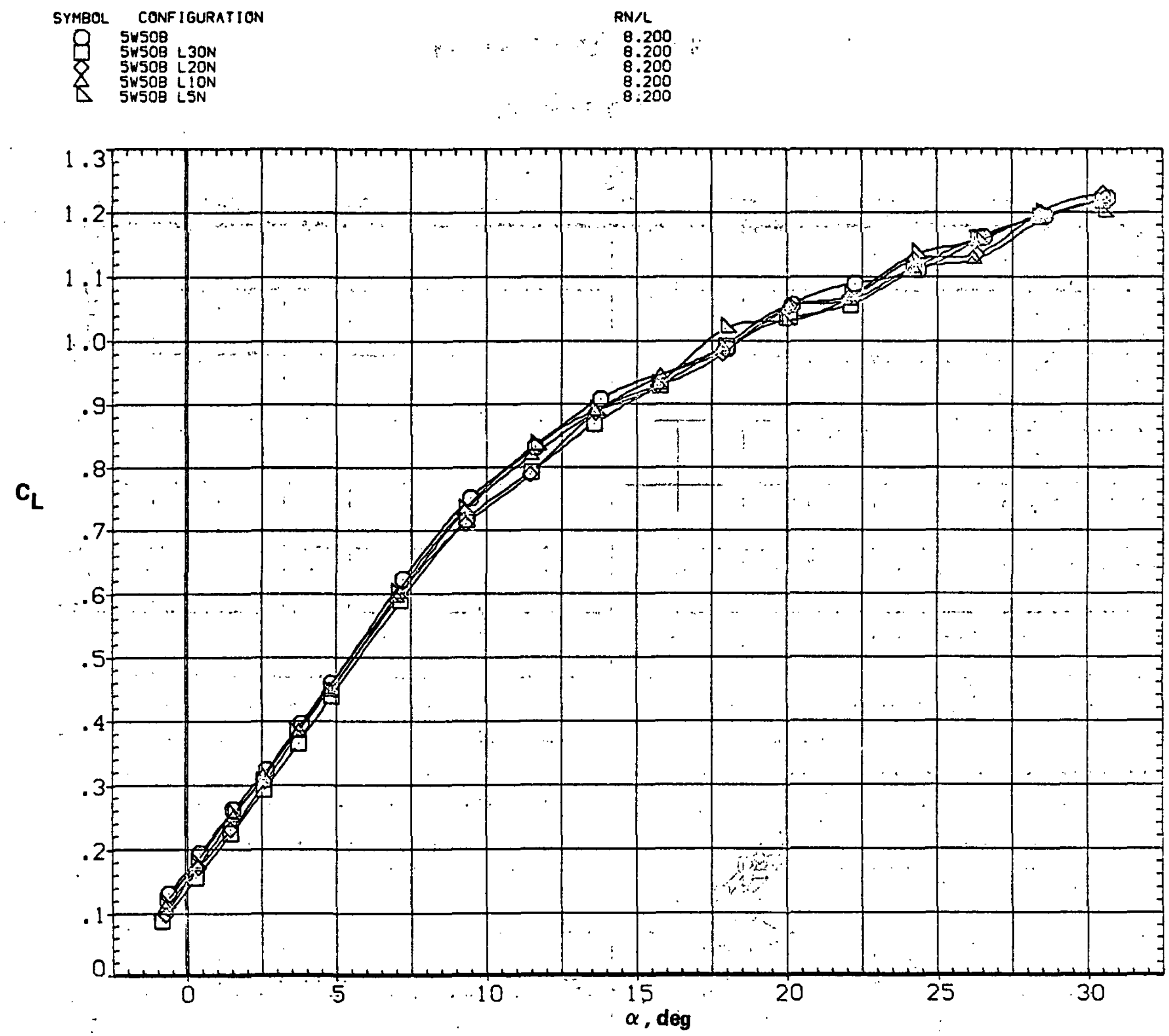

(a) C_L vs α

Figure 15.– Effect of drooped-nose flaps on the static longitudinal characteristics of the oblique wing: flaps on downstream wing panel only, $\Lambda = 50^\circ$, $M = 0.95$.

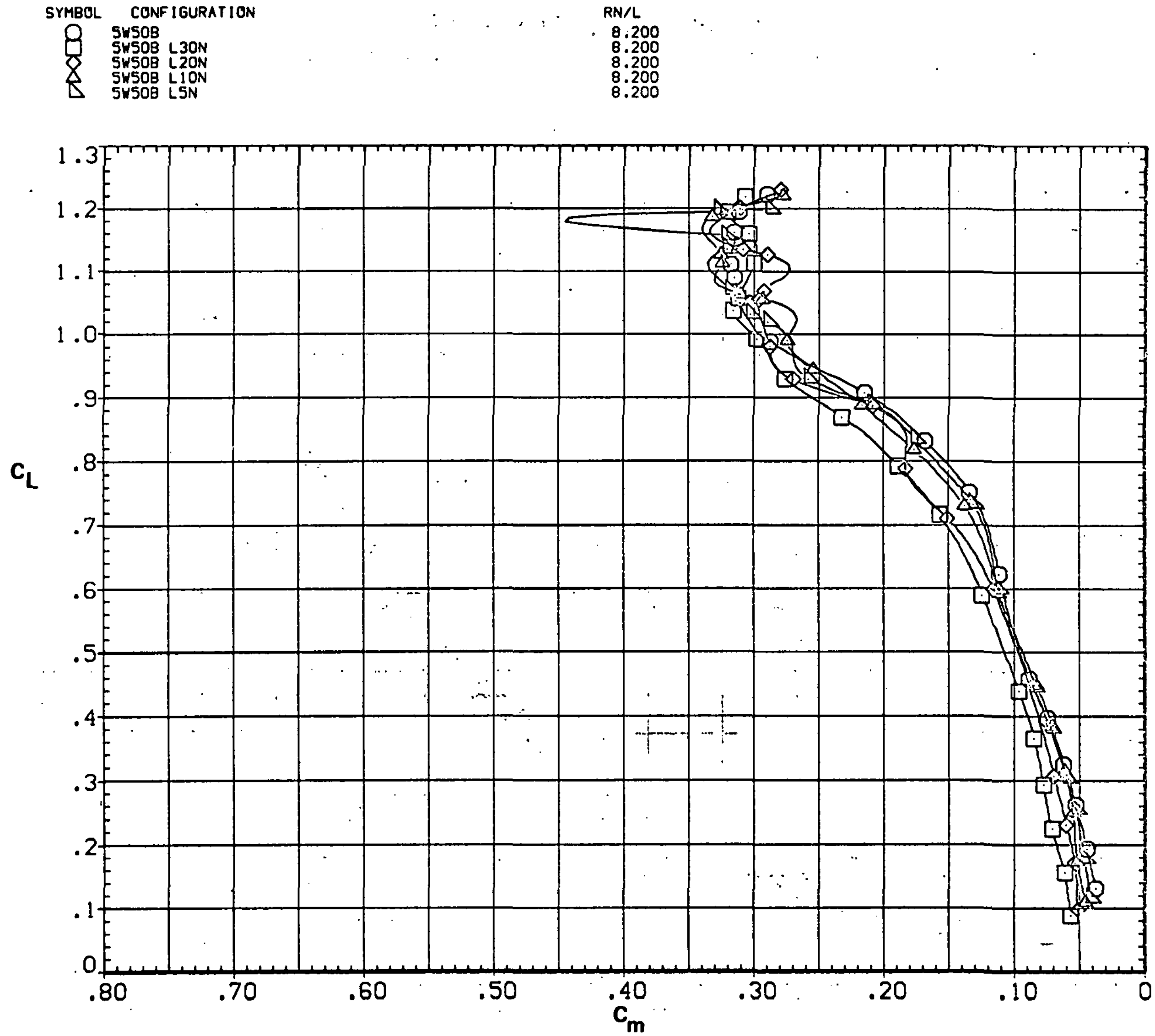

(b) C_L vs C_m

Figure 15.– Continued.

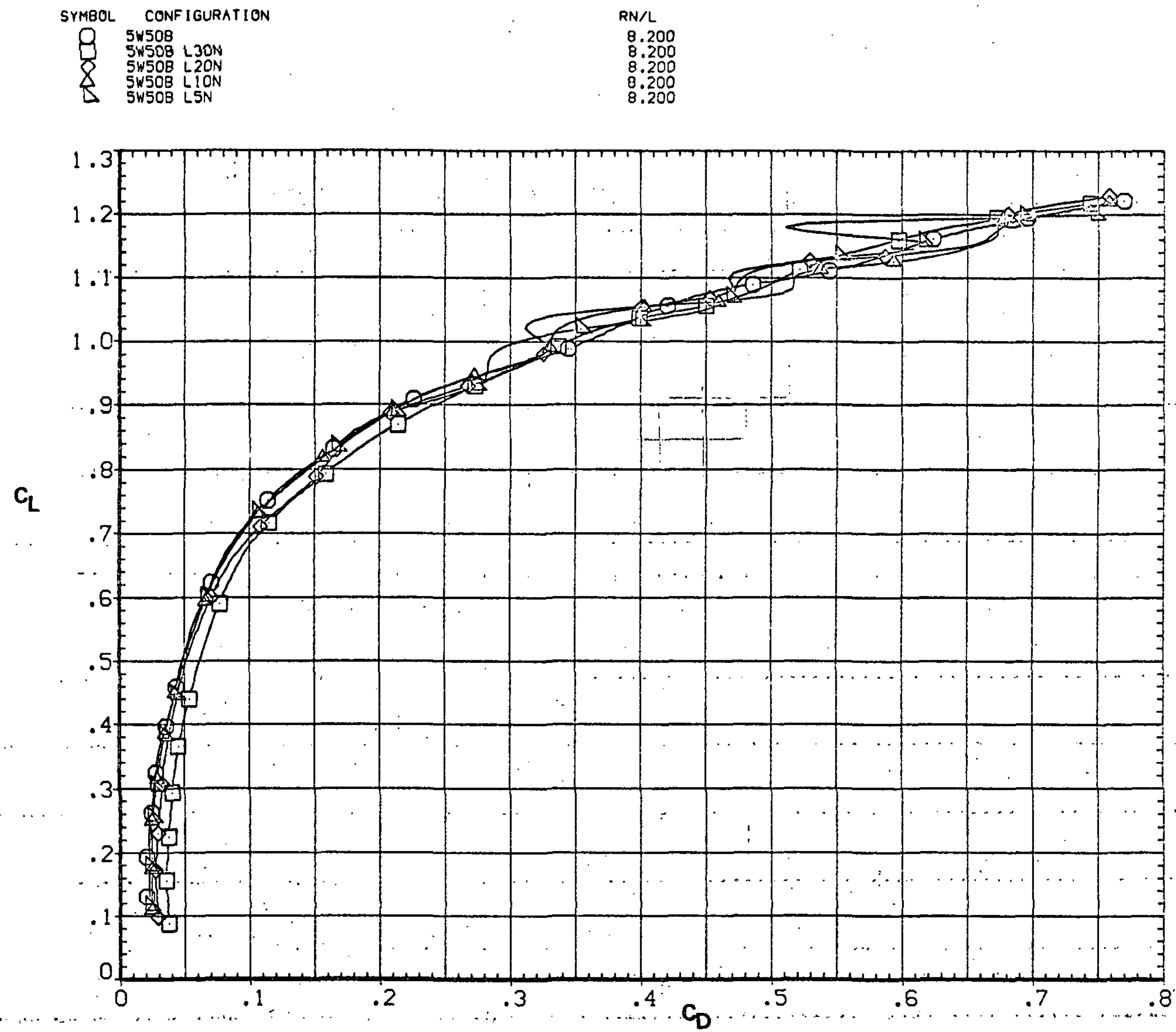

(c) C_L vs C_D

Figure 15.– Continued.

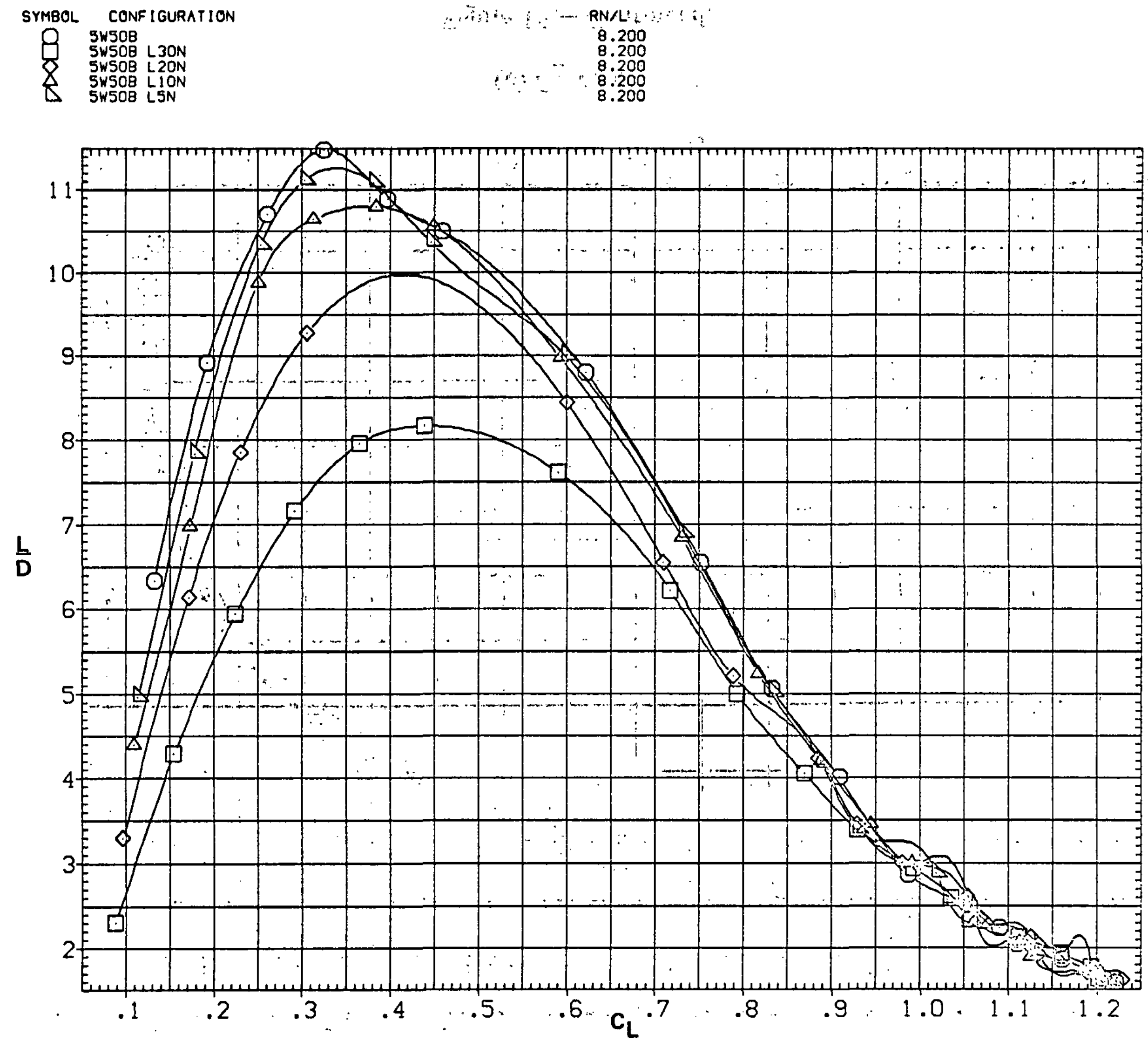

(d) L/D vs C_L

Figure 15.– Continued.

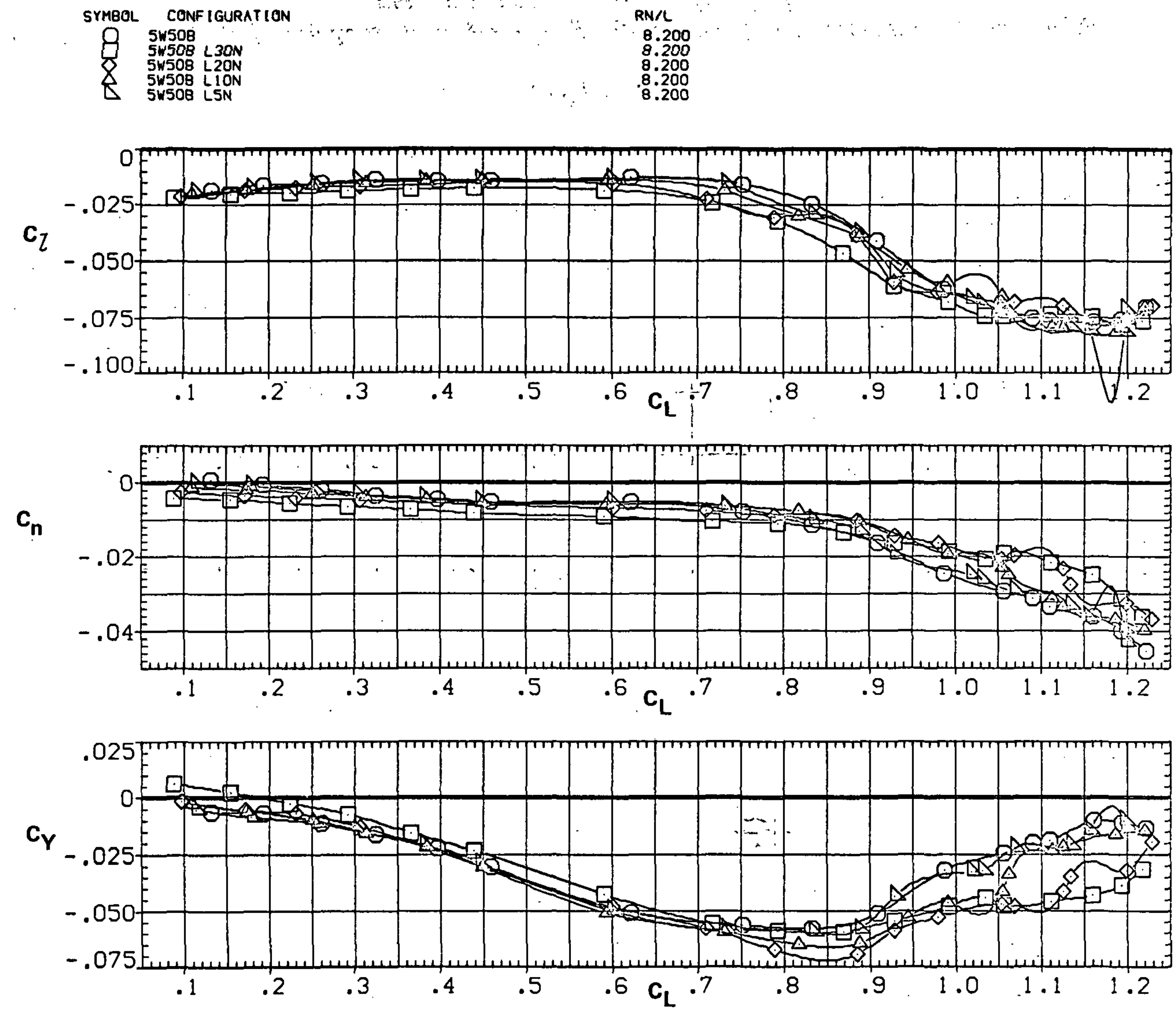

(e) C_l, C_n, and C_Y vs C_L

Figure 15.– Concluded.

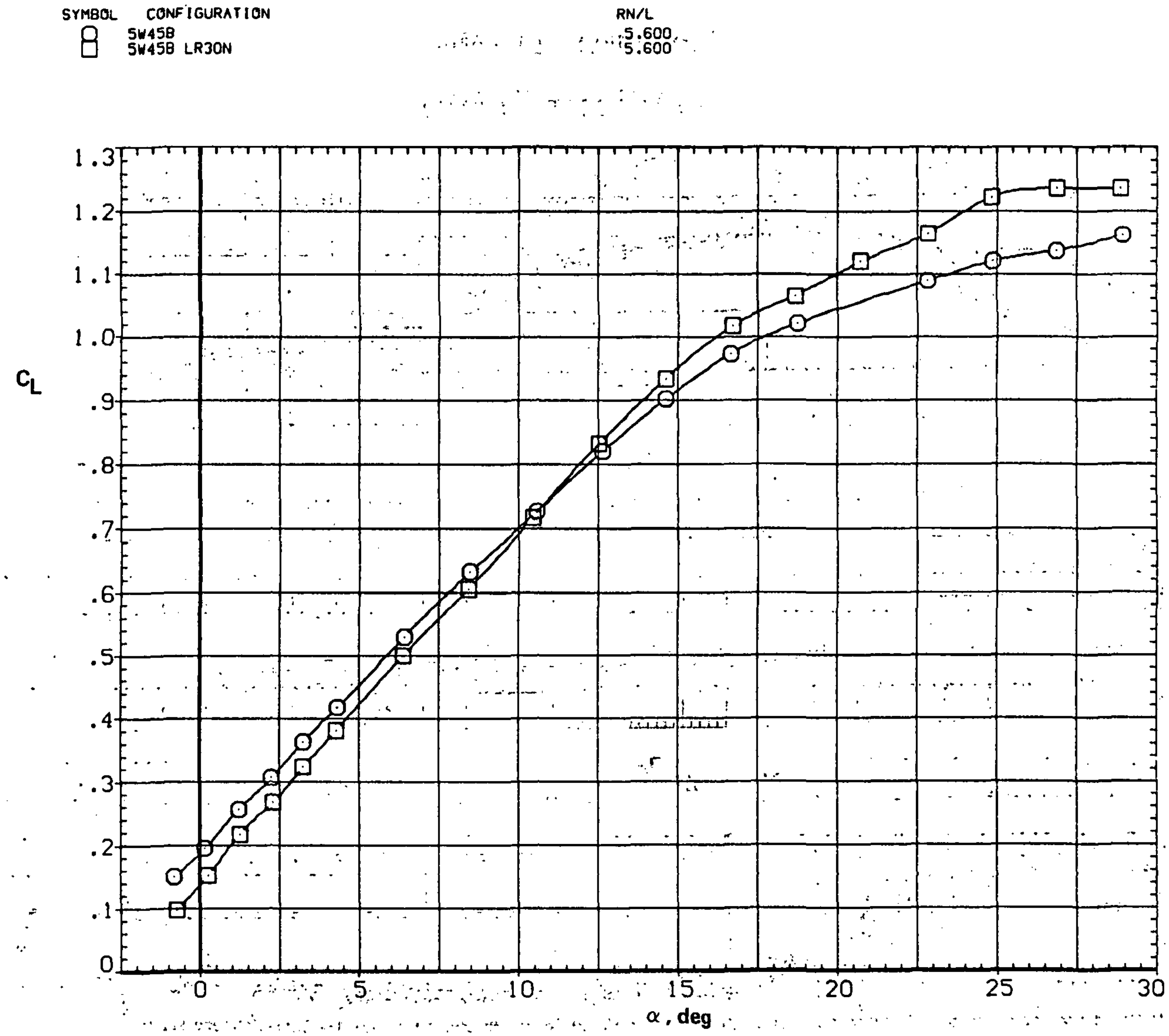

(a) C_L vs α

Figure 16.– Effect of drooped-nose flaps on the static longitudinal stability characteristics of the oblique wing: flaps on both wing panels, $\Lambda = 45°, M = 0.25$.

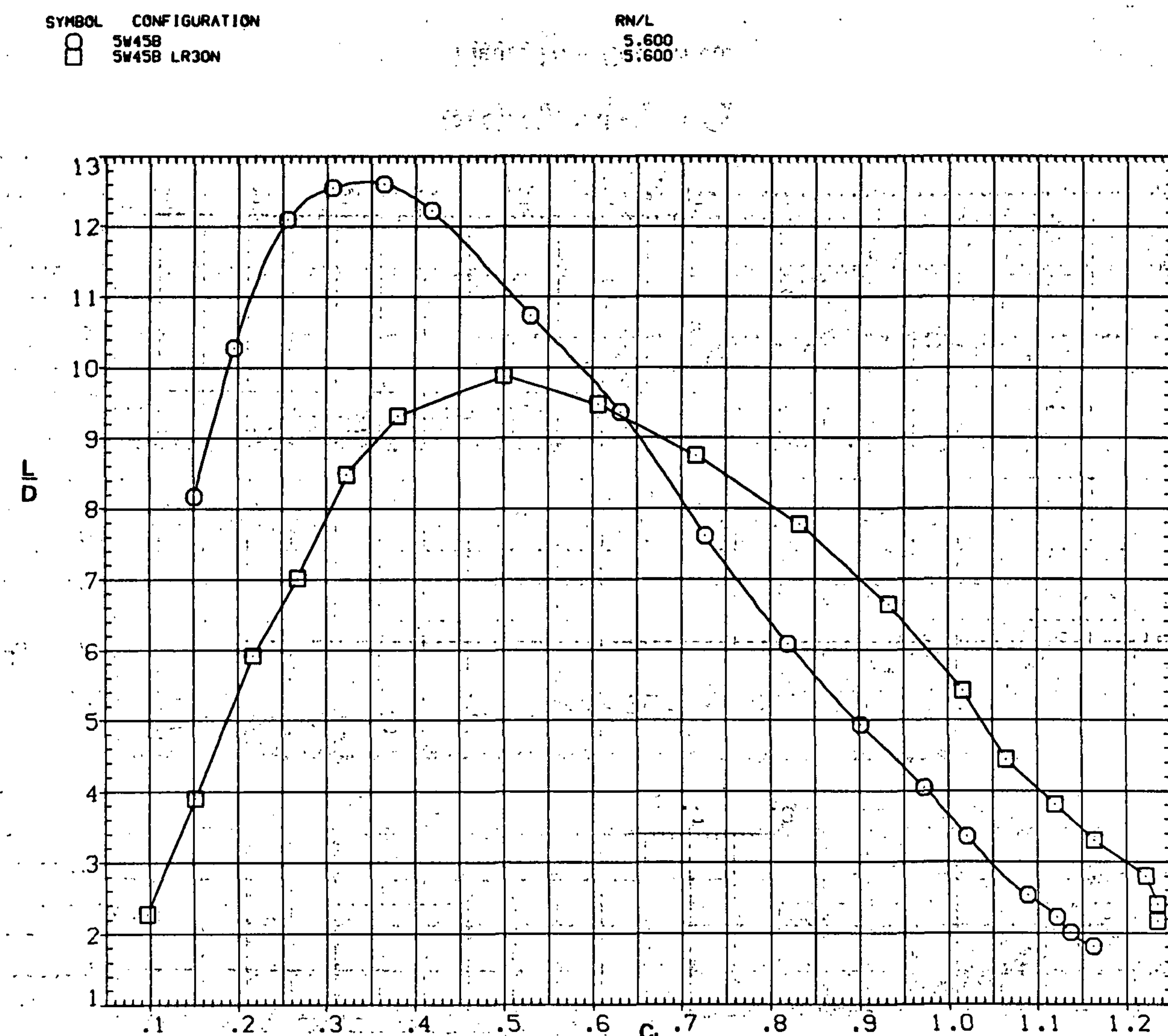

(d) L/D vs C_L

Figure 16.– Continued.

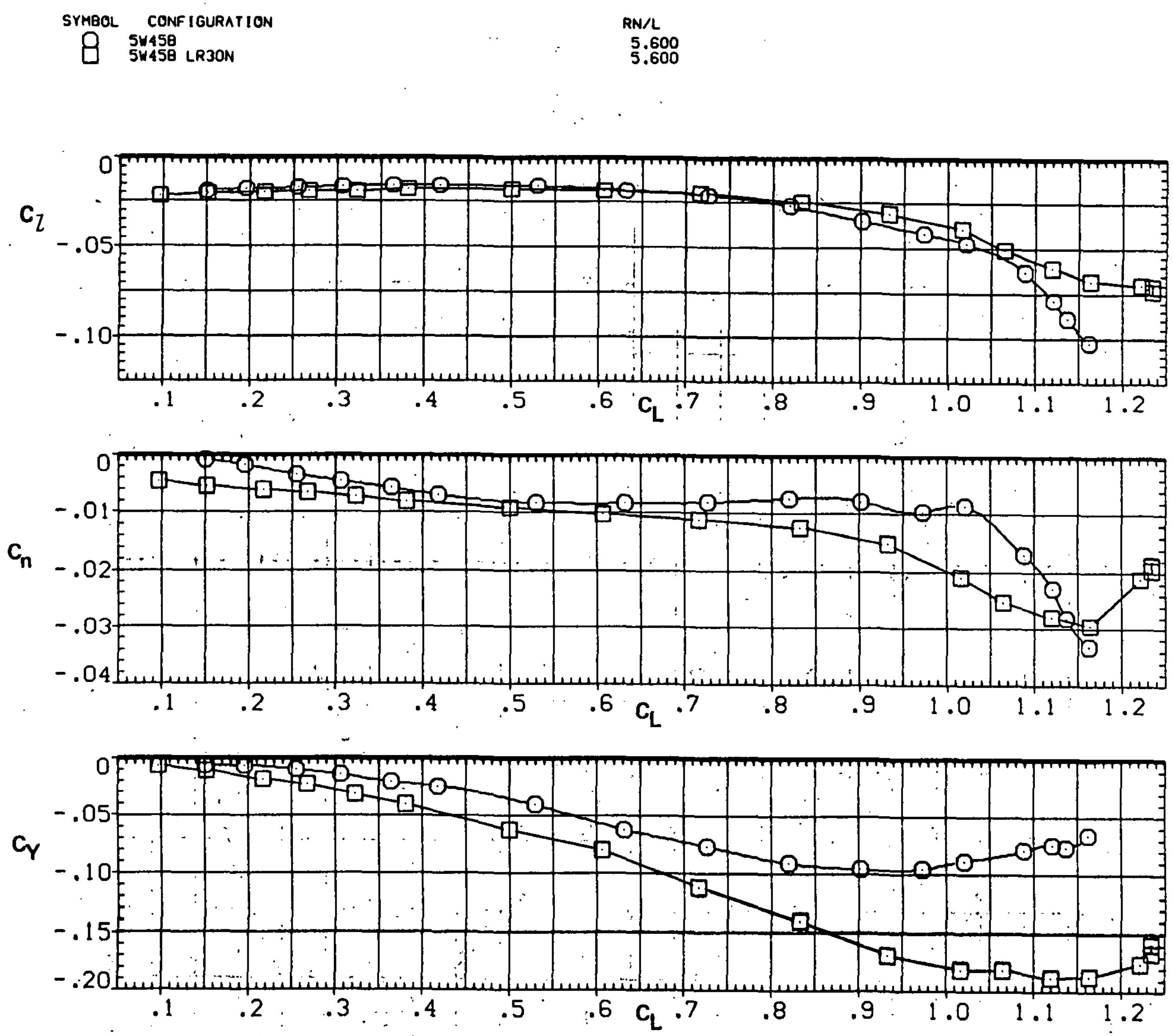

(e) C_l, C_n, and C_Y vs C_L

Figure 16.– Concluded.

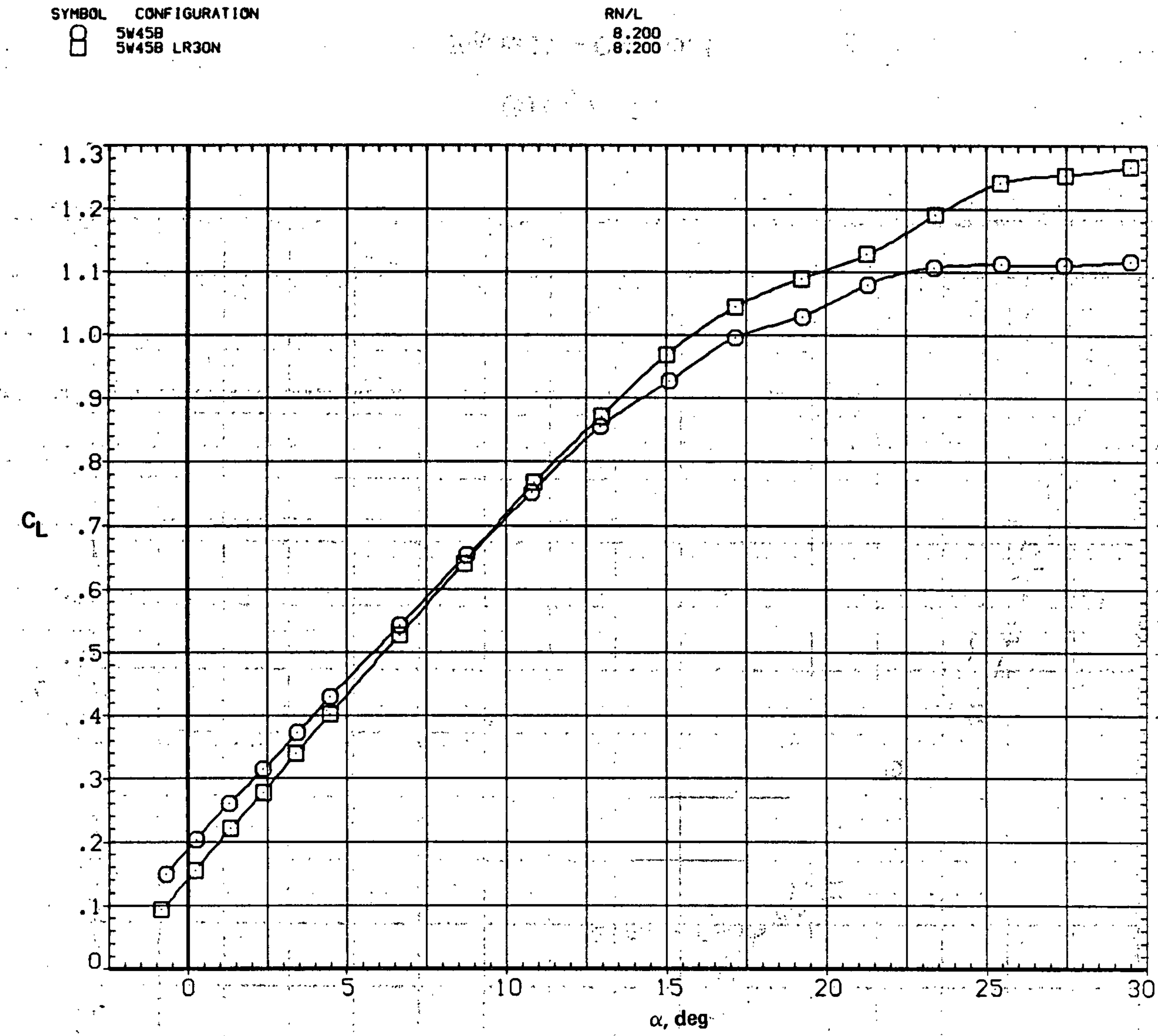

(a) C_L vs α

Figure 17.– Effect of drooped-nose flaps on the static longitudinal characteristics of the oblique wing: flaps on both wing panels, $\Lambda = 45°$, $M = 0.4$.

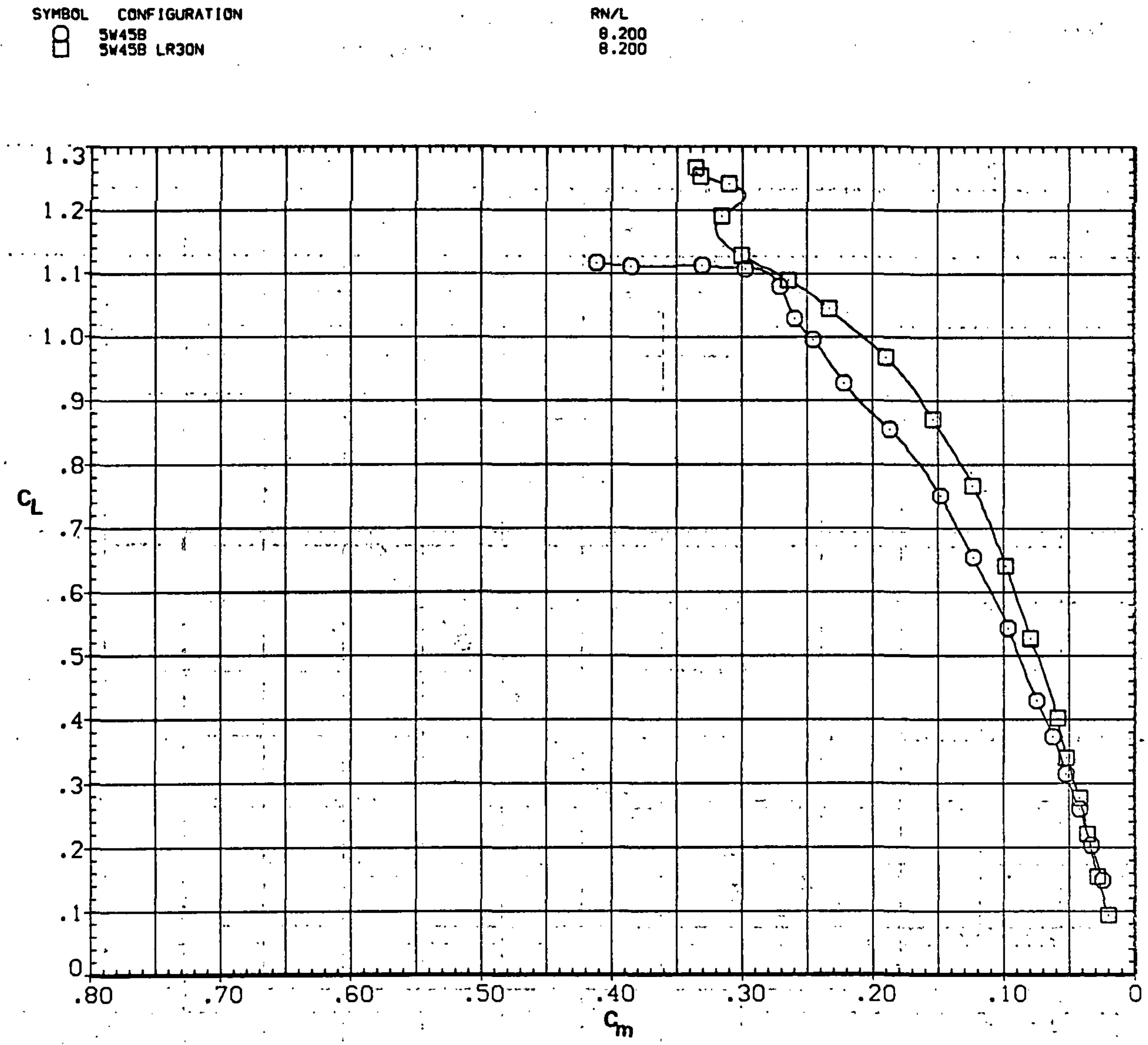

(b) C_L vs C_m

Figure 17.– Continued.

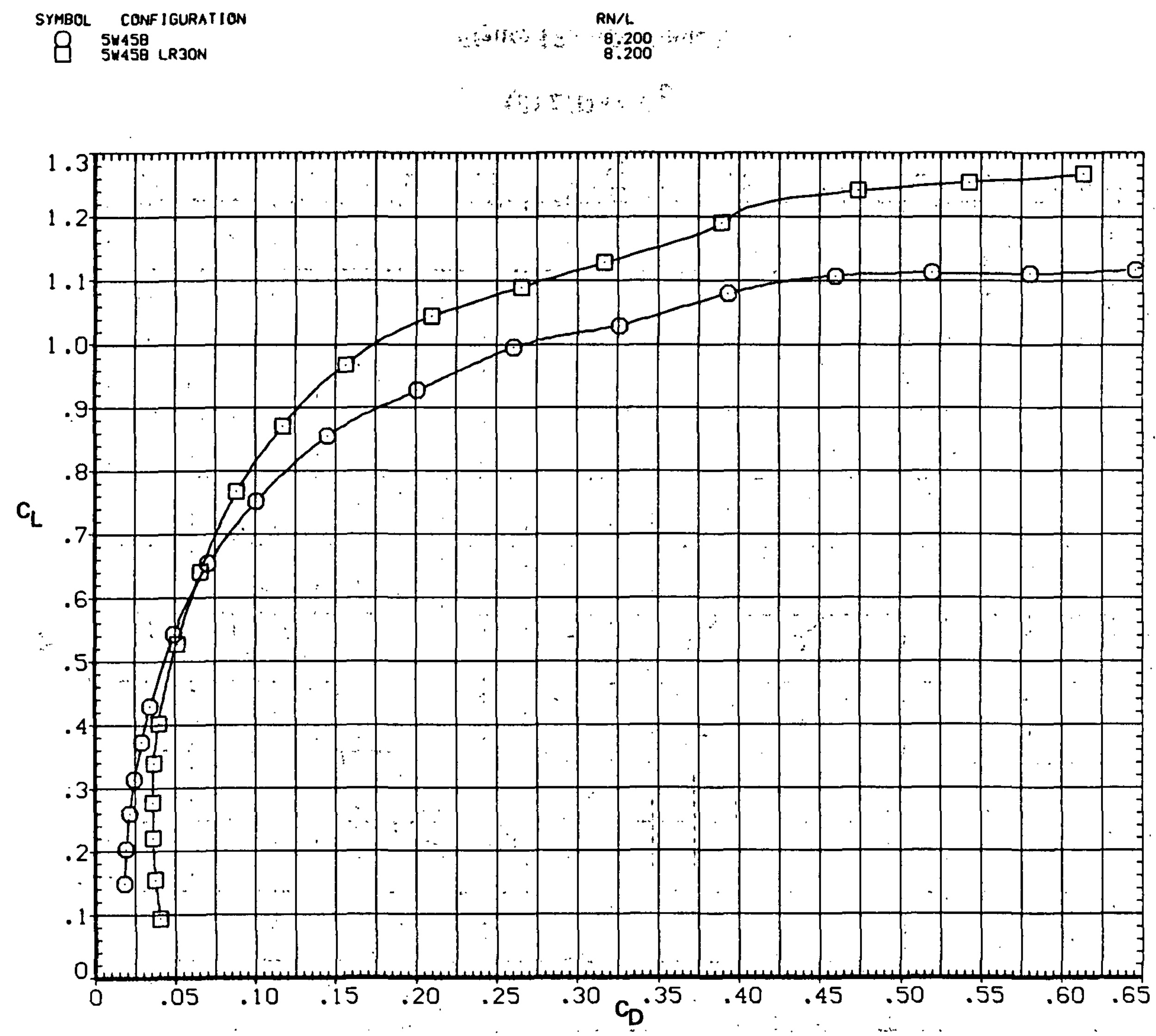

(c) C_L vs C_D

Figure 17.– Continued.

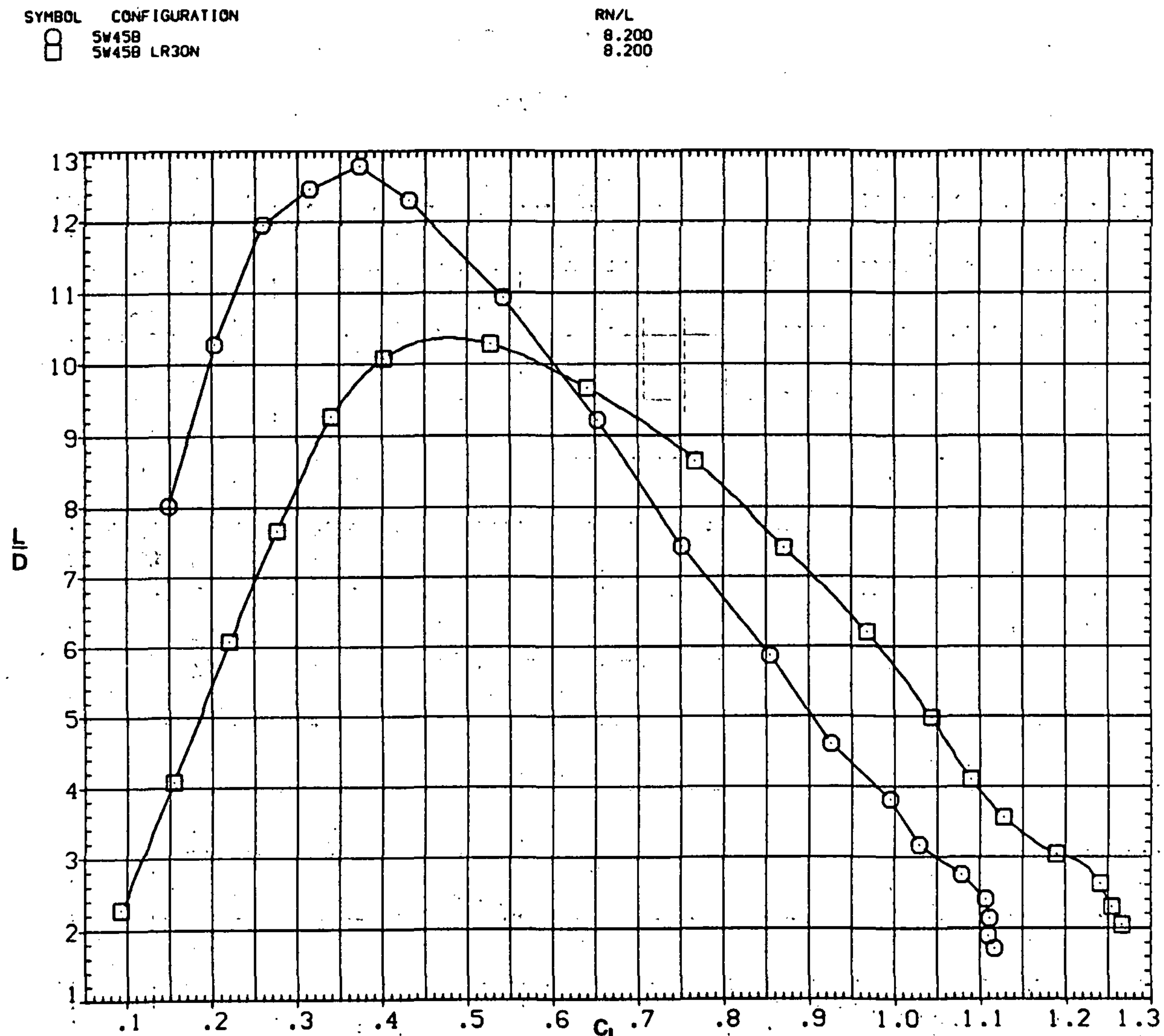

(d) L/D vs C_L

Figure 17.– Continued.

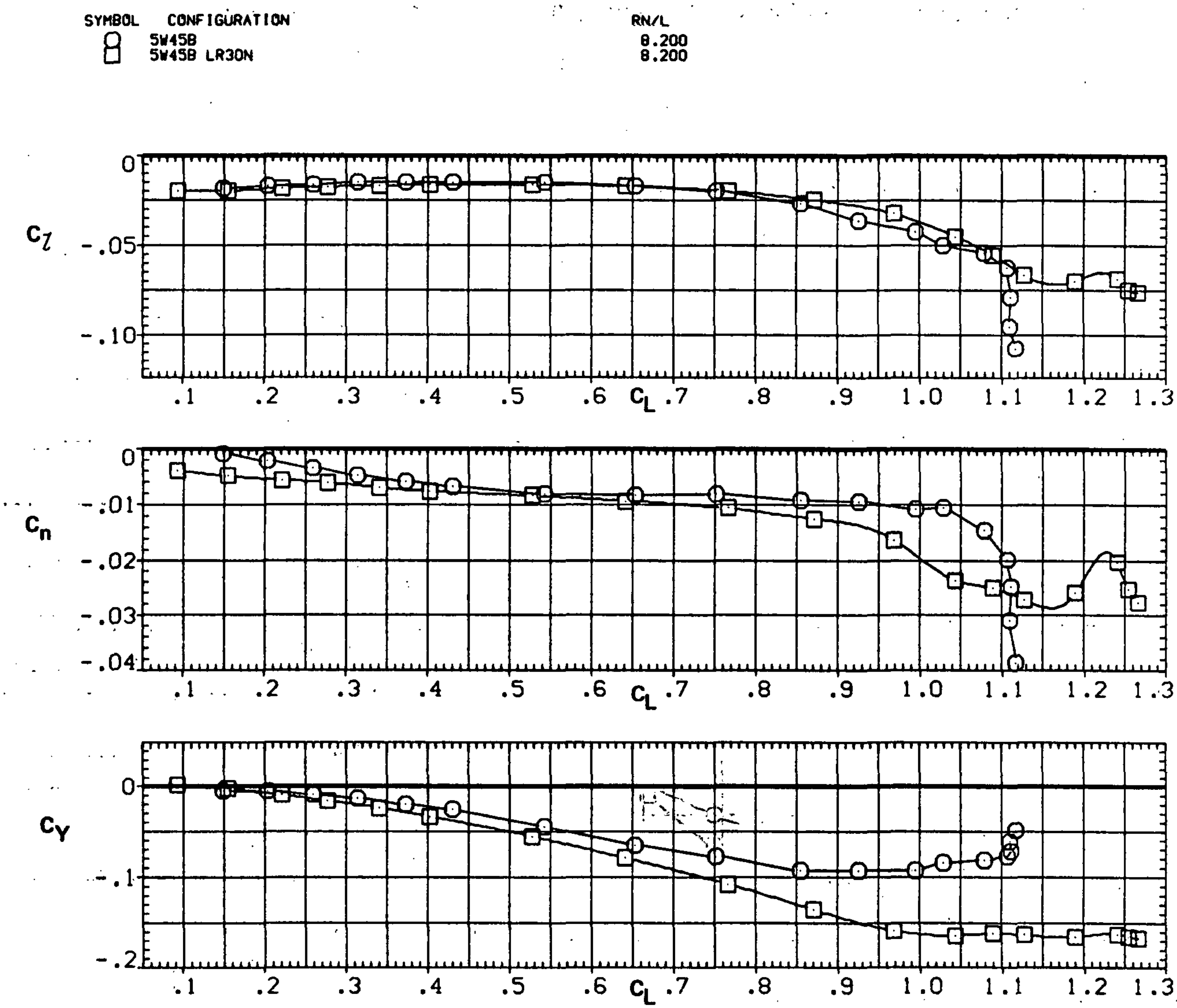

(e) C_l, C_n, and C_Y vs C_L

Figure 17.– Concluded.

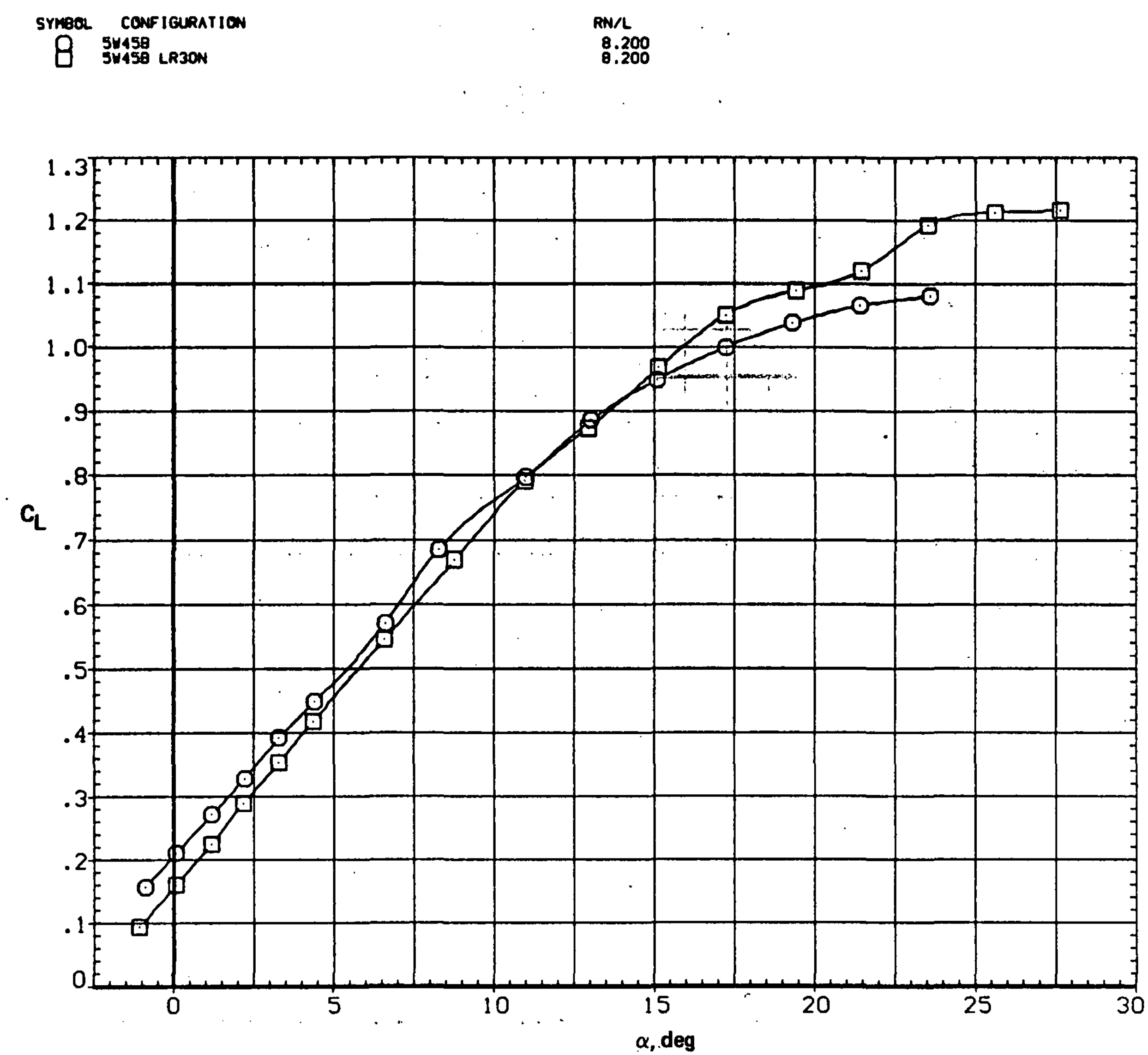

(a) C_L vs α

Figure 18.– Effect of drooped-nose flaps on the static longitudinal stability characteristics of the oblique wing: flaps on both wing panels, $\Lambda = 45°, M = 0.6$.

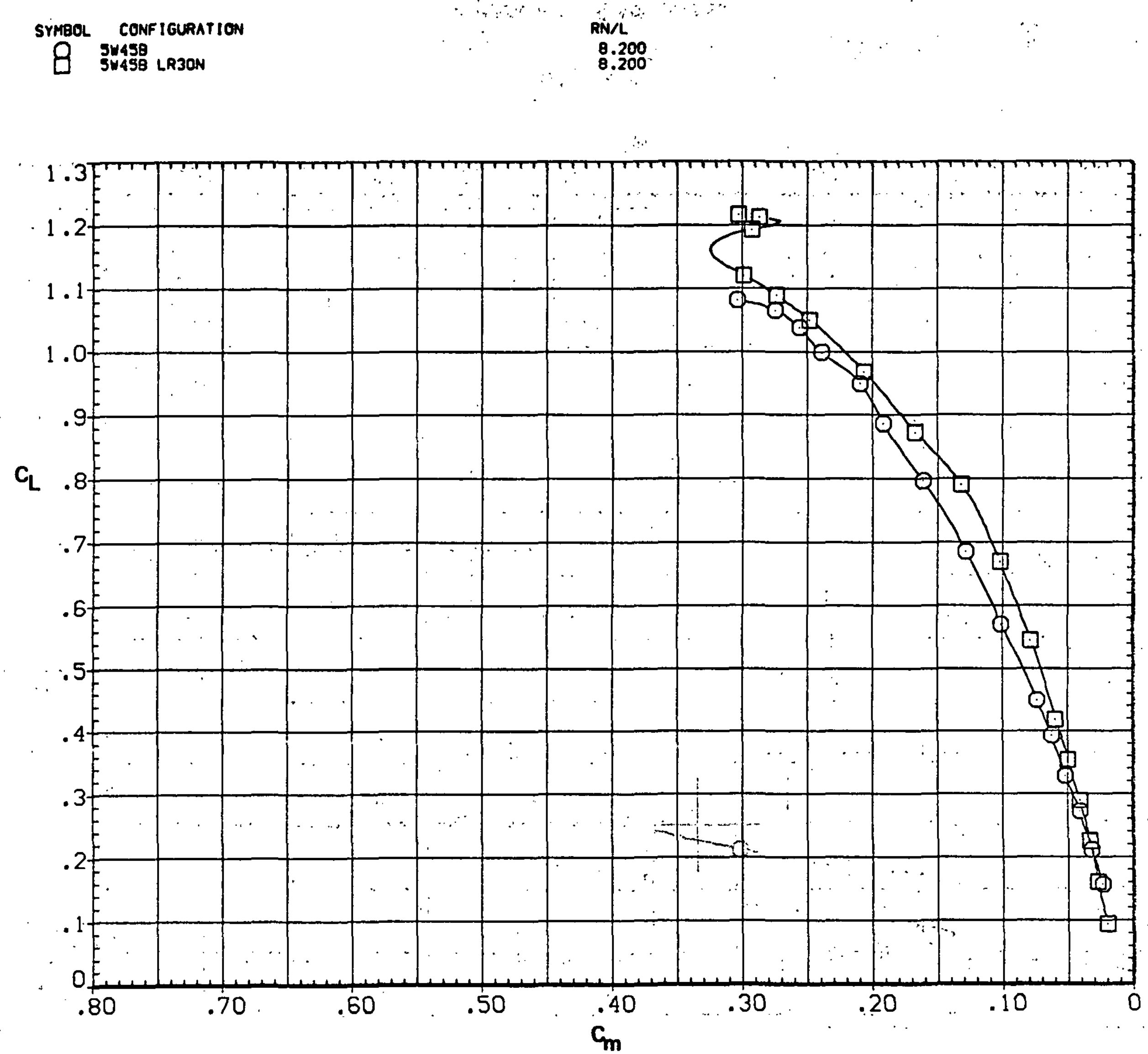

(b) C_L vs C_m

Figure 18.– Continued.

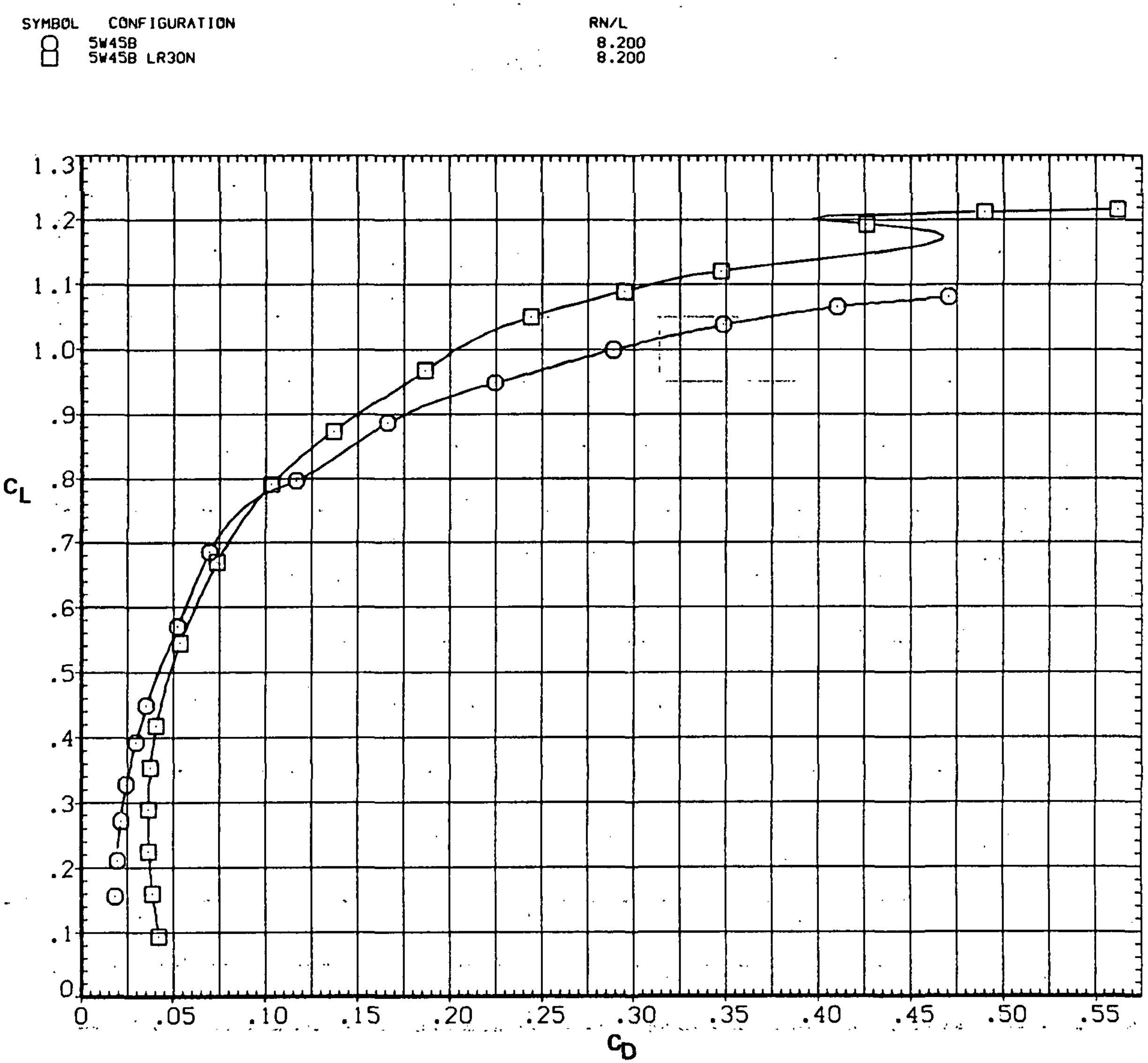

(c) C_L vs C_D

Figure 18.– Continued.

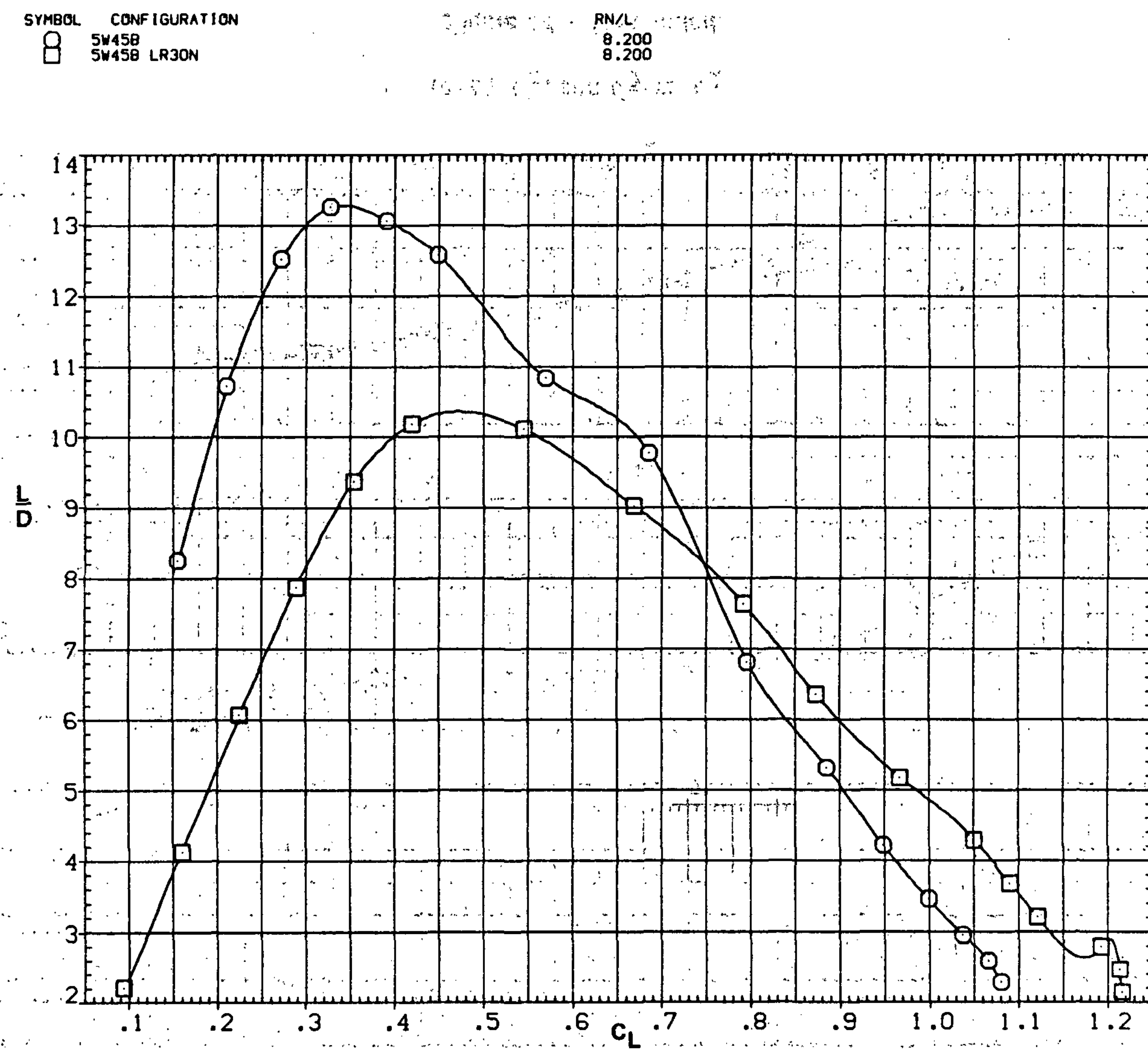

(d) L/D vs C_L

Figure 18.– Continued.

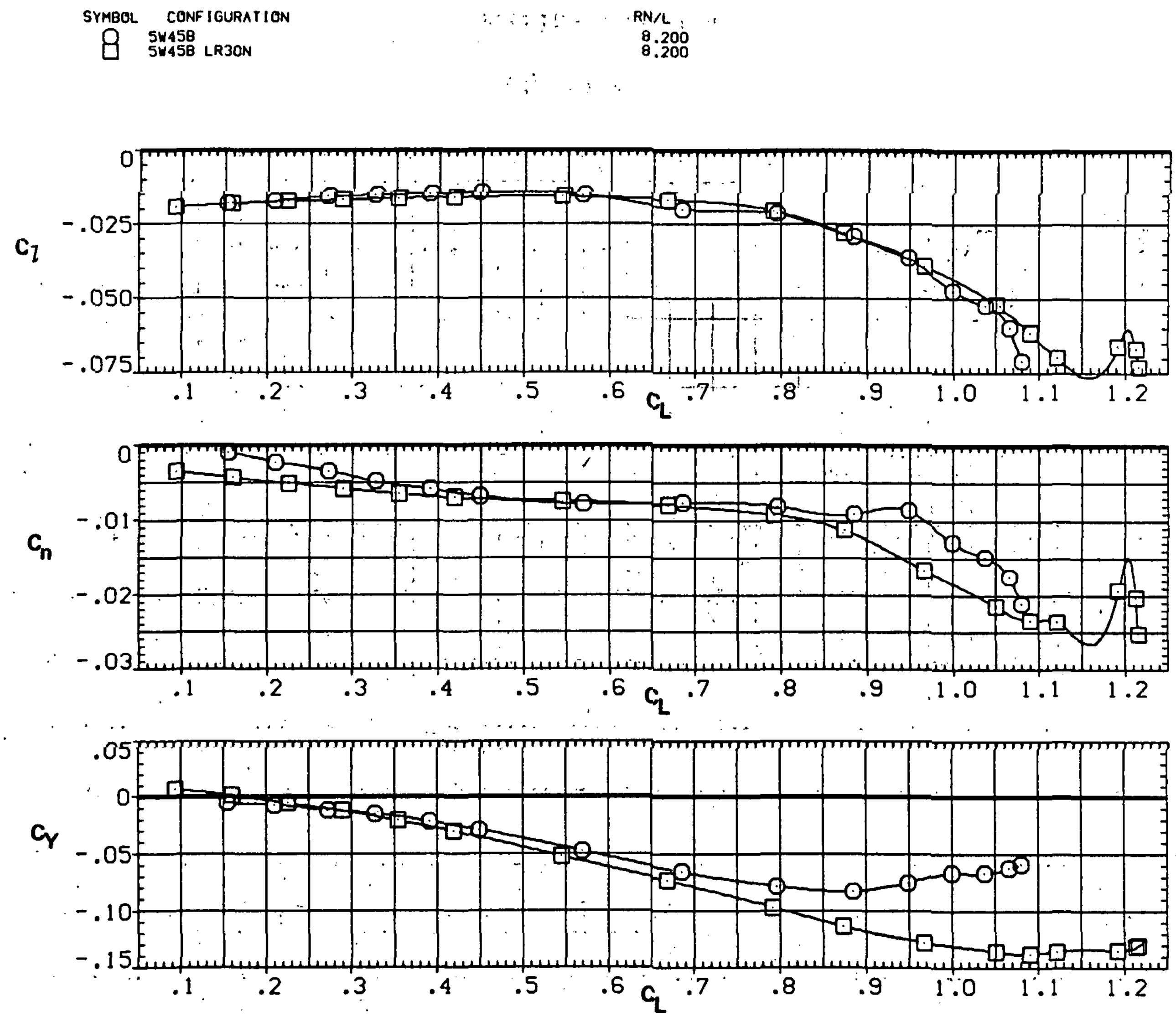

(e) C_l, C_n, and C_Y vs C_L

Figure 18.– Concluded.

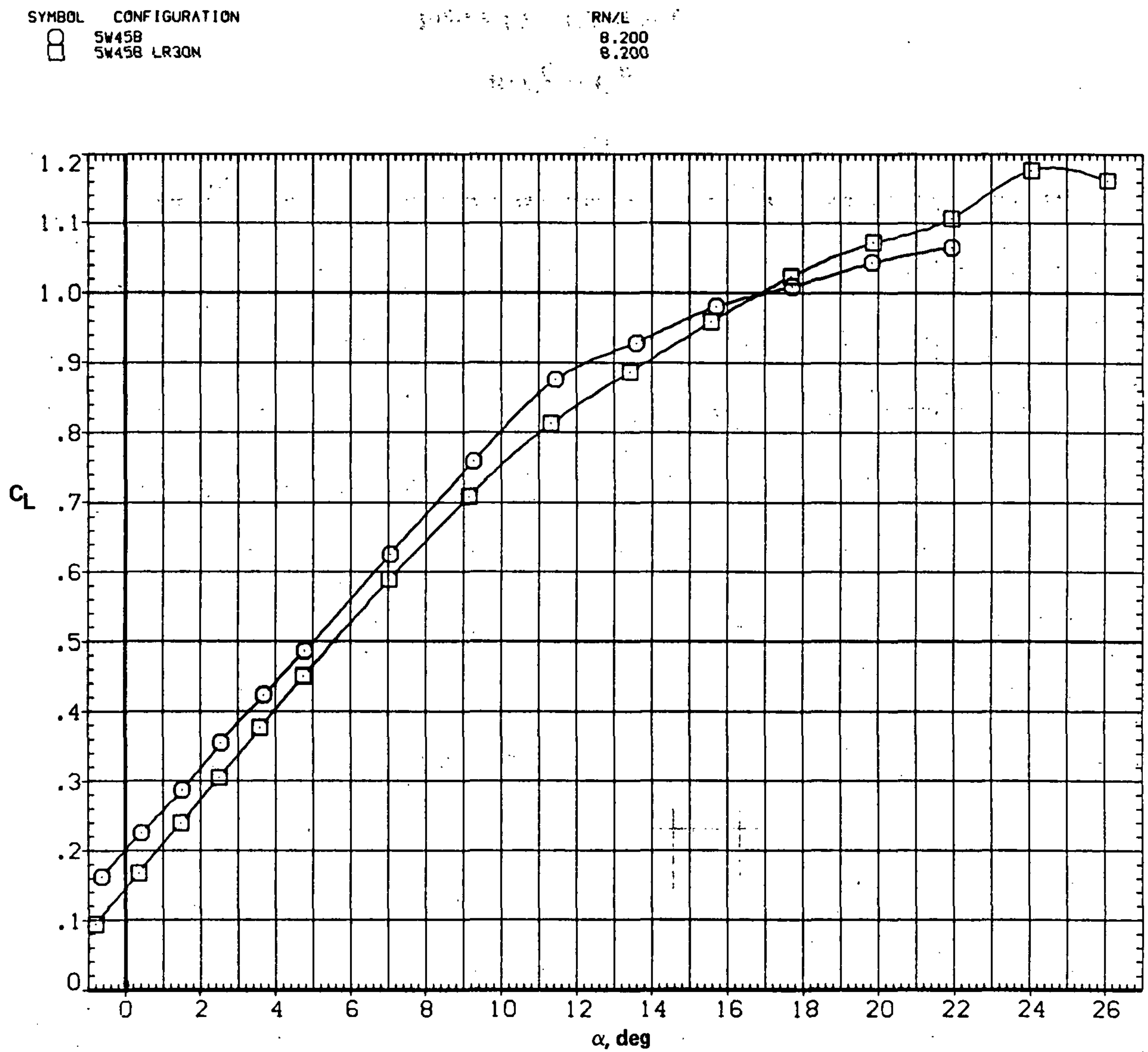

(a) C_L vs α

Figure 19.– Effect of drooped-nose flaps on the static longitudinal characteristics of the oblique wing: flaps on both wing panels, $\Lambda = 45°$, $M = 0.8$.

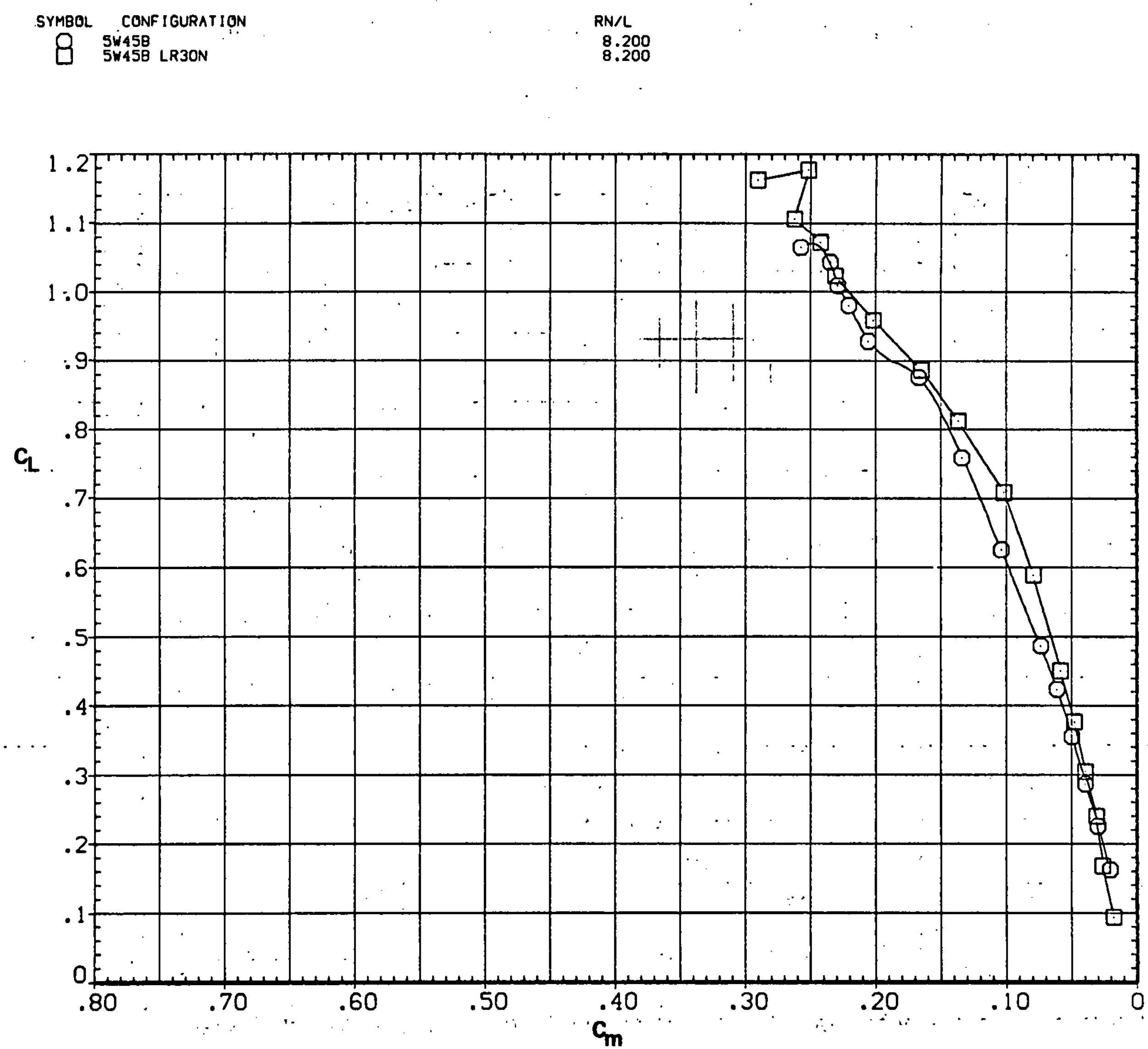

(b) C_L vs C_m

Figure 19.– Continued.

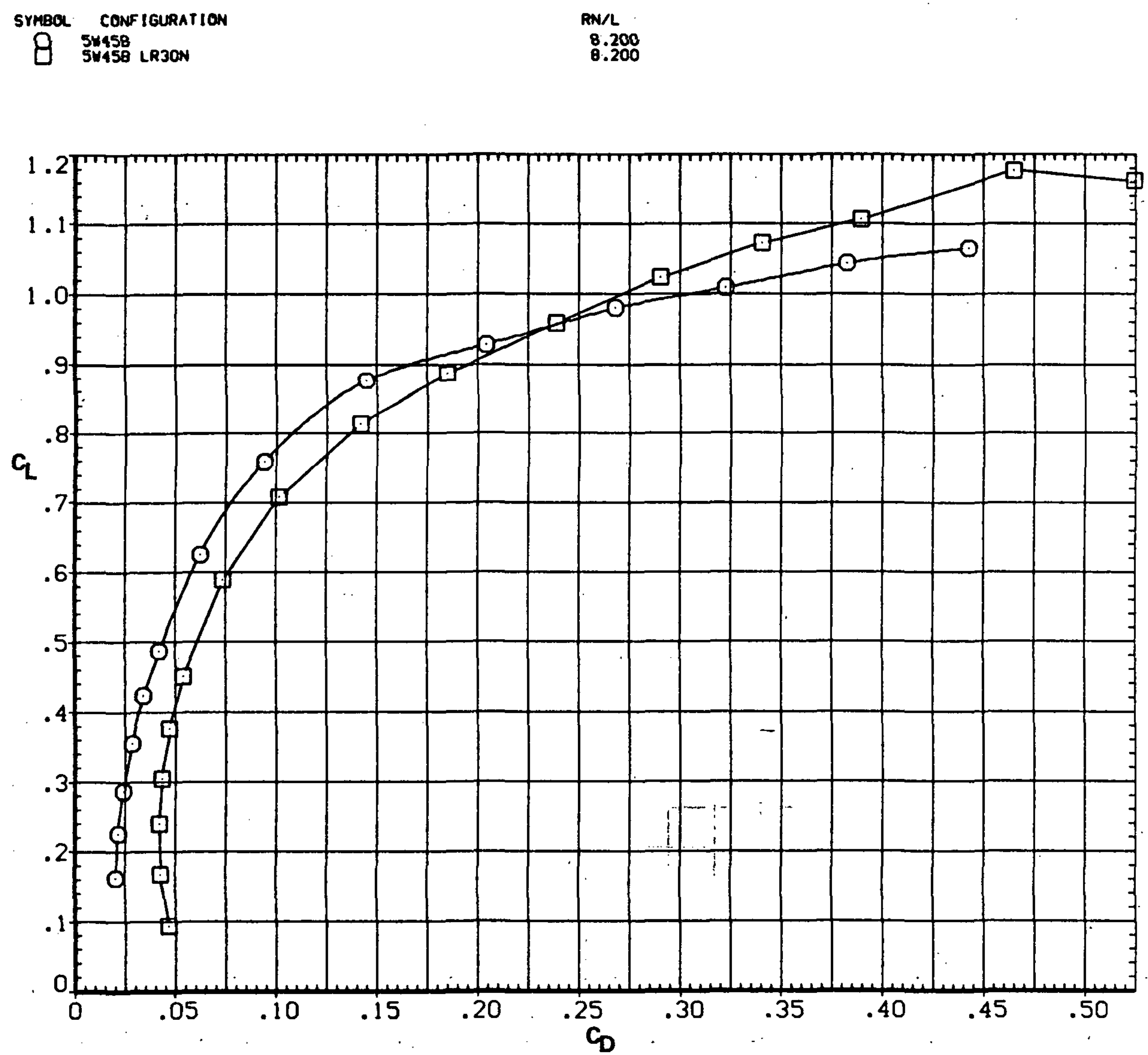

(c) C_L vs C_D

Figure 19.– Continued.

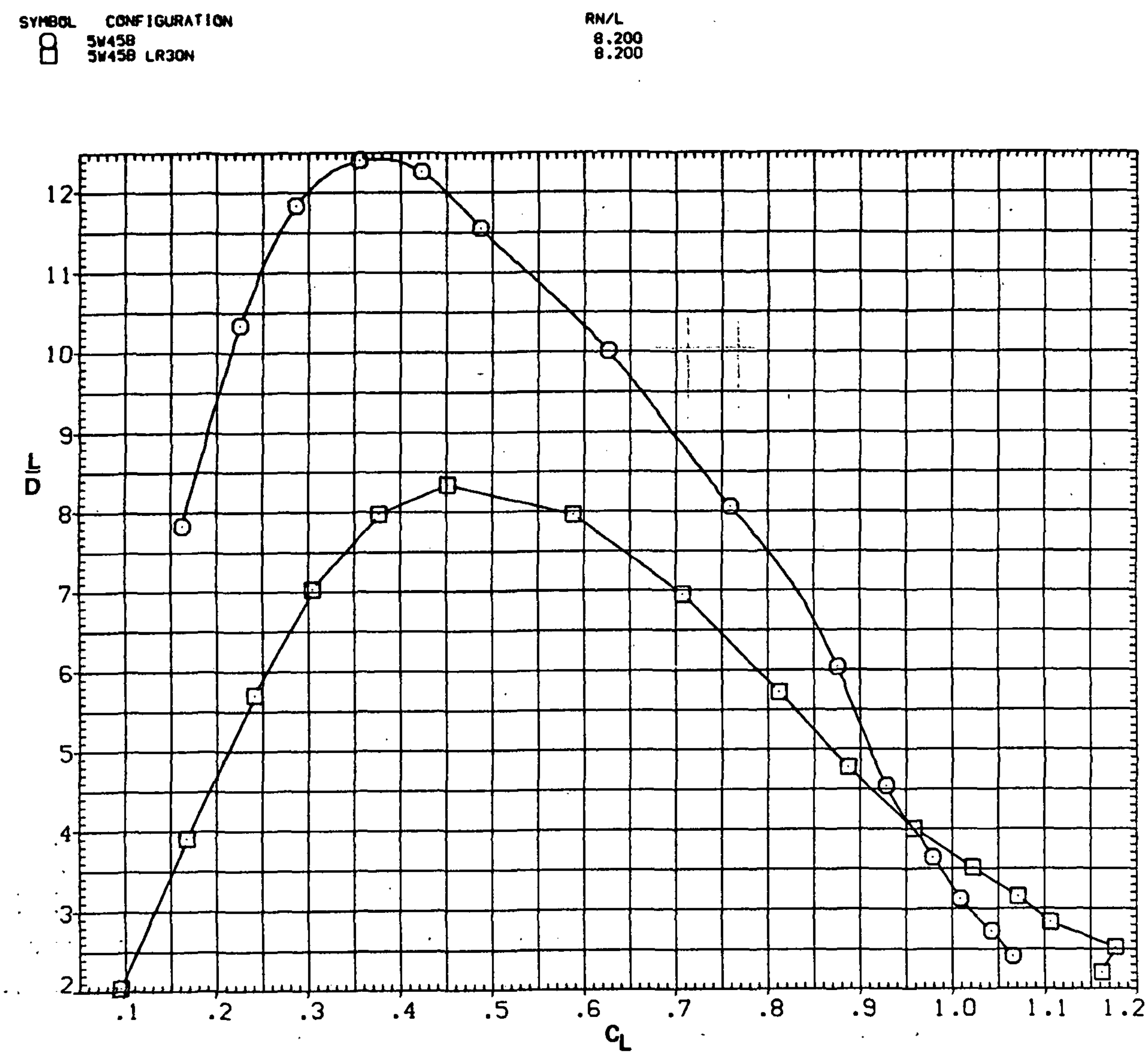

(d) L/D vs C_L

Figure 19.– Continued.

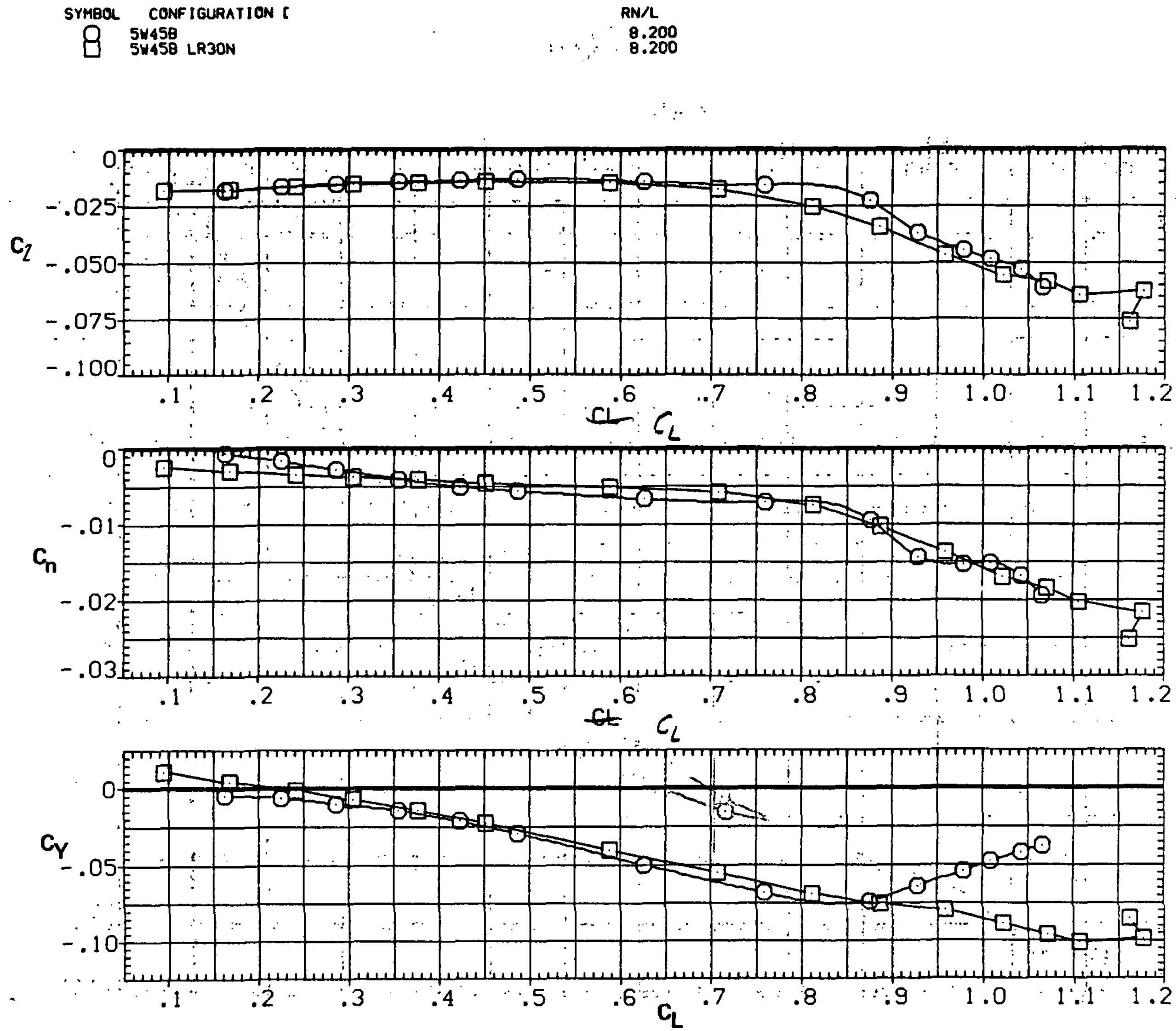

(e) C_l, C_n, and C_Y vs C_L

Figure 19.– Concluded.

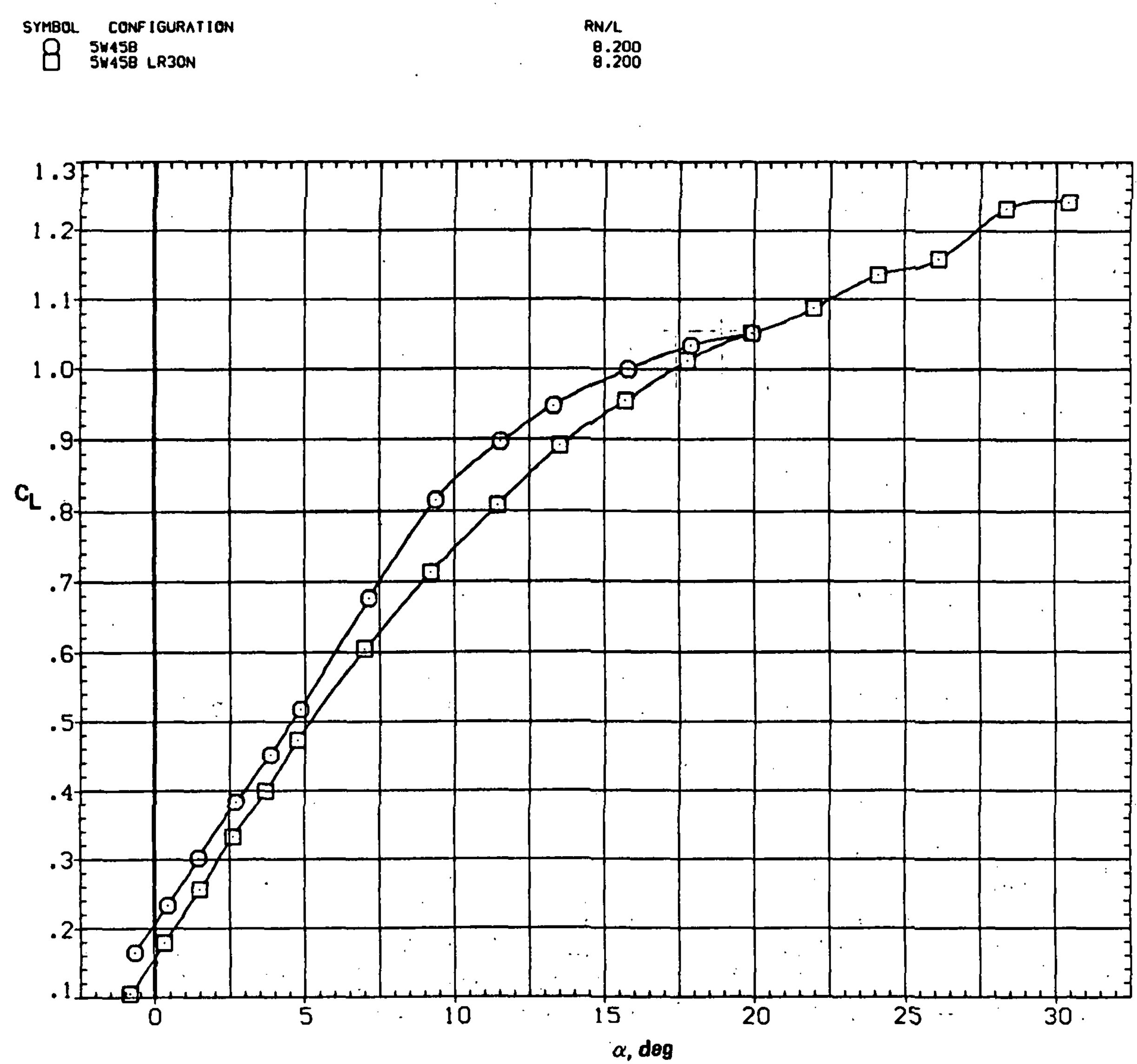

(a) C_L vs α

Figure 20.– Effect of drooped-nose flaps on the static longitudinal characteristics of the oblique wing: flaps on both wing panels, $\Lambda = 45°$, $M = 0.9$.

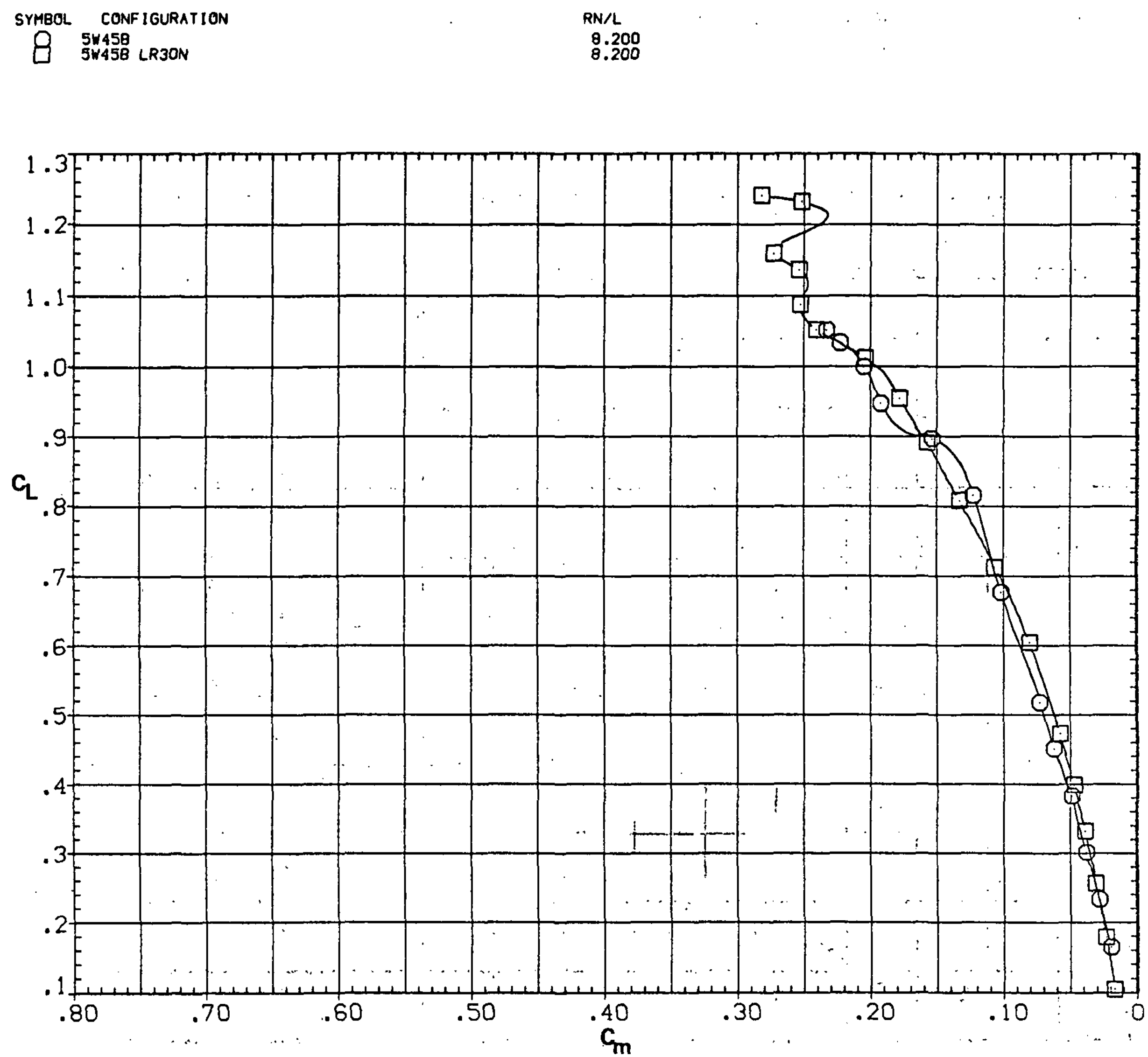

(b) C_L vs C_m

Figure 20.—Continued.

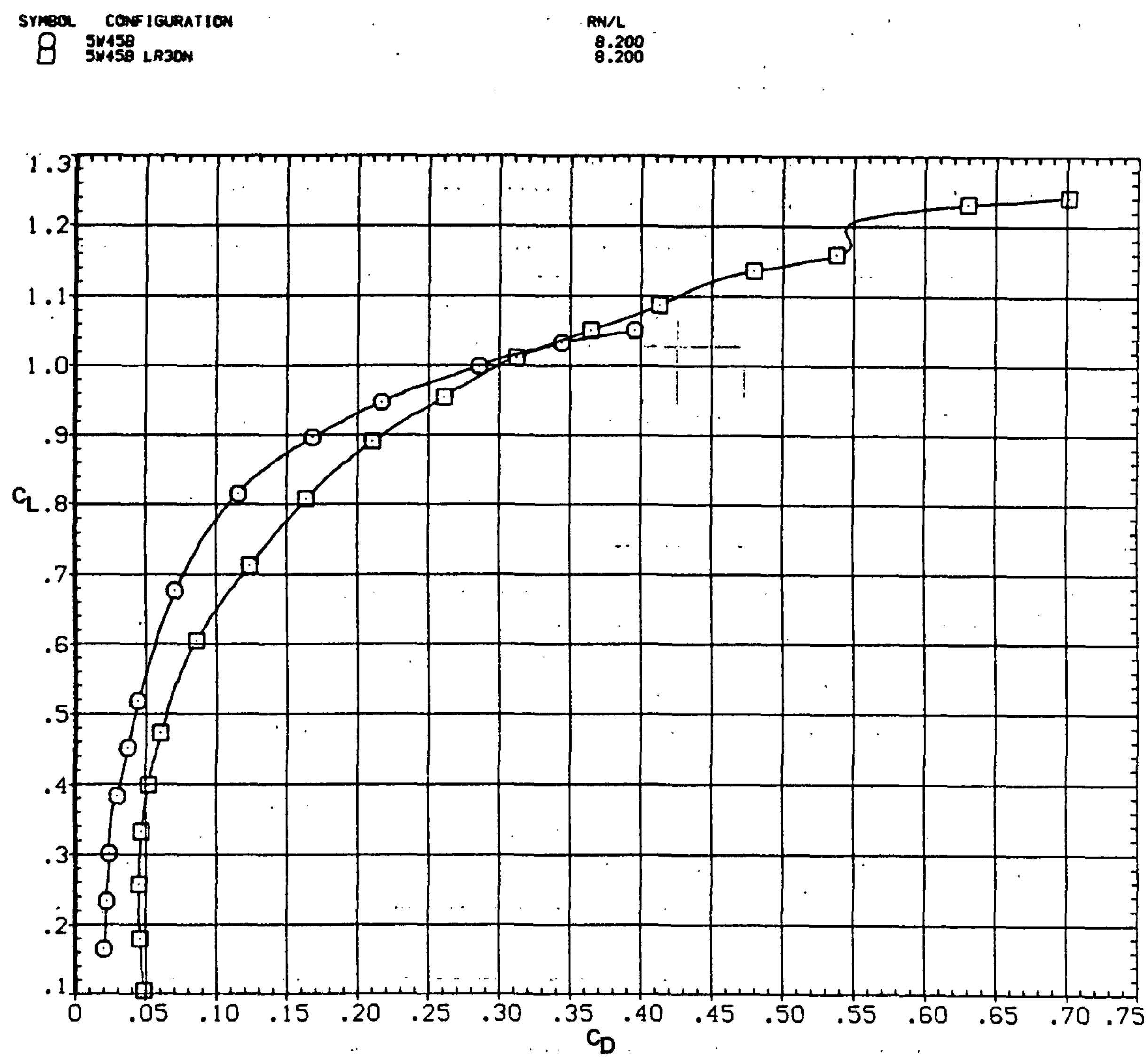

(c) C_L vs C_D

Figure 20.– Continued.

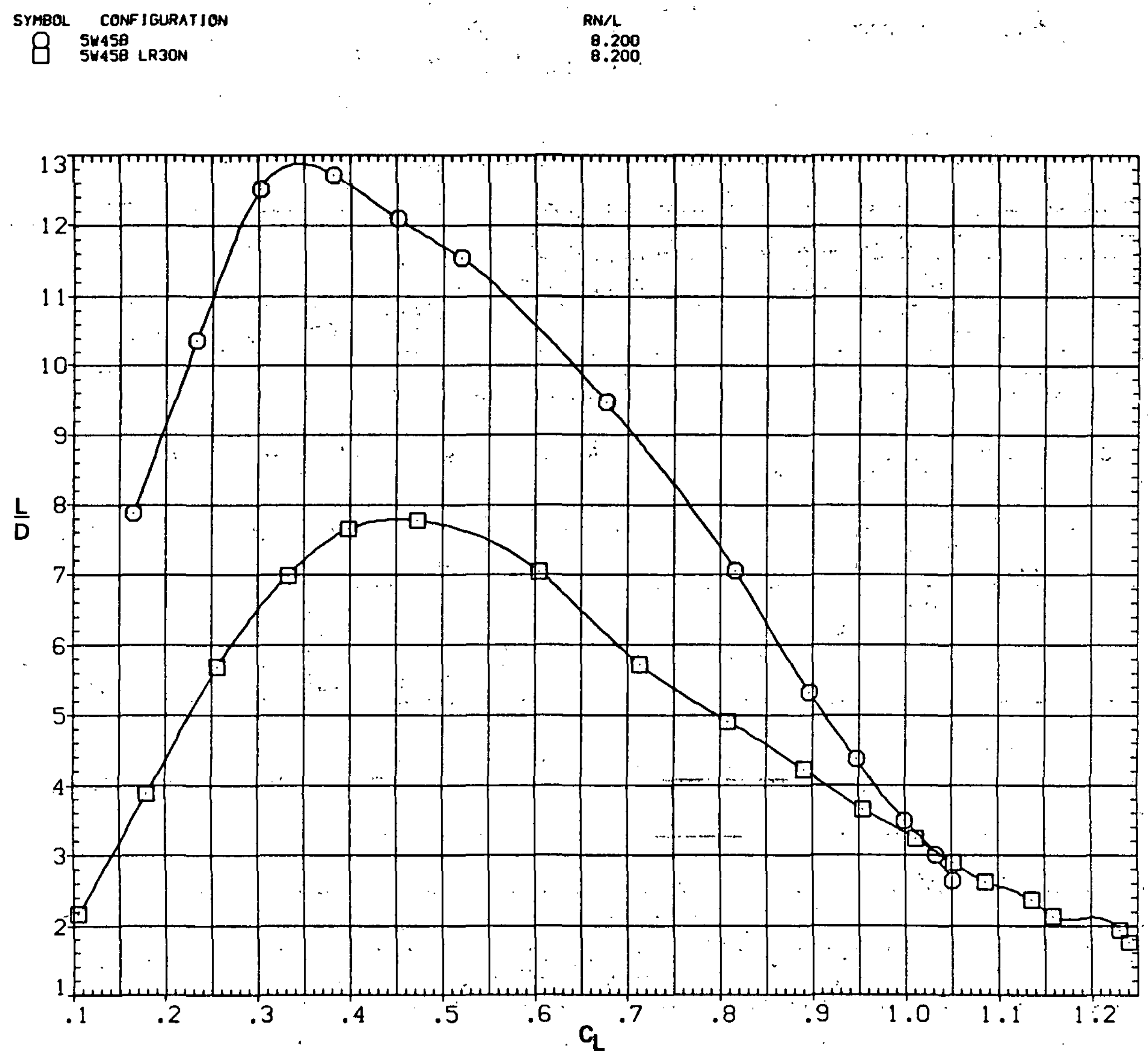

(d) L/D vs C_L

Figure 20.– Continued.

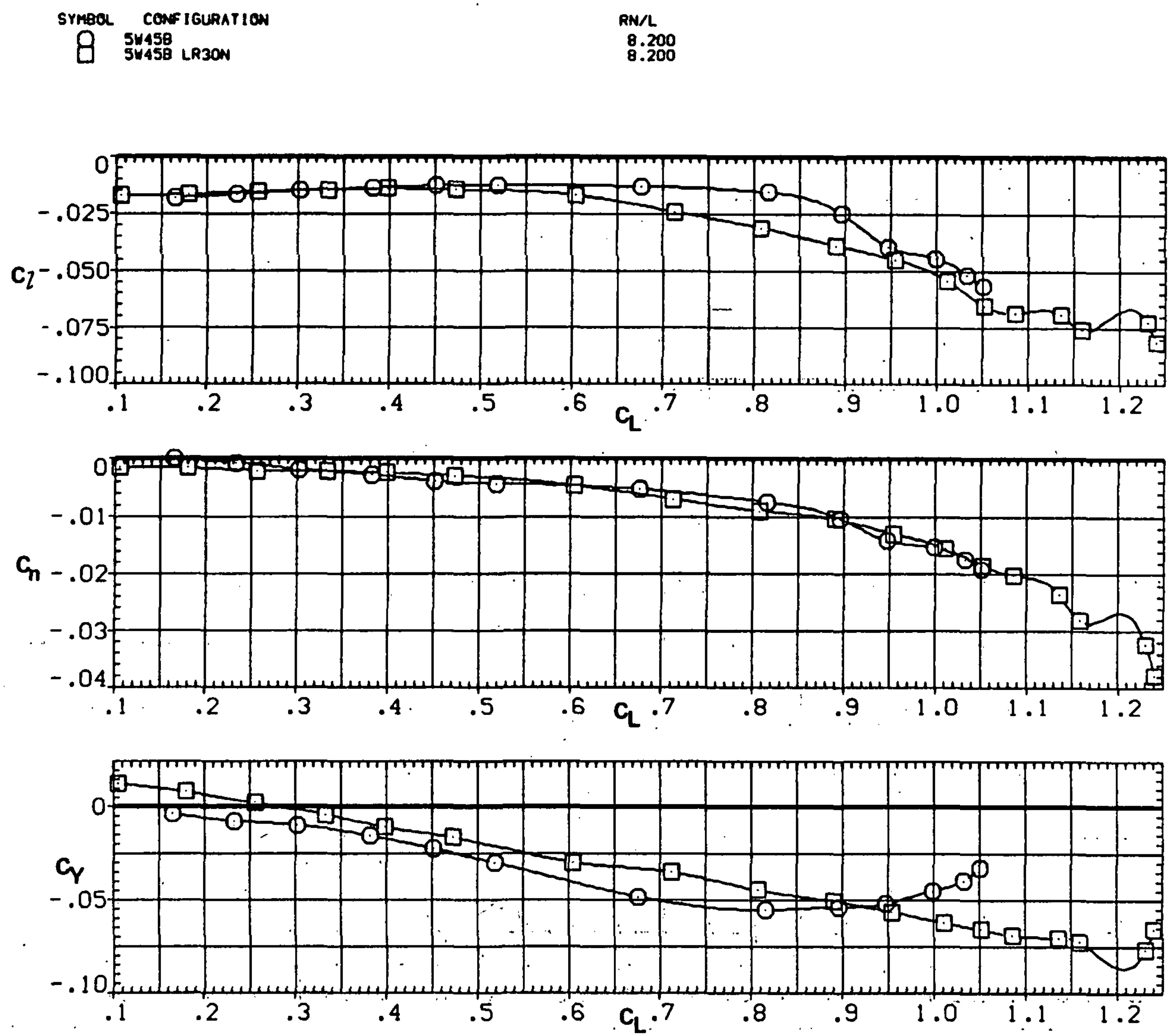

(e) C_l, C_n, and C_Y vs C_L

Figure 20.– Concluded.

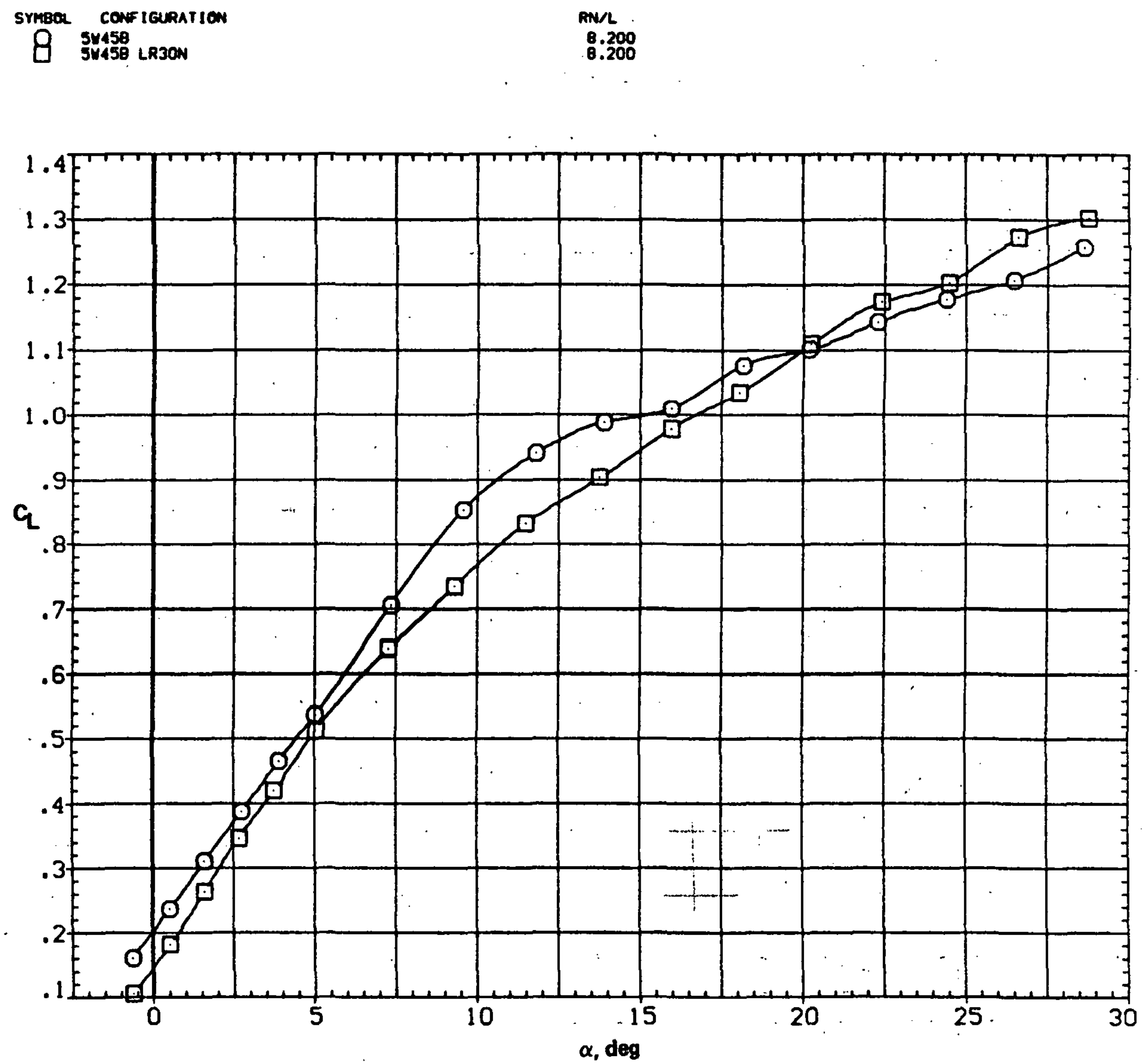

(a) C_L vs α

Figure 21.– Effect of drooped-nose flaps on the static longitudinal characteristics of the oblique wing: flaps on both wing panels, $\Lambda = 45°$, $M = 0.95$.

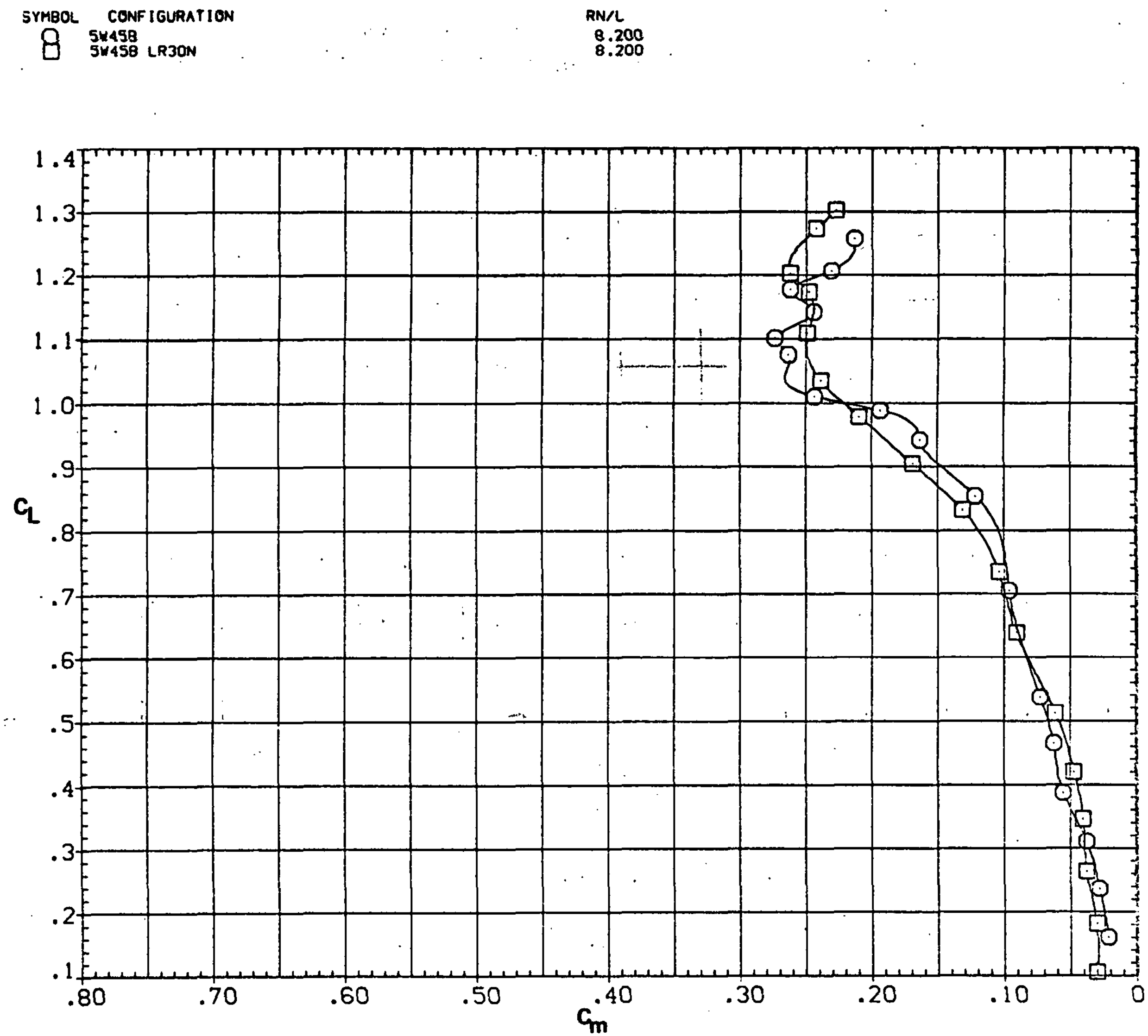

(b) C_L vs C_m

Figure 21.– Continued.

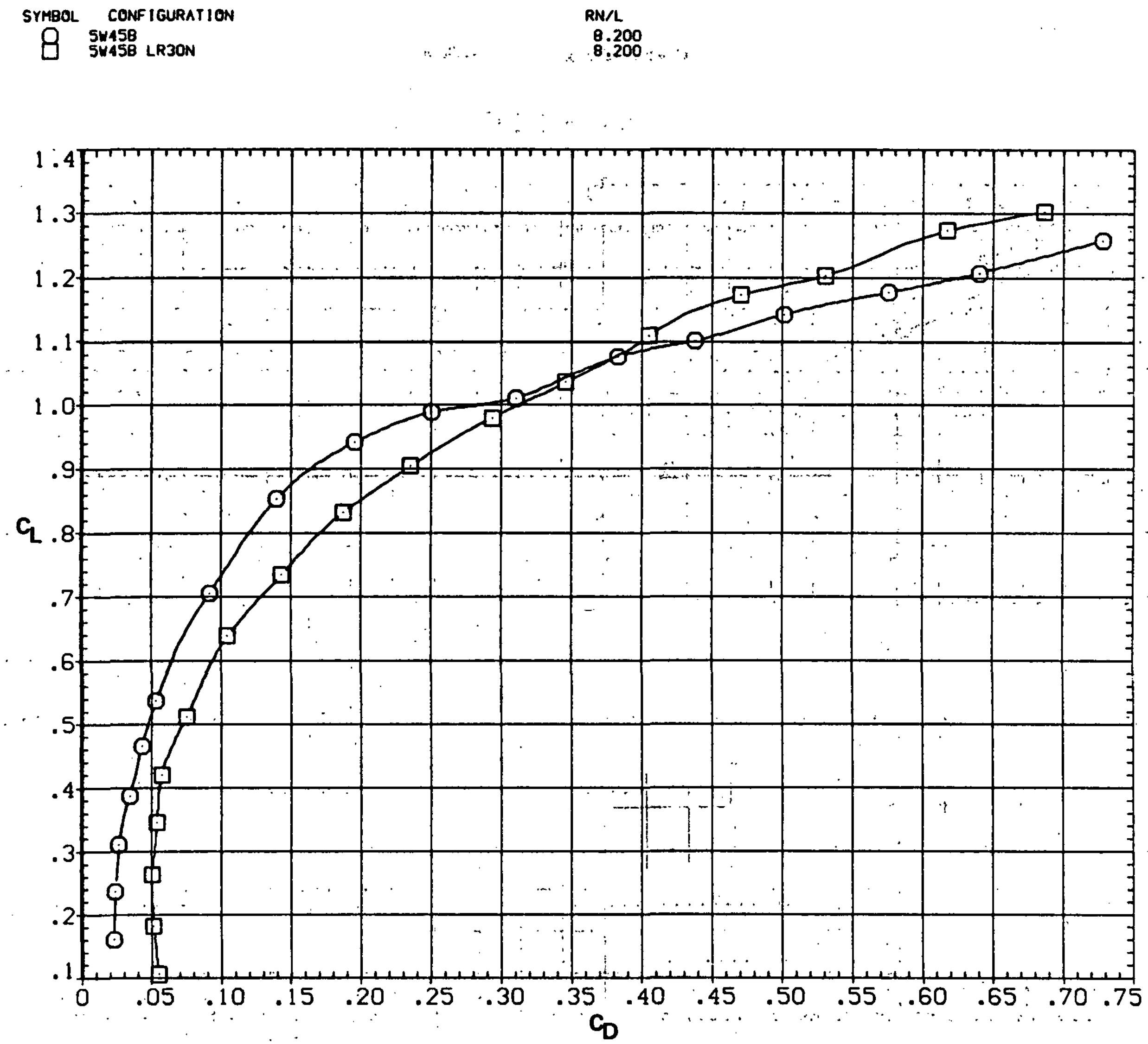

(c) C_L vs C_D

Figure 21.– Continued.

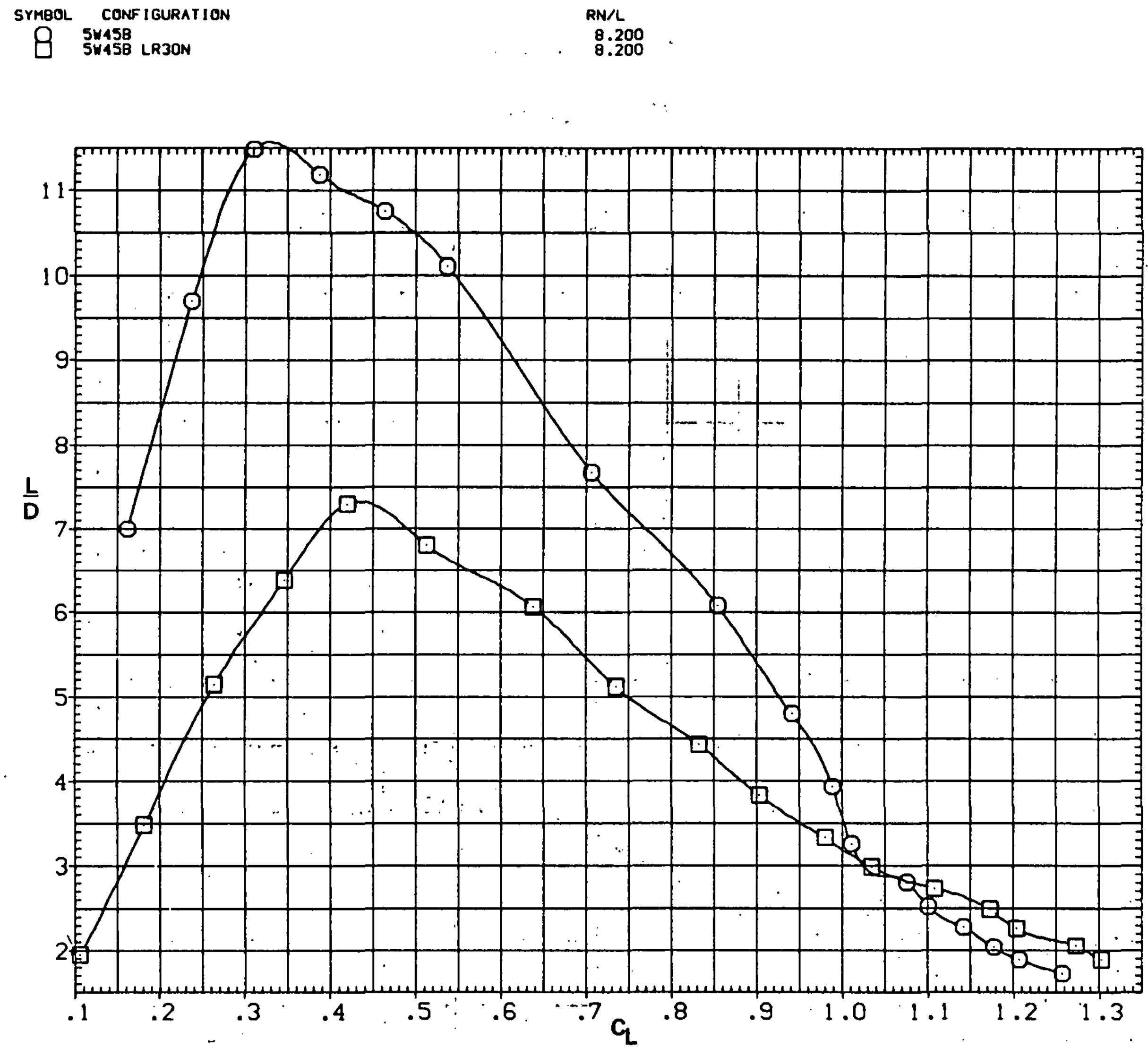

(d) L/D vs C_L

Figure 21.– Continued.

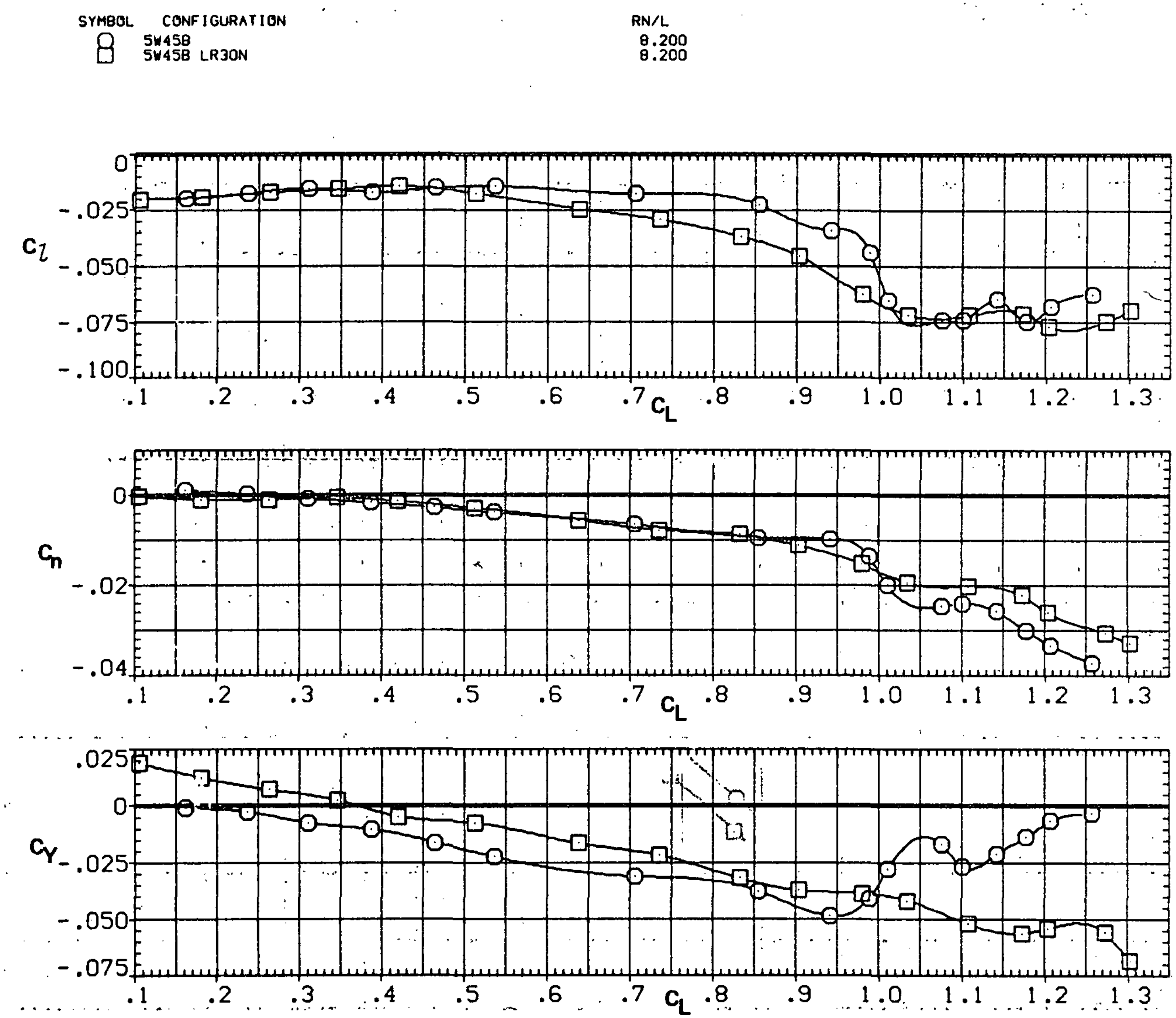

(e) C_l, C_n, and C_Y vs C_L

Figure 21.– Concluded.

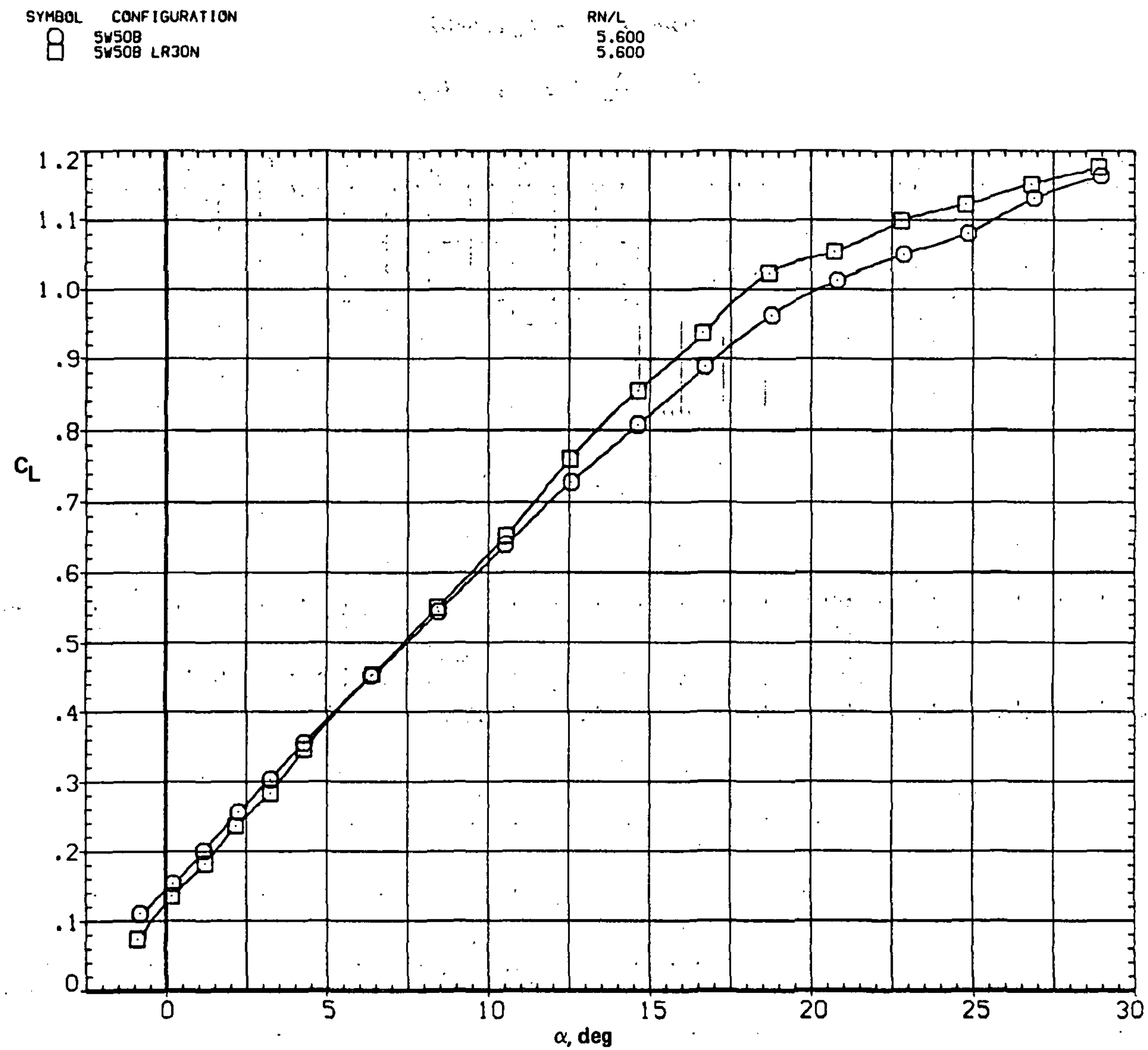

(a) C_L vs α

Figure 22.– Effect of drooped-nose flaps on the static longitudinal characteristics of the oblique wing: flaps on both wing panels, $\Lambda = 50°, M = 0.25$.

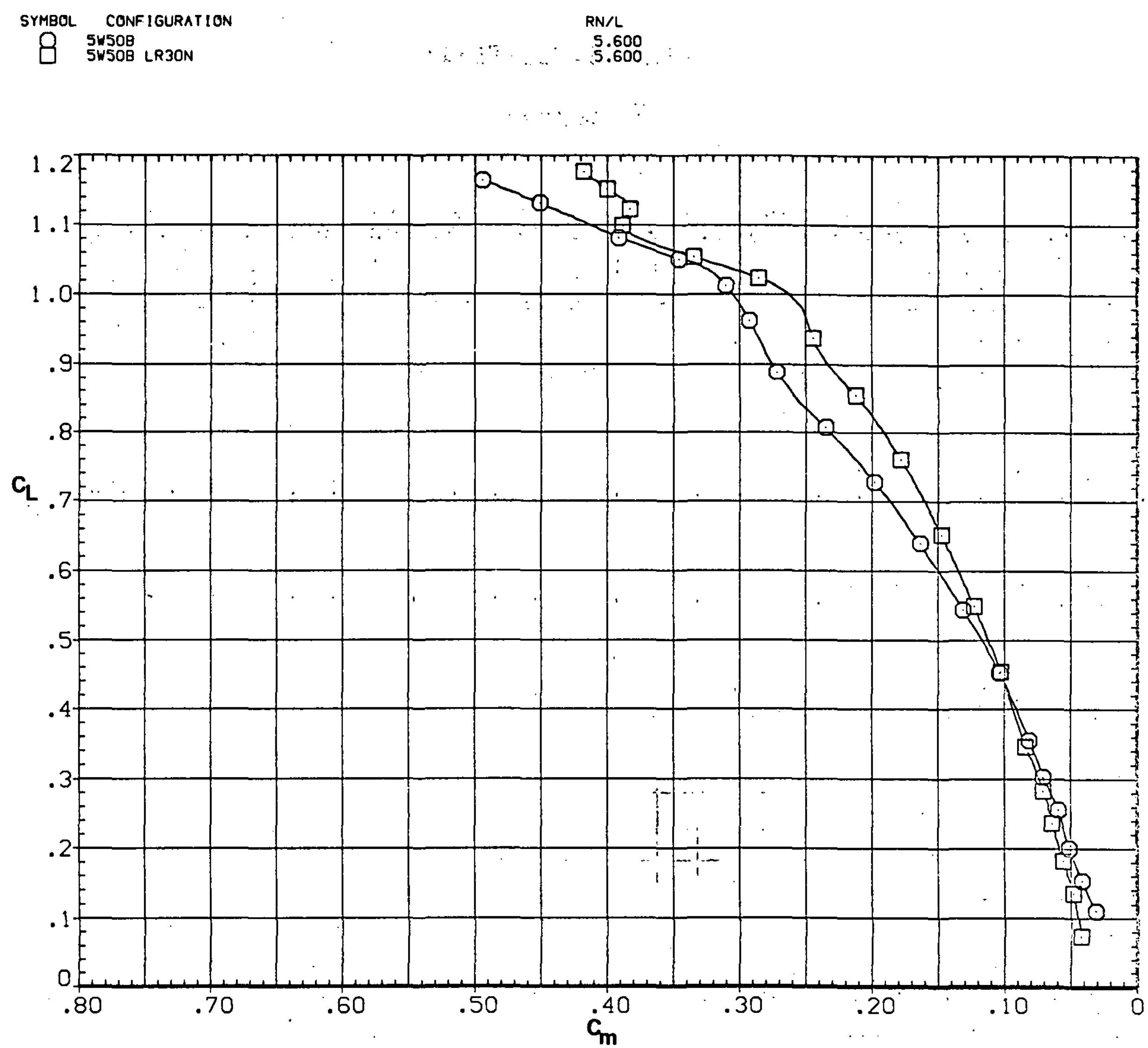

(b) C_L vs. C_m

Figure 22.– Continued.

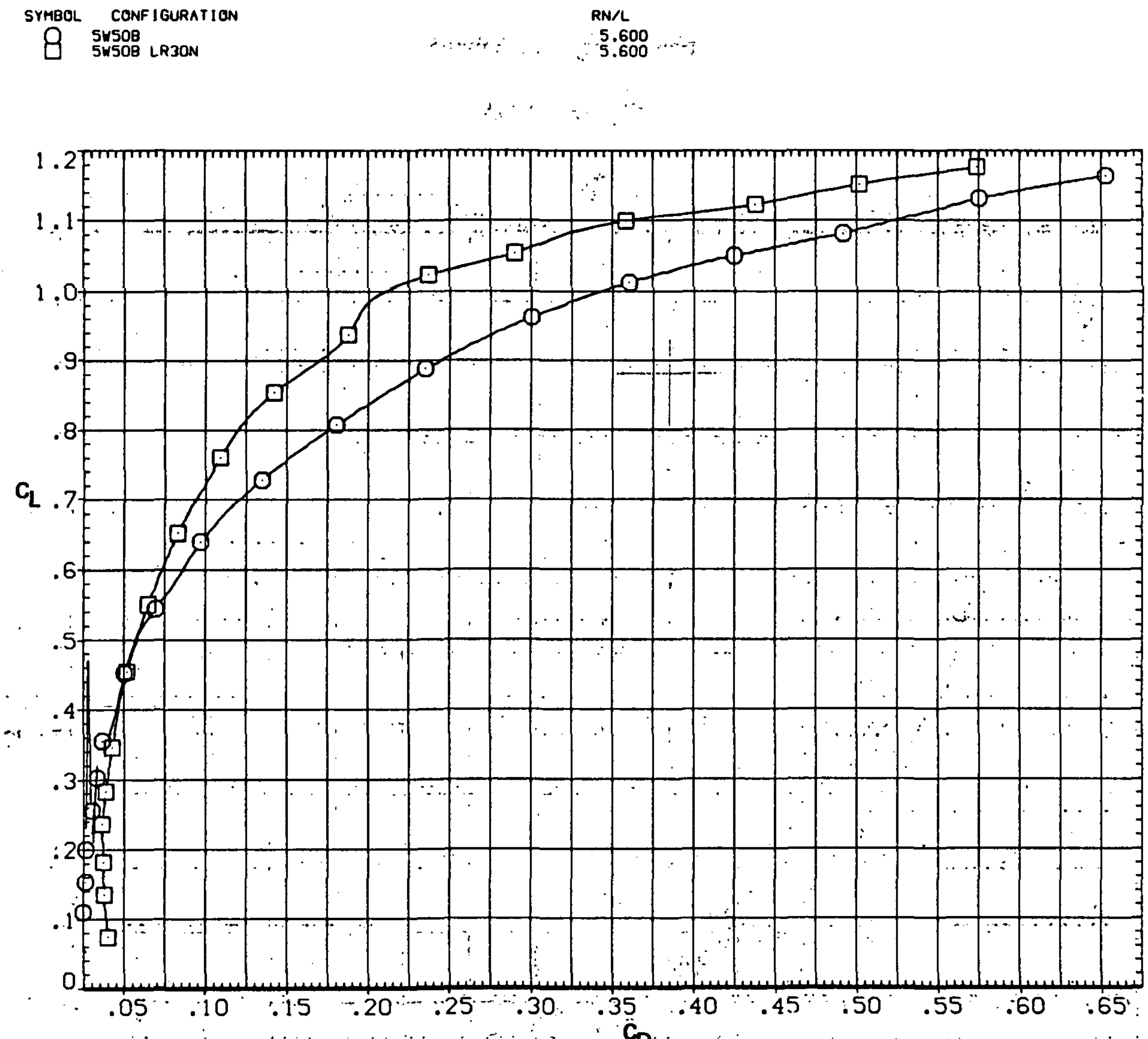

(c) C_L vs C_D

Figure 22.– Continued.

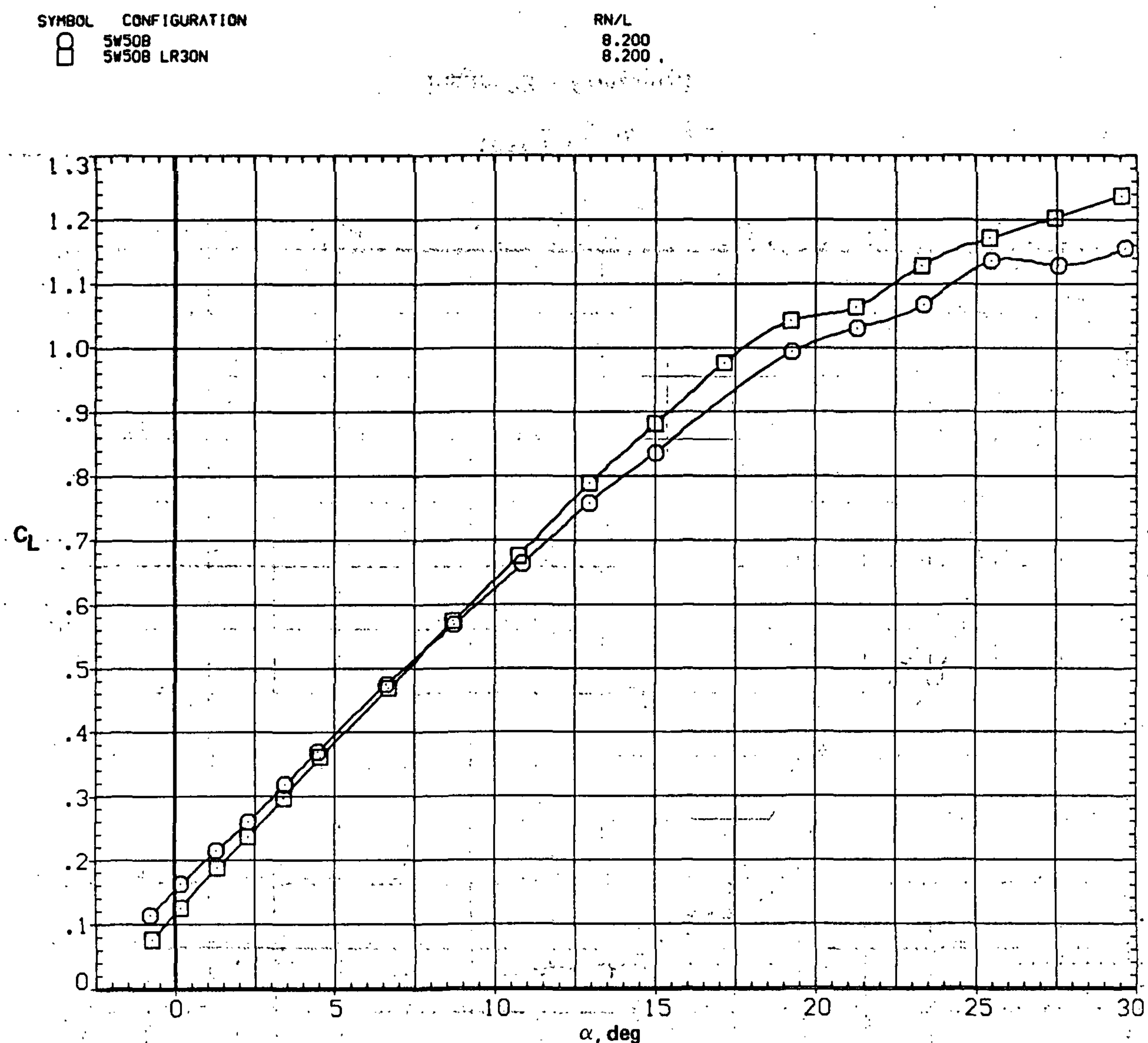

(a) C_L vs α

Figure 23.– Effect of drooped-nose flaps on the static longitudinal characteristics of the oblique wing: flaps on both wing panels, $\Lambda = 50°$, $M = 0.4$.

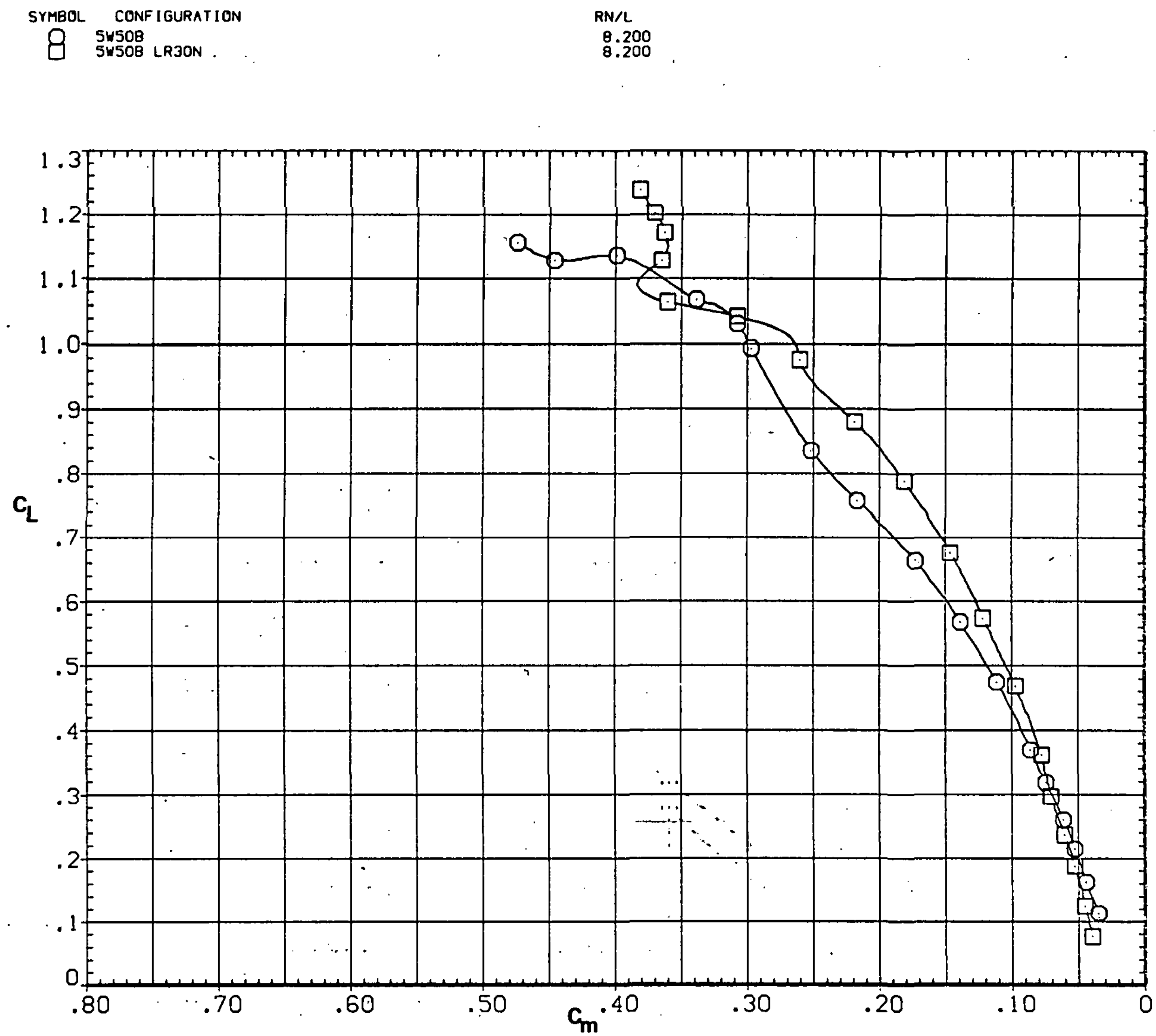

(b) C_L vs C_m

Figure 23.– Continued.

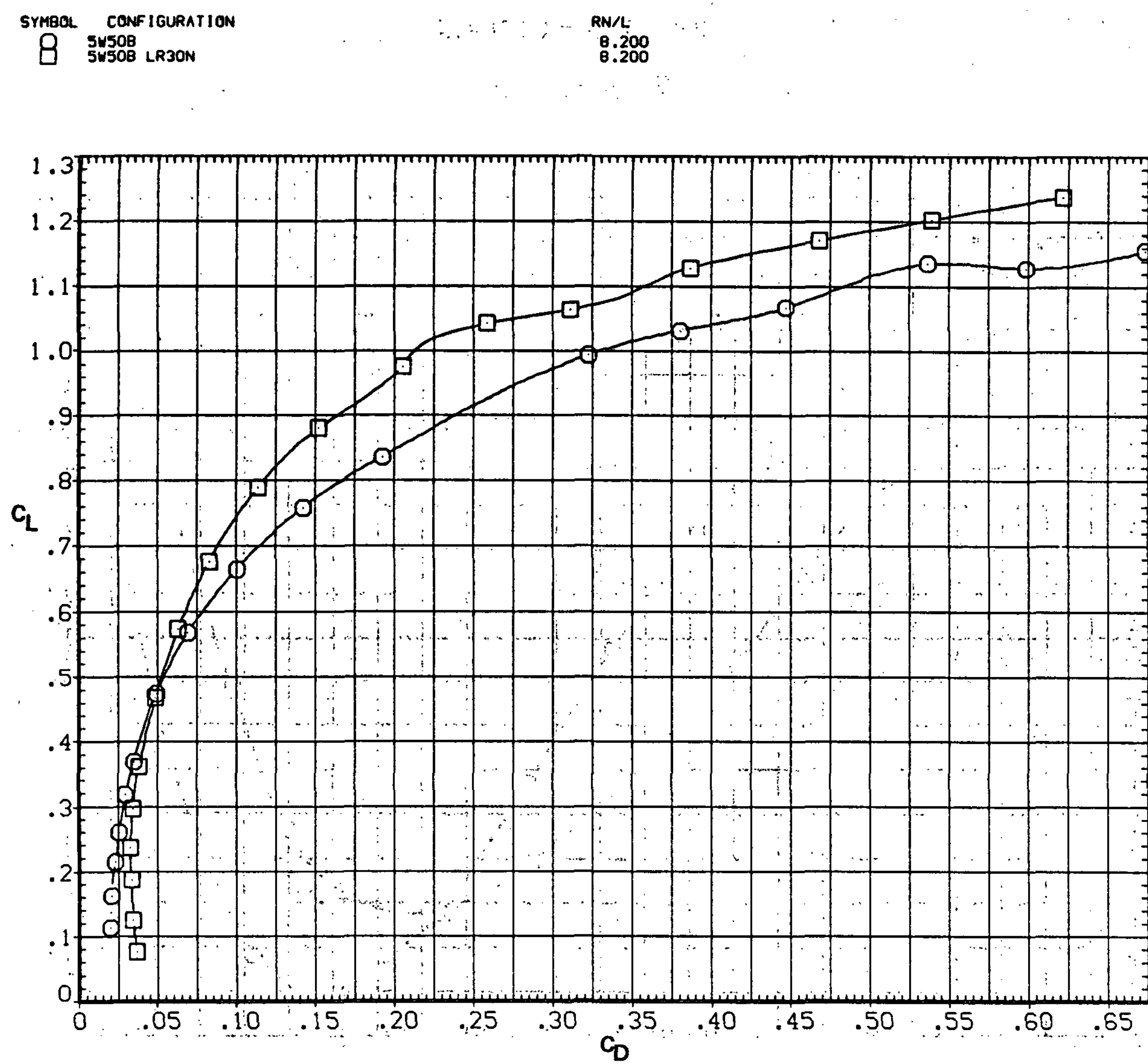

SYMBOL CONFIGURATION
5W50B
5W50B LR30N
RN/L
8.200
8.200
C_L
1.3
1.2
1.1
1.0
.9
.8
.7
.6
.5
.4
.3
.2
.1
0
.05
.10
.15
.20
.25
.30
.35
.40
.45
.50
.55
.60
.65
C_D

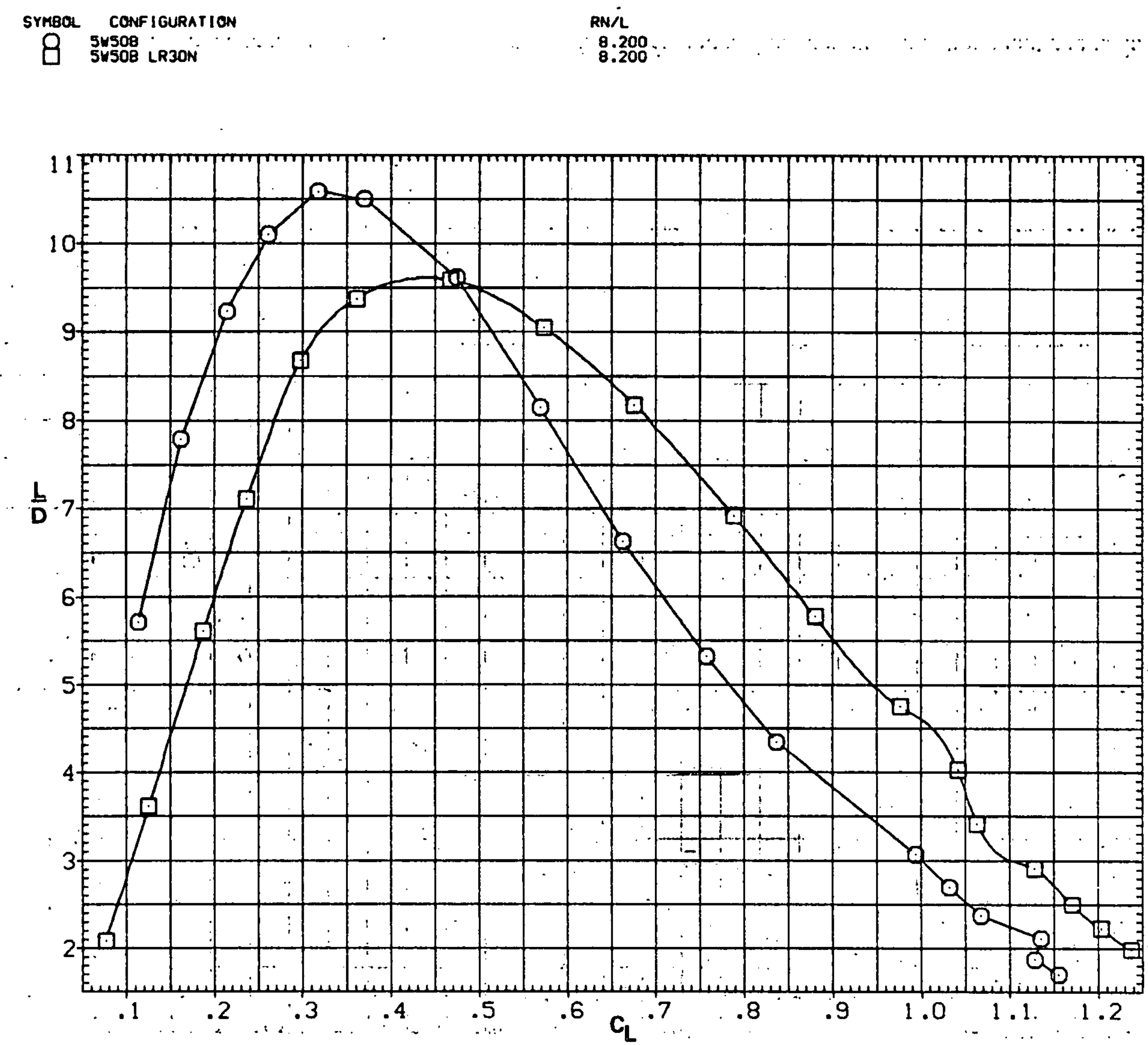

(d) L/D vs C_L

Figure 23.– Continued.

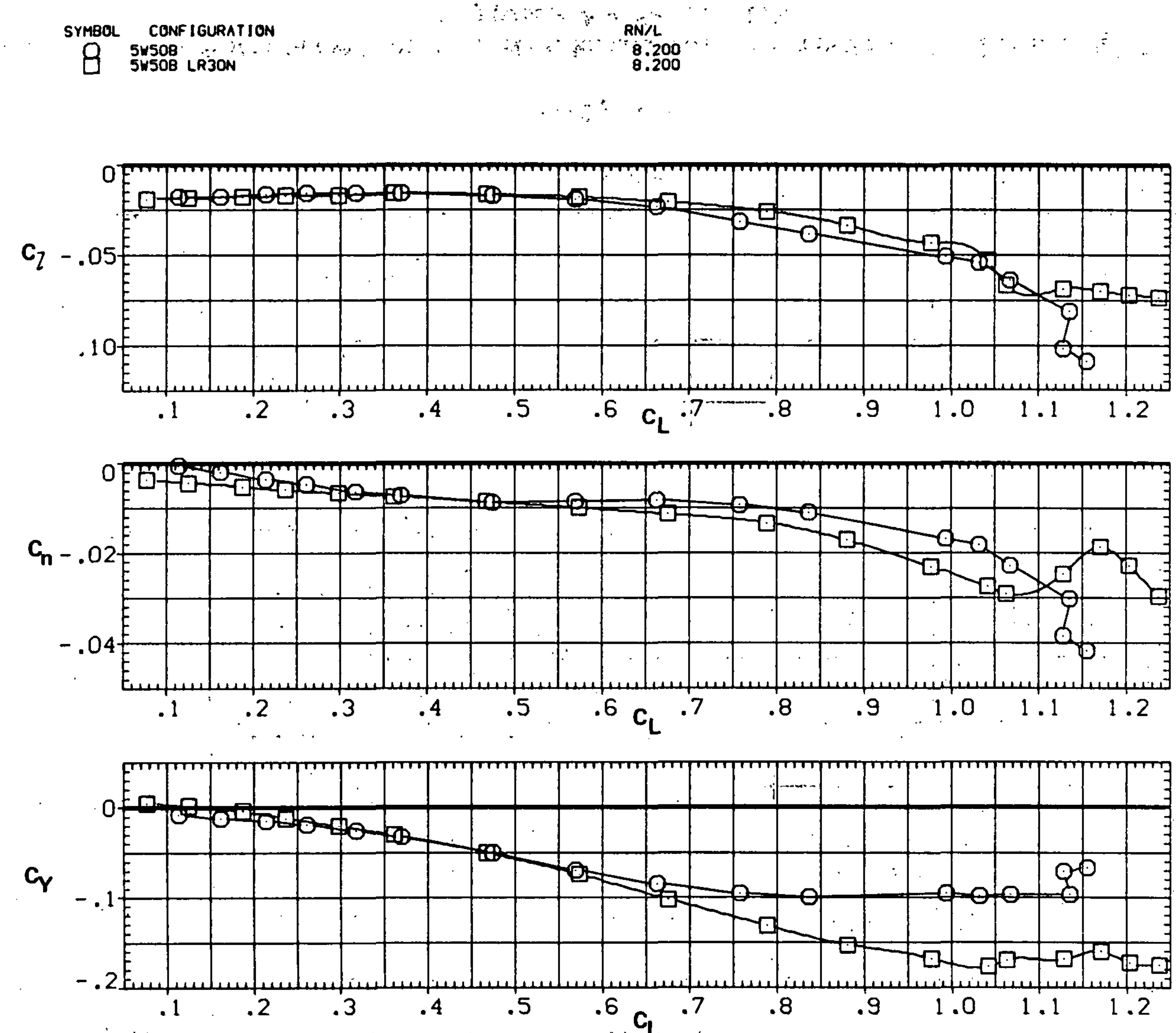

(e) C_l, C_n, and C_Y vs. C_L

Figure 23.– Concluded.

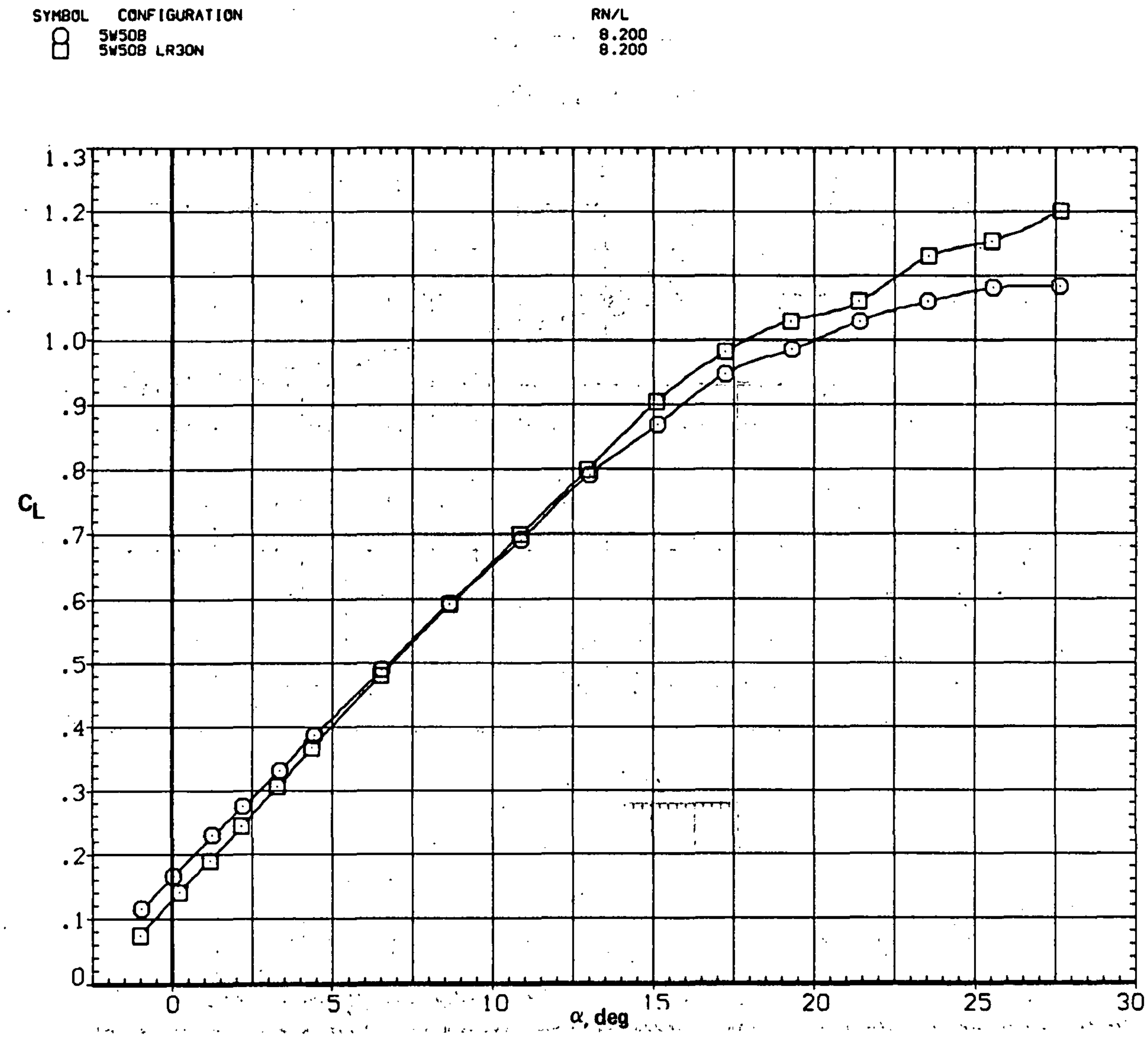

(a) C_L vs α

Figure 24.– Effect of drooped-nose flaps on the static longitudinal characteristics of the oblique wing: flaps on both wing panels, $\Lambda = 50°, M = 0.6$.

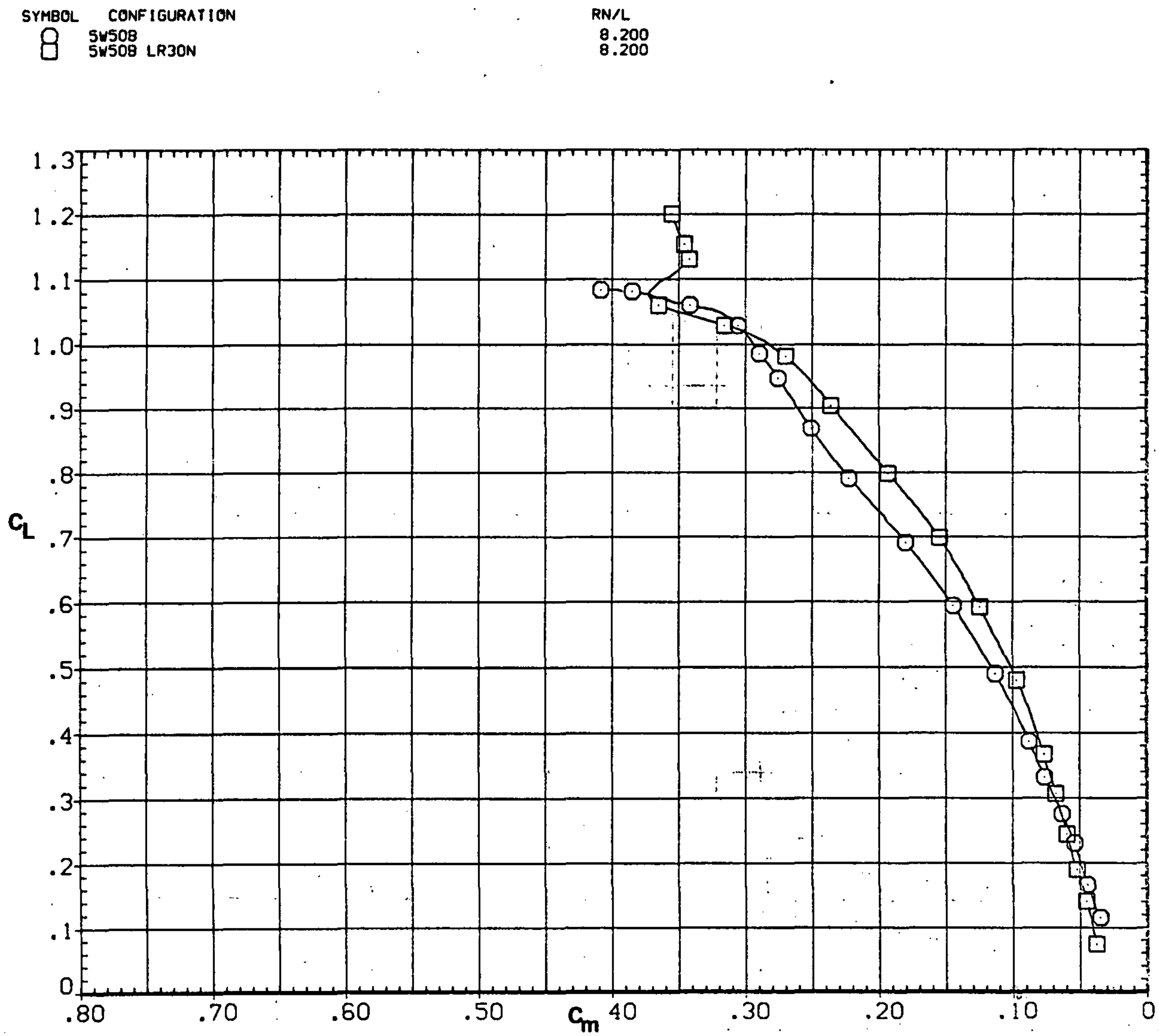

(b) C_L vs C_m

Figure 24.– Continued.

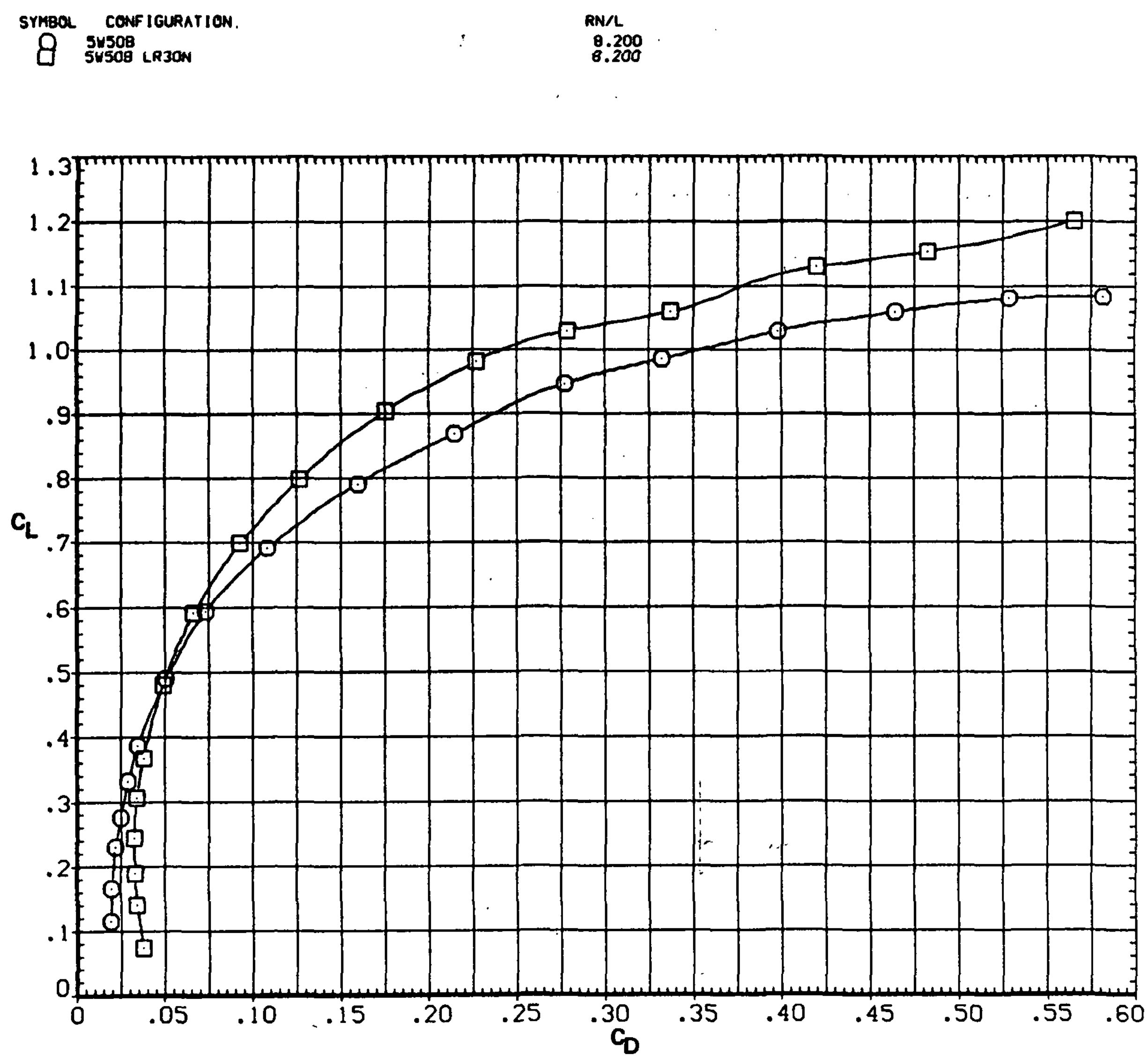

(c) C_L vs C_D

Figure 24.– Continued.

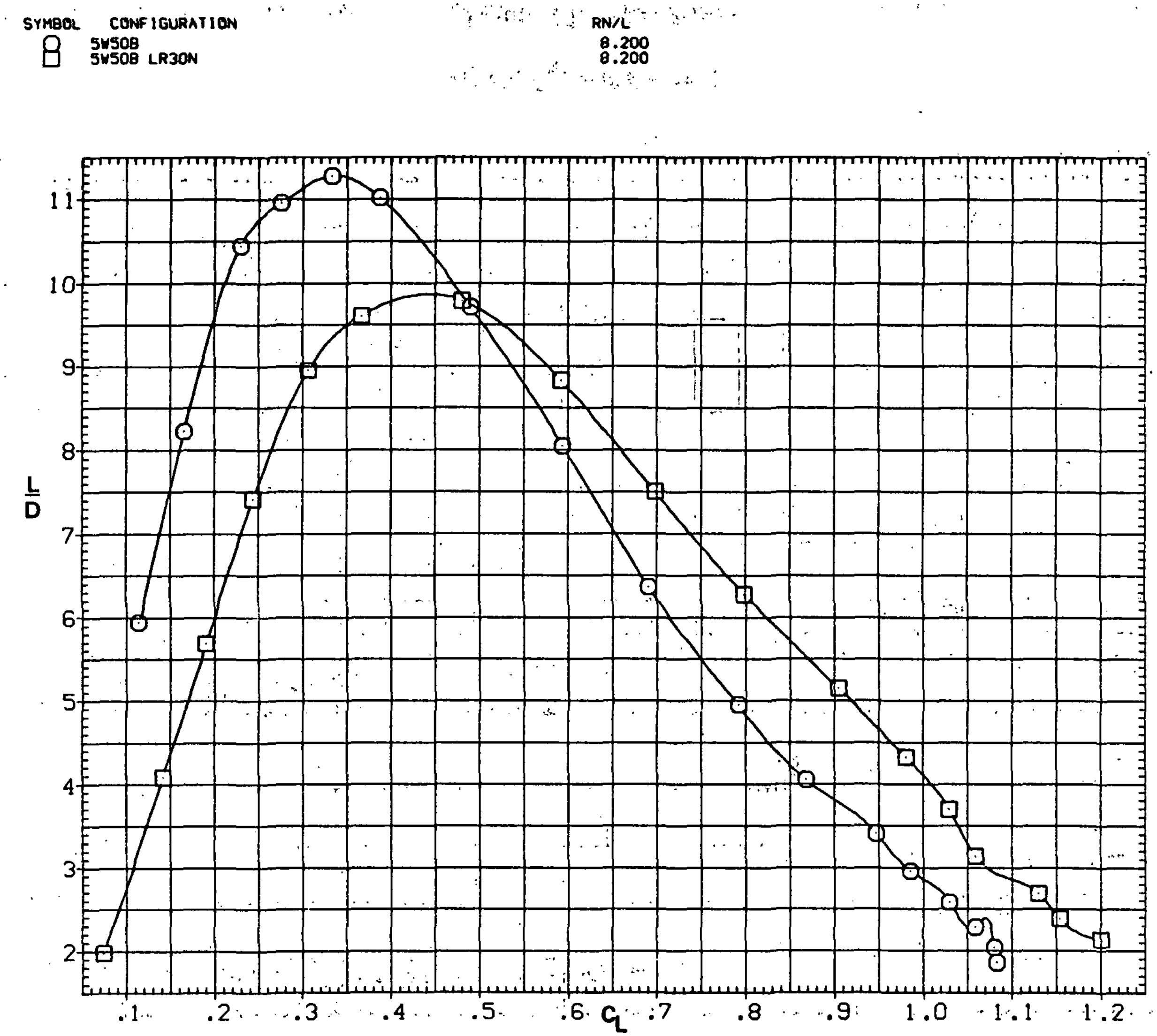

(d) L/D vs C_L

Figure 24.– Continued.

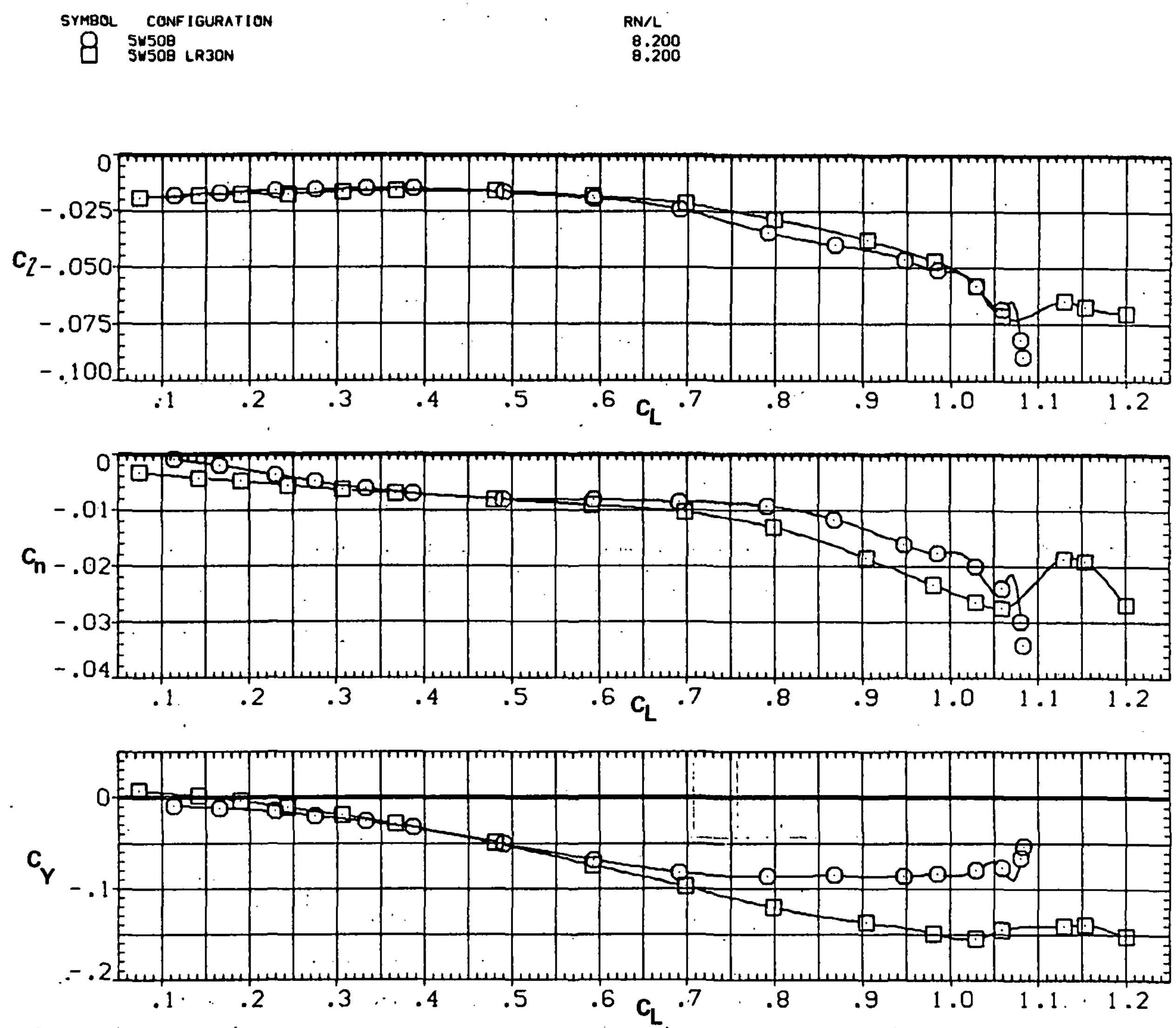

(e) C_l, C_n, and C_Y vs C_L

Figure 24.—Concluded.

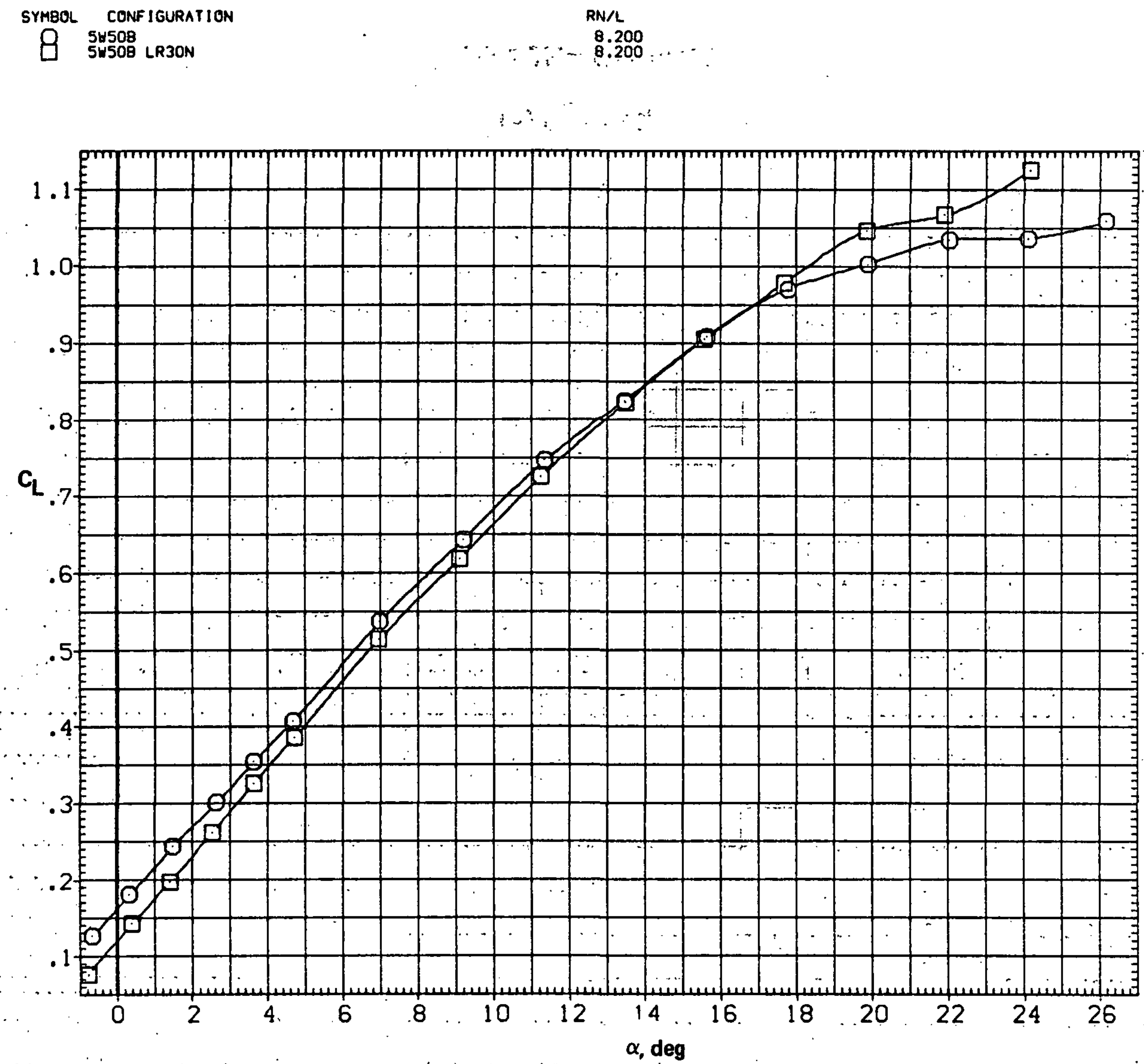

(a) C_L vs α

Figure 25.– Effect of drooped-nose flaps on the static longitudinal characteristics of the oblique wing: flaps on both wing panels, $\Lambda = 50°$, $M = 0.8$.

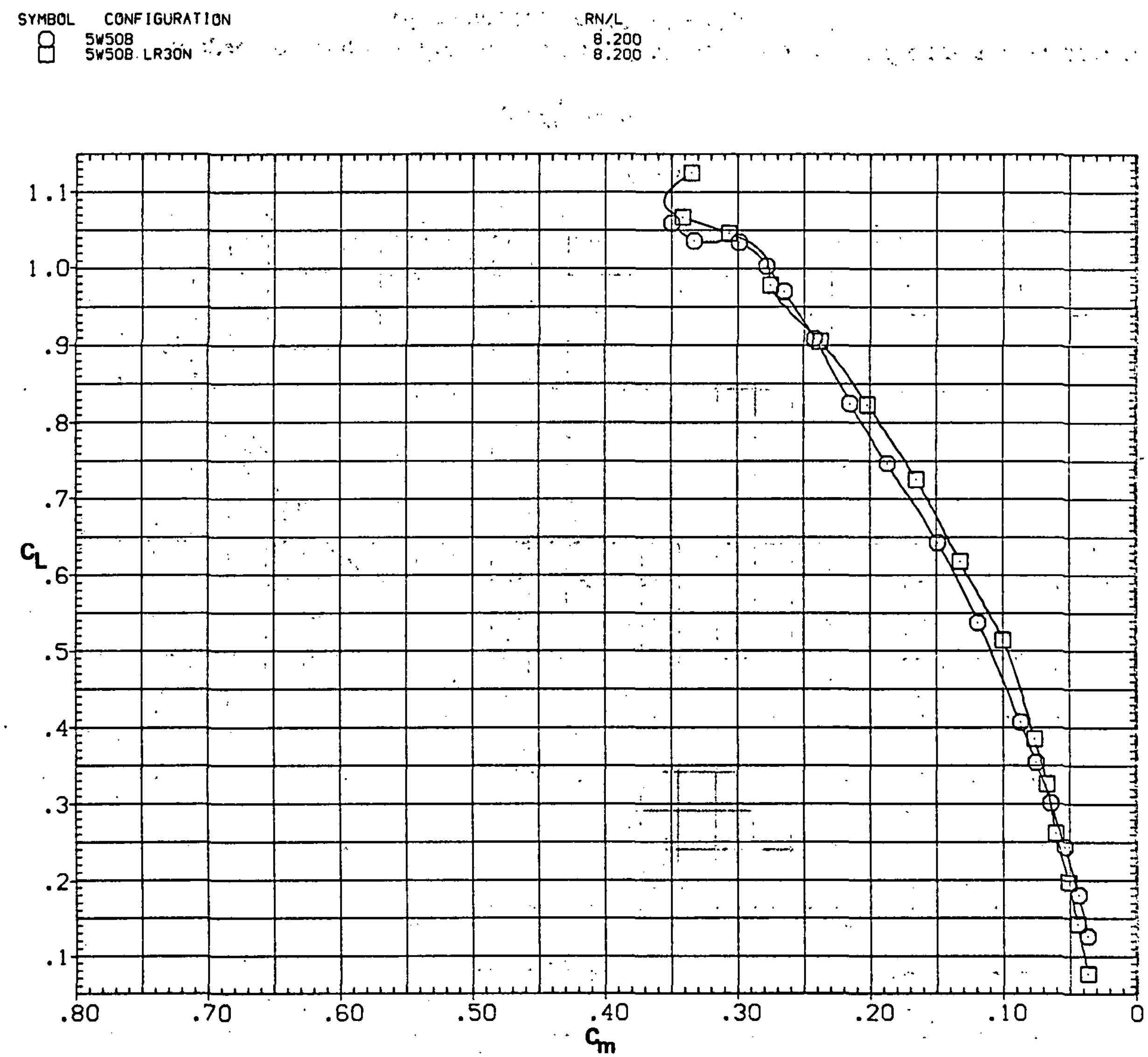

(b) C_L vs C_m

Figure 25.– Continued.

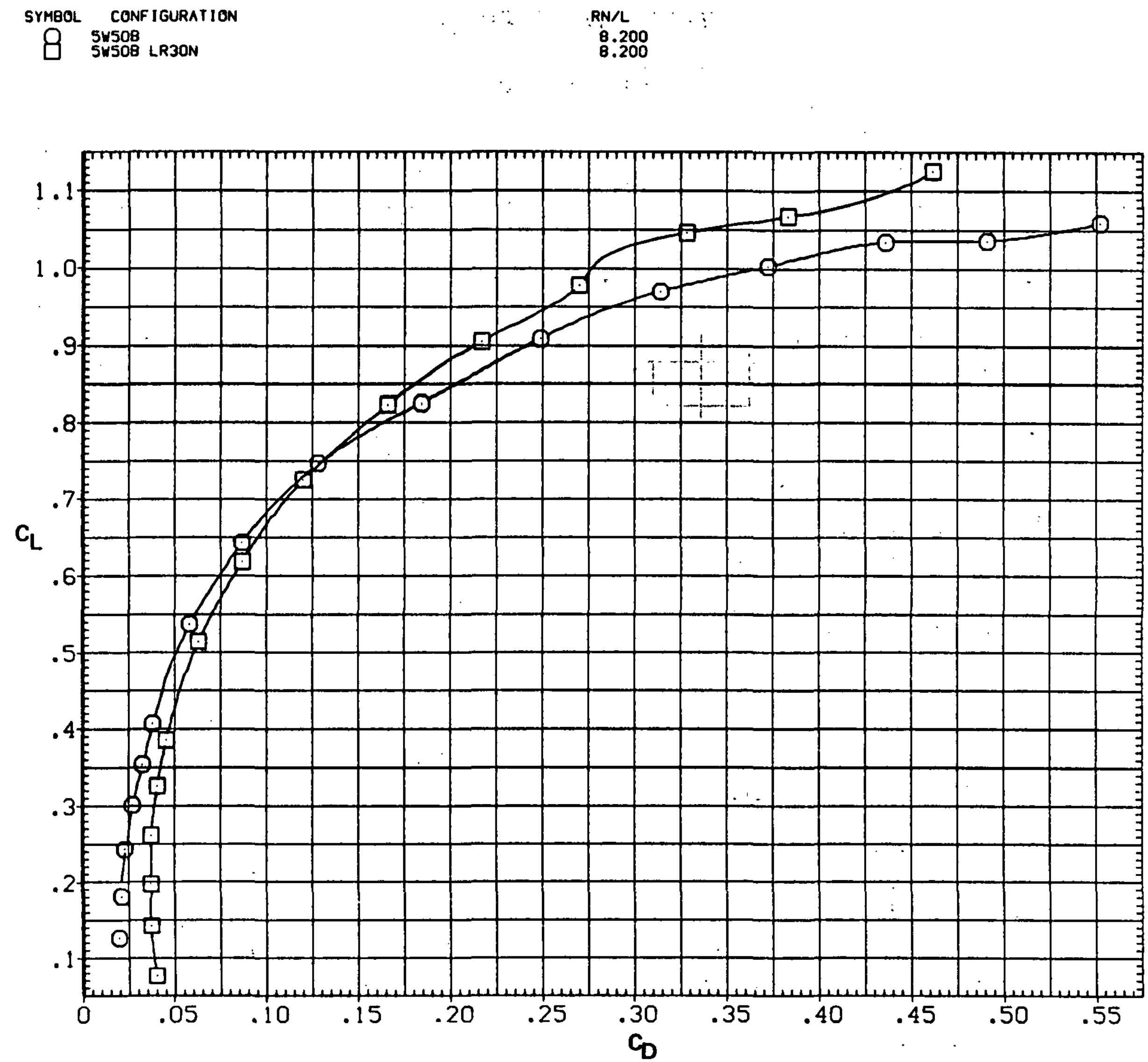

(c) C_L vs C_D

Figure 25.– Continued.

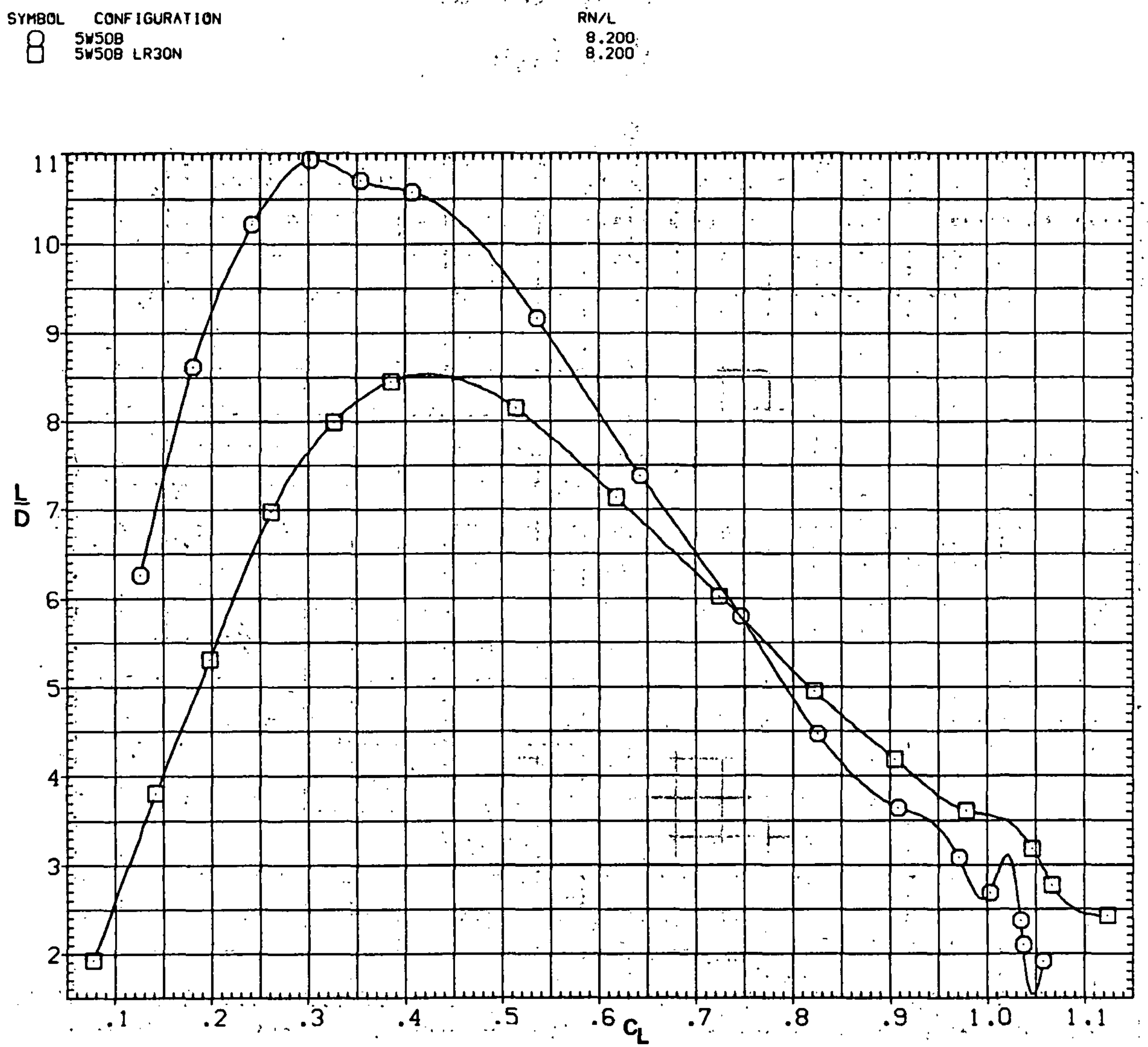

(d) L/D vs C_L

Figure 25.– Continued.

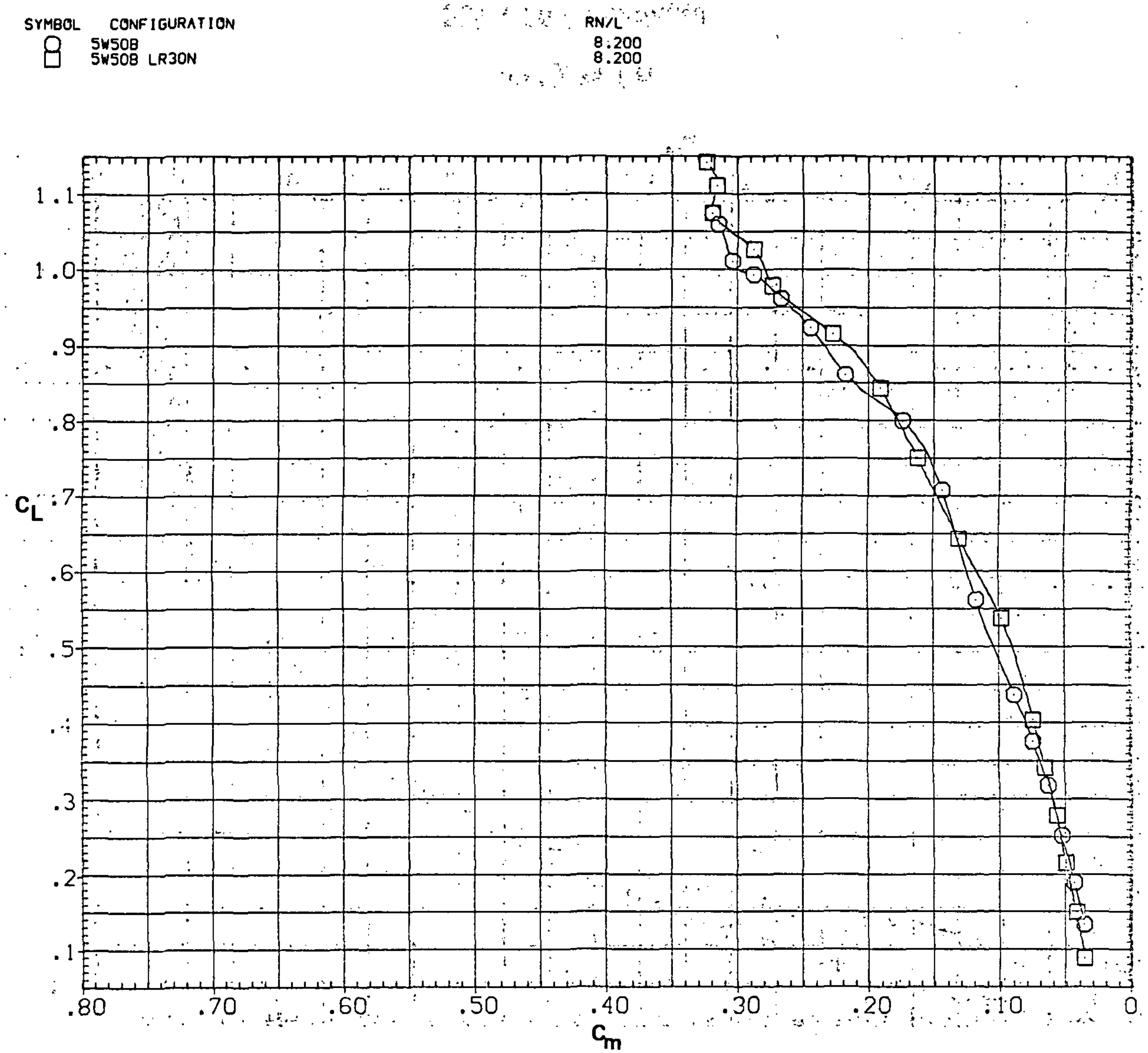

(b) C_L vs C_m

Figure 26.– Continued.

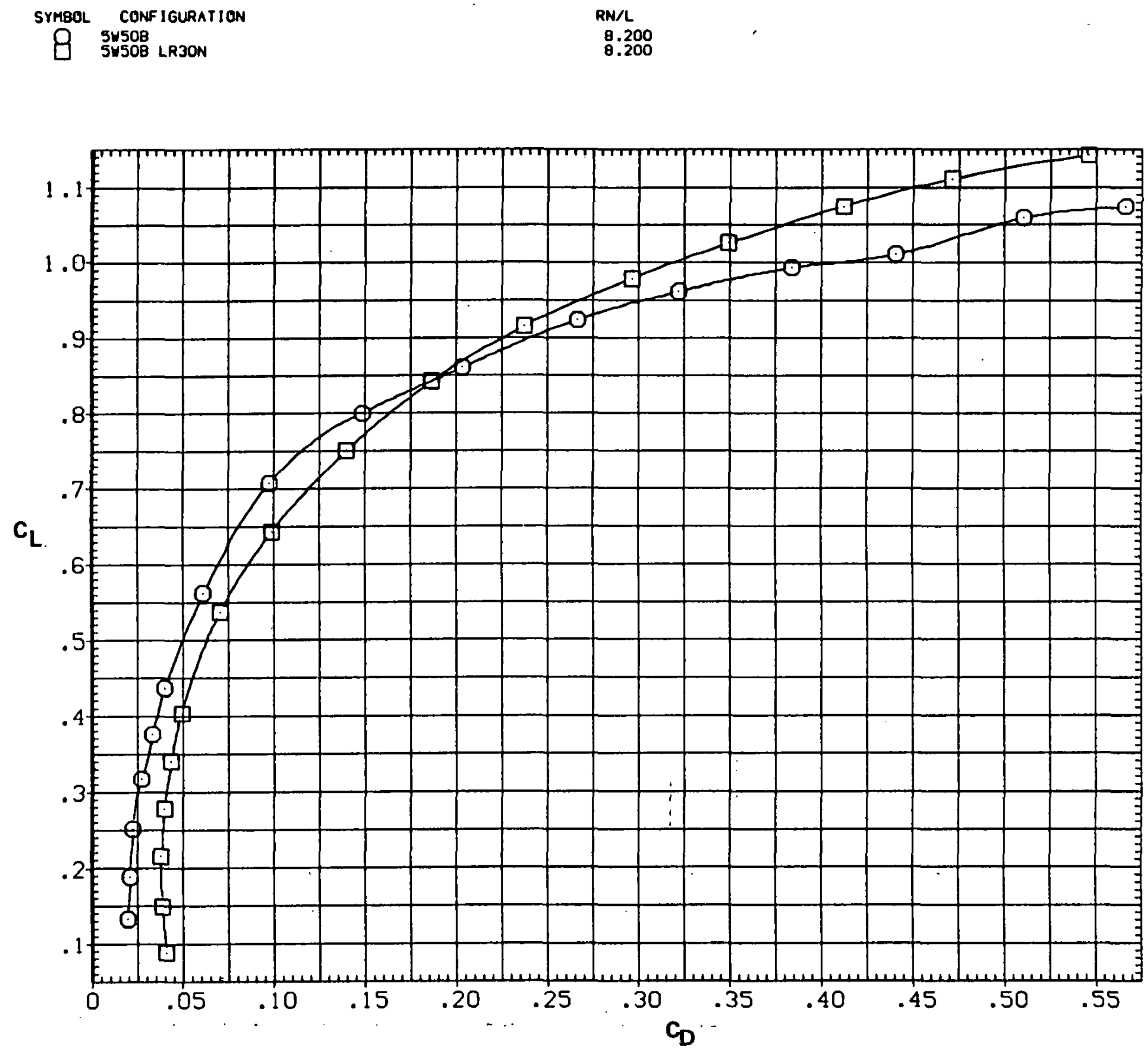

(c) C_L vs C_D

Figure 26.– Continued.

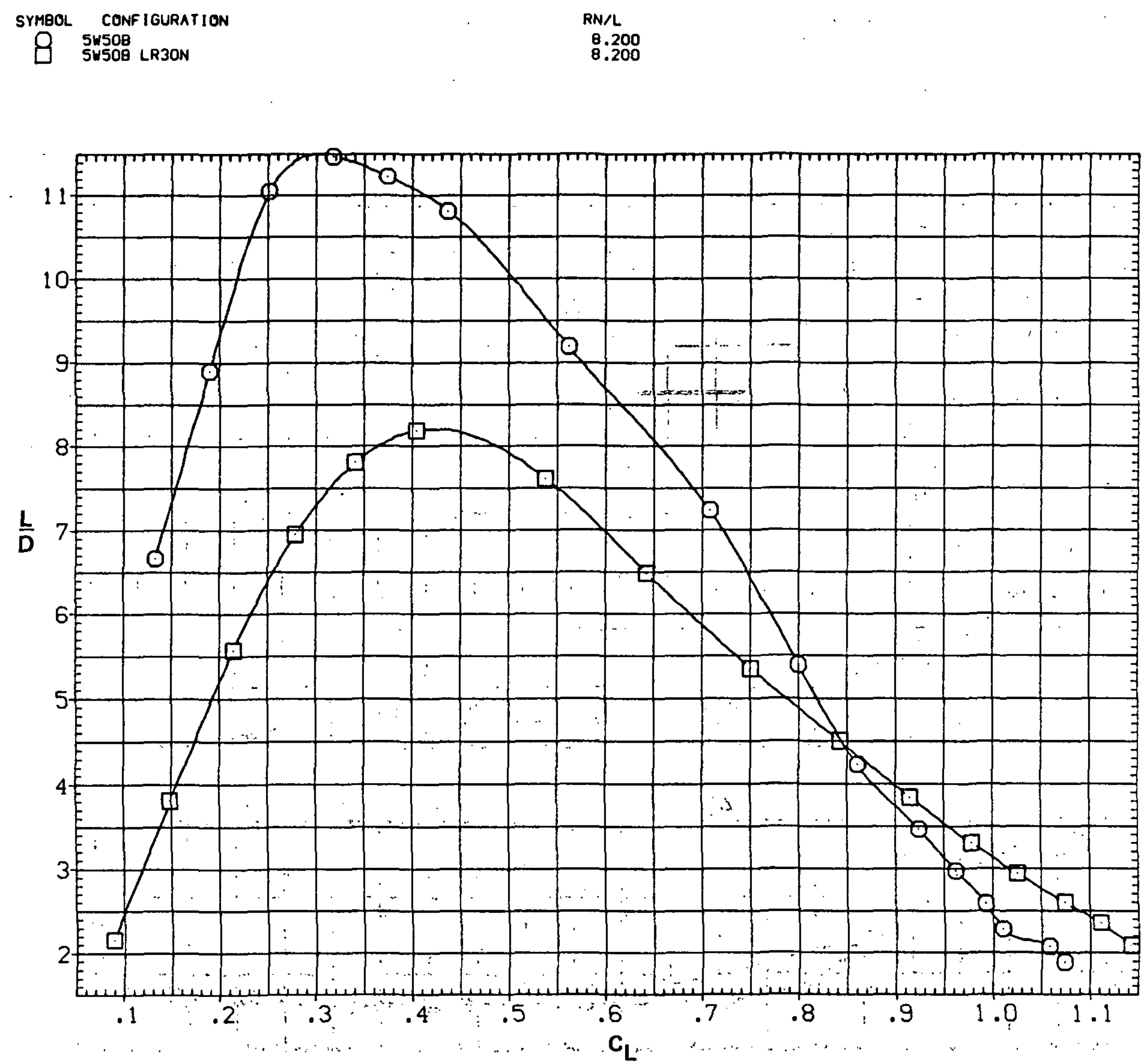

(d) L/D vs C_L

Figure 26.– Continued.

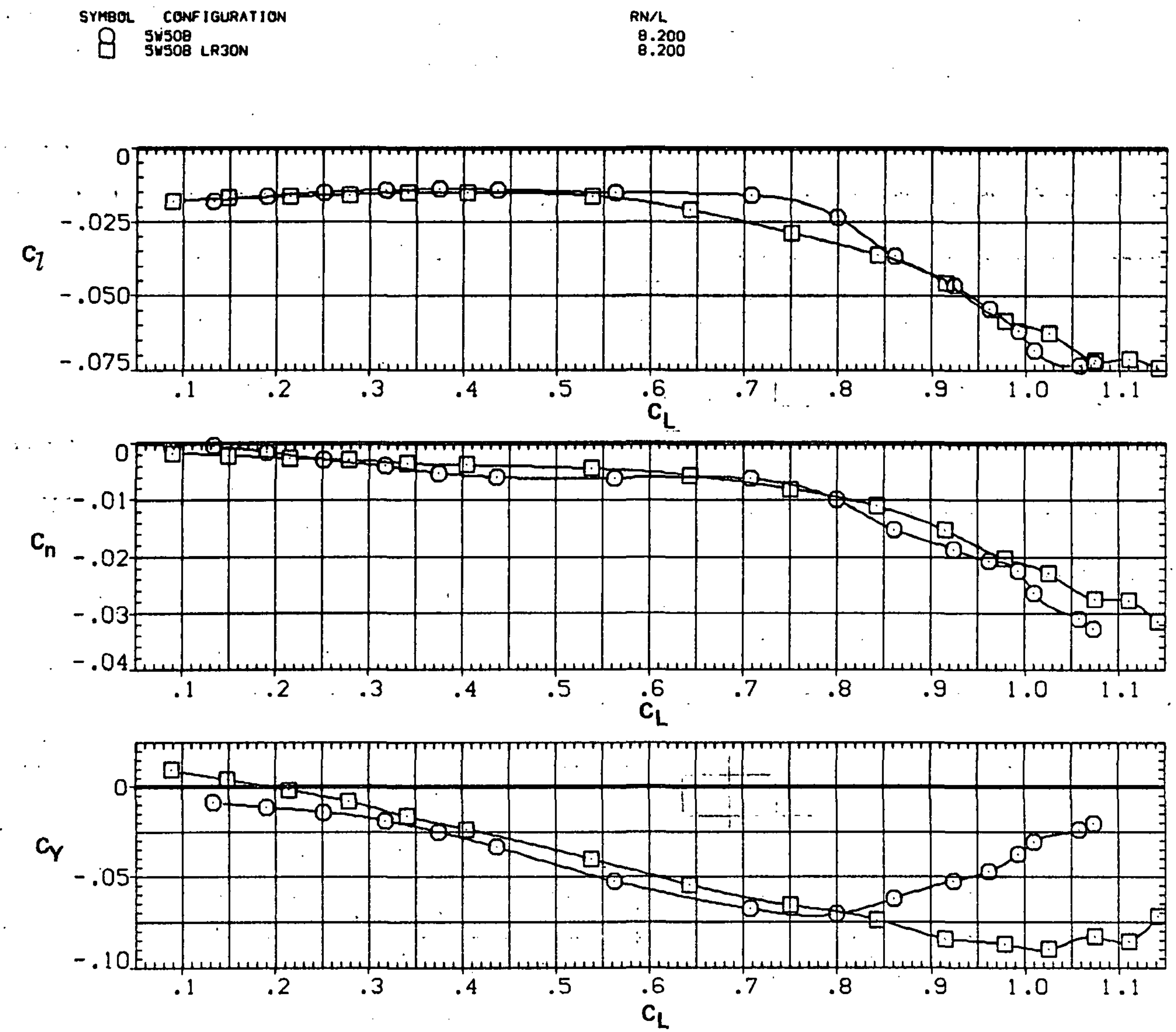

(e) C_l, C_n, and C_Y vs C_L

Figure 26.– Concluded.

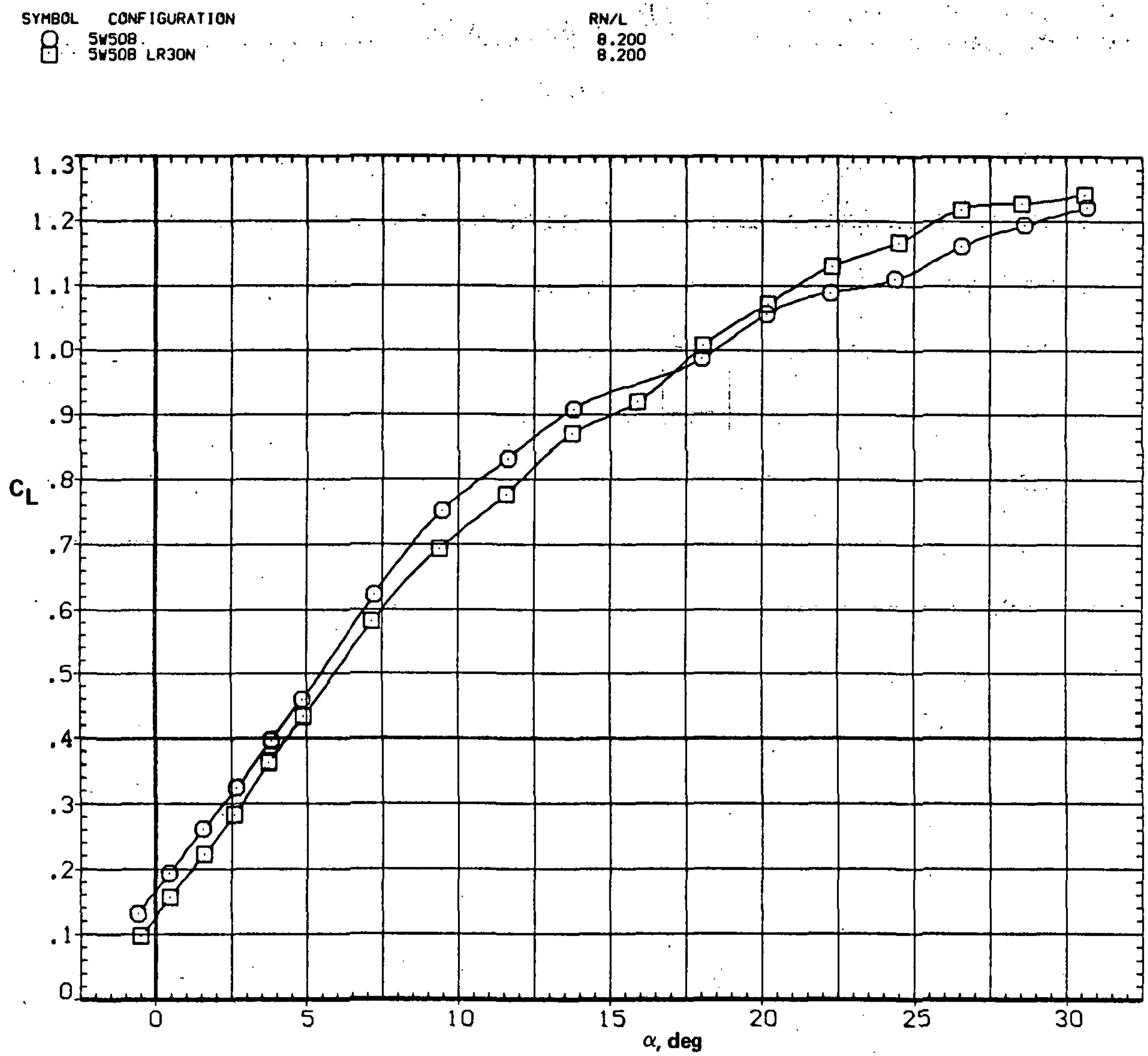

(a) C_L vs α

Figure 27.– Effect of drooped-nose flaps on the static longitudinal characteristics of the oblique wing: flaps on both wing panels, $\Lambda = 50°$, $M = 0.95$.

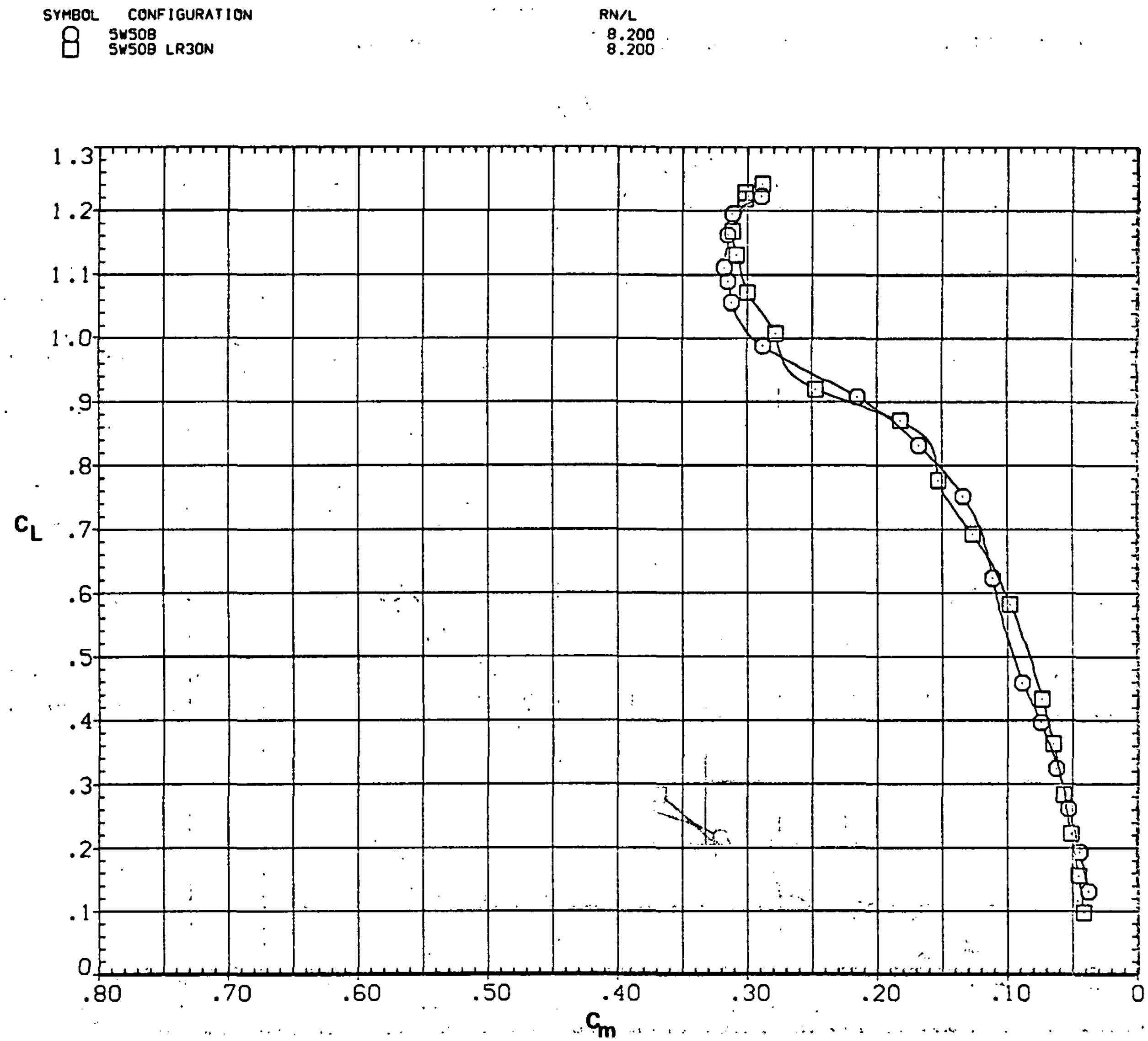

(b) C_L vs C_m

Figure 27.– Continued.

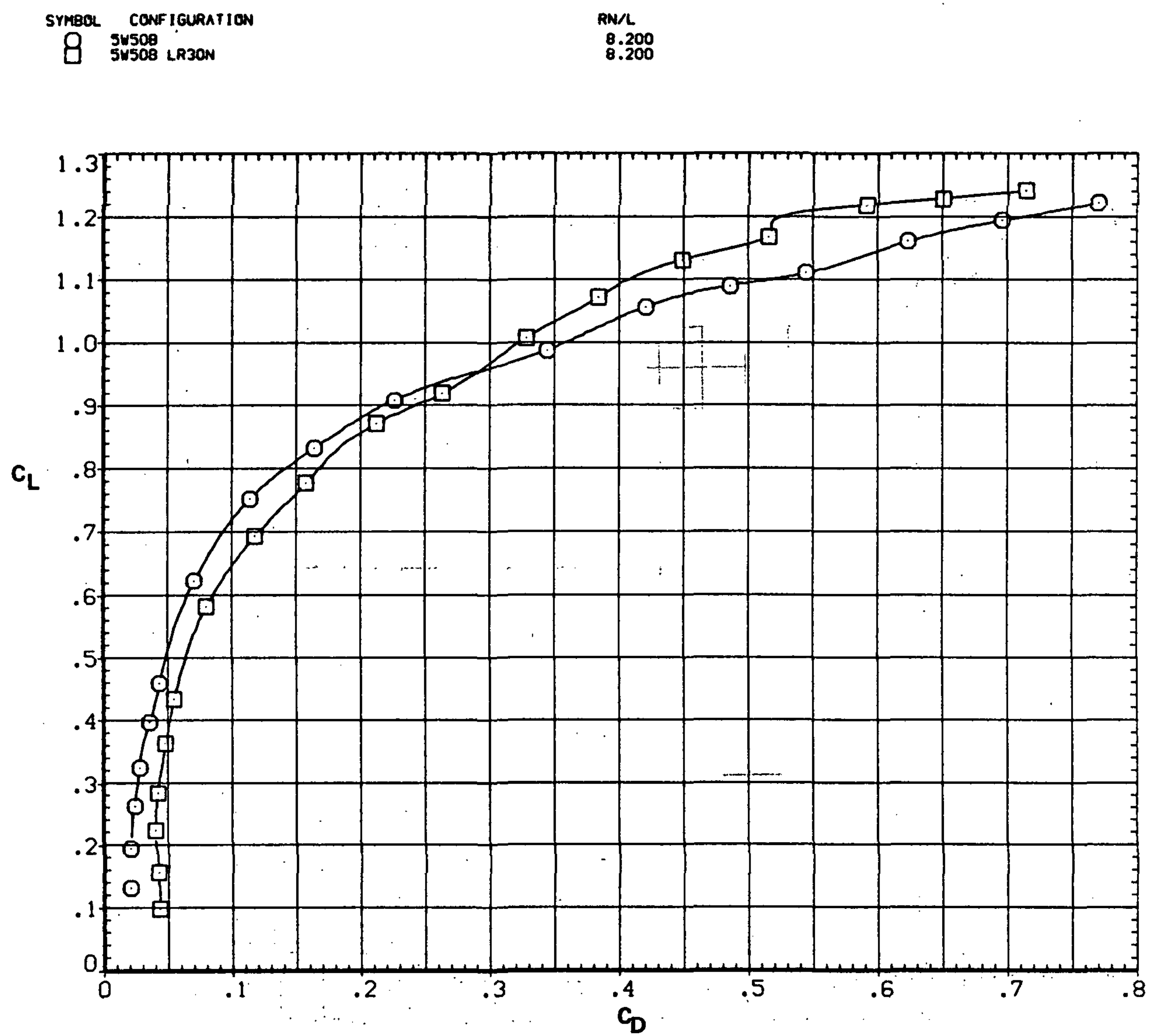

(c) C_L vs C_D

Figure 27.– Continued.

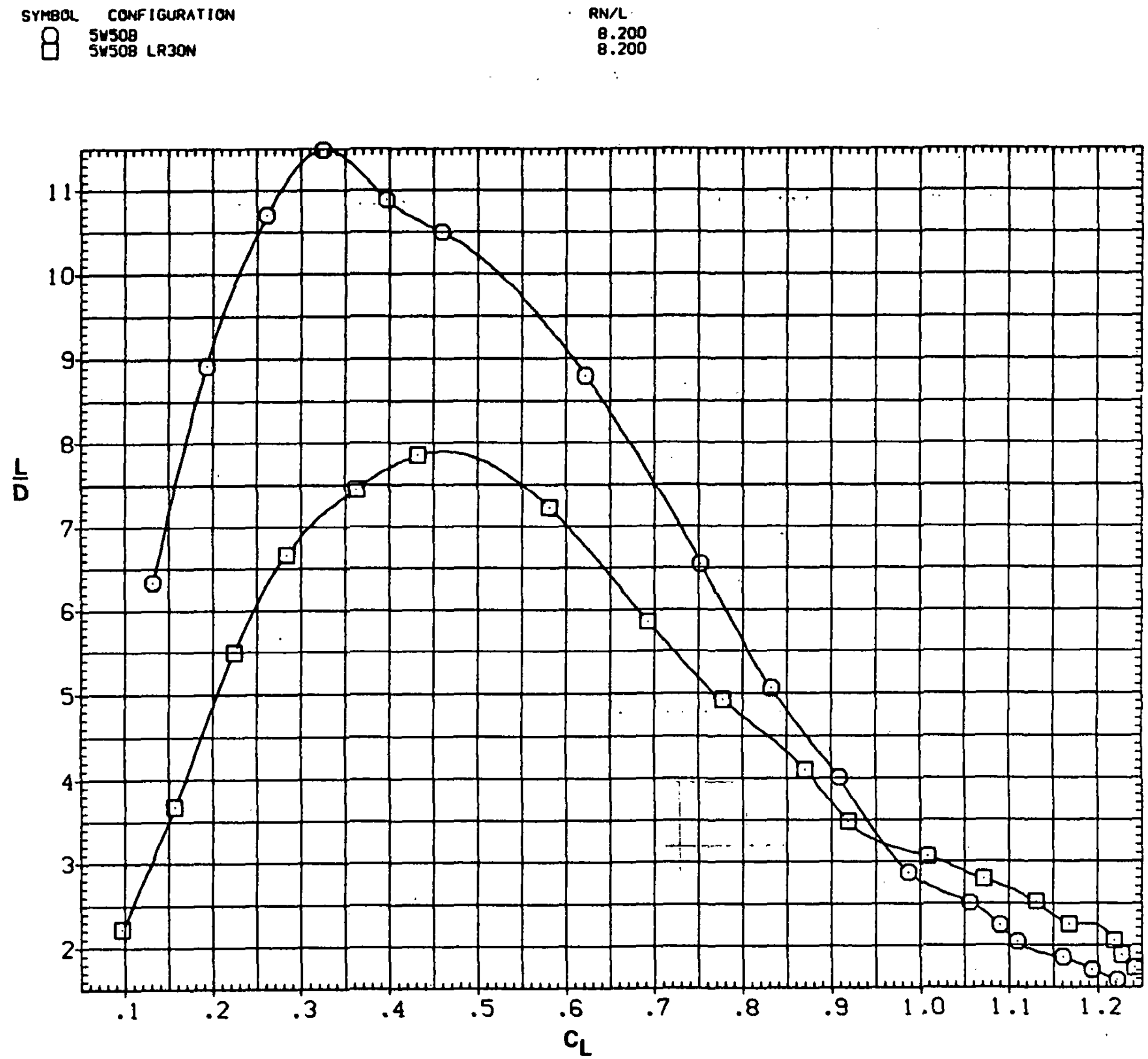

(d) L/D vs C_L

Figure 27.– Continued.

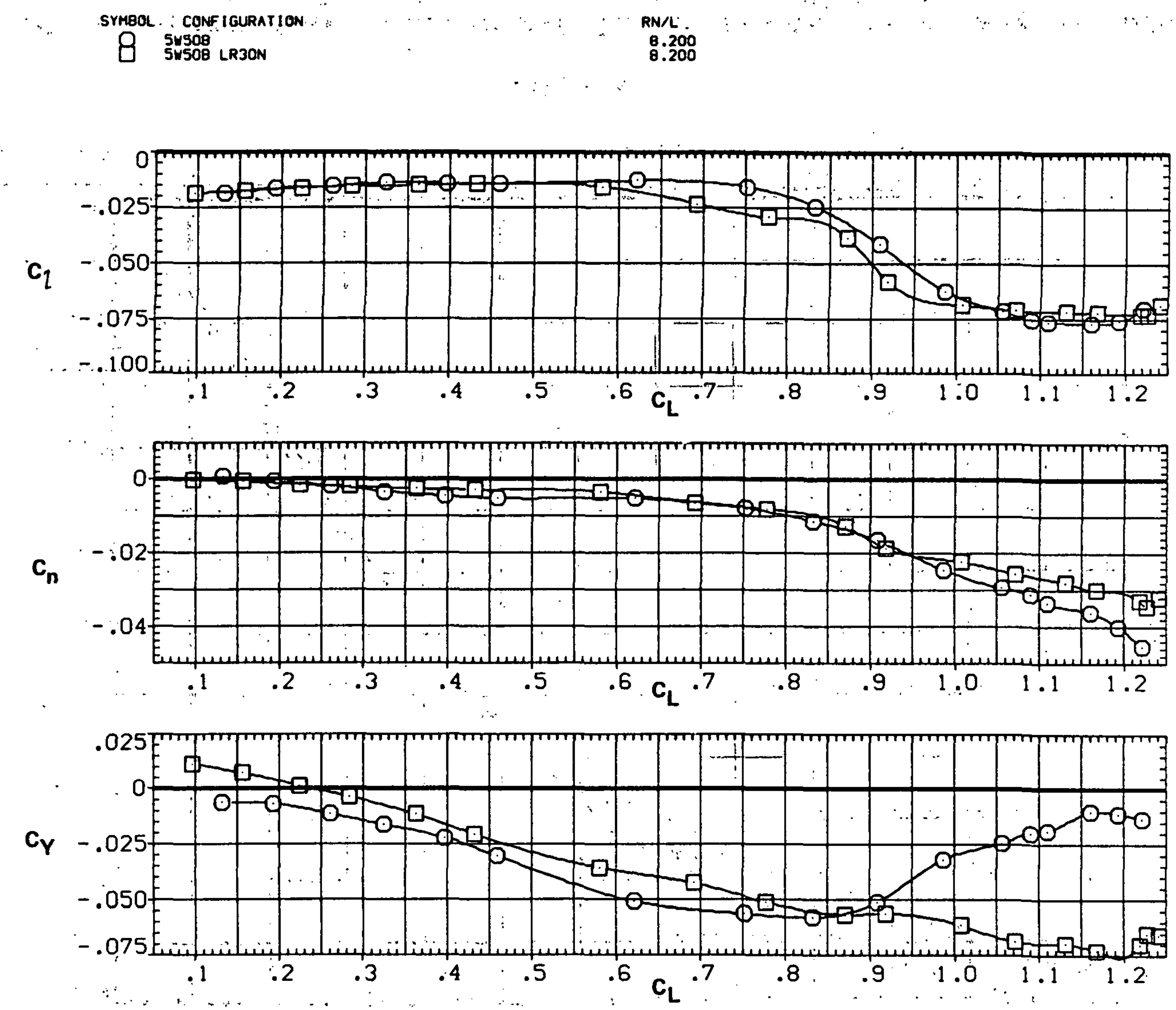

(e) C_l, C_n, and C_Y vs C_L

Figure 27.– Concluded.

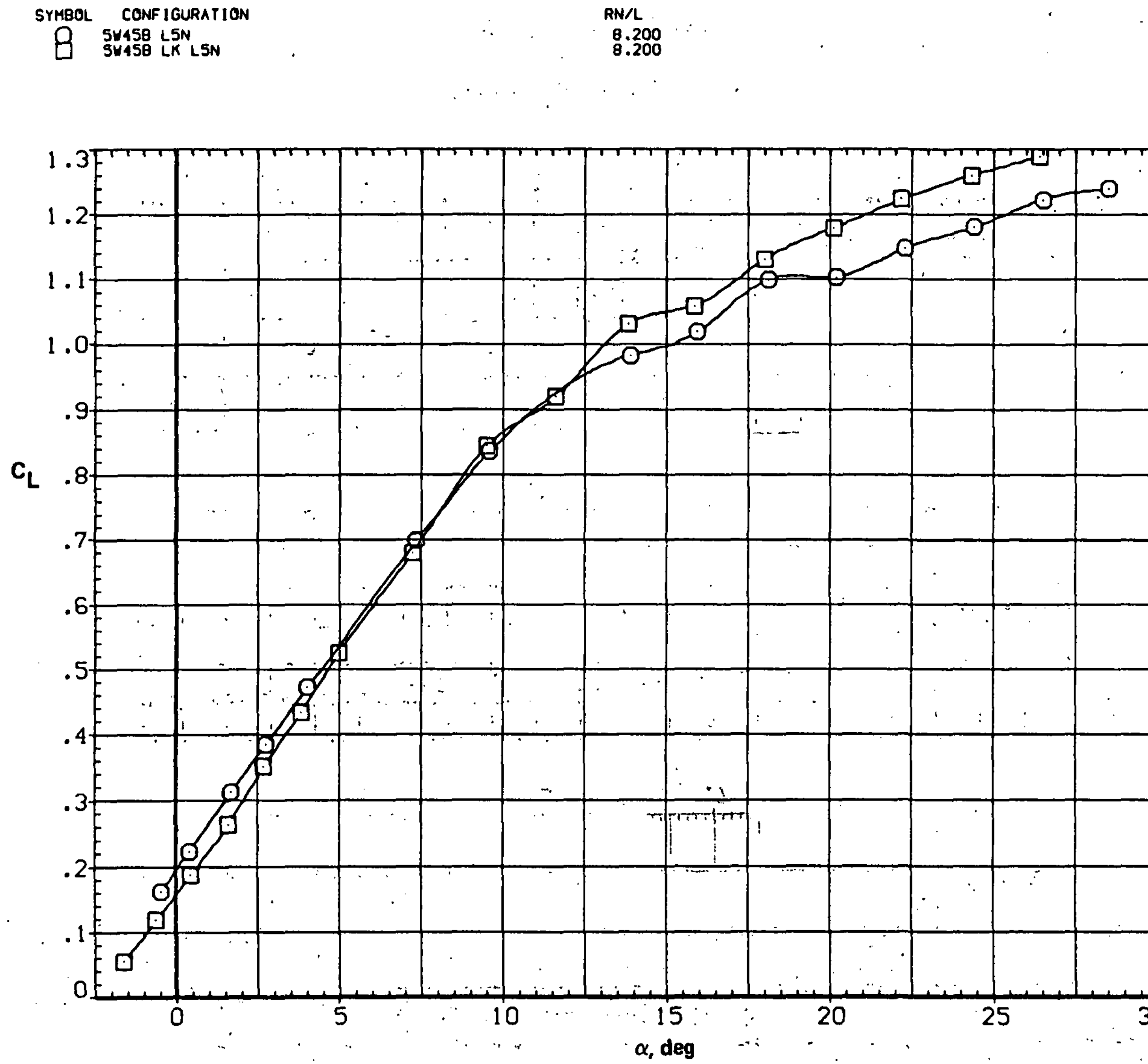

(a) C_L vs α

Figure 28.– Effect of Krüger-nose flaps on the static longitudinal characteristics of the oblique wing equipped with drooped-nose flaps: flaps on downstream wing panel only, $\Lambda = 45°$, $M = 0.95$.

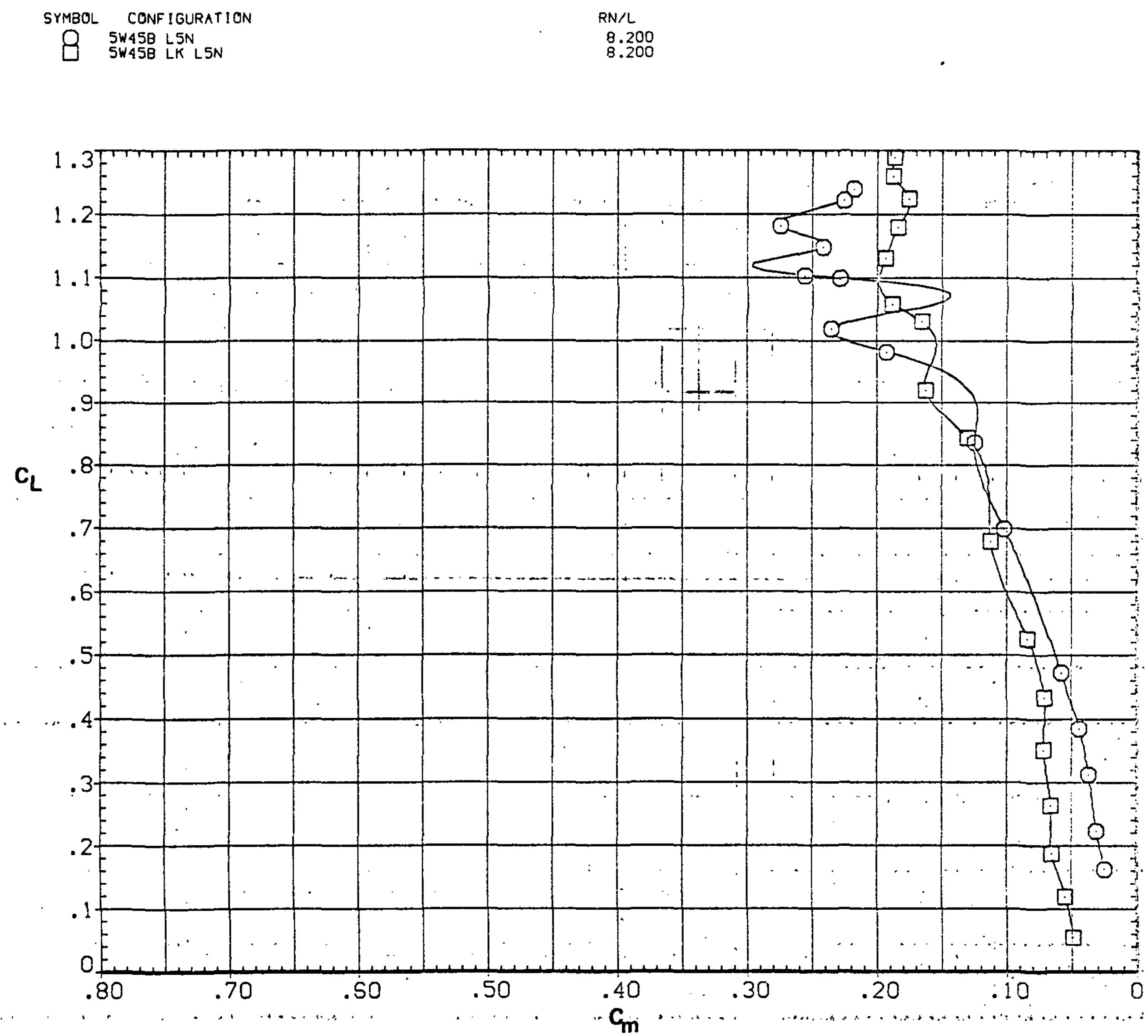

(b) C_L vs C_m

Figure 28.– Continued.

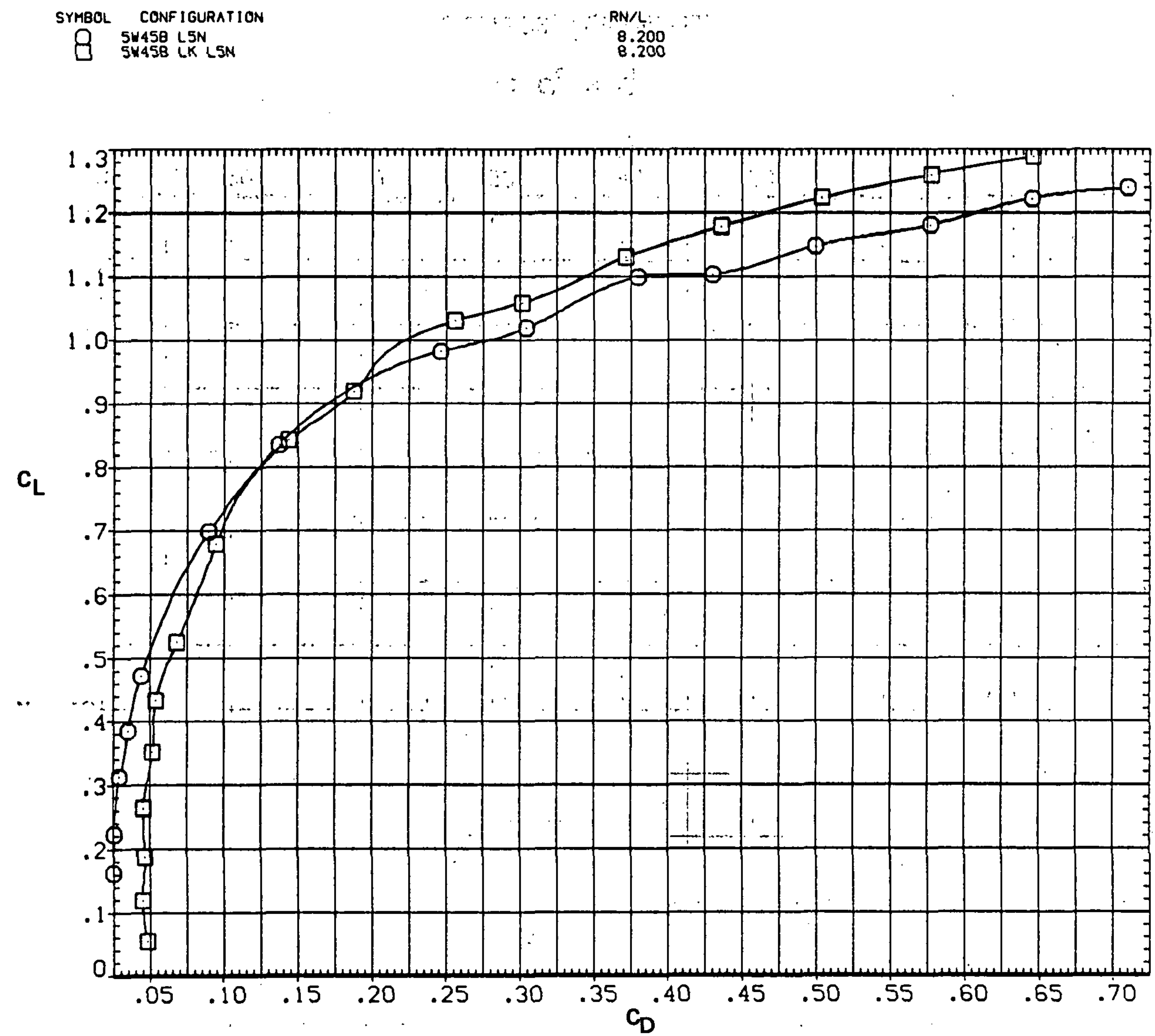

(c) C_L vs C_D

Figure 28.– Continued.

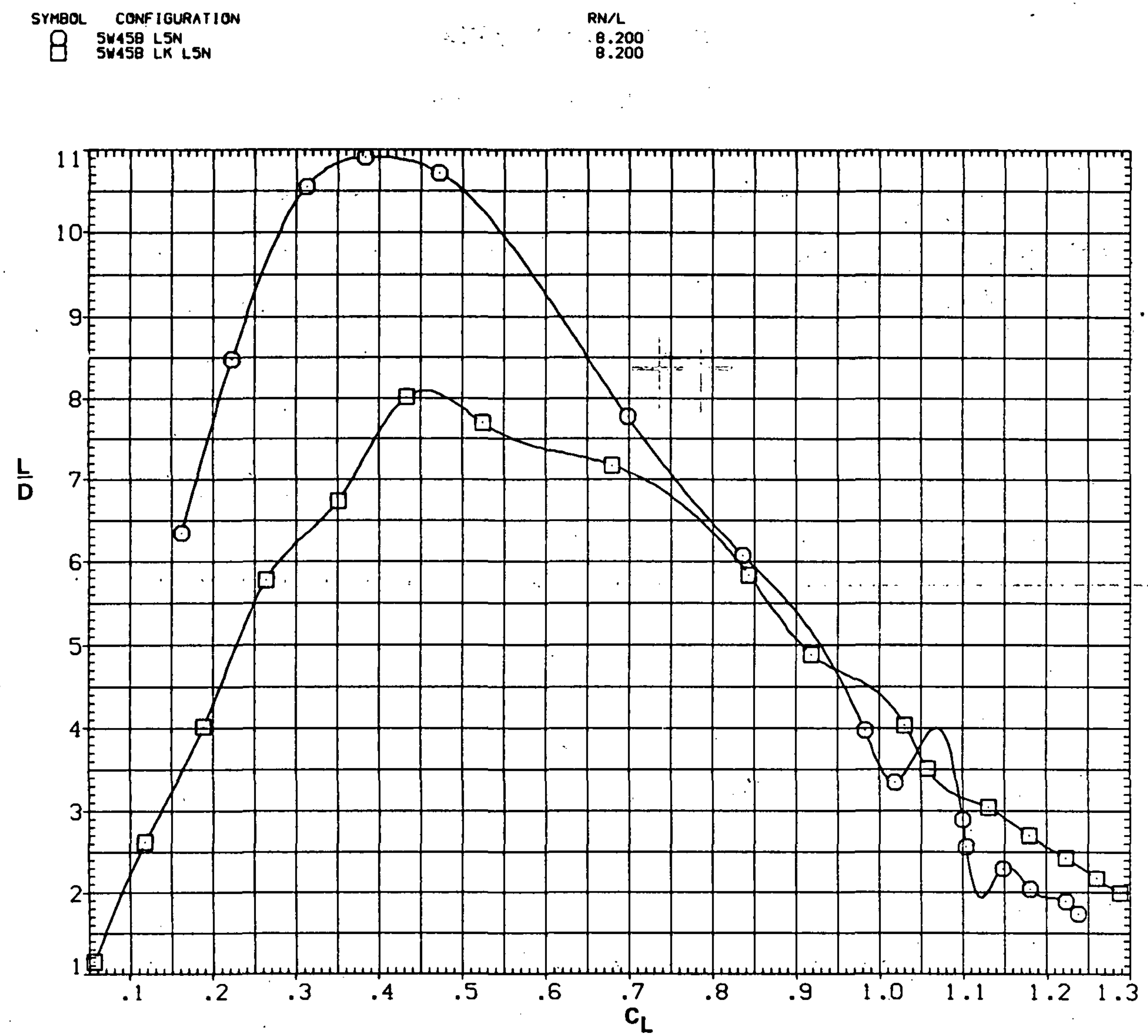

(d) L/D vs C_L

Figure 28.– Continued.

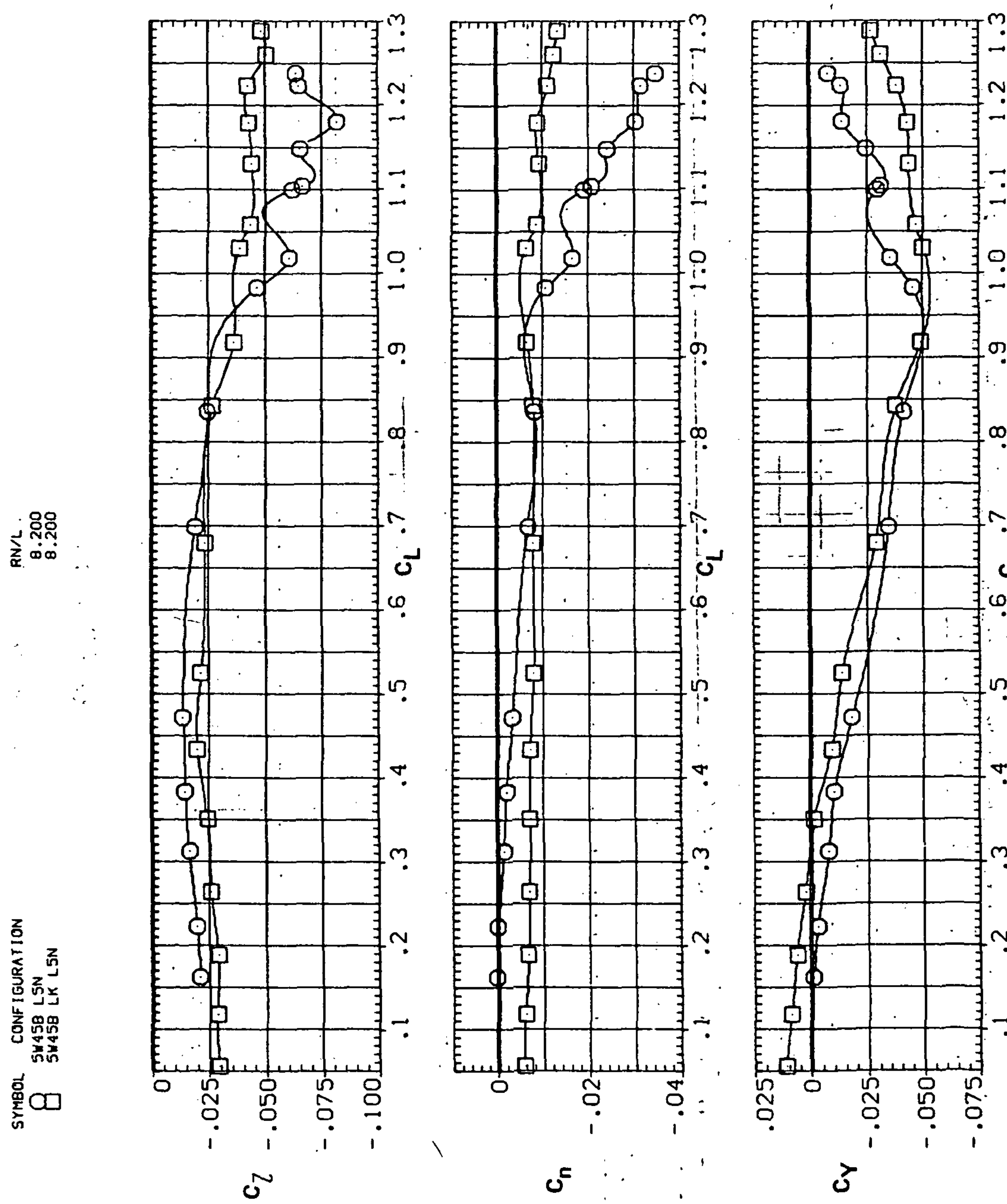

(e) C_l, C_n, and C_Y vs C_L

Figure 28.– Concluded.

*U.S. GOVERNMENT PRINTING OFFICE: 1976 - 735-004/3

"The aeronautical and space activities of the United States shall be conducted so as to contribute . . . to the expansion of human knowledge of phenomena in the atmosphere and space. The Administration shall provide for the widest practicable and appropriate dissemination of information concerning its activities and the results thereof."

—NATIONAL AERONAUTICS AND SPACE ACT OF 1958

NASA SCIENTIFIC AND TECHNICAL PUBLICATIONS

TECHNICAL REPORTS: Scientific and technical information considered important, complete, and a lasting contribution to existing knowledge.

TECHNICAL NOTES: Information less broad in scope but nevertheless of importance as a contribution to existing knowledge.

TECHNICAL MEMORANDUMS: Information receiving limited distribution because of preliminary data, security classification, or other reasons. Also includes conference proceedings with either limited or unlimited distribution.

CONTRACTOR REPORTS: Scientific and technical information generated under a NASA contract or grant and considered an important contribution to existing knowledge.

TECHNICAL TRANSLATIONS: Information published in a foreign language considered to merit NASA distribution in English.

SPECIAL PUBLICATIONS: Information derived from or of value to NASA activities. Publications include final reports of major projects, monographs, data compilations, handbooks, sourcebooks, and special bibliographies.

TECHNOLOGY UTILIZATION PUBLICATIONS: Information on technology used by NASA that may be of particular interest in commercial and other non-aerospace applications. Publications include Tech Briefs, Technology Utilization Reports and Technology Surveys.

Details on the availability of these publications may be obtained from:

SCIENTIFIC AND TECHNICAL INFORMATION OFFICE

NATIONAL AERONAUTICS AND SPACE ADMINISTRATION

Washington, D.C. 20546